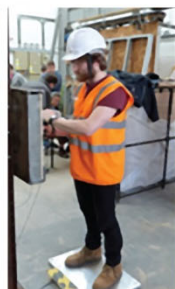# Proceedings of the 54th UK annual conference on human responses to vibration

24th -26th September 2019
Edinburgh Napier University
Craiglockhart Campus
Scotland, United Kingdom

Local Chair: Dr. Mark D. Taylor
General Chair: Professor Setsuo Maeda

54th UK HRV 2019
Edinburgh Napier University

WELCOME

Co-hosted by

Edinburgh Napier
UNIVERSITY

REACTEC
INFORM : PROTECT : DEPLOY

Proceedings of the 54th UK Conference on Human Responses to Vibration

24th - 26th September 2019

Edinburgh Napier University
School of Engineering the Built Environment
Edinburgh, Scotland

Local chair: Dr. Mark D. Taylor
Edinburgh Napier University

General chair: Prof. Setsuo Maeda
Nottingham Trent University

Co-host: Reactec Ltd.

Online version: 1st November 2019

Contents

1 Welcome

Welcome to Edinburgh Napier University and the City of Edinburgh. Napier Technical College was founded in 1964, taking its name from John Napier, the inventor of logarithms and the decimal point, who was born in 1550 in the medieval tower house of Merchiston Castle (the site of the University's Merchiston campus). His statue stands in the tower of Merchiston Castle today. An opening ceremony was held on 23 February 1965. In 1966, it was renamed Napier College of Science and Technology. In 1974, it merged with the Sighthill-based Edinburgh College of Commerce to form Napier College of Commerce and Technology, which became a Central Institution in 1985.
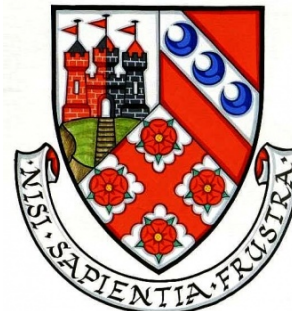
The college was renamed Napier Polytechnic in 1986 and in the same year acquired the former Hydropathic hospital buildings at Craiglockhart. In June 1992 the institution officially became Napier University. At a ceremony witnessed by over 700 staff and students, Lord James Douglas Hamilton and the then Principal, William Turmeau, unveiled the new University sign at Merchiston. In 1994, Napier University acquired its Craighouse Campus. In 1996, the university gained a new Faculty of Health Studies through a merger between the Scottish Borders College of Nursing and Lothian College of Health Studies. In February 2009 it became Edinburgh Napier University
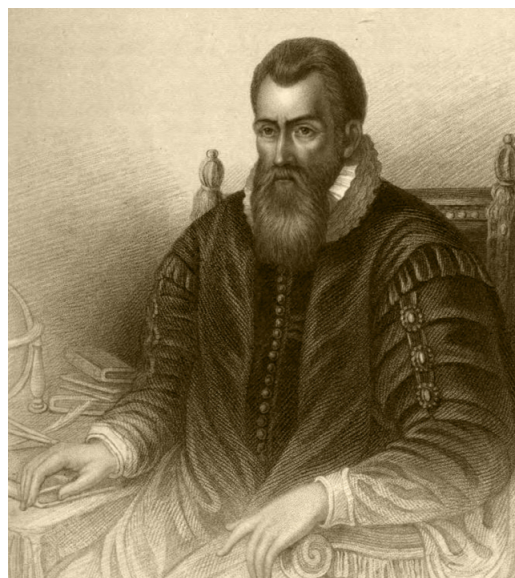
Edinburgh Napier has been awarded the Queen's Anniversary Prize twice. Its most recent win came in 2015, when it was recognised for its work in timber engineering, sustainable construction and wood science. The motto of the University, Nisi sapientia frustra (meaning "Without knowledge, [all is] in vain"), echoes the motto of the City of Edinburgh, Nisi Dominus frustra (meaning "Without [the] Lord, [all is] in vain"). We wish you all a successful conference and we hope you enjoy your stay in the City of Edinburgh.

2 Professor Michael Griffin

Professor Michael Griffin sadly passed away on 17 August 2019. He was Professor of Human Factors within Engineering and Physical Sciences at the University of Southampton. Professor Griffin was actively involved in establishing the UK Conference on Human Responses to Vibration and has contributed to our field extensively over many years.

Professor Griffin's research focussed on human responses to vibration. He obtained a PhD in the Institute of Sound and Vibration Research 1972. After a period as a Research Fellow, he was appointed as a Lecturer in the Institute of Sound and Vibration Research in 1977, a Senior Lecturer in 1984, and Professor of Human Factors in 1991.

Professor Griffin provided lectures on 'Human Factors in Engineering' and 'Human Responses to Vibration' for graduate and postgraduate programmes at the University of Southampton. He is the author of more than 600 publications including 250 papers in peer-reviewed scientific journals, the author of the 'Handbook of Human Vibration', and the author of chapters in more than 20 other books.

Professor Griffin was the Chairman of the British Standards Institution Sub-Committee on human responses to mechanical vibration and shock, a member of relevant ISO and CEN Committees, and a member of the International Advisory Committees of Conferences on Hand-arm Vibration and Whole-body Vibration. He was a member of the Ergonomics Society, the Human Factors and Ergonomics Society, and the Aerospace Medical Association.

Our thoughts and condolences are with his family and friends.

3 Previous conferences

1968 University of Southampton, Institute of Sound and Vibration Research
1968 University of Birmingham
1969 Royal Aircraft Establishment, Farnborough
1970 Loughborough University of Technology
1971 University of Southampton, Institute of Sound and Vibration Research
1971 University College, Swansea
1972 University of Sheffield
1973 University of Salford
1974 Westland Helicopters Limited, Yeovil
1975 University of Southampton, Institute of Sound and Vibration Research
1976 Royal Military College of Science, Shrivenham
1977 UOP Bostrom, Northampton
1978 National Institute of Agricultural Engineering, Silsoe
1979 Royal Aircraft Establishment, Farnborough
1980 University College, Swansea
1981 Heriot-Watt University, Edinburgh
1982 Health and Safety Executive, Cricklewood
1983 National Institute of Agricultural Engineering, Silsoe
1984 Heriot-Watt University, Edinburgh
1985 British Rail, Derby
1986 Loughborough University of Technology
1987 Royal Military College of Science, Shrivenham
1988 INRS Nancy, France
1989 AFRC Institute of Engineering Research, Silsoe
1990 University of Leeds
1991 Health and Safety Executive, Buxton
1992 University of Southampton, Institute of Sound and Vibration Research
1993 Army Personnel Research Establishment, Farnborough
1994 Institute of Naval Medicine, Alverstoke
1995 Silsoe Research Institute, Silsoe
1996 Motor Industry Research Association, Nuneaton
1997 University of Southampton, Institute of Sound and Vibration Research
1998 Health and Safety Executive, Buxton
1999 Ford Motor Company Ltd, Dunton, Essex
2000 University of Southampton, Institute of Sound and Vibration Research
2001 QinetiQ, Farnborough
2002 Loughborough University
2003 Institute of Naval Medicine, Alverstoke
2004 RMS Vibration Test Laboratory, Ludlow

2005 Health and Safety Executive, Liverpool
2006 QinetiQ, Farnborough
2007 University of Southampton, Institute of Sound and Vibration Research
2008 Caterpillar, Leicester
2009 Loughborough University
2010 Institute of Naval Medicine, Alverstoke
2011 Health and Safety Laboratory, Buxton
2012 University of Southampton, Institute of Sound and Vibration Research
2013 Andreas Stihl Limited, Ascot
2014 Health and Safety Laboratory, Buxton
2015 University of Southampton, Institute of Sound and Vibration Research
2016 Institute of Naval Medicine, Alverstoke
2017 Cranfield University, Shrivenham
2018 Andreas Stihl Ltd. and Health and Safety Executive, Ascot
2019 Edinburgh Napier University and Reactec Ltd., Edinburgh

4   Conference programme

DAY 1 Tuesday 24th September 2019
11:00   12:00   Registration
12:00   13:00   Lunch
Welcome and introductions
13:00   13:05   Mark Taylor   Welcome and domestics
13:05   13:10   Jacqui McLaughlin   Welcome from Reactec Ltd.
Session 1: Keynote speech
Chair: Mark Taylor
13:10   13:40   Paul Pitts   UK Health and Safety Executive
13:45   14:15   Chris Oliver   King James IV Professor
14:15   14:30   Photograph on lawn
Session 2: HAV1
Chair: Paul Pitts
14:40   16:20   Presentations (Papers 10,11,19,22 and 23)
16:20   16:35   Panel discussion
Session 3: HAV2
Chair: Chris Oliver
16:40   18:00   Presentations (Papers 8,9,13 and 21)
18:00   18:15   Panel discusson
18:15   19:30   Informal meal and drinks reception
END OF DAY 1

DAY 2 Wednesday 25th September 2019
Session 4: WBV1
Chair: Peter Johnson
09:10   10:30   Presentations (Papers 2,7,14 and 15)
10:30   10:45   Panel discussion
10:45   11:15   Tea/coffee break and exhibits
Session 5: WBV2
Chair: Gurmail Paddan
11:15   12:35   Presentations (Papers 6,16 and 18)
12:35   12:50   Panel discussion
12:50   14:00   Lunch buffet
Session 6: Keynote speech
Chair: Mark Taylor
13:45   14:15   Peter Johnson, University of Washington
14:30   16:00   Tour of historical Edinburgh (drop of in city centre)
19:30   20:00   Drinks reception at Craiglockhart Campus
20:00   23:00   Conference dinner (formal with Scottish entertainment)
END OF DAY 2

DAY 3 Thursday 26th September 2019
Session 7: WBV3
Chair: Kazuhito Kato
09:30   10:30   Presentations (Papers 3,4 and 5)
10:30   10:45   Panel discussion
10:45   11:15   Tea/coffee break and exhibits
Session 8: WBV4
Chair: Mohammed Fard
11:15   12:15   Presentations (Papers 1,12 and 20)
12:15   12:30   Panel discussion
Session 9: Conference close
Chair: Setsuo Maeda
12:30   12:45   Consideration of the 55th UK HRV Conference 2020
12:45   12:50   Confernece close
12:50   14:00   Lunch buffet
Session 10: Conference special tour
14:20   17:00   Tour of Forth Bridges at South/North Queensferry

5   Delegates

Surname	First name	Afiliation
Anderson	Leif	Reactec Ltd.
Barbeau	Romain	Faurecia Automotive Seating
Carre	Matt	University of Sheffield
Cavacece	Massimo	University of Cassino and of Southern Lazio
Cherry	Morag	Edinburgh Napier University
Coe	Tom	Royal National Lifeboat Institution
Cooper	Laura	Edinburgh Napier University
D'Amore	Francesco	University of Southampton
Ebe	Kazushige	Bridgestone Corporation
Fairley	Hans	Andreas Stihl Ltd.
Fard	Mohammed	Royal Melbourne Institute of Technology
Gunston	Tom	Finch Consulting Ltd.
Houssein	Peerally	Skanska UK Plc.
Hawker	Antonia	UK Health and Safety Executive
Hida	Takenori	The University of Tokyo
Hossain	Mahbub	Yamaguchi University Graduate School of Medicine
Johnson	Peter	University of Washington
Junglin	Xu	Chiba University
Kato	Kazuhito	NHK Spring Co. Ltd.
Keiichi	Hiroshinge	Kyushu Nutrition Welfare University
Khalil	Hamzah	University of Sheffield
Lawrie	Yvonne	Edinburgh Napier University
Maeda	Setsuo	Nottingham Trent University.
Malloy	Nick	Reactec Ltd.
Mclaughlin	Jacqui	Reactec Ltd.
Oliver	Chris	Edinburgh Napier University
Paddan	Gurmail	Institute of Naval Medicine
Pitts	Paul	UK Health and Safety Executive
Qiu	Yi	University of Southampton
Steel	Chris	UK Health and Safety Executive
Taleshi	Naser	University of Exeter
Tarabini	Marco	Politecnico di Milano
Taylor	Mark	Edinburgh Napier University
Ye	Ying	University of Southampton
Yin	Weitan	University of Southampton
Yoshizawa	Mutsuhiro	Takenaka Corporation
Zhuang	Yi	University of Southampton

6 Information for presenters

Please meet with your session chair immediately after the end of the session before that in which you will be speaking. Provide your presentation as a single PowerPoint file to the organisers (either Mark Taylor or Yvonne Lawrie) during the break prior to your session. The presentation may be quickly tested prior to your session.

Each presentation is allowed 20 minutes. This can be broken down into 15 minutes presentation time and 5 minutes for technical questions and change of presenters. If more in-depth discussion is required we encourage delegates to have a discussion during the breaks. You are expected to finish your presentations before the end of the time allowed. This will allow the audience to ask any questions related to their technical understanding of your presentation. The session chair will gently warn you when you reach the end of your allotted time. Please try to avoid over-running to ensure all speakers get equal time to present.

For the discussion at the end of your session you will be asked to join the other speakers at the front of the room. The chair will then direct the discussion and questions. During the panel discussion, please phrase your answers so that they can be understood by anyone who has not heard the question.

Thank you for your consideration of these guidelines and we look forward to hearing your contribution to the conference.

7   Information for session chairs

Please meet the presenters for your session immediately after the end of the session before the one you are chairing. Introduce presenters briefly stating their name and affiliation. Warn speakers 5 minutes before the end of the time allocated for the presentation: " 5 minutes remaining". If they are still speaking, please warn them again: "2 minutes remaining". If they continue after the allotted time please say: "Please finish as soon as possible".

Presenters are expected to finish their presentation at least 2 minutes before the time allocated in the programme. This will allow the audience to ask any questions related to the understanding of the presentation. If the audience has no questions the chair is encouraged to ask a question. For the panel discussion at the end, all presenters should be invited to come to the front of the room. Please chair the discussion so that it involves the audience and all the presenters. Please bring the session to a close at the time indicated on the programme. Thank you for your contribution to organising and managing the conference.

8   Session 1: Keynote Presentation

Session chair: Mark Taylor

Professor Chris Oliver King James IV Professor Royal College Surgeons of Edinburgh

Professor Oliver has contributed to over 400 publications and presentations on hand fracture management, physical activity, bionic hand technology, medical informatics and has led writing of chapters to a variety of leading postgraduate text books, written many invited articles in both the hand surgery literature and appeared in national media. He has published regularly in peer-reviewed speciality journals and produced educational websites. He has an interest in prediction of longevity and active ageing. Professor Oliver is an Associate Research Fellow in the Edinburgh Napier University Transport Research Institute.

Paul Pitts, Noise and Vibration Principal Scientist, Health and Safety Executive

Paul Pitts has spent 37 years working as a specialist noise and vibration scientist with the Health and Safety Executive. In addition to vibration studies in foundries, ship building, forestry and many other industries, Paul has contributed to the development of HSE guidance on vibration in the workplace and has provided tools for employers on their duties to assess and control vibration risks. Paul was also contributed to the European guidance on implementation of EU Directive 2002/44 on the health and safety requirements regarding the exposure of workers to the risks arising from physical agents (vibration). Paul has represented the UK on European and International Standards committees for many years. He was convenor and project lead of the ISO working group responsible for the 2005 revision of ISO 8041. He was convenor of the European and International standards groups on hand-arm vibration. Paul has recently become the Chair of the International Advisory Committee on Hand-Arm Vibration.

Medical issues surrounding vibration exposure and chronic pain

Prof Christopher W. Oliver
King James IV Professor Royal College Surgeons of Edinburgh
Retired Consultant Trauma Orthopaedic Surgeon, Royal Infirmary Edinburgh
Associate Research Fellow, Transport Research Institute, Edinburgh Napier University
c.oliver@napier.ac.uk   Twitter @CyclingSurgeon

This plenary lecture will outline the authors clinical experience as a consultant trauma orthopaedic surgeon treating patients whom have been exposed to vibration exposure.

The author will relate his experiences with upper limb neuropathies, HAVS, vibration exposure in cyclists and chronic pain.

A full copy of the lecture slides at www.researchgate.net/profile/Chris_Oliver9/research

Vibration risk assessment - evaluation of exposures to vibration, control and measurement strategies

Paul Pitts
Health and Safety Executive,
Harpur Hill, Buxton, SK17 9JN, UK
paul.pitts@hse.gov.uk

ABSTRACT

Long-term exposure to hand-arm vibration from powered machinery is known to present a risk of damage to the hand and arm.

In Great Britain, the actions required of employers controlling vibration exposure and providing health surveillance are defined in Regulations based on European Directive 2002/44/EC. Assessment of hand-arm vibration risk is an important part of the process of controlling risk. However, assessment does not need to be onerous, or complicated; it needs to be suitable and sufficient so that it leads to the appropriate control of exposure.

This paper discusses the requirements for evaluation of risk and how the appropriate level of assessment will produce timely, suitable and effective control actions.

1 ASSESSMENT OF HAND-ARM VIBRATION RISK

1.1 What is a risk assessment?

Health and Safety Executive (HSE) guidance on risk assessment [1] says:
> *"A risk assessment is not about creating huge amounts of paperwork, but rather about identifying sensible measures to control the risks in your workplace."*

and goes on to say:
> *"What you must do is make sure you know about the main risks and the things you need to do to manage them responsibly."*

The purpose of a risk assessment is therefore to identify whether control is required and identify which control measures are appropriate. A key part of the assessment is an exposure evaluation. The format and precision required of that evaluation will depend on where an employer is in the process of determining and controlling risks.

1.2 Initial evaluation of risk

A risk evaluation can be relatively simple; ask some basic questions:
- Do we use hand-held or hand guided power tools, or holding other vibrating surfaces?
- Are they used for a significant amount of time?

We now know who is at risk and an indication of those at greater risk (due to the longer handling times). This is sufficient information to allow us to consider some initial controls.

1.3 Initial Controls

Ideas and advice on controlling risks can come from review work processes with workers, supervisors and other managers, experiences reported by similar industry groups, trade associations and equipment suppliers.

Use the hierarchy of control for considering how to control vibration risks:

ELIMINATION:	Why do we use these machines – can we do the job in a different way to avoid risk?
SUBSTITUTION:	Are these machines the best machines to do the work – can we find suitable lower-vibration machines?
ENGINEERING CONTROL:	Can we modify the work or the task to reduce the risks?
ADMINISTRATION:	Are the machines in good condition, well maintained, using the right accessories? Are the machines being used correctly – do the workers need additional training? Can we limit the time spent using the machines?
PERSONAL PROTECTION:	Are machine operators keeping their hands and body warm and dry?

1.4 Initial assessment review

The initial assessment may identify simple changes that reduce vibration risks. In some cases, these changes may be sufficient such that all the likely vibration risks have been removed or reduced to a point where further control is not necessary.

If there is a remaining risk, this will need to be addressed, and the next stage of risk assessment is likely to require more detailed information and perhaps a numerical evaluation of exposure.

2 EVALUATION OF HAND-ARM VIBRATION EXPOSURE

For workplace risks, EU Directive 2002/44/EC[2] does not require measurement of vibration. It says:

> *"the employer shall assess and, if necessary, measure the levels of mechanical vibration to which workers are exposed"*

and:

> *"The level of exposure to mechanical vibration may be assessed by means of observation of specific working practices and reference to relevant information on the probable magnitude of the vibration corresponding to the equipment or the types of equipment used in the particular conditions of use, including such information provided by the manufacturer of the equipment."*

Information from a variety of (non-measurement) sources, including manufacturer's data, can therefore be used to estimate likely vibration levels in the workplace.

HSE recognises that manufacturer data does not always reflect the vibration experienced during real use[3] and recommends comparing values from multiple sources; in this way vibration values are confirmed by a second source. HSE publishes its own list of likely in-use vibration values[4] to assist this process.

3 MEASUREMENT OF VIBRATION

Where the existing data is insufficient or inconsistent, it may be appropriate to perform measurements. ISO 5349-1[5] defines how vibration exposure should be evaluated. This standard

provides the basis for both the daily exposure action and limit values in regulations[6], and the requirements for declaration of vibration emission values for manufacturers or suppliers of machinery. Guidance on practical measurement is provided in ISO 5349-2[7].

Instrumentation should satisfy the requirements of the appropriate instrumentation standard i.e. ISO 8041-1[8]. This general standard for vibration instrumentation provides a good basis for ensuring the errors of measurement are minimised, and that the instrument is capable handling vibrations from a wide range of rotary and percussive machines.

Since ISO 5349-1 and ISO 5349-2 were published in 2001, there have been substantial changes in measurement instrumentation. It has become more accessible, easier to use, lower cost and smaller in size. However, the challenges of hand-arm vibration measurement in the workplace have not necessarily become easier. It remains important that a measurement is carefully planned, to account for variations of vibration levels which may be introduced by changes in:

- machine and machine operator,
- workpiece and work materials,
- inserted tools (drill bits/ abrasives etc.),
- postures and applied forces,
- fatigue and engagement of the operator,
- environment (e.g. noise, temperature), etc.

Devices are now available that enable a form of personal vibration exposure monitoring which offer new opportunities and challenges. For HSE it is important to understand the strengths and weaknesses of new and novel measurement systems. For users, it is important to understand how such systems can properly contribute to their measurement objectives.

4   MEASUREMENT PLANNING

There is a risk of measurements being made for no clear purpose – it becomes an exercise in collecting data. Measurements should not be made without a clear plan of how to assess and act on the information those measurements provide. Remember, the purpose of risk assessment is to identify those individuals at risk and to consider how those risks might be managed.

The employer should have a clear plan for their measurements. The plan will show how the results will feed into an improved understanding of vibration risks and then into decisions on controlling those risks.

Continual personal exposure monitoring is not required by Regulations in Great Britain[9] (or Directive 2002/44/EC). Monitoring may be useful for a limited period. If monitoring is used, it should be planned, with clear objectives and instructions, for example, specifying the actions expected of individuals using the monitor, particularly when exposure alerts are raised.

5   SUMMARY AND CONCLUSIONS

The risk assessment process is a critical component of the control of vibration risks. Assessment does not need to be onerous, or complicated; it needs to be suitable and sufficient so that it leads to the appropriate control of exposure.

Measurement is not always required for a risk assessment. Sufficient information can be obtained from other sources.

Where measurements are undertaken it is important to understand the limitations of measurement and to have a clear plan for how the results from those measurements will feed in to the risk assessment process.

REFERENCES

[1] Health and Safety Executive "Risk assessment - A brief guide to controlling risks in the workplace" HSE INDG 165 (rev 4) [Online]. Available: http://www.hse.gov.uk/pubns/priced/indg163.pdf. [Accessed 10 April 2019].

[2] European Parliament, Council, DIRECTIVE 2002/44/EC OF THE EUROPEAN PARLIAMENT AND OF THE COUNCIL of 25 June 2002 on the minimum health and safety requirements regarding the exposure of workers to the risks arising from physical agents (vibration), OJ L 177, 6.7.2002, p. 13–20.

[3] Shanks EP, Hewitt SM and Pitts PM, "Investigation of the relationship between vibration emission and in-use vibration for electrical tools," Canadian Acoustics vol. 39, no. 2 , pp. 104-105, 2011.

[4] HSE "Sources of vibration magnitude data" http://www.hse.gov.uk/vibration/hav/source-vibration-magnitude-app3.pdf Page visited: 10 April 2019

[5] International Organization for Standardization, ISO 5349-1:2001 Mechanical Vibration and Shock – Evaluation of human exposure to hand-transmitted vibration – Part 1 General requirements, ISO, 2001.

[6] HSE, "Hand-arm vibration The Control of Vibration at Work Regulations 2005 Guidance on Regulations (L140) (ISBN 978 0 7176 65655)," Second Edition 2018. [Online]. Available: http://www.hse.gov.uk/pubns/books/l140.htm. [Accessed 30 July 2019].

[7] International Organization for Standardization, ISO 5349-2:2001 Mechanical vibration – Measurement and evaluation of human exposure to hand-transmitted vibration – Part 2: Practical guidance for measurement at the workplace, ISO, 2001.

[8] International Organization for Standardization, ISO 8041-1:2017 Human response to vibration – Measuring Instrumentation – Part 1: General purpose vibration meters, ISO, 2017.

[9] HSE "Vibration exposure monitoring Q&A" http://www.hse.gov.uk/vibration/hav/advicetoemployers/vibration-exposure-monitoring-qa.pdf , Page visited: 10 April 2019

9   Session 2: HAV 1

Session chair: Paul Pitts

Encouraging the control of Vibration – HSE update

Chris Steel[1] & Emma Shanks[1]
Field Operations Division & Science Division
Health & Safety Executive
Edinburgh EH4 3UE
UK
Chris.steel@hse.gov.uk

ABSTRACT

This paper presents examples of good practice that have been developed by duty holders and the Health and Safety Executive (HSE) to focus on the control and reduction of hand-arm vibration in the workplace. The HSE has been encouraging trade associations, professional bodies and companies to develop their own sector specific information on practical means to reduce the use of vibrating power tools. In most instances this work has been developed in partnership with the HSE and looks at developing management and design awareness of hand-arm vibration to push the control of vibration up the management structure. The paper presents a selection of practical improvements that have been introduced across a range of key industries where hand-arm vibration syndrome is a known risk and reviews what this means for the HSE's enforcement procedures.

1   INTRODUCTION

HSE's overall aims

Part of the HSE mission is to prevent ill-health in Great Britain's work-places (HSE 2009). To comply with the Vibration Regulations, employers need to assess the risks from vibration and plan how to control the risks (HMSO, 2005). In 2016 Hand-Arm Vibration Syndrome (HAVS) accounted for 46% of all ill-health RIDDOR reports made to the HSE (Hounslea, 2017) which suggests an ongoing risk associated with the use of powered hand tools. The focus for HSE inspectors is to ensure dutyholders understand the level of risk and exposure to their employees and to then encourage a focus on the control of vibration and any residual risk.

In an effort to encourage employers to focus their activities on control measures the HSE noise and vibration specialist inspectors and scientists have been actively encouraging trade associations and professional bodies to provide guidance to their members on reasonably practicable control of hand-arm vibration. In addition, engagement with these associations has also allowed the HSE to develop new case studies or to review existing control methods. This paper sets out a selection of the guidance that has been published and is yet to be published (as of May 2019) and will serve as a consolidation of current good practice on the control of hand-arm vibration primarily across the construction sector.

With around 75% of all Health related RIDDORS in the Construction industry being related to hand-arm vibration (Hounslea 2017) it was considered appropriate to focus activities within the construction sector. The first two key strands of control that were considered were:

1) the design aspect of construction work which may allow for the removal or reduction of hand-held power tool usage and

2) the demolition activities, particularly those associated with the removal of concrete and masonry where impulsive power tools are commonly used.

Steel fabrication was highlighted by the Noise and Vibration team as another area where RIDDOR reporting of HAVS was prevalent from the manufacturing industry. Inspections highlighted the use of hand-held grinders in the fabrication of structural as an area where improvement could be achieved. The nature of the structural steel industry also made it a suitable as it is common for employees in this sector to split their time between a factory/workshop setting and a construction setting as they fabricate then install their products. Structural steel production provides the third strand of control to feed into the construction sector.

1.2 Background to the requirement for Control

General procedures for the control of vibration exposure are detailed under Regulation 6(3) which are (HMSO, 2005):
A. Other working methods which eliminate or reduce exposure to vibration;
B. Choice of work equipment of appropriate ergonomic design which, taking account of the work to be done, produces the least possible vibration;
C. The provision of auxiliary equipment which reduces the risk of injuries caused by vibration;
D. Appropriate maintenance programmes for work equipment, the workplace and workplace systems;
E. The design and layout of workplaces, work stations and rest facilities;
F. Suitable and sufficient information and training for employees, such that work equipment may be used correctly and safely, in order to minimise their exposure to vibration;
G. Limitation of the duration and magnitude of exposure to vibration;
H. Appropriate work schedules with adequate rest periods; and the provision of clothing to protect employees from cold and damp.

These regulations follow the general principles of prevention set out in Schedule 1 of the Management of Health and Safety at Work Regulations 1999 (HMSO, 1990) and the hierarchy of controls, i.e.: elimination, substitution, engineering controls, administrative controls and personal protective equipment (PPE). These principles are hierarchical, with a priority on collective control over individual control. Actions such as limiting the duration of exposure, the provision of PPE (such as in the form of clothing etc) and work scheduling are placed below actions such as eliminating tool use, substituting for other lower vibration tools or looking for adaptions to existing tools to limit their vibration magnitudes.

1.3 What success would look like

Success would be measures based on the level of response from each industrial sector and we would look for actual documented commitment from the trade associations or the production of cases studies that the HSE can use to disseminate the message on control.

The second measurement for successes would be to produce information that can be adopted by the general HSE inspection teams for use in the field. This led to the development of internal links with the Noise and Vibration team within the HSE and the Construction Health Sector team.

2 STRAND 1 - DESIGN

2.1 Background

HSE's Construction Sector Health team have focused on the development of easily identifiable matters of evident concern that they can be provided to the construction inspection teams. Information had been developed for the control of dusts but there remained a requirement for updated information on the control of noise and hand-arm vibration. An initial discussion paper was produced within the HSE for dissemination to the Construction Health Sector team who would then take this information for comment and agreement with their local industry liaison groups.

The document 'Safety in Design, noise and vibration' provided examples of how architectural design choices could be altered in order to reduce the need for vibrating hand held power tools on site and aimed to demonstrate in the following key areas:
- How architectural preference can impact on control of hand-arm vibration,
- How tendering and costing procedures can be used to inform the risk assessment process for hand-arm vibration,
- How investigation and management of utilities repair can reduce exposure to hand-arm vibration,
- How standard planning information can be used to inform workplace noise control,
- How good practice in material specification can reduce exposure to hand-arm vibration,
- How good practice in detailed design can reduce exposure to hand-arm vibration,
- How modern methods of construction and lead to better control of hand-arm vibration on site and in the factory.

The document was reviewed by industry partners and identified a set of key control methods which were seen as reasonably practicable case studies.

2.2 Case studies

2.2.1 The construction of non-standard rooms where timber strapping is selected

The design of rooms with vaulted ceilings and curved walls can require significant lining out using timber straps to achieve the desired shape. Where the base construction is concrete there is a lot of drilling producing noise, HAV and dust exposure.

Options to reduce exposure would be:
a. Can the same look be achieved with alternative construction methods, e.g. pre-formed curved concrete, prefabricated timber products such as Cross Laminated timber (CLT), cast in situ concrete which closer follows the final required shape or moderns plastic based stretch ceiling systems.
b. Alternative fixing systems – The adoption of a metal stud framework or metal lining systems would have needed fewer fixing points into the concrete (metal lining systems and suspended ceiling grids can often have fixing points which are as far apart as 1200 mm). In addition, free standing metal stud work is often slimmer in profile than timber stud work to achieve the same heights and so could be accommodated where dimensions are tighter.
c. Better design of preferred fixing systems – Timber strapping is generally required to be fixed at closer centres than metal frame systems of the same thickness. The use of thicker timber battens/straps and even free-standing timber studwork could have been considered if room dimensions had allowed. This would have reduced or eliminated a significant number of the required drilled fixing points. Allowing for a marginally larger room footprint

(around 40 to 50mm at the perimeter) would have provided the extra space need to accommodate these adjustments to the system.

2.2.2 The use of tendering and pricing processes to estimate and control hand-arm vibration exposure

Clients can instruct tendering contractors that packages will be awarded on the basis of both cost control and quality. Splits of 60% cost and 40% quality are common. Contractors can be encouraged or expected to include assessment of health and safety issues as part of the overall job quality. Completion of work packages and contracts can also include payment and bonus structures that allow for demonstrable controls of health and safety, e.g. bonus payment for no work place injuries occurring during a project. Proving bonus payments for the control of health risks is likely to be more difficult as these may not present themselves until well after a contract is concluded. This does not mean that the control of health issues cannot be accounted for when considering the quality of a tender.

A client requests a quotation for the removal of damp and bossed plasterwork within a number of housing association dwellings. This activity requires the use of noise and vibration emitting tools and also carries a significant risk to dust control. The wining contractor operates the following control system:

a. From previous assessments of this type of work they have established accurate estimations of tool usage per square meter to clear plaster. Therefore, they can estimate the likely hand-arm vibration and noise exposure levels for any single employee based on the number of square meters of work they can complete in any given day.
b. The contractor's surveyor measures up the total area of plaster work to be removed including information on whether plaster is "to the hard" or on timber straps (the contractor has different noise and vibration exposure data for each type).
c. The contractor has a simple pricing Excel spreadsheet set up to allow for costing of time, labour and materials. In addition, the Excel spreadsheet includes a calculation which takes the number of man hours to complete the job and determines how many employees would be need on site in order to limit total exposure to vibration to any single employee. Pricing for the project is therefore intrinsically linked to the control of vibration and noise as the number of workers needed is a function of controlling exposure.
d. During the project the level of exposure to any individual employee can be cross referenced with their normal weekly output records (as employees are paid based on productivity). Where employees are found to have accrued significant levels of overtime, their work activities can be rotated or adjusted in order to limit their exposure (e.g. they are moved from removal work to re-instatement or clearing work). The system means that workers are not required to self-record exposure which has inherent difficulties.

Client Awareness
a. The contractor is able to show at tender stage the expected noise and vibration exposure levels to the client and so fulfils part of the quality expectation of the tender process.
b. The provision of this information also allowed the client to more accurately interrogate other quotations where lower project fees indicated that cost cutting was at the expense of worker safety.

2.2.3. Management of utilities repairs to allow for better control of road working activities that may expose employees to hand-arm vibration

The repair of underground electrical cables usually requires the need to dig up road surfaces and the nature of the work means that it is often responsive rather than planned. This creates a conflict

between the need to re-connect the electrical supply as quickly as possible and the need to control workers exposure to HAV. A system has been adopted to help better schedule work and reduce risk of Noise, HAV and possibly dust exposure:

a. The use of single shot auto-re-closer fuse in the sub-station network means that electrical supplies can be maintained while persistent faults are investigated. This is because an auxiliary fuse is automatically brought into use when a fault trips the primary fuse. An automated message is issued to the repair team and the auxiliary fuse allows them to take more time scheduling and programming work as the electrical supply is not interrupted. This means that repair work can be more easily scheduled rather than having to be unplanned and reactive.
b. Using portable electrical generators and daisy chaining, where necessary, to ensure electrical supplies are maintained during repair also allows more time to schedule and organise work as it removes the pressure placed on utility suppliers to re-establish as quickly as possible the power supply to their customers.
c. The use of cable sniffers allows for sample holes to be drilled in order to pin-point the location of a fault and reduce the need to break out significant areas of road surface.

By adopting these procedures work can be more easily managed by the utility provider with the core benefit of reduce the duration of any electrical supply down time.

2.2.4 Controlling exposure to hand-arm vibration through specification where alternative materials and products can provide similar performance

Selecting products and materials that are produced in large quantities under automated factory conditions or which use more common manufacturing methods can reduce exposure to risk for both workers on the construction site as well as for workers further up in the supply chain. Similarly, the use of alternative materials, which have the potential to provide the same performance, should be considered if they reduce exposure to noise, vibration and dust. Examples of good practice were;

a. The use of standard coloured timber door blanks as suspended baffles allowed for the architectural quality of a school to be enhanced without the need for the manufacture of a significant number of bespoke panels. The initial option for bespoke panels was likely to lead to more working on site (there was initial discussion about part manufacturing the baffles on site from base materials). By using mass produced door blanks this risk was eliminated and a significant cost saving was made to the project.
b. The manufacture of bespoke architectural concrete block and artificial stone is likely to require factory and manufacturing processes which result in factory workers being exposed to higher levels of hand-arm vibration and noise. It is likely to be beneficial to discuss alternative options which achieve the same or similar finishes without the need for entirely or partially bespoke product. Selecting coloured concrete architectural blocks and mouldings for external feature finishes often required the use of hand rammers in the production process to ensure that the colour of the product is even and consistent. Consideration of natural concrete colours rather than bespoke colours can provide the manufacture with the opportunity of supply products which use self-compacting concrete and thereby avoiding the exposure of their workforce to noise and vibration.
c. Plastic kerbs reduce handling and lifting issues as well as reducing exposure to workplace noise, dust and hand-arm vibration as they can be cut with a hand saw. These could be considered on projects where the performance of these kerbs meets the required performance specification.

d. Where appropriate, aerated concrete or lightweight thermal block for internal building skins can be used to reduce the need for cutting with power tools or percussive tools. These materials can be cut with handsaws, so reducing exposure to workplace noise, hand-arm vibration and even dust. Their lighter weights also reducing manual handling risks.

e. Slotted block work for large sports halls allows for a finished treatment surface that can deal with architectural acoustic issues (i.e. highly reverberant rooms) while negating the need to install wall mounted acoustic baffles. The fitting of wall linings requires exposure to workplace noise, hand-arm vibration and involves working at height.

f. Core cutting of concrete floors and walls was identified as a potential workplace noise, dust and hand-arm vibration risk and so alternative means of construction were considered. This highlighted the possibility of using pre-formed 'top hats' or sleeves which could be placed in position on permanent and temporary form work prior to any concrete pour. As a result, no core cutting would be required and the noise, vibration and dust risk would be minimised or eliminated.

3 STRAND 2 – DEMOLITION

3.1 Background

An approach was made to the Drilling and Sawing Association (DSA) to request that they consider the development of a guidance document for their members, and the wider construction industry, to detail good practice with regards to the removal of concrete. The focus of the information was to look at reducing noise, dust and hand-arm vibration. The document, to be held by the DSA, is in the late staged of publication with the following examples of good practice have been identified.

3.2 Removal of Concrete floor slabs

The removal of large areas of concrete slab using only hand-held breakers or demolition hammers is unacceptable where it is likely to take longer than 15 minutes (tool trigger time). In many instances the use of floor saws, wire cutting systems, robotic peckers and core cutters can be used to achieve the same results. These methods are often faster, more efficient and likely to reduce, noise, vibration, dust and MSD issues. There are several alternative processes available. One of the following should be adopted on site.

A) Bursting Method - The use floor cutting saws or rail mounted saws to define the work area to be removed. Followed by core cutting to allow for hydraulic bursting tools to be used. For larger areas the burst concrete can then be broken up and removed using a digger arm with a bucket attachment.

B) Cut and lift method – Diamond core cutters are used to create lifting points and to allow starting points for the use of floor saws, rail mounted saws or wire saw cutters. Cut sections are then lifted out of position and removed for disposal.

3.3 Reduction of existing concrete slab depth to create a pit or trench

It is often necessary to reduce the height or level of a concrete floor to allow for the insertion of heavy machinery, remove concrete screeds/toppings or simply to increase floor to ceiling heights in existing buildings. Similarly, it is often necessary to break out section of concrete walls to slap out doors or create openings. The use of hand-held breakers or demolition hammers as the sole means of removal of concrete for this type of task is unacceptable. The following methodology is expected.

Scoring of cutting area using either a rail mounted diamond saw or hand held or trolley mounted power cutter (e.g. cross cut saw). Cuts should be deeper than required depth. This creates concrete strips that can then be broken off using manual tools (e.g. pry bar) or a hand-held breaker. As concrete

stirps are easier to remove than breaking out across an area the overall level of vibration exposure is reduced

The traditional method would be to form the void using demolition hammers and impulsive drills. The use of a cutting system could be adopted which is similar in nature to the process describe for the removal of concrete at floor level. A circular cutting disc is used to create break out sections which can be removed using a hand tool. This methodology would be a credible means of removal for walls with a depth of up to 400 mm and should produce lower levels of hand-arm vibration than would be expected from the use of traditional impulsive power tools. Caveat – Removal of concrete using only hand-held breaker or demolition hammer is only acceptable were the duration of trigger time on the tool does not exceed 15 minutes or where the volume of concrete to be removed does not exceed 45 litres in any single working day.

3.4 Core cutting – adopting engineering controls

Coring through concrete slab and concrete/masonry walls is a typical construction task undertaken on both refurbishment and new build constructions. The cutting of more than 15 holes by any single operator in a typical working day is likely to exceed the exposure action value. In such instance's duty holders are expected to consider the use of a coring rig.

Coring rigs improve the quality of a core cut and reduce exposure to hand-arm vibration and MSD risks as there is no need to support the tool or maintain physical contact with the tool motor. Some coring rigs are also fitted with automatic feeds further reducing the need to physically interact with the tool when in use.

3.5 Plinth Removal – Adopting Engineering Controls

The removal of concrete plinths solely with hand held breakers or demolition hammers is likely to be an unacceptable working practice where tool use durations exceed 30 minutes (tool trigger time). Bursting concrete would be acceptable as would the use of chemical bursting agents. Horizontal coring rigs can also be used for the removal of concrete plinths or pads, particularly where it is necessary to limit disturbance to existing structures of machinery. With the use of temporary supports, it can be possible to remove concrete with minimal disturbance and with limitations of exposure to hand-arm vibration, dust and safety hazards. Caveat – The use of hand held breakers or demolition hammers to remove small areas of concrete where the tool use duration can be limited to less than 30 minutes is acceptable as is the use of hand held breakers and demolition hammers where access is severely restricted or where they are required for dressing or minor finishing work.

4 STRAND 3 – STRUCTURAL STEEL SUPPLY

4.1 Background

An approach was made to the British Constructional Steel Association (BCSA) to request that they consider the development of a guidance document for their members, and where possible, the wider fabrication industry. The BCSA were already in the process of addressing this issue and so had developed a range of activities which focused on the reduction of hand-held grinder use. This was already identified as a health and safety concern for the BCSA. As with the DSA document the BCSA document is in the last stages of publication and contains practical advice on control. The following details some of the reasonably practicable methods that have been identified by the BCSA and the HSE.

4.2 Pre-Blasting structural steel for preparation

The blasting of steelwork before it is taken into the preparation area will reduce the need to remove the surface scale and rust for marking off. This significantly reduces the use of grinders and improves the safety of operators as the scale can react violently to heat sources and causes skin burns or serious eye injuries.

Pre-blasting the steel prior to preparation and fabrication work will also improve the general workplace environment and housekeeping as the amount of dust and debris in the workplace is significantly reduced. blasting can be a significant source of noise and so adequate hearing protection should be supplied to and used by those undertaking the task. Where pre-blasting of the steelwork is not an option, the mill scale that needs to be removed can be carried out by using a pre-heat torch that caused the scale to expand and break free, personal protective equipment will be required to be worn to protect against the hot scale.

4.3 Quality Assurance Procedures in Weld Preparation

The unnecessary grinding of all free edges and joints prior to welding should be challenged. There is often a statement in the welding procedure that says all cut edges must be ground before welding. This is only required if the hardness of the cut edge exceeds 450 HV10 but rather than test the edge hardness produced by the cutting process the management solution is made easy if the instruction is given to grind the edges whether or not they need to be dressed this way?

Testing carried out by BCSA Members shows that the edge hardness of 450 HV10 is not exceeded by thermal cutting and therefore grinding should only take place on free edges where corrosion protection calls for ISO 8501-3 grade P3 where edges must be ground to a 2mm radius before coating, in such cases the clients specification has precedence over EN 1090-2.

4.4 Disproportionate Specifications

Some Architects, Designers or Engineers may specify that welds or edges of steel are dressed by grinding, if this is for a genuine technical reason then this will be required, however some Architects, Designers or Engineers will specify that such dressing takes place purely for appearance (aesthetics), where this occurs they should be challenged to justify why this is required when the principles of ERIC (Eliminate, Reduce, Inform & Control) from the CDM Regulations 2015 should be employed.

The CDM Regulations 2015 require that Designers when considering health and safety risks are expected to do what is reasonable at the time that the design is prepared to take into account current industry knowledge and practice. Therefore, the elimination of the use of tools that create the risks can be driven by the Designer when and where the aesthetics are the only reason for specifying excessive use of dressing/grinding tools, especially when the final location of the component will not be readily visible.

4.5 Use of Appropriate Tools

Quite often the grinder is too readily available for operators to pick up and dress or clean steel. Proprietary tools are available for removing debris from flame cutting such as steel scrapers and deburring tools for cleaning dross from drilled holes.

a. Bevelling Tools: A variety of hand held mechanical milling machines are available that can put the smaller weld preparation on the edge of steel, or for the removal of the sharp edge to produce the chamfer required to enable the coatings specification to be met.
b. Deburring Tools: Drilled holes can be de-burred by the use of countersink drill bits used with hand held electric (or rechargeable) tools, this will not eliminate the use of vibratory tools but it will assist in the reduction of the use of the tools that are of a higher risk.

5   DISCUSSION & CONCLUSIONS

4.1 General Comments

Most of the control methods outlined in this paper are neither particularly new nor are they particularly difficult. In many instances they represent methodologies which will improve the construction and/or manufacturing processes where they are used. The advancement in the control of hand-arm vibration is the development of agreements across a range of professional agencies on what good enough looks like. Previously we have seen the potential for discrepancies across activities which can lead to variations in the HSE enforcement expectations. By gaining agreement from the industry partners this achieves three key improvements.

1 – There is a clearer level of understanding on what reasonably practicable control looks like in terms of real world examples for anyone involved in these industries to see.

2 – Employers not adopting these processes and methods become more obvious to the industry as poor performers.

3 – There are clearer lines of enquiry and enforcement for our inspectors.

The HSE's general approach of goal setting with regards to achieving health and safety standards remains intact as we are allowing, under guidance of the HSE, employers and their representatives to detail what they believe good practice looks like. In many instances the conversations with the professional bodies took the form of the HSE Inspectors asking why some processes were not more common place and being told by the professional bodies that they were just as frustrated by this fact.

The underlying requirement of the Government to avoid a creeping increase in regulatory burdens on industry is also achieve due to the agreed nature of the control methods and the publication of them in industry held guidance. For most industries, while there is a desire to work free of unnecessary red tape there is often an equally strong desire to define what are 'professional practices', partly to ensure the perception of an industry sector as competent and partly to protect the professional standing of those involved in that industry sector.

The documentation referenced within this paper has generally yet to be published by the relevant industry group but there are expected to be released within the next six to twelve months. The control measures detailed within this document would then be fed to our general Health and Safety Inspectors and as part of any ongoing priority inspection programmes with a particular focus on construction. It is expected that this may not occur until there has been a bedding in time for these documents so that they become established as current good practice. The HSE Noise and Vibration team intend to reference this work in any industry engagement work that they undertake. After this bedding in period it is anticipated that a review of working practices would take place during our typical inspection cycles to review how widely the controls are being adopted and it is likely that enforcement will result for any organisations found to be lacking.

4.2 Conclusions

The process of approaching industry bodies and asking them to get involved in developing control guidance for hand-arm vibration exposure has been encouraging. All of the trade associations approached readily supplied time and resources to complete the task.

There was a concern within the HSE that the proposed guidance we received would be of a poor quality but we generally found that the industry partners were prepared to adopted what may have

once been seen as specialist work as general good practice, in some instanced, beyond what the HSE would expect. This highlighted the possibility that industry improvement which naturally occurs provides an opportunity to move the control standards for health and safety forward.

The process allows for clear lines on what good looks like without increasing the regulatory burden and without shifting the focus on control away from that of goal setting. Employers are still free to use any reasonably effective alternative means. The documentation that is expected to be produced should make it simpler for both employers and regulators to identify good practice.

REFERENCES

1. HMSO, L140, Controlling Vibration at Work, The Control of Vibration at Work Regulations 2005, Guidance on Regulations, HMSO; Norwich 2005.
2. A. Hounslea, HSE Internal assessment, Memo issued by HM Specialist Inspector, 2017
3. HMSO, Statutory Instrument, Health and Safety, The Control of Vibration at Work Regulations 2005, HMSO, London
4. HMSO. Statutory Instrument. 1999 No.3241 Health & Safety. The Management of Health and Safety at Work Regulations 1990, HMSO. London.
5. HMSO. Statutory Instrument, Health and Safety at Work etc. Act 1974, HMSO, London

An Exploratory Study Comparing Three Rivet Guns and the Hand Arm Vibration Exposures Transmitted Through the Upper Extremities

Peter W. Johnson [1,3], Per Reinhall [2], Wadih Zaklit [2,3,4], Livia Anderson [2,3],
Szymon Sarnowicz [2,3], Cassidy Quigley [2,3], Richard Gardner [3,4], Riley HansonSmith [3,4],
Hyoung Frank Ryou [1]
[1] Department of Environmental and Occupational Health Sciences,
University of Washington, Seattle, WA, USA
[2] Department of Mechanical Engineering, University of Washington, Seattle, WA, USA
[3] Boeing Advanced Research Center, University of Washington, Seattle, WA, USA
[4] The Boeing Company, Everett, WA, USA

ABSTRACT

This pilot study was conducted to evaluate the vibration exposures associated with three different rivet guns. Two experienced mechanics each used the three different rivet guns and simulated riveting against a load cell. Tri-axial vibration was measured from the barrel and handle of the rivet gun; small, battery-powered, self-contained Inertial Measurement Units (IMUs) measured the surface vibrations transmitted through the tool operators' hands, forearms and upper arms; and a wearable wrist watch device measured vibration exposures at the right wrist. The measurements indicated that the barrels of the rivet guns had two-fold higher vibration exposures than the tool handles. In contrast, the vibration magnitudes measured from right and left arms did not match the tool-based measurement trends. The percentages of the tool-born exposures transmitted through the right arm were generally two-fold higher than the left arm. Finally, the wrist watch device appeared to accurately estimate the magnitude of the tool-born exposures measured at the right hand.

1   INTRODUCTION

Employees in the manufacturing sector, including those in the aerospace industry, can be exposed to high levels of vibration, contact stress, and repetitive motion. Mechanics that use rivet guns and bucking bars can be exposed to tool-induced hand-arm vibration (HAV). Over time, some mechanics may experience shoulder pain, musculoskeletal problems, and/or develop Raynaud's syndrome or vibration induced white finger.

Workers engaged in percussive riveting operations tend to experience more musculoskeletal disorders than those of vascular nature. High-frequency vibration is thought to be responsible for damage to the soft structures of the fingers and hands, while low-frequency vibration with high amplitude (percussive tools) is thought to be more strongly associated with injuries to the wrist, elbow and shoulder (Griffen, 1990).

In a recent systematic review and meta-analysis of the literature, Nilsson et al. (2016) demonstrated that workers who are exposed to HAV are 4-5 times more likely to develop vascular and neurological diseases. Unlike vascular and sensorineural disorders, demonstrating the association between HAV and musculoskeletal disorders (MSDs) is more difficult since vibration and impact forces occur concurrently. However, a recent study demonstrated that occupational exposures to whole-body or hand–arm vibration were associated with MSDs of the shoulder and neck (Charles et al., 2018). In addition, a study by Kihlberg and Hagberg (1997) compared workers using impact and non-

impact hand-held power tools, and their analysis demonstrated that workers using low frequency impact tools reported more symptoms in the elbows and shoulders while those working with the high frequency power tools reported more wrist symptoms.

The objective of this study was to instrument three different rivet guns to measure and compare the vibrations transmitted to the left and right hands of the tool operator using methods outlined in the ISO 5349-1 standard. Further, an exploratory portion of the study consisted of using self-contained inertial measurement units to measure vibration transmitted through the tool operators' left and right hands, forearms and upper arms. The goal was to determine whether there were differences in vibration exposures across the three riveting guns, whether there were differences in tool-transmitted vibration to the operators' left and right hands, and whether there were differences in the vibration transmitted through the operators' upper extremities. In addition, a wearable wrist watch device worn on the right wrist was evaluated for estimating the ISO 5349-1 measured vibration exposure occurring at the tool handle.

2   METHODS

2.1   Subjects and Tools

In this pilot test, two experienced aerospace mechanics participated as subjects. The experimental procedures were approved by the University of Washington Human Subjects Review Board and subjects gave their informed consent to participate in the experiments.

The two mechanics used three different rivet guns in the experiment. The rivet guns differed slightly in mass and percussive power. All three rivet guns were recoilless models made by Atlas Copco (Stockholm, Sweden). The first rivet gun (R1), model RRH10P-TS, had the lowest power and is typically used for medium duty riveting tasks. The second gun (R2), modelRRH12P-TS, was an intermediate power gun typically used for heavier duty riveting tasks. Finally, the third gun (R3), model RRH14P-TS, had the most power for more extreme riveting tasks. Key specifications of the rivet guns are provided in Table 1.

Table 1. Key specification for each rivet gun. DEV is the tool manufacturer's Declared Emission Value and K is the tool-based measurement uncertainty factor.

Specification	R1	R2	R3
Stroke	118 mm	153 mm	188 mm
Energy/Blow	13.0 J	16.0 J	19.5 J
Blows/Sec	25 Hz	20 Hz	18 Hz
Weight	2.0 kg	2.1 kg	2.2 Kg
DEV	5.1 m/s²	4.4 m/s²	5.4 m/s²
K	1.7 m/s²	1.1 m/s²	2.9 m/s²

2.2   Experimental Protocol

The experimental task consisted of having the experienced mechanics simulate riveting with each of the three rivet guns by applying force against a 225 kg capacity load cell (Model WMC-500; MFg; City, State). Force measurements were recorded from the load cell at 20 KHz. In addition, a ±5000 g, 2 - 4000 Hz, triaxial accelerometer (Model SEN040, Larson Davis; Depew, NY) was mounted to the rivet gun and collected the vibration data at 20 KHz. The task consisted of sets of ten simulated riveting trials each lasting 1 second. For the first set of the ten rivets the tri-axial accelerometer was secured to the barrel of the rivet gun where the left hand contacted the tool. For the second set, the tri-axial accelerometer was secured to the handle of the rivet gun where the right hand gripped the handle. For logistical reasons and time constraints, the order of the tools and barrel and handle measurements were not randomized.

In addition, the exploratory part of this study was to measure vibrations transmitted through the operators' right and left arms using 3.4 x 2.2 x 0.9 cm tri-axial inertial measurement units (IMUs)

mounted to the back of the hands, middle of the forearms over the ulna, and middle of the lateral aspect of the upper arm using an aggressive double-sided medical tape. The battery-powered IMUs (Model AX-3; Axivity Ltd; Newcastle upon Tyne, UK), had 512 Mb of internal memory, a ±16 g's measurement range, a bandwidth of 0 – 1000 Hz and collected the vibration data at 3200 Hz. Finally, a wrist-worn accelerometer device (HAVWear; Reactec; Edinburgh, UK) was secured to the right wrist of the subjects. This wrist-mounted device, through the use of a transfer function, was designed to capture and estimate the average tool-born exposures for the right hand.

2.3   Data Processing and Analysis

With the exception of the HAVWear device, which had its own ISO 5349-1 transfer function, all the acceleration data were analyzed employing the Wh filter as outlined in the ISO 5349-1 standard (ISO 5349-1, 2001). For the subject, the vibration exposures from the ten one second riveting sets from the barrel and handle of the rivet gun were analyzed separately. The same methods were used to calculate the exposures in the left and right hands, forearms and arms using the IMUs. The HAVWear device, using its proprietary transfer function, calculated the vibration exposure based on the vibration data collected between the start and end of the ten riveting sets. The operators would scan an RFID label on each tool with the HAVWear device to indicate the beginning and end of a riveting set, with vibration exposures for each set labeled and stored in the device's memory.

The tri-axial accelerometer and IMU data were based on the 10 simulated individual riveting episodes with the median and interquartile ranges calculated for each subject. Due to the way it collected and stored data, the HAVWear device was only capable of providing subject averages for each of the 10 riveting episodes per set (barrel and handle). With all devices, the tool averages were based on the mean of the two subjects. Due to the small sample size, no inferential statistical analyses were performed, and general trends were compared between upper extremities and tools.

3   RESULTS

The top graph in Figure 1 depicts a summary of the vibration magnitudes measured on the barrel and handle of the tested rivet guns. The result demonstrated that there were differences in the vibration magnitudes measured across all three rivet guns. The vibration measurements at both the barrel and handle exhibited a trend with rivet gun R1 having the highest magnitude, R2 had intermediate levels, and R3 had the lowest magnitude of vibration. The vibration magnitudes measured at the barrel were about 2-fold higher compared to the vibration magnitudes measured at the handle. The top graph of Figure 1 also shows that there was relatively good correspondence between the vibration magnitudes measured at the three rivet gun handles (orange bars) and the tool-measured vibration magnitudes estimated by the wrist-mounted HAVWear devices (blue bars).

Figure 2 shows the vibration magnitudes measured at three different upper extremity locations: the hands, forearms and upper arms, respectively. The trends of the differences in the vibration magnitudes measured between the barrel (left hand) and handle (right hand) and across the three tools did not correspond with the IMU vibrations measured from the back of the hands, and middle of the forearms and upper arms.

In order to understand how much of the tool-born vibrations were transmitted through the chain of the upper extremities, the vibration magnitudes measured at each proximal location in the left and right upper extremities were expressed as percentage of the vibration measured at the barrel and handle of the tool. The transmissibility results, shown as percentages in Figure 1, indicated that the percentage of vibrations transmitted through the right arm were at least double the amount transmitted through the left. In addition, the percentage of the vibration transmitted through the arms increased across the three guns (R1-R2-R3).
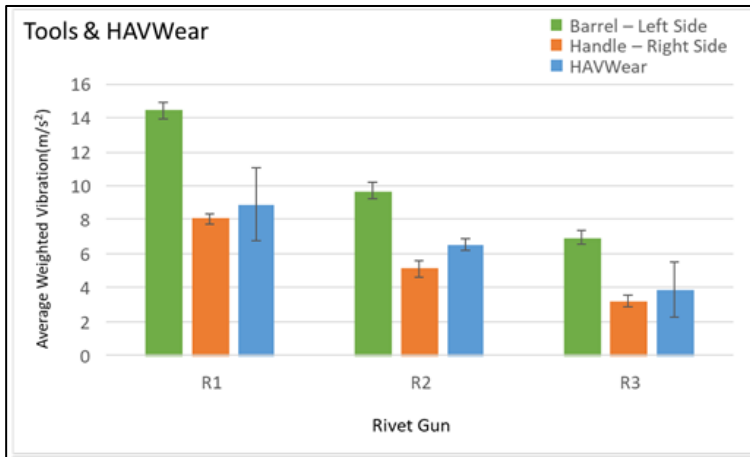
Figure 1. Mean (standard error) vector sum tool accelerations by rivet gun measured at the barrel (green, held by the left hand) and handle (orange, held by the right hand) and the HAVWear vibration exposure estimates (blue, from the right wrist).
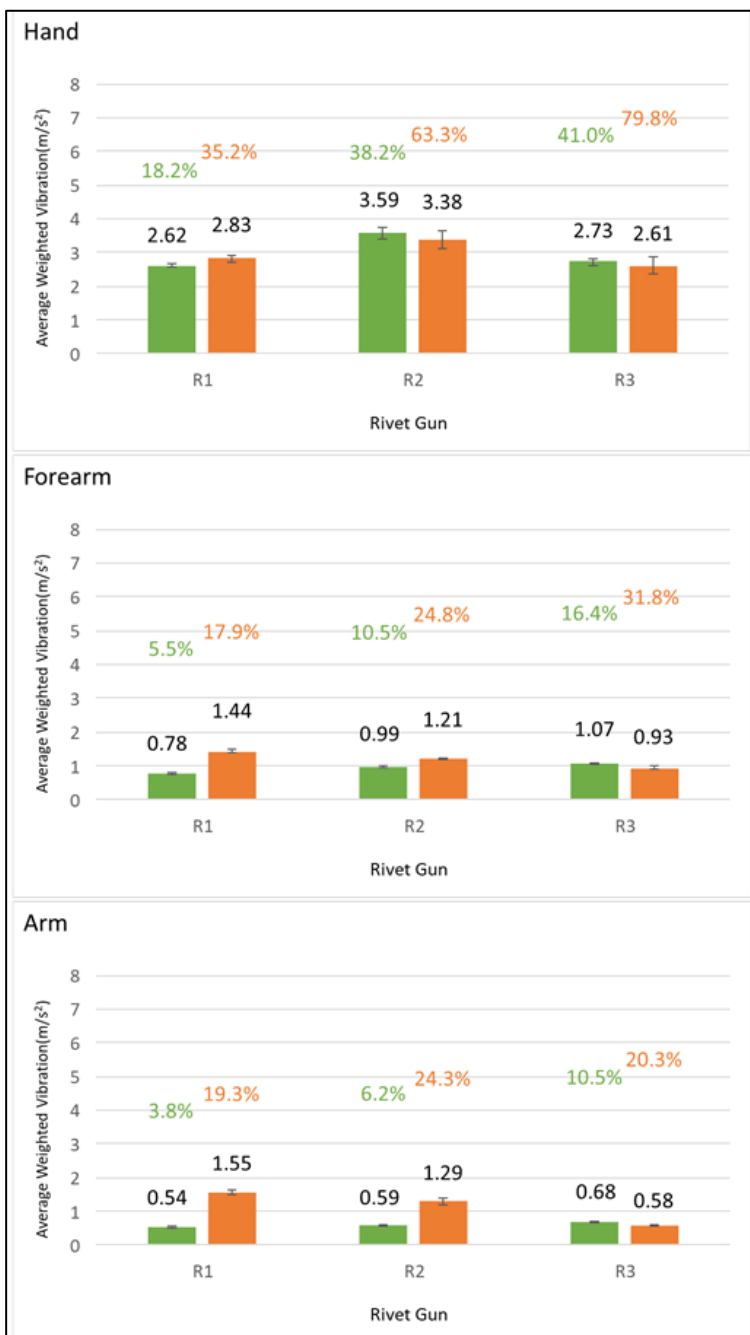

Figure 2. Mean (standard error) IMU vibration measurements from the back of the hands (top graph), forearms (middle graph) and upper arms (bottom graph) of the left (green) and right (orange) upper extremities. The green and orange values represent the percentage of the barrel (left side) and handle (right side) measured vibration transmitted through the upper extremities. (Note: the difference in scale of this graph relative to first graph).

4 DISCUSSION

The results indicated that there were consistent differences in the magnitude of the vibration transferred from the tool to the left and right hands. With all tools, the barrel transmitted vibrations to the left hand were almost twice the magnitude of the vibration transmitted through the handle to the right hand. However, the vibration magnitude differences measured at the barrel (left) and handle (right) of the tool and across tools were not seen in the IMU vibration measurements from the upper extremities.

There was more consistency in the transmissibility results measured between the left and right extremities and across the three tools. In general, the transmissibility measured from the right arm were at least two-fold of those measured in the left arm. These transmissibility deltas may be due differences in stiffness between the left and right arms. With the right arm gripping the tool handle and responsible for the riveting force, it seems plausible for the right arm to have greater stiffnesses than the left arm, and as a result, greater potential to transmit vibration. The respective operating frequencies of rivet guns R1, R2 and R3 were 25, 20 and 18 Hz, respectively. As the operating frequency of the rivet guns decreased, transmissibility increased across tools (R1-R2-R3) in both left and right arm vibration measurements.

Resonant frequencies at the back of the hand, middle of the forearm and middle of the upper arm were shown to be approximately 35, 30 and 25 Hz, respectively, in a study by Welcome et al., (2015). The operating frequency of rivet gun R1 (25 Hz) was closest to resonant frequency of the forearm and upper arm and may partially explain the decreasing vibration magnitudes measured across the guns in the right forearm and upper arm.

Another interesting consistency in the data across all tools and both subjects was the similarity in vibration magnitude estimated by the HAVWear device and the actual ISO 5349-1 vibration measured from the handle of the tool (top graph Figure 1). The wrist-mounted HAVWear device measured the tri-axial vibration at the wrist and used a proprietary transfer function to estimate the tool-born vibration occurring at the tool-hand interface. While these results are just preliminary and based on a small sample size, the similarity in measurements is encouraging given how variable HAV measurement tends to be. Greater testing with more subjects and different tools is merited before broader conclusions can be drawn.

Despite all the consistent trends, this study does have some inconsistencies and limitations. There were differences between the Declared Emission Values (DEV) of our tool-measured vibration exposures. However, this was not unexpected. DEV's are derived using a test standard where the tool is suspended in the air by a string and the tool is gripped by three different operators in a typical fashion with a known downward force applied to the tool while vibration is measured during a tool activation cycle of 8-16 seconds. Our tool-measured vibration values were higher than the DEVs and may not reflect actual field exposures and tool trends due to operating the riveting guns against a stationary load cell. The goal in our study was to create a very controlled riveting task with limited potential for variability. Another inconsistency was that the IMU measurements from the back of hands did not match either the tool-measured vibration trends between the left (barrel) and right (handle) vibration measurements. We are uncertain if hand compliance or the resonant frequency of the hand contributed to these differences. Finally, the greatest limitation is the small sample size of just two subjects; however, our within subject variability was not large, so it appeared the subjects performed tasks relatively consistently.

Despite the small sample size, we felt the exploratory results of the HAVWear may have potential for larger scale and field-based exposure assessment studies. The HAVWear device has been more actively used and tested in the construction industry in the United Kingdom. The desirable aspect of the HAVWear device, if it is relatively accurate estimating the tool-born vibration for the targeted tools and/or tasks, is its ability to less invasively collect a tool operator's vibration exposure; not over just a single day, but over weeks, months or even years. Although not used in this study, the HAVWear device has a docking station where it sends both tool-related and subject-based vibration exposure data to the cloud for subsequent analysis. This longitudinal, long-term data collection may

be essential for developing and better determining the dose-response relationship between vibrating tool use and the onset and development of vibration-related musculoskeletal disorders.

5   ACKNOWLEDGEMENTS

REFERENCES

[1] Charles, L.E., Ma, C.C., Burchfiel, C.M. and Dong, R.G., 2018. Vibration and ergonomic exposures associated with musculoskeletal disorders of the shoulder and neck. *Safety and health at work*, *9*(2), pp.125-132.

[2] Griffin, M.J., 1990. Handbook of human vibration. Academic Press Limited. London.

[3] Nilsson, T., Wahlström, J. and Burström, L., 2017. Hand-arm vibration and the risk of vascular and neurological diseases—A systematic review and meta-analysis. PLoS One, 12(7), p.e0180795.

[4] International Organization for Standardization (ISO), 2001. Mechanical vibration guidelines for the measurement and the assessment of human exposure to hand-transmitted vibration. ISO 5349-1, 2001. ISO, Geneva, Switzerland

[5] Welcome, D.E., Dong, R.G., Xu, X.S., Warren, C., McDowell, T.W. and Wu, J.Z., 2015. An examination of the vibration transmissibility of the hand-arm system in three orthogonal directions. International journal of industrial ergonomics, 45, pp.21-34.

Effects of vibration directions, postures and velocity levels on measurements of the mechanical impedance of the hand-arm system

Massimo Cavacece[1]
University of Cassino and Southern Lazio, Department of Civil and Mechanical Engineering,
Via G. Di Biasio n.43, 03043 Cassino (FR), Italy
cavacece@unicas.it

Graziella Aghilone[2]
University La Sapienza of Rome, Pharmacy and Medicine Faculty,
Piazzale Aldo Moro n.5, 00185, Rome (RM), Italy
graziella.aghilone@uniroma1.it

ABSTRACT

The characteristics of hand-arm vibration generated by the operation of power tools depends on the dynamics of the coupled hand-tool system. The assessment methodologies require repetitive measurements involving representative human subjects, test conditions and inter- and intra-subject variabilities. The applications of mechanical equivalent or biodynamic models of the human hand-arm system offer considerable potential to carry out assessments through analytical and experimental analyses. So the involvement of human subjects could be considerably reduced. If the statistical model considers the interaction between human hand-arm system and power tool, the statistical model could permit efficient evaluations of the tool design factors and vibration attenuation devices.

1   INTRODUCTION

Hand-transmitted vibration can influence human comfort, the performance of activities and health [1]. The various effects of hand-transmitted vibration are influenced by the complex biodynamic responses of the fingers, hands and arms [8]. Several physical and biodynamic factors, such as intensity, frequency and direction of HAV, duration and pattern of exposure, grip force and posture can play a rule of degeneration on human hand-arm system [4].

The mechanical impedance of the human hand-arm system was measured within the frequency range of 20-1500 Hz by Lundström and Burström [2]. A handle, specially designed for such measurements, was used. The studies were carried out on eight healthy male subjects during different experimental conditions defined by three different hand-arm postures, hand grip forces 25-75 [N], velocity 27-53 [mm/s] and direction of the vibration stimuli.

Biodynamic response of the human hand-arm system exposed to sinusoidal and random vibration is characterized in terms of the driving point impedance [13]. The driving point mechanical impedance (MI) characteristics are measured for various test conditions to determine the influence of grip force and nature of vibration on the response behaviour of the human hand-arm system [14].

The impedance characteristics measured under different test variables revealed the following aspects: (i) the biodynamic response characteristics of hand-arm system may be obtained by using

mechanical impedance techniques [5]; (ii) the measured impedance data exhibits a high degree of inter-subject variations that may attributed to the differences in weights and sizes of hands of the subjects [6]; (iii) the effect of grip force and the excitation frequencies on the driving point impedance is significant [7]; (iv) the impedance characteristics differed under sinusoidal and stochastic excitation [3].

The objective of the study of Besa et al. was to describe the methodology applied to analyse the influence of certain factors that could affect the transmission and absorption of energy by the hand-arm system. The Authors affirmed that the characterisation of the mechanical impedance of the hand-arm system makes it possible to define the vibration power absorption frequency weighting filters for the accelerations measured in the tool handle [9].

Dong et al. estimated the biodynamic responses distributed at fingers and palm based on the total response of the hand-arm system. The Authors confirmed that the skin of the hand is effectively involved in the response at very high frequencies (>500 Hz) [11]. Therefore, the Authors affirmed that the skin tissues, compressed against the handle surface, have a displacement relative to the handle surface.

In the study of Adewusi, laboratory experiments were performed to obtain estimates of transmission of Z_h-axis handle vibration to the underlying bone/joint structures of the wrist, elbow and the shoulder of the human hand-arm system under different combinations of grip and push forces, excitation magnitudes and different postures [10].

Welcome et al. characterized the vibration transfer functions distributed on the entire hand-arm system in three orthogonal directions. The dominant vibration frequencies of many tools such as grinders, chainsaws, impact wrenches, and orbital sanders are in the range of 80-160 Hz. Implications of the results for risk assessment are that such vibration exposures are thus likely to be primarily associated with finger or hand disorders [12].

This research estimates the effects of different vibration sources on mechanical impedance of the human hand-arm system. The analysis examines the interquartile range and median value of mechanical impedance real part, obtained by effect of grip and push action.

2   STATISTICAL MODEL OF THE HAND-ARM SYSTEM

A number of mechanical equivalent models have been developed to characterize the biodynamic response characteristics of the human hand-arm under vibration. The biodynamic response can be described in terms of through-the-hand arm and to-the-hand response functions. The through-the-hand-arm response function describes the transmission of vibration to specific segments of the hand and forearm. The to-the-hand biodynamic response function relates the motion at the hand-handle interface to the force at the driving point.

The hand-arm vibration (HAV) models could permit efficient evaluations of the tool design factors and vibration attenuation devices. It can be distinguished distributed-parameter HAV models and lumped-parameter models.

The biodynamic response in terms of driving-point mechanical impedance (MI) is given by the following relation:

$$Z = \frac{F}{v},$$ (1)

where Z is complex MI, v is velocity measured at the driving point and F is the driving force.

A deterministic model is defined by a set of parameters. The bound of a deterministic model is that performs the biodynamic response of human hand-arm system for a given set of initial

conditions. A very important aspect is represented by the working conditions of workers. The grip and push forces and working postures may be highly variable by using a power tool. A wide range of forces can be generated on hand-arm system. In addition, very little knowledge exists on the natural frequencies and dissipative properties of human hand-arm system. For this reason the current state of knowledge on the vibration behaviour of the human human hand-arm system does not permit a quantitative evaluation of the models in terms of their natural frequencies and dissipative properties.

Conversely, in a stochastic model or statistical model, randomness is present, and variable states are not described by unique values, but rather by functions of descriptive statistics.

3   INFLUENCE OF THE DIRECTION

The real parts of the mechanical impedance values of hand–arm system are presented in Fig.1, obtained by effect of transmission direction. The graph of mechanical impedance, obtained along Xh direction, is lower in the field frequency 0-20 Hz; it assumes a maximum value at 40–50 Hz and a minimum value at 100 Hz. The graph of mechanical impedance, obtained along Z_h direction, is higher in the field frequency 0-200 Hz. Measured data of mechanical impedance real part, obtained by effect of transmission direction (Fig.1), present the interquartile range IQR and median value proposed in Table 1.

Table 1 : Median value and interquartile range of measured data of mechanical impedance real part, obtained by effect of direction

Direction	Median value	Interquartile range
	[N s m^{-1}]	
X_h	246.69	144.61
Y_h	86.9	64.18
Z_h	147.79	87.01

Measured data of mechanical impedance real part (MI), obtained by effect of direction, offers a wide IQR and high median values along X_h axes. The IQR and median value of MI, allong X_h axis is greater than MI evaluated along Y_h and Z_h axis.
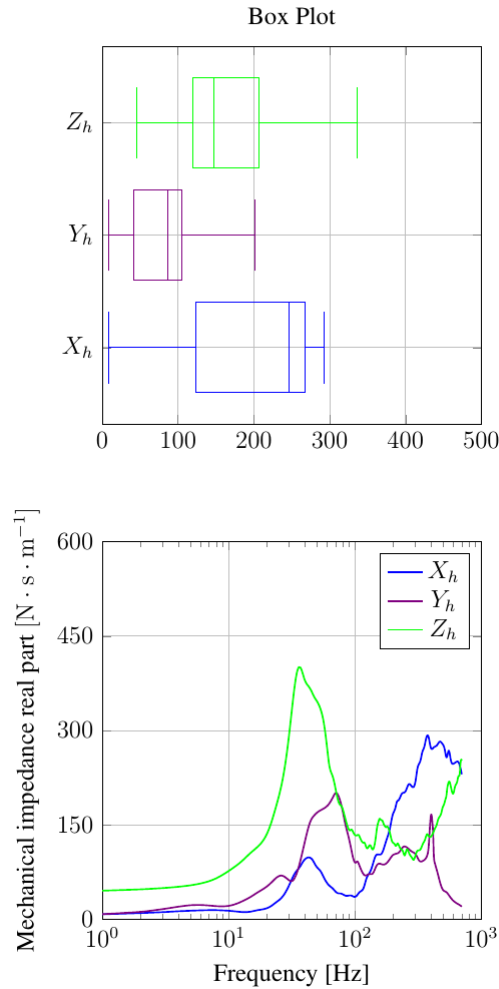
Figure 1: The interquartile range of measured data of mechanical impedance real part, obtained by effect of transmission direction

4   EFFECT OF EXCITATION MAGNITUDE

The real parts of the mechanical impedance values of hand-arm system are presented in (Fig.2) obtained by effect of excitation magnitude. The graphs of mechanical impedance, obtained by effect of excitation magnitude (Fig.2), have similar trend. The graphs present maximum value at 50 Hz and minimum value at 125 Hz. Measured data of mechanical impedance real part, obtained by effect of excitation magnitude, present the IQR and median value proposed in Table 2.

The increment of excitation magnitude expandes IQR, increases median values and generates different upper quartile values:

- $\circ$ $a_w = 15$ [m $\cdot$ s^{-2}]: upper quartile = 214.96 [N $\cdot$ s $\cdot$ m^{-1}];
- $\circ$ $a_w = 30$ [m $\cdot$ s^{-2}]: upper quartile = 251.68 [N $\cdot$ s $\cdot$ m^{-1}].

Table 2 : Median value and interquartile range of measured data of mechanical impedance real part, obtained by effect of excitation magnitude

Magnitude a_w	Median value	Interquartile range
m s^{-2}	[N s m^{-1}]	
15	155.85	91.44
30	166.83	125.42
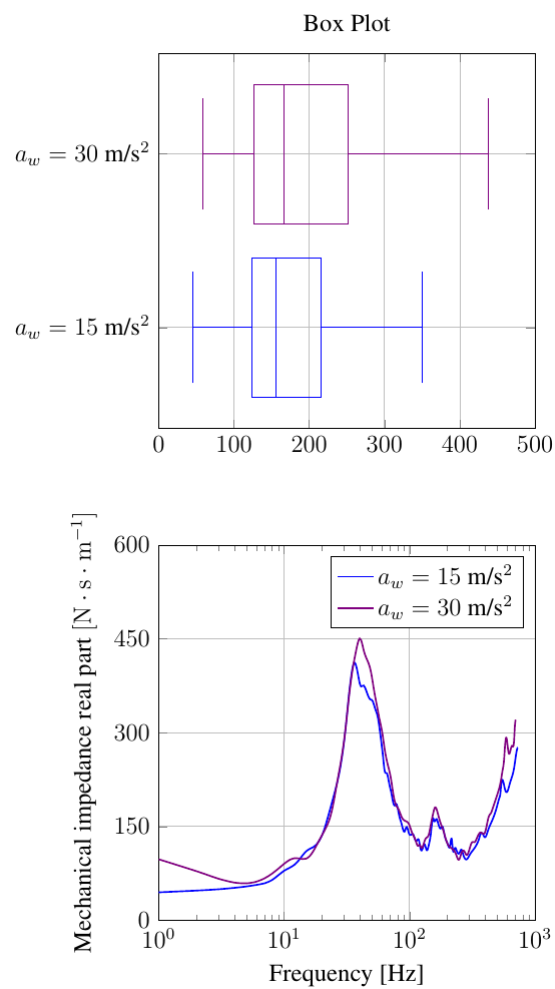
Figure 2: The interquartile range of measured data of mechanical impedance real part, obtained by effect of excitation amplitude

5   INFLUENCE OF THE VIBRATION LEVEL

The comparison of mechanical impedance, obtained with equal postures and grip forces but with different vibration levels, offers some interesting aspects. At low frequencies (0-10 Hz), the magnitude of mechanical impedance is higher for low stimulus amplitude (vibration level 27 [mm · s^{-1}]).

The mechanical impedance of lowest stimulus amplitude seems to be especially pronounced than ones obtained by stimulus amplitude 38 and 53 [mm · s^{-1}] in the frequency range from 20 to 100 Hz (Fig.3). For against, the mechanical impedance, obtained by vibration level 27 [mm · s^{-1}], is lower in the field of high frequencies (400-1000 Hz).

The mechanical impedance, obtained by vibration level 27 [mm · s^{-1}], assumes the maximum value at 50 Hz. Instead, the magnitudes of mechanical impedance, obtained for velocity 38 and for velocity 53 [mm · s^{-1}], assume the maximum value at 40 Hz.

In addition, the magnitudes of the mechanical impedance, obtained for velocity 27 [mm · s^{-1}], 38 [mm · s^{-1}] and 53 [mm · s^{-1}] indicated a tendency to two minima, once close to 80-100 Hz and the other close to 300 Hz. These results can indicate two different resonant frequency areas for the hand-arm system. The mechanical impedance increased from 100 Hz.

Measured data of mechanical impedance real part, obtained by different hand-arm postures (Fig.4) present the IQR and median value proposed in Table 3.

The comparison of measured data shows that the mechanical impedance real part, obtained by velocity 53 [mm · s^{-1}], presents a wide IQR and high median value.

Table 3: Median value and interquartile range of measured data of mechanical impedance real part, obtained by effect of vibration level

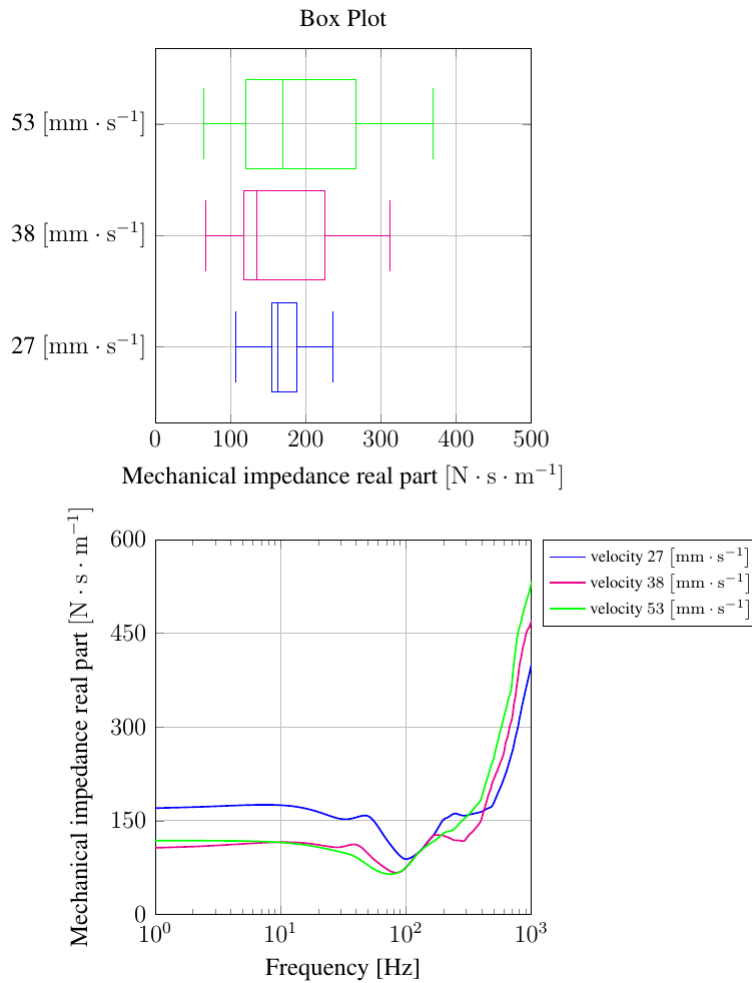| Vibration level	Median value	Interquartile range
[mm s^{-1}]	[N s m^{-1}]	
27	155.06	32.56
38	135.24	108.15
53	169.78	147.11

Figure 3: Magnitudes of the driving point mechanical impedance (MI) obtained for velocity 27 mm/s, 38 mm/s, 53 mm/s with posture 3 and grip force 50 N

6   EFFECT OF COMBINED ACTION OF GRIP FORCE AND PUSH FORCE

The real parts of the mechanical impedance values of hand-arm system are presented in Fig.4, obtained by effect of grip force and push force. At low frequencies, the magnitude of mechanical impedance, obtained by push force 20 N and grip force 0 N, is lower. The magnitudes of mechanical impedance, obtained by effect of grip force and push force, reach the maximum value at 20–80 Hz; after 80 Hz, they decrease in the frequency range from 80-200 Hz to obtain a minimum value at about 200 Hz; after 200 Hz, they increase in the field of high frequencies. The magnitude of mechanical impedance is lower for push force = 20 N and grip force = 0 N in the frequency range from 80 to 200 Hz.

Measured data of mechanical impedance real part, obtained by effect of combined action grip force and push force, present interquatile ranges (IQR) from 32 to 116.50 [N · s · m^{-1}] and median values median value from 102.3 to 209.94 [N · s · m^{-1}] (Fig.4).

In detail, measured data of mechanical impedance real part, obtained by effect of grip force and push force, present the IQR and median value proposed in Table 4.
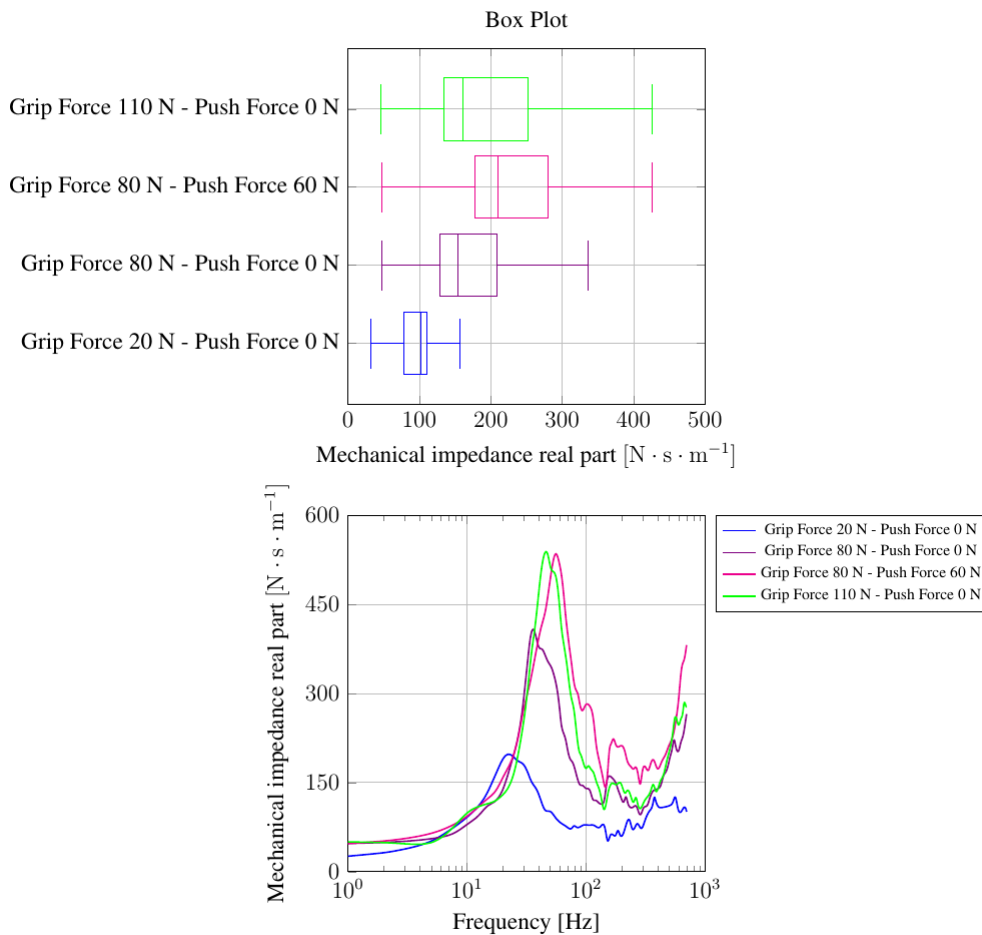
Table 4: Median value and interquartile range of measured data of mechanical impedance real part, obtained by effect of grip force and push force

Grip Force	Push Force	Median value	Interquartile range
[N]		[N s m^{-1}]	
20	0	102.53	32.17
80	0	153.60	87.18
80	60	209.94	102.21
110	0	161.34	116.51

The grip force greatly influences the values of mechanical impedance real part. The increment of grip force amplifies IQR and increases median value. Therefore, the values of grip force and of push force plays an important rule on the tension of the muscles of human hand-arm system.

Figure 4: The interquartile range of measured data of mechanical impedance real part, obtained by effect of grip force and push force

7 INFLUENCE OF THE POSTURE OF HUMAN HAND–ARM SYSTEM

The influence of the posture of human hand-arm system on real parts of the mechanical impedance values (MI) is proposed in Fig.6. The postures are indicated in Fig.5 as mentioned by study of Lundström and Burström [2].

(a) Posture 1   (b) Posture 2   (c) Posture 3
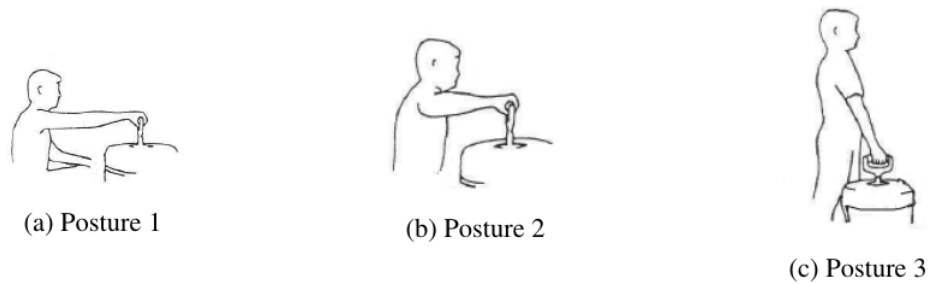
Figure 5: Different human hand-arm postures

The different hand-arm postures generated pronounced differences between impedance curves for the lower frequency region, i.e. below about 300 Hz. The mechanical impedance for Posture 3 appears mainly marked in the frequency range from 0 to 70 Hz than the mechanical impedance obtained for Posture 1 and Posture 2. The MI for Posture 3 assumes a minimum value at 100 Hz.

The MI for Posture 3 increases with the frequency in the frequency range 100-1000 Hz. The graphs of MI for Posture 1 and Posture 2 increase with the frequency from 20 Hz to 100 Hz (Fig.6). The MI for Posture 1 and Posture 2 reach the maximum value at 100 Hz. They decrease in the frequency range from 20–300 Hz to obtain a minimum value at about 300 Hz. The MI for Posture 1 and posture Posture 1 increase in the frequency range 300-1000 Hz.

Measured data of mechanical impedance real part, obtained by different hand-arm postures (Fig.6) present the IQR and median value proposed in Table 5.

Table 5: Median value and interquartile range of measured data of mechanical impedance real part, obtained by effect of the posture of human hand-arm system

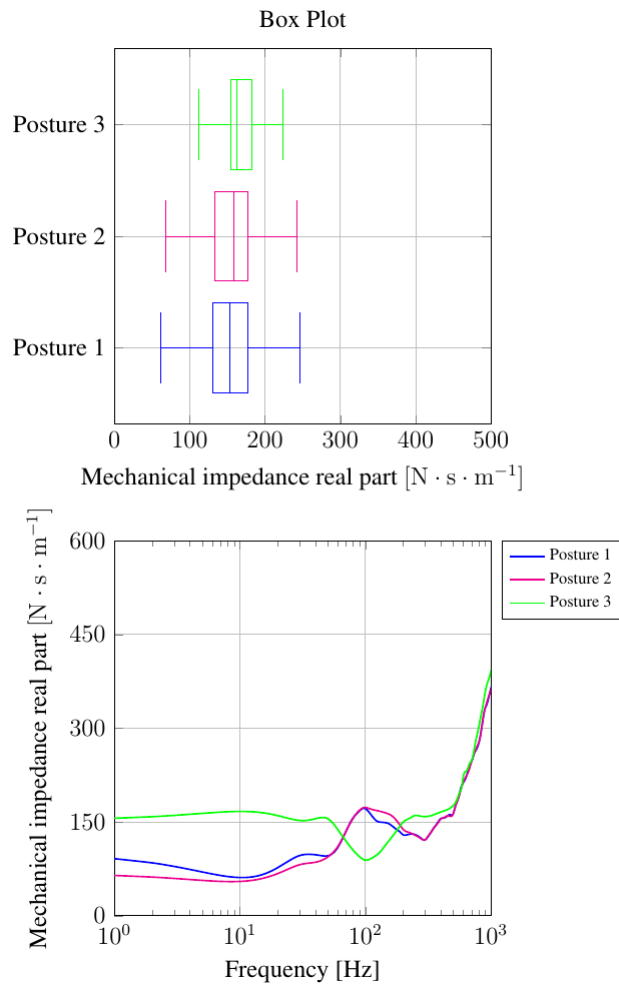| Posture	Median value	Interquartile range
		[N s m^{-1}]
1	153.87	47.07
2	158.42	44.03
3	162.88	27.94

Figure 6: Magnitudes of the driving point mechanical impedance (MI) obtained for Posture 1, Posture 2 and Posture 3 with grip force 50 N, vibration level 27 mm/s

8   DISCUSSION

The results of this study suggest that the driving-point mechanical impedances distributed at the fingers and the palm of the hand can be approximately estimated from the total response of the entire hand-arm system using the statistical model of the hand-arm system. The method proposed in this study provides a new approach to extend the applications of these experimental data, which may accelerate the quantification and understanding of the distributed biodynamic responses. Statistical model considers the variable states represented by functions of descriptive statistics.

Series of measurements observed over frequency (Fig.7), containing statistical noise and other inaccuracies, are evaluated by Kalman filtering (Fig.8). The comparison shows a good agreement between the MI values obtained by statistical method and MI values obtained by deterministic model.
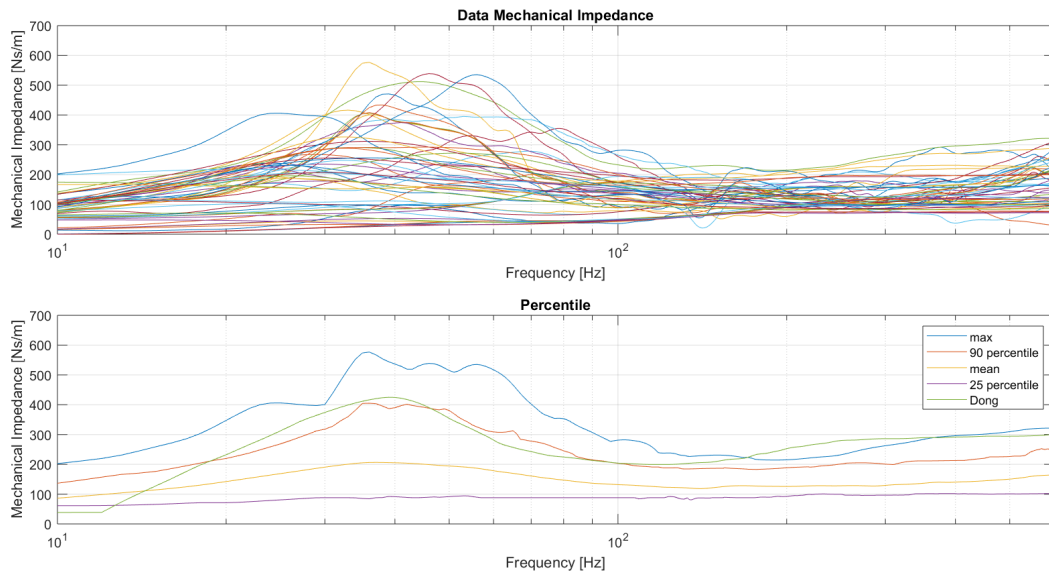
Fig.7 : Series of measurements
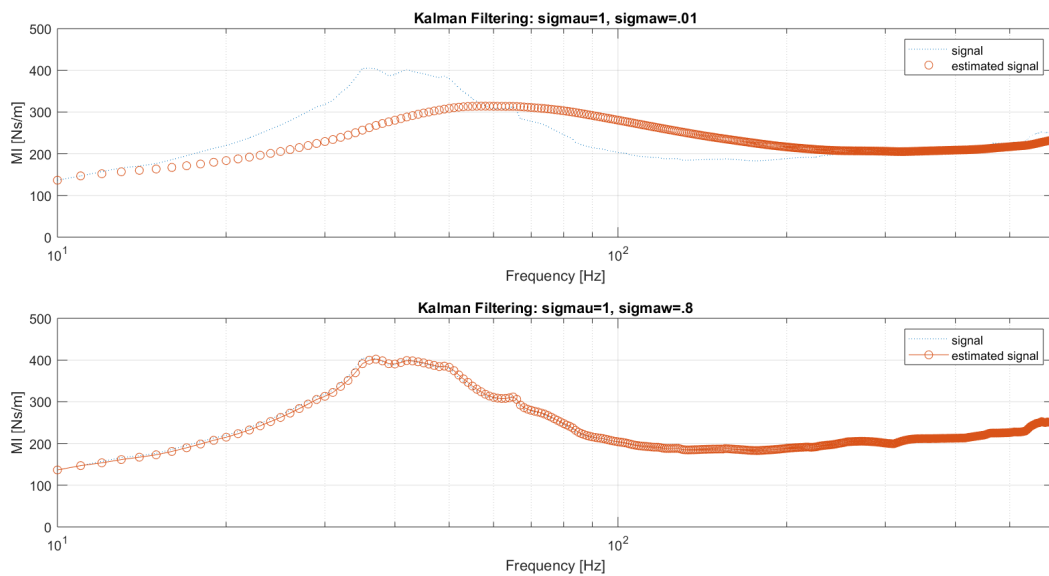
Fig.8: Series of measurements observed by Kalman filtering

9   CONCLUSION

This study confirmed that the most reliable approach to represent the biodynamic responses distributed at the fingers and the palm of the hand is to create the model using the

experimental data. Vibration data are separately measured at the fingers and the palm. The models defined in this study can be used to analyze the design of many tools and anti-vibration devices. The statistical model, proposed in this study, is also applicable for further model development.

REFERENCES

[1] E.G. Tasker, "Assessment of vibration levels associated with hand-held roadbreakers", Scandinavian Journal of Work, Environment & Health, 12, 407-12, 1986

[2] R. Lundström, L. Burström, "Mechanical Impedance of the human hand–arm system", International Journal of Industrial Ergonomics, 3, 235-242, 1989

[3] R. Gurram, S. Rakheja, G.J. Gouw, "Mechanical Impedance of the human hand–arm system subject to sinusoidal and stochastic excitations", International Journal of Industrial Ergonomics, 16, 135-145, 1995

[4] Z. Xu, H.C. Ding, M.P. Ding MP, "A study of dose-effect relationships for vibration induced white finger", Proceedings of the 5th International Conference on Hand–Arm Vibration, 305-308, Kanazawa, Japan, 1990

[5] M.J. Griffin, "Measurement, evaluation, and assessment of occupational exposures to hand-transmitted vibration", Occupational and Environmental Medicine, 54, 73-89, 1997

[6] P. Marcotte, Y. Aldien, P.-E. Boileau, S. Rakheja, J. Boutin, "Effect of handle size and hand-handle contact force on the biodynamic response of the hand-arm system under z_h-axis vibration", Journal of Sound and Vibration, 283, 1071–1091, 2005

[7] R.G. Dong, T.W. McDowell and Daniel E. Welcome, "Biodynamic Response at the Palm of the Human Hand Subjected to a Random Vibration", Industrial Health, 43, 241-255, 2005

[8] R.G. Dong, D.E. Welcome, T. W. McDowell, J. Z. Wu, A. W. Schopper, J. Z. Wu, A. W. Schopper, "Frequency weighting derived from power absorption of fingers-hand-arm system under z_h-axis vibration", Journal of Biomechanics, 39, 2311-2324, 2006

[9] A.J. Besa, F.J. Valero, J.L. Suner, J. Carballeira, "Characterisation of the mechanical impedance of the human hand-arm system: The influence of vibration direction, hand-arm posture and muscle tension", International Journal of Industrial Ergonomics, 37, 225-231, 2007

[10] S.A. Adewusi, S. Rakheja, P. Marcotte, J. Boutin, "Vibration transmissibility characteristics of the human hand-arm system under different postures, hand forces and excitation levels", 329, 2953-2971, 2010

[11] R.G. Dong, S. Rakheja, T. W. McDowell, D.E. Welcome, J. Z. Wu, "Estimation of the biodynamic responses distributed at fingers and palm based on the total response of the hand-arm system, International Journal of Industrial Ergonomics", 40, 425-436, 2010

[12] D.E. Welcome, R.G. Dong, X.S. Xu, C. Warren, T.W. McDowell, Z.J. Wu, "An examination of the vibration transmissibility of the hand-arm system in three orthogonal directions", International, Journal of Industrial Ergonomics, 21-34, 2015

[13]   S. Hewitt, R. Dong, T. McDowell, D. Welcome, "The Efficacy of Anti-vibration Gloves", Acoust Aust, 44, 121-127, 2016

[14]   M. Cavacece, G. Aghilone, "Biodynamic responses at the fingers and the palm of the human hand-arm system under different vibration sources", 14th International Conference on Hand-Arm Vibration, Bonn, Germany, ISBN 978-3-86423-228-2, 21-24 May 2019

Validity of VPT (Vibrotactile Perception Threshold) as an Indicator of Human Response to Vibration Exposure

Setsuo Maeda[1], Kazuhisa Miyashita[2]

[1] Visiting Professor, School of Science and Technology, Nottingham Trent University,
Clifton Lane, Nottingham, NG11 8NS, UK,
setsuo.maeda@ntu.ac.uk

[2]President, Wakayama Medical University,
811-1, Kimiidera, Wakayama City, Wakayama Prefecture, 641-8509, JAPAN,
miyaka@wakayama-med.ac.jp

ABSTRACT

This paper firstly reviews the research on Vibrotactile Perception Threshold (VPT) together with the ISO standards concerning VPT measurement and evaluation, and the use of VPT in different countries. The relationship between the measurements of vibration dose and VPT are then examined in order to consider the future use of VPT as an indicator of human response to vibration exposure.

1   INTRODUCTION

As show in Figure 1, following prolonged use of hand-held tools workers may develop Hand-Arm Vibration Syndrome (HAVS), which affects the vascular, nervous and musculoskeletal systems at the hands (Mansfield, 2004). Vascular disease results in finger blanching (Raynaud's phenomenon) and finger coldness. Neurological disease results in pain, dysesthesia, paraesthesia, tingling and numbness. Musculoskeletal disease results in pain, loss of muscle power and manual dexterity, and deformity of bones and joints. A shift in the Vibrotactile Perception Threshold (VPT) has historically been used in a number of countries for the diagnosis of HAVS, especially the diagnosis of neurological damage (International Organization for Standardization, 2001).
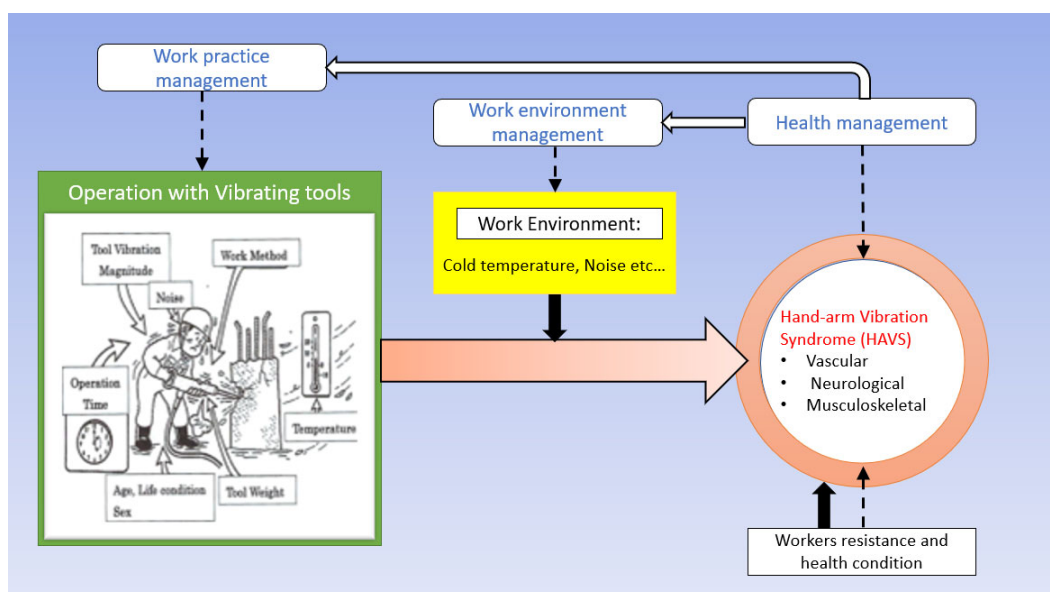

Figure 1. Relationship between Vibration Dose and HAVS.

This paper begins with a review of existing research involving VPT followed by a review of ISO standards relating to the topic and how various countries are using the technique for the diagnosis of HAVS symptoms. The paper goes on to highlight some specific research which has used VPT to assess the human response to vibration and the relationship between the measurement of vibration dose and VPT. Finally, the paper gives consideration to the future of VPT as an indicator of human response to vibration exposure.

2 VIBROTACTILE PERCEPTION THRESHOLD AND EXISTING RESEARCH

As detailed in the standard ISO 13091-1 (International Organization for Standardization, 2001), VPT is defined as skin surface acceleration level at which there is a 50 % positive response rate for detecting a pure-tone oscillatory stimulus in the psychometric function. After prolonged vibration exposure from the use of hand-held tools (Figure 1), workers can develop a chronic disorder known as Hand-Arm Vibration Syndrome (HAVS). The increased awareness of the risks posed by this sensory neuropathy has resulted in an interest in quantitative sensory testing (QST) for screening and diagnosis of vibration-induced neuropathy.

Radzyukevich(1969) (Radziukevich, 1969) suggested that the temporary threshold shift (TTS) in vibrotactile perception threshold at the end of a working day was correlated with the permanent threshold shift (PTS) that would develop over a longer period of time. Malinskaya et al (1964) (Malinskaya et al., 1964) found that the mean TTS of workers after a day of work that included vibration exposure was an indicator of the PTS of vibratory sensation that occurred in the group after 10 years of exposure. These findings suggest that the TTS after daily exposure may be used to indicate the PTS after prolonged exposure to vibration. Based on these results, further research looked to determine the relationship between TTS in VPT and other influencing factors of hand-arm vibration exposure, such as those highlighted in Annex D of ISO 5349-1 (International Organization for Standardization, 2001a).

The measurement of VPT as an indicator of PTS is used as a diagnostic criterion, in order to determine the risk for development of HAVS. A significant level of research has been undertaken using VPT as an intermediary in the relationship between the different vibration exposure conditions and the human response to vibration. A survey for VPT papers, revealed around 1000 papers by Google Scholar ("Vibrotactile Perception Thresholds - Google Scholar," n.d.) and around 600 papers by PubMed ("Temporary Threshold Shift - PubMed - NCBI," n.d.), indicating the significance of VPT in the research of the human response to vibration.

3 ISO STANDARDS OF VPT MEASUREMENT EQUIPMENT

The significance of VPT has also been demonstrated by the development of the international standards ISO 13091-1 and ISO 13091-2 (International Organization for Standardization, 2003, 2001). ISO 13091-1 is an equipment standard relevant for the inspection of peripheral nerve dysfunction in Hand-Arm Vibration disorders. This equipment for neurological function tests works by measuring VPT on the fingertip. The ISO 13091-2 relates to the interpretation of the measured VPT results according to the ISO 13091-1 equipment. Within the academic environment, VPT measurement has been widely used to diagnose the neurological disorder caused by Hand-Arm vibration exposure (Gandhi et al., 2011). While the UK, Japan, China and Poland are all countries which have adopted VPT as a means of diagnosing HAVS, application of the diagnosis criteria is not fully consistent. Table 2 summarises the equipment used and diagnostic criteria for countries adopting VPT for HAVS diagnosis.

Table 1 Existing VPT Standards

Country	Equipment	Diagnosis Criteria
ISO Standard	ISO13091-0	ISO13091-2
UK	Vibrotactile meter	Not clear
Japan	RION AU-02B	More than 7.5dB at 125Hz (Normal Temperature)
China	RION AU-02B	17.5dB at 125Hz and 250Hz
Poland	Vibrotactile meter Type MCW80 or Pallethesiometer P8 (EMSON-MAT)	Normal <126dB Slightly abnormal 127-131dB Moderate abnormal 132 -141dB Severely abnormal >141dB (dB ref 10-6ms^{-2})

4   RELATIONSHIP BETWEEN VIBRATION DOSE AND VPT FROM HUMAN RESPONSE TO VIBRATION EXPOSURE

Within the significant research into human response to vibration, many researchers have measured the hand transmitted vibration on the tool handle without considering the affecting factors described by Annex D of the ISO5349-1 standard. Measurement of vibration on the tool handle is undertaken to establish a vibration dose. The vibration dose of a daily exposure to HAV is proposed as $A(8) = a_{hv}\sqrt{t/8}$, where a_{hv} is notionally the hand transmitted vibration (in m/s^2) and t is the time (in hours) of exposure. The approach of measuring vibration on a tool handle together with an estimated time of exposure has been used to establish a relationship between the daily dose value and the likelihood of developing symptoms of finger blanching over extended periods of daily exposure as shown in ISO5349-1 (International Organization for Standardization, 2001a). The factors identified in annex D of ISO5349-1 highlight that the measurement of vibration on the tool handle will not fully represent the vibration transmitted to the hand and arm system i.e. the hand transmitted vibration. Review of historic research also shows that studies were often based on an estimation of tool usage time from time study methods, as opposed to measurement of actual exposure time.

The release of the standards ISO5349-1 (International Organization for Standardization, 2001a), ISO5349-2 (International Organization for Standardization, 2001b), and ISO 8041 (International Organization for Standardization, 2005), has resulted in a focus of measuring vibration on the tool handle, despite ISO 5349-1 identifying the following factors as affecting Hand-Transmitted vibration:

> ISO 5349 recognizes the presence of factors that may influence vibration exposure, which are not accounted for in the standard:
> - Direction of the vibration
> - Working method and operator's skill
> - Age, constitution and health
> - Coupling forces (grip and feed forces)
> - Hand, arm and body posture
> - Condition of the machinery and accessories/workpieces used

The idea of a daily dose $A(8) = a_{hv}\sqrt{t/8}$ as required to inform risk management, would suggest that if A(8) has the same magnitude, then any worker being deployed to this activity will be facing a uniform risk from the tool vibration exposure in the workplace. Furthermore, it has been considered that tool manufacturer's Vibration Declaration Values can be used as a_{hv} for risk management purposes. While controlled to stringent test protocols it is recognised that these declaration values seldom represent the tool activity in a real working environment (Health and Safety Executive (HSE), 2019). As shown in Figure 1, research highlights the difficulties of A(8) following ISO5349 as an adequate indicator of risk, such as the effect of 1) handle diameter (Shibata and Maeda, 2008), 2) postures (Maeda and Shibata, 2008, 2007), 3) coupling forces (Maeda et al., 2007), and 4) subjects (Maeda et al., 2019). From such research although the A(8) values were often consistent, the human response to vibration, such as TTS values were not the same. Many researchers are reporting that the human response to vibration is affected by the issues highlighted in Annex D of ISO 5349-1 without identifying an alternative approach or consideration.

4.1   Handle diameter

The purpose of this paper (Shibata et al, 2008)was to study the Temporary threshold shifts (TTSs) of fingertip VPT under controlled conditions, and the effects of handle size in combination with vibration frequency, amplitude, and frequency weighting; on human response to HAV. Ten healthy male subjects were exposed to two levels of HAV: 125Hz-5.0m/s^2 and 125Hz-20.0m/s^2 (represented as a combination of vibration frequency and rms acceleration) using two different handles (22 and 35 mm in diameter) excited by a shaker. A simplified version of method of limits were used to measure VPT and TTS were then calculated as the difference between fingertip vibrotactile perception thresholds measured before and after 5 min vibration exposure. At 125Hz-5.0m/s^2 vibration, the handle size significantly affected TTS in VPT. In contrast, the handle size did not have a significant effect at 125Hz-20.0m/s^2 vibration. These results suggest that handle size is more sensitive to the TTS in fingertip VPT under relatively lower vibration level. From a viewpoint of risk assessment to HAV exposure, TTS after short-term exposure to HAV is indicative of likelihood of developing HAVS from long-term exposure to HAV. Since, the long-term effect has been the accumulation of repeated short-term effect of HAV, these results suggest that the tool handle size should be designed based on diminishing TTS.
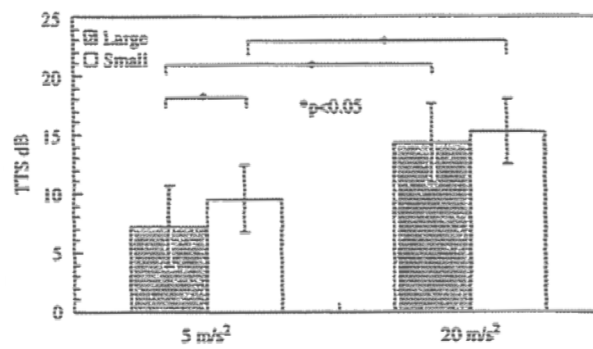

Figure 2. Comparison of TTS vs. different handle size under the same vibration magnitudes.

Within the study vibration measurements were taken at the shaker handle using a vibrometer, and vibration magnitude was unchanged with different handle diameters, despite the TTS differences shown in Figure 2. The results mean that hand-transmitted vibration was different with each handle diameter, but a measurement on the tool handle is not effective in representing this difference.

4.2   Operator Posture

Maeda et al (Maeda and Shibata, 2007) report results of an investigation into A(8) evaluation effects of hand-transmitted vibration on TTS of VPT on the finger. The hand-transmitted vibration was applied with an electric tool to the right hand of five male subjects with four different working postures. The threshold of 125 Hz vibratory sensation was measured at the tip of the right forefinger before and after vibration exposure. The study reported that the TTS following vibration exposure was significantly different in the four different working postures. In contrast, the vibration delivered, as measured on the tool handle, did not correlate with the TTS readings. The results suggest that a measurement of vibration on the tool following ISO 5349-1 will not predict the variations in physiological effects from hand-arm transmitted vibration from different working postures.

A.

B.

Subjects	Posture 1	Posture 2	Posture 3	Posture 4
1	8.37	13.76	11.74	9.16
2	9.97	9.96	9.96	10.67
3	10.67	13.39	11.72	14.35
4	10.00	12.95	13.25	12.61
5	6.63	10.87	6.56	9.96
Mean TTS	9.13	12.19	10.65	11.35

C.
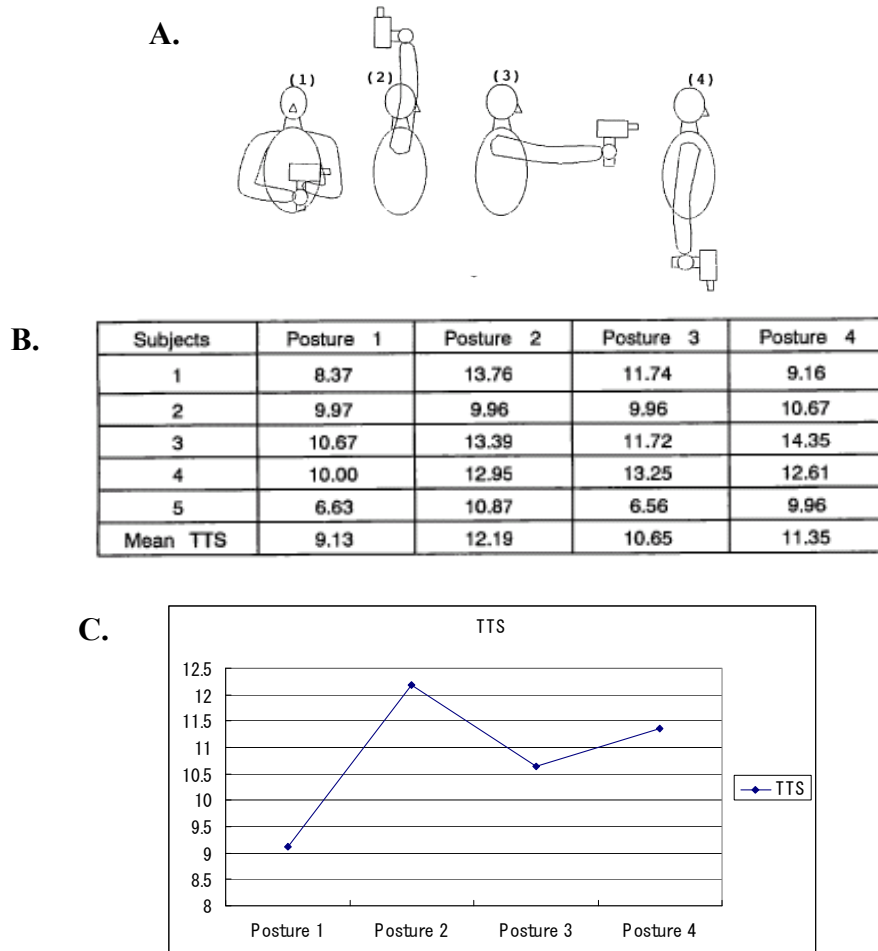
Figure 3. Comparison of TTS vs. different postures under the same vibration magnitudes, including a graphical description of the postures (A), the results obtained for all subjects (B) and the relationship between posture and TTS (C).

In a similar manner, another study (Maeda and Shibata, 2008) sought to investigate the effect on TTS of VPT at the finger with differing work postures. Subjects were exposed to the hand-held tool with the exposure time of 5 min at different positions in the working surface. A controlled condition with no vibration was included. In order to obtain the TTS in the fingertip VPT, the VPT were measured before and after the subjects were exposed to hand-transmitted vibration from the hand-held tool. The results of TTS were different at different positions in the working surface, even though the hand-held tool vibration magnitudes, as measured on the tool handle according to ISO 5349-1, were the same.
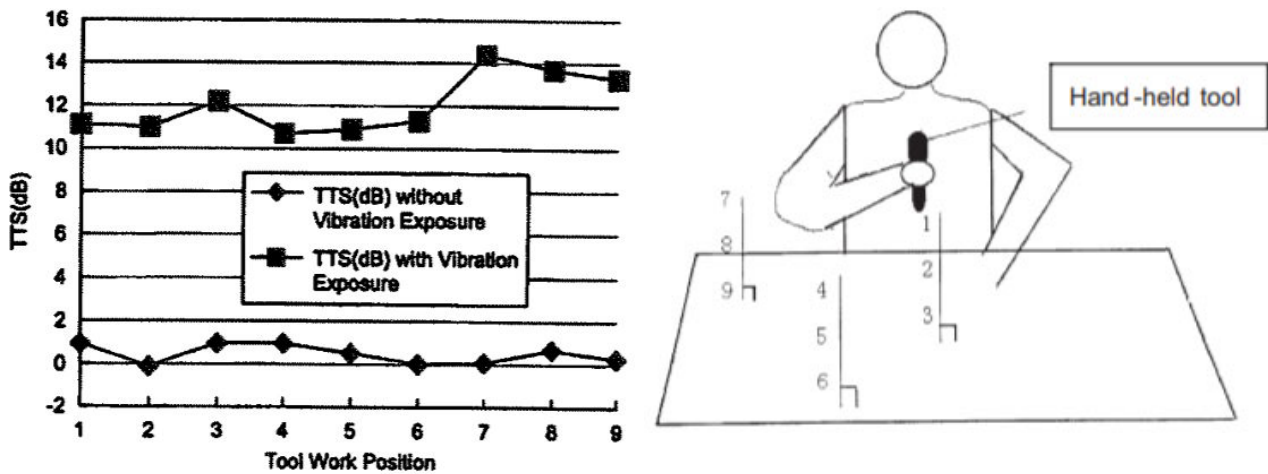
Figure 4. Comparison of TTS vs. different position with the same vibration magnitude. On the left, TTS results obtained for each of the positions. On the right, a diagram depicting the 9 positions used.

Figure 4 shows the changes in TTS with different postures, while the vibration magnitude, measured according to ISO 5349-1, remained unchanged. These results mean the hand-transmitted vibration was different and translated into varying physiological effects. Therefore, in order to predict the impact of posture at the different positions on the human response, equipment or considerations outside ISO 5349 may be required.

4.3   Coupling forces

In this study (Maeda et al., 2007), the effect of coupling action and frequency was assessed using TTS for subjects exposed to a constant ISO-weighted acceleration (8 m/s^2 rms) under a grip-only action and a combined grip and push action at 16 and 125 Hz. The experiments were performed with twelve healthy subjects; six American males and six Japanese males with mean ages of 23.5 and 24.5 years old, respectively. All the subjects were non-smokers. None of the subjects had been exposed to high levels or long periods of HAV occupationally or in their leisure time activities. The experiments were approved by the Research Ethics Committee of Japan NIOSH and US NIOSH.

As shown in Figure 5A, the vibration exposure test apparatus consisted of an electro-mechanical shaker mounted horizontally on a table, a closed loop controller, a power amplifier, an instrumented handle, and a data acquisition system. The instrument handle consisted of two parts; the base and the measuring cap. Two force sensors were placed between the two parts along the centreline of the handle and were used to measure the grip and dynamic response forces. An accelerometer was positioned on the measuring cap at the centre point of the handle to measure the vibration amplitude of the handle. A force plate was used to measure the applied push force. Similar apparatuses were setup in Japan NIOSH and US NIOSH. Two different systems were used to determine the TTS – the RION system for the Japanese subjects and the HVLab system for the American subjects. Following the 5 minutes exposure the shaker was turned off and the test subject immediately returned to the vibration perception test apparatus to get ready for the TTS testing. Beginning at 30 seconds following the completion of the vibration exposure, the TTS was continuously measured for 30 seconds at the corresponding exposure frequency (either 16 or 125 Hz). Following the first TTS measurement, additional TTS measurements were taken at 2.5, 4.5, 6.5, and 8.5 minutes, as well as at 10 minutes for the Japanese. The test subjects were given a 30-minute rest period to allow for the effects of the vibration exposure to wear off. Following the rest break, another 30-second vibration perception threshold measurement was performed and was used as a new baseline for the next test treatment. A balanced design of the testing order of the six exposure treatments among each group of subjects was used in this study. The tests were performed over a two-day period.
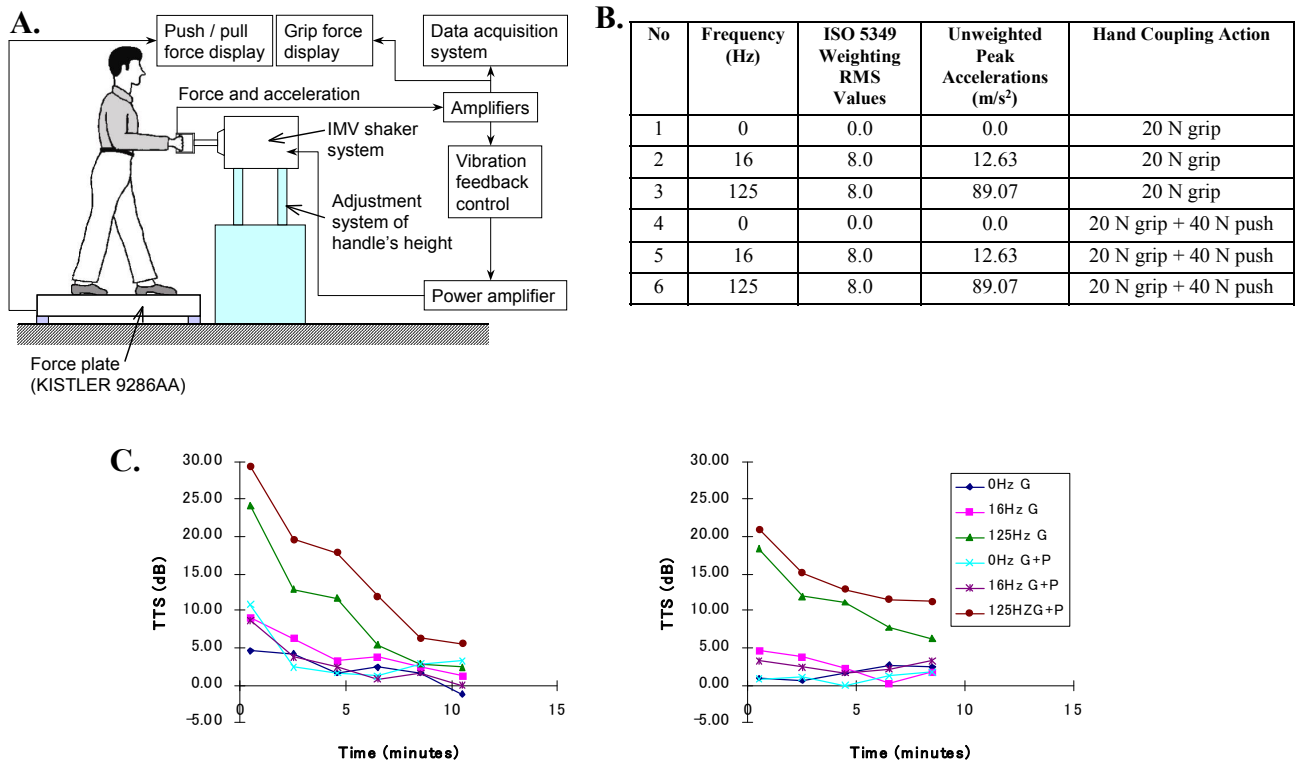
No	Frequency (Hz)	ISO 5349 Weighting RMS Values	Unweighted Peak Accelerations (m/s^2)	Hand Coupling Action
1	0	0.0	0.0	20 N grip
2	16	8.0	12.63	20 N grip
3	125	8.0	89.07	20 N grip
4	0	0.0	0.0	20 N grip + 40 N push
5	16	8.0	12.63	20 N grip + 40 N push
6	125	8.0	89.07	20 N grip + 40 N push

Figure 5. Comparison of TTS vs. different coupling forces, including the experimental setup (A), conditions tested (B) and results obtained for both groups (C).

As shown in Figure 5, the TTS at the test frequency of 125 Hz differs due to coupling action even though the frequency-weighted rms acceleration magnitude was the same value. It is clear that the TTS was affected by the coupling action at the higher frequency. The trends are similar between the Japanese and American subjects; however, the ranges of TTS are different. The Japanese subjects start with higher threshold shifts but end the tests closer to the baseline measurements. Despite the same frequency-weighted rms acceleration values, the TTS of VPT were affected by the coupling action, indicating that the coupling action affects a worker's physiological response to vibration exposure. Based on these results, the authors suggested that the coupling action be taken into account to assess the risk of the hand-transmitted vibration exposure.

During the study vibration measurements on the tool handle following ISO5349-1 did not vary with different coupling action, while the TTS varied as shown in Figure 5. These results mean the hand-transmitted vibration were different with the different coupling force levels.

4.4   Individual subjects

Maeda et al (Maeda et al., 2019) studied the relationship between the current ISO5349-1 and ISO5349-2 standard measurement results and the human response to vibration, as indicated by a measurement of TTS in VPT with different subjects.

The research demonstrated that while the measurement of vibration on the tool handle following ISO5349-2 was essentially constant, the TTS in VPT for individual subjects showed a wide range of values.   Prior research has determined that increasing TTS measurements corresponded to an increasing level of hand-arm vibration magnitude. From the results in Figure 6, the hand-transmitted vibration exposure is increasing across the subject group. However, measurement on the tool handle following ISO 5349-2 appears to not reflect the hand-transmitted vibration through from the handle to the human.
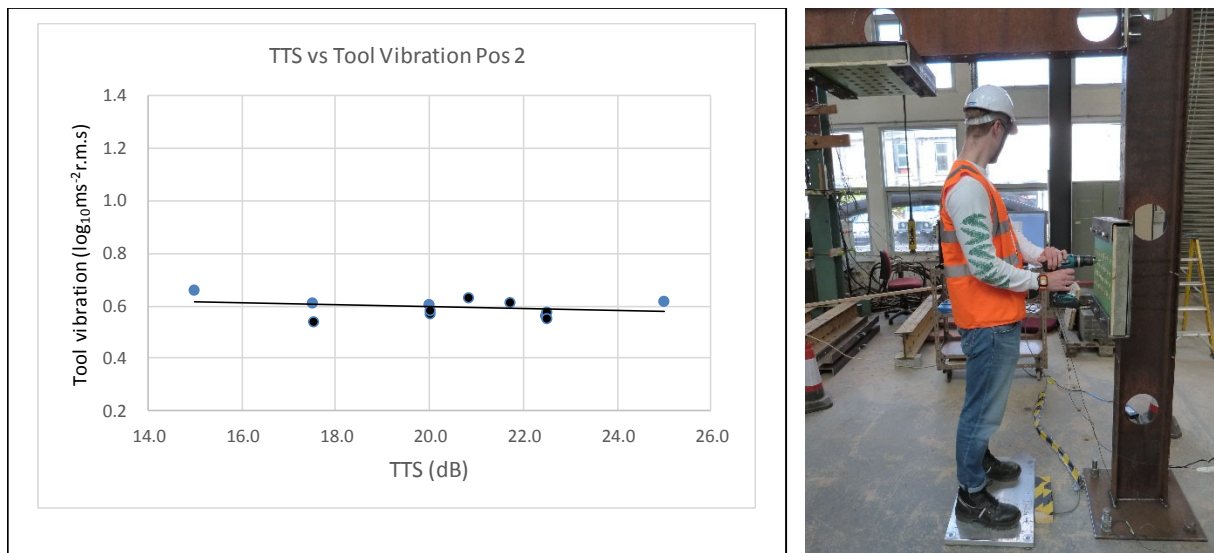
Figure 6. Comparison of TTS vs. tool vibration magnitude in several subjects, operating tools in the position illustrated on the right side of the figure.

5 DISCUSSION

The four studies above highlight that a measurement of vibration magnitude on a tool handle may not represent the hand transmitted vibration to the worker. The major part of historic research into the human response to vibration has been based on measurement of vibration on the tool handle without including the affecting factors of Annex D of the ISO5349-1 standard. This historic research has established a vibration daily dose, the $A(8) = a_{hv}\sqrt{t/8}$, as a method of assessing the likely risk of progression of HAVS as a disease. Regulators have adopted the daily dose as an administrative control to establish safe working conditions such as guidance released by the UK's Health and Safety Executive HSE (Health and Safety Executive (HSE), 2019). Assessments of daily dose based only on measurements on the tool handle are unlikely to include all the factors which affect the vibration transmitted through to the hand and arm from the tool handle.

It should be noted that historic research was limited by the availability of equipment only really suited for short duration measurements of vibration on the handle of the tool. Equipment which could not discern the factors included in Annex D of ISO 5349-1 very easily to directly measure the hand transmitted vibration. Research has therefore been dominated by the simple measuring method on the tool handle to evaluate the hand-transmitted vibration. Leading to potentially inadequate controls have being determined to manage workers risk with assessments made without consideration of the factors of Annex D of ISO5349-1.

It may be possible to determine a better relationship between the hand-transmitted vibration (including the affecting factors of Annex D of ISO5349-1 standard) and the human response to vibration if a more direct measurement of the hand transmitted vibration in the real work place, such as figure 1 depicts, can be achieved. Researchers have shown the effects, such as the transmissibility, coupling forces, postures, and so on, without being able to identify a means of determining the hand transmitted vibration inclusive of these effects. A direct measurement of the vibration transmitted to the hand and arm which can be gathered during normal work is required.

The dose from a measurement following ISO5349-1 and ISO5349-2 does not relate fully with the human response to vibration with different subject in the workplace under the varied conditions of the workplace. Therefore, this value is not ideal for workplace exposure risk management. The experiments here presented show results in which, the human response to vibration as indicated by a measurement of TTS, varied depending on four different factors in a manner which was very inconsistent with a measurement of vibration taken in accordance with ISO5349 taken on the tool handle. This means the vibration magnitude on the tool handle will not fully account for workplace exposure risk. Therefore, in order to prevent HAVS in the workplace, consideration should be given to personal exposure risk management of the individual worker instead of the workplace exposure risk management.

Maeda et al [16] examined a wearable sensor for determining hand-transmitted vibration magnitude as part of personal exposure risk management. The authors showed the hand-transmitted vibration magnitude equations on the human by the following equations:

$$a_{hx}(t) = a_x(t)H_{FW}Ha_xHb_xHc_xHd_xHe_xHf_xHg_xHh_xHi_xHj_xHk_xHl_x$$

$$a_{hy}(t) = a_y(t)H_{FW}Ha_yHb_yHc_yHd_yHe_yHf_yHg_yHh_yHi_yHj_yHk_yHl_y$$

$$a_{hz}(t) = a_z(t)H_{FW}Ha_zHb_zHc_zHd_zHe_zHf_zHg_zHh_zHi_zHj_zHk_zHl_z$$

where a_x, a_v, a_z are the vibration levels emitted by the tool, a_{hx} a_{hv} a_{hz} are hand-transmitted vibration levels, H_{FW} represents the ISO 5349-1 frequency weighting and Ha,b,…l are the weighting factors identified within ISO 5349 Annex D.

Further collaborative research is required to move this work forward and be appropriately considered by the standards authorities.

6   CONCLUSIONS

In this study, a body of research has been reviewed to highlight the limitations of using assessments of daily exposure to HAV as a means of safely controlling workers activities based on vibration magnitude data from measurements on a tool handle following ISO5349-1. Research work into factors influencing the human response to vibration as determined by the measurement of the temporary threshold shift in vibrotactile perception strongly indicate that dose estimations based on vibration magnitude from the tool grip point do not take into account important factors. These factors which limit the appropriateness of measurements taken on the tool handle are highlighted in annex D of ISO53490-2.

The availability of more practical sensor technologies should drive a review of current standards to address the limitations of ISO5349 and establish a more direct measurement of hand transmitted vibration which better correlates with human response in order to improve the suitability of assessments against which workplace controls are designed.

7 BIBLIOGRAPHY

Gandhi, M.S., Sesek, R., Tuckett, R., Bamberg, S.J.M., 2011. Progress in Vibrotactile Threshold Evaluation Techniques: A Review. J. Hand Ther. 24, 240–256. https://doi.org/10.1016/j.jht.2011.01.001

Health and Safety Executive (HSE), 2019. Hand-Arm Vibration: The Control Of Vibration At Work Regulations 2005, L140. HSE Books.

International Organization for Standardization, 2005. ISO 8041:2005 [WWW Document]. ISO 80412005. URL http://www.iso.org/cms/render/live/en/sites/isoorg/contents/data/standard/03/01/30145.html (accessed 6.6.19).

International Organization for Standardization, 2003. ISO 19091-2:2003 [WWW Document]. ISO 19091-22003. URL https://www.iso.org/standard/27716.html (accessed 6.6.19).

International Organization for Standardization, 2001a. ISO 5349-1:2001 [WWW Document]. ISO 5349-12001. URL http://www.iso.org/cms/render/live/en/sites/isoorg/contents/data/standard/03/23/32355.html (accessed 6.6.19).

International Organization for Standardization, 2001b. ISO 5349-2:2001 [WWW Document]. ISO 5349-22001. URL https://www.iso.org/standard/27511.html (accessed 6.6.19).

International Organization for Standardization, I., 2001. ISO 13091-1:2001, Mechanical vibration -- Vibrotactile perception thresholds for the assessment of nerve dysfunction -- Part 1: Methods of measurement at the fingertips. Multiple. Distributed through American National Standards Institute.

Maeda, S., Shibata, N., 2008. Temporary threshold shifts (TTS) of fingertip vibrotactile perception thresholds from hand-held tool vibration exposures at working surface. Int. J. Ind. Ergon. 38, 693–696. https://doi.org/10.1016/j.ergon.2007.10.005

Maeda, S., Shibata, N., 2007. Problem of A(8) Evaluation. Presented at the 15th Japan conference on Human Response to Vibration, Japan.

Maeda, S., Shibata, N., Welcome, D.E., Dong, R.G., 2007. Effect of coupling action on temporary threshold shift (TTS) of vibrotactile perception, in: Proceedings of 11th International Conference on Hand-Arm Vibration. Presented at the 11th International Conference on Hand-Arm Vibration, Bologna.

Maeda, S., Taylor, M.D., Anderson, L.C., McLaughlin, J., 2019. Determination of hand-transmitted vibration risk on the human. Int. J. Ind. Ergon. 70, 28–37. https://doi.org/10.1016/j.ergon.2019.01.002

Malinskaya, N.N., Filin, A.P., Shkarinov, L.N., 1964. Problem of occupational hygiene in operating mechanized tools. Vestnik Academy of Medical Science U.S.S.R.

Mansfield, N.J., 2004. Human Response to Vibration. CRC Press.

Radziukevich, T.M., 1969. Interrelationship between temporary and permeanent shifts in the threshold of vibration and pain sensitivity under the effect of local vibration. Gig. Tr. Prof. Zabol. 13, 20–23.

Shibata, N., Maeda, S., 2008. Effect of tool handle diameter on temporary threshold shift (TTS) of vibrotactile perception. Int. J. Ind. Ergon. 38, 697–702. https://doi.org/10.1016/j.ergon.2007.10.006

Temporary Threshold Shift - PubMed - NCBI [WWW Document], n.d. URL https://www.ncbi.nlm.nih.gov/pubmed/?term=Temporary+Threshold+Shift (accessed 9.12.19).

Vibrotactile Perception Thresholds - Google Scholar [WWW Document], n.d. URL https://scholar.google.co.uk/scholar?hl=en&as_sdt=0%2C5&q=vibrotactile+perception+thresholds&btnG=&oq=Vibrotactile+Perception+Threshold (accessed 9.12.19).

Human machine interactions and the human response to vibration

Leif Anderson [1], Francisco Diaz [1]
Reactec Ltd.
Vantage Point, 3 Cultins Road, EH11 4DF, Edinburgh, UK
leifanderson@reactec.com, franciscodiazmayoral@reactec.com

Setsuo Maeda [2]
Nottingham Trent University, School of Science and Technology
Clifton Lane, NG11 8NS, Nottingham, UK
setsuo.maeda@ntu.ac.uk

Mark D. Taylor [3]
Edinburgh Napier University, School of Engineering and The Built Environment
10 Colinton Road, EH10 5DT, Edinburgh, UK
m.taylor@napier.ac.uk

ABSTRACT

Prolonged occupation exposure to a vibration source at the hands can result in a disease known as hand-arm vibration syndrome. As the condition is irreversible, all current efforts to combat this disease involve the reduction of vibration exposure through risk assessment and health surveillance of those at risk. The current standard for vibration assessment (ISO 5349) introduced a method of vibration measurement based on the placement of sensors on the tool handle, however a multitude of factors recognised within the standard exist which can affect actual vibration exposure to the individual. This study investigates the effect of one of these factors; operator posture, its impact on hand transmitted vibration and the relationship between the assessment method and an evaluation of the human response to that vibration. By evaluating the human response to vibration and complementing the standardised method with a wearable sensor device, the authors demonstrate the effects of posture on human vibration exposure in a typical civil engineering application and evaluate the relative significance of this phenomenon in different scenarios.

1   INTRODUCTION

Hand-arm vibration syndrome (HAVS) is an industrial disease caused by prolonged exposure to a source of vibration affecting the hands of an individual, such as sustained occupational exposure to mechanised vibrating tools. This condition manifests with neurological, vascular and musculoskeletal symptoms. Some of the most characteristic symptoms include finger blanching, pain, loss of dexterity, numbness, dysesthesia and paraesthesia. (Mansfield, 2004).

HAVS presents itself as a progressive and irreversible condition, and as such, prevention and accurate assessment of exposure constitute the only tools currently available to deal with the disease. As a condition predominantly linked to occupational exposure, the currently established method for assessment of the vibration exposure and disease progression is standardised and contained in the ISO 5349 document (International Organization for Standardization, 2001a). Following this standard, vibration exposure is assessed based on determining the duration of exposure and through the placement of sensors on the tool handle to measure acceleration magnitude at this position. This measurement is commonly accepted as the hand-arm vibration magnitude and used as a unique magnitude (together with exposure time) to assess the risk perceived by a tool operator.

1.1 Factors affecting vibration exposure and posture effects

However, clause 4.3 of ISO 5349-1 states that although the standardised method of vibration assessment involves the measurement of vibration at the tool surface, it is reasonable to assume that the resulting biological effects depend to a large extent on the coupling between the hand and the vibration source.

Furthermore, Annex D in the same document acknowledges and identifies the presence of multiple factors that affect the exposure to hand-transmitted vibration in the real work environment. Some of these factors include the direction of the vibration, skill and working method, individual constitution, hand and body posture, or coupling forces. In order to achieve an accurate assessment of vibration exposure, the contribution of these factors will have to be characterised and fully understood.

This study focuses on determining the effect of posture on the vibration exposure to the operator in an applied environment where desired posture may be affected by other factors such as operator physiology. With the incorporation of some of the known limitation outlined within Annex D by replicating a real work environment for the experiment the authors seek to illustrate their significance in the context of risk management. To evaluate both the effect on tool emitted vibration and the effect on vibration transmitted to the individual it is desirable to include both a standardised on-tool measurement in accordance with ISO 5349 and a modern wearable sensor, worn on the subject.

The motivation to consider a wearable device within the study arises from the commonly accepted notion that the standard method for calculating exposure requires a skilled technician and a controlled environment to execute a repeatable assessment. In practise, a measurement spanning minutes is unlikely to capture the variability in day-to-day tasks undertaken by tool operators in different activities and industries. The CEN technical report CEN/TR 15350 (British Standards Institution, 2013) identifies the difficulty in capturing all the factors affecting the vibration level of a tool and recognise the expense of doing so, advising that a range of factors would need to be considered to make an ideal assessment of vibration exposure.

1.2 Vibrotactile perception threshold

Vibrotactile perception threshold (VPT) is defined in ISO standard 13091-1 (I. International Organization for Standardization, 2001) as the skin surface acceleration capable of triggering a 50% response rate for detection by the individual. This minimum threshold for detecting vibration in the fingertip has often been used as a diagnostic technique to assess neurological damage in HAVS (Radziukevich, 1969).

Existing research links the temporary threshold shift (TTS) in the VPT after short durations of acute vibration exposure with the long-term permanent threshold shift that would develop over a longer period of time with a similar exposure (Malinskaya et al., 1964). For this reason, TTS may be used as an indicator of risk to the human subject arising from interaction with a specific vibration source.

Based on this body of research, TTS is used during the present study as an indicator of the human response to a period of vibration exposure. Vibration measurements, both at the tool and on the subject, will be compared with this indicator to determine the effectiveness of such methods at predicting the human response to the vibration and the potential risk for HAVS development.

2   MEASUREMENT OF HAND-ARM VIBRATION ON THE SUBJECT

The wearable device used in the study (HVW-002, Reactec Ltd.) is mounted in the wrist of the subject by means of a nylon webbing strap and adjusted using a velcro arrangement in the strap. The orientation of the device is controlled by aligning the flat surface of the device with the wrist of the operator, in such a direction that the wearer will be able to read the display on the device.

This device includes a triaxial accelerometer, implemented through a MEMS device (LIS3DSH, ST Microelectronics). The operation range of this accelerometer is limited to ±8g, and the recommended temperature range is -40ºC and +85ºC.

This accelerometer captures the vibration on the wrist at a sampling frequency of 1.6kHz, to allow for a total captured frequency range between 0Hz and 800Hz. Acceleration data from each axis is captured and processed sequentially by converting from time domain to frequency domain through a 1024-point Fourier analysis incorporating a Hanning window function. At the specified sampling frequency of 1.6kHz, 1024 samples are captured in a total of 0.64s. Samples are captured in cycles of 1.5s, and the remaining 0.86s are used by the device to process the previously obtained sample.

The 1024-point FFT results in a total of 512 power spectrum coefficients in the 0-800Hz frequency range. However, only data within the 0-650Hz is processed, discarding the coefficients 417 to 512. In equations 1 to 3 the coefficient 'i' represents the frequency coefficient index, with values between 0 and 416. Conversely, the coefficient 'n' represents each of the samples, one captured every 1.5s, which increases in relation to the total duration of the tool vibration recording.

For each sample, the sum of the frequency weighted FFT magnitude values for each of the axes is calculated, using equations 1 to 3 for each (n) frame:

$$a_{rhx}(n) = \sqrt{\sum w_{rhx}(i)^2 \cdot a_{hx}(n,i)^2} \tag{1}$$

$$a_{rhy}(n) = \sqrt{\sum w_{rhy}(i)^2 \cdot a_{hy}(n,i)^2} \tag{2}$$

$$a_{rhz}(n) = \sqrt{\sum w_{rhz}(i)^2 \cdot a_{hz}(n,i)^2} \tag{3}$$

Where w_{rhx}, w_{rhy} and w_{rhz} are frequency weighted transfer functions specifically designed to account for the transmissibility of the hand-wrist system and replicate the ISO 5349-1 weighting function. $a_{hx/y/z}$ defines each of the 417 coefficients that belong to a given frame, which are weighted and combined to obtain a unique magnitude $a_{rhx/y/z}$ for each axis. These transfer functions were determined by the manufacturer in a separate piece of research. (Maeda et al., 2019).

For each of the three axes, a running average is determined independently after each frame *n*, using the equations 4 to 6, respectively:

$$a_{rhx} = \sqrt{\frac{\sum_n a_{rhx}(n)^2}{n}} \tag{4}$$

$$a_{rhy} = \sqrt{\frac{\sum_n a_{rhy}(n)^2}{n}} \tag{5}$$

$$a_{rhz} = \sqrt{\frac{\sum_n a_{rhz}(n)^2}{n}} \tag{6}$$

Finally, the running averages of the three axes are combined using equation 7, in order to determine the overall vibration magnitude over the duration terminated by (n):

$$a_{rhv} = \sqrt{a_{rhx}^2 + a_{rhy}^2 + a_{rhz}^2} \qquad (7)$$

3 EXPERIMENTAL METHODOLOGY

3.1 Test Subjects

In order to study the effect of vibration on the human body, a total of 12 male subjects with no previous history of vibration exposure participated in the study. All participants were non-smokers with an age range restricted between 20 and 31 years of age (mean = 22.2 and standard deviation = 3.2) to minimise the effect of age on subject response to vibration (Venkatesan et al., 2015). In accordance with ISO 13091-1 (I. International Organization for Standardization, 2001), the participants were not allowed to smoke, consume caffeine or alcohol during the duration of the experiment.

All participants wore steel toe-capped safety boots with a rubber outsole, complying with ISO 20345:2011 (International Organization for Standardization, 2011). In order to minimise additional factors affecting the human-tool interface, no gloves were worn during the tests. Screening was undertaken to ensure that all participants were clear of medical conditions and occupational history that would have an impact upon the test results. The experiment was approved by the Edinburgh Napier University research ethics committee, all subjects were willing volunteers and individual consent was obtained prior to commencing the experiments.

3.2 Vibrotactile temporary threshold shift

TTS is defined as the difference, expressed in dB, in the vibrotactile threshold before and after exposure to vibration (Maeda and Griffin, 1993; Yonekawa et al., 1998). Testing was limited to two sessions per day for each operator, in order to allow a minimum of 4h of rest between each test. The expression used to calculate TTS was:

$$TTS\ (dB) = VPT_A - VPT_B \qquad (8)$$

Where VPT_B corresponds to the baseline vibrotactile perception threshold before the vibration exposure and VPT_A is the vibrotactile perception threshold after the exposure.

Vibrotactile sensitivity VPT_B was obtained 3 min prior to the start of the tool activity, and VPT_A within 30 seconds after the test was completed. A vibrotactile sensation meter (RION type AU-02A) was used for the assessment of the vibrotactile perception threshold, by delivering pulses of 125Hz and varying intensities to the tip of the index finger. To ensure consistency, subjects were asked to maintain a constant force of 2N with their index finger, as measured using a digital scale connected to a display. VPT was determined by gradually adjusting the intensity of the pulses, and recording the minimum intensity at which the stimulus became perceptible. Three measurements were obtained within a 30 second frame, and the final result for each individual and test is obtained by averaging these three results.

Ambient temperature within the test laboratory was maintained at 20 °C ± 4 °C for the duration of all tests, verified using a Grant 2020 Series Squirrel data logger with four thermocouples. Subject fingertip temperature was measured and recorded during each TTS assessment. This was undertaken using a thermocouple attached to a digital display (RS 206–3738). If the subject's fingertip temperature was lower than 23 °C, the subject was instructed to warm their finger such that throughout the experiment, all subject's fingertip temperature was maintained at greater than 25 °C.

The effect of fingertip temperature has been previously characterised by previous research (Harada and Griffin, 1991), and should be kept constant to avoid external variance in the results.

3.3   Test procedure

In order to study the effects of posture on vibration exposure, a total of 8 test conditions were considered, composed by the combination of 4 tools and 2 working postures. The tools used to generate the vibration exposure during the study and their relevant mechanical properties are detailed in Table 1. All of these tools are rotary demolition hammers, used in their hammer drill configuration to produce holes in a block of concrete.

Table 1: Tools used in the experiment

	Tool 1	**Tool 2**	**Tool 3**	**Tool 4**
Manufacturer	Makita	Makita	Milwaukee	Bosch
Model	HR4011C	HR4011C	Kango 950 SDS	GBH 11 DE
Blows per minute	1350	2750	1950	2250
Mass [Kg]	6.3	6.3	11.8	11.1
Declared vibration magnitude [m/s^2]	4.5	4.5	11.0	24.0
Declared uncertainty [m/s^2]	1.5	1.5	2.0	1.5
Blow energy [J]	6.2	6.2	20	18

The two working postures considered are depicted in Figure 1. The first posture involves drilling downwards into a block of concrete, with the weight of the tool resting on the drill bit and the operator merely guiding the tool. The second posture involved drilling horizontally into concrete, with the weight of the tool born by the operator and significant force applied against the substrate in order to maintain the hammer action.
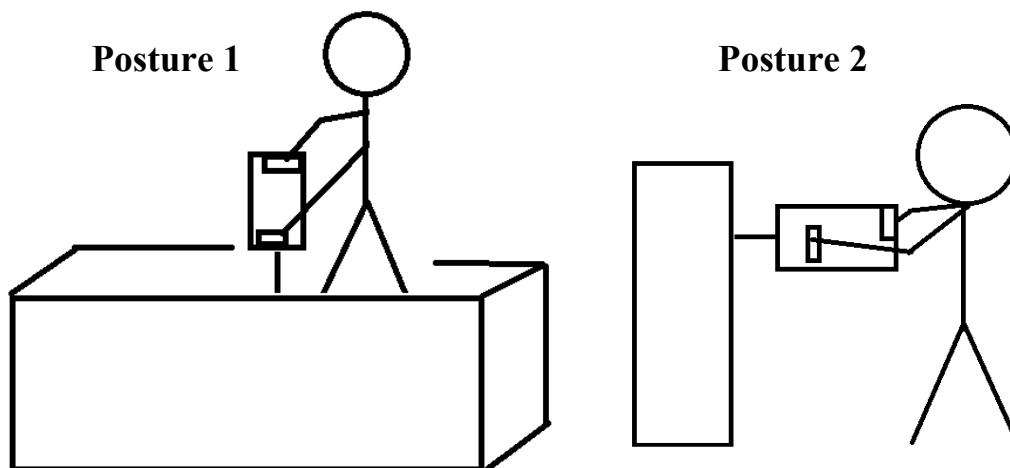
Figure 1: Working postures studied during the experiment. Posture 1 (left) involved vertically drilling into a block of concrete, while Posture 2 (right) had the operator drilling horizontally.

Vibration data was obtained from accelerometers mounted on the tool handle, according to the specifications of ISO 5349-1 and ISO 5349-2 (International Organization for Standardization, 2001a, 2001b), and the obtained signals were processed in compliance with the standards. Two sensors were used: a Svantek SV106 and a Brüel & Kjær 4520-001, both compliant with ISO8041 standard (International Organization for Standardization, 2005). Furthermore, the subjects wore a wrist mounted wearable device (HVW-002, Reactec Ltd.) to capture vibration data concurrently with the on-tool sensors.

A test was performed for each of the participants, and each of the tool/posture combinations. The test procedure for each one of the individual tests is depicted in Figure 2. Vibrotactile perception was assessed 3 minutes prior to the vibration exposure, and subjects were instructed to operate the corresponding tool in the indicated position for a total of 2 minutes continuously. Within 30 seconds of finishing the tool operation, the VPT of the subject was measured again. In order to avoid interference between tests. A minimum of 4 hours was allowed between two tests for any given subject.

All subjects were given induction training on how to operate and grip each tool. However, subjects were not experienced tool operators and demonstrated a degree of variability in tool operation performance.
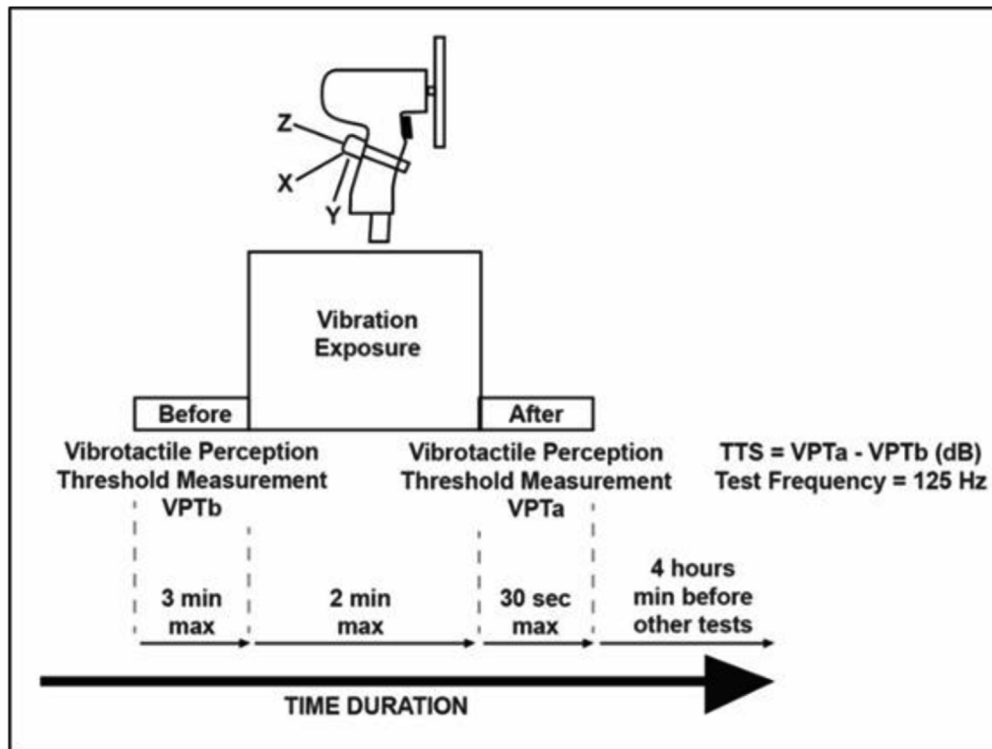
Figure 2: Test procedure sequence for each of the individual tests. One test was performed for each of the subjects, and each of the tool/posture combinations

4   RESULTS AND DISCUSSION

With 12 participants each performing tests with 4 tools in two separate body postures, the total number of tests conducted for the experiment was 96. Two tests were discarded from further analysis due to displacement of the sensors on the tool handle. Every test included two minutes of continuous tool operation, preceded and followed by measurements of VPT. All of the vibration results obtained are detailed in Table 2.

Table 2: All results obtained during the study, grouped by posture and tool.

		On-tool vibration [m/s²]		On-subject vibration [m/s²]		TTS [dB]	
		Mean	S.D.	Mean	S.D.	Mean	S.D.
Tool 1	Posture 1	5.3	0.6	7.3	1.9	13.3	1.6
	Posture 2	5.5	0.7	8.0	1.6	14.0	3.1
Tool 2	Posture 1	9.0	0.9	10.4	1.8	14.2	2.7
	Posture 2	8.3	1.5	10.9	1.9	14.7	2.1
Tool 3	Posture 1	15.6	2.0	19.0	4.0	16.6	4.0
	Posture 2	10.6	1.3	14.7	3.9	12.7	2.9
Tool 4	Posture 1	17.3	1.9	24.9	5.0	16.0	3.2
	Posture 2	12.2	2.0	19.7	5.3	14.1	2.5

4.1 Inter-operator effects on vibrations

One of the primary motivations for adoption of monitoring technology capable of gathering data on an individualised fashion lies in the limitations of using a single vibration magnitude value to accurately predict vibration exposure. Whether the applied vibration magnitude value comes from a manufacturer declared value or from an ISO 5349-1 compliant measurement, it is hypothesised that this value will be hard to extrapolate to every scenario in a work environment. Factors likely to preclude such an effective extrapolation are in fact listed within Annex D of ISO 5349-1. In particular physicality and technique of the operator is listed as likely to affect the vibration transmitted to the individual.

Figure 3 offers a graphical representation of the vibration magnitude distributions obtained for each tool across the cohort of operators. Both measurement methods, on the tool and on the subject reveal a spread in the vibration magnitudes detected. It can be observed that for each of the tools, the emitted vibrations fall within a wide range instead of a single constant value. There is a notable difference between tools 1 and 2, with a lighter weight, lower energy output and easier operation; and tools 3 and 4, heavier, more powerful and more technique dependent. This is noteworthy as the investigators selected tools which were broadly considered to be similar and would all be considered suitable for the test activities and could reasonably have been hired under the same class of tool from tool hire centre. In the case of the first two tools, the spread observed is narrower, which combined with overall lower vibration magnitudes translates into a reduced risk of incorrect vibration estimation. However, the heavier and higher impact energy tools 3 and 4 show a large spread between operators, combined with higher overall vibration magnitudes. In both tools, regardless of the measurement method, the operator with the highest vibration levels is exposed to more than twice the vibration magnitude received by the operator with the lowest vibration.

These results reveal the difficulty of accurately assessing the exposure risk which a tool operator may be exposed by using a single magnitude for a given tool, and the potential advantage of real time vibration assessment on an individual basis.
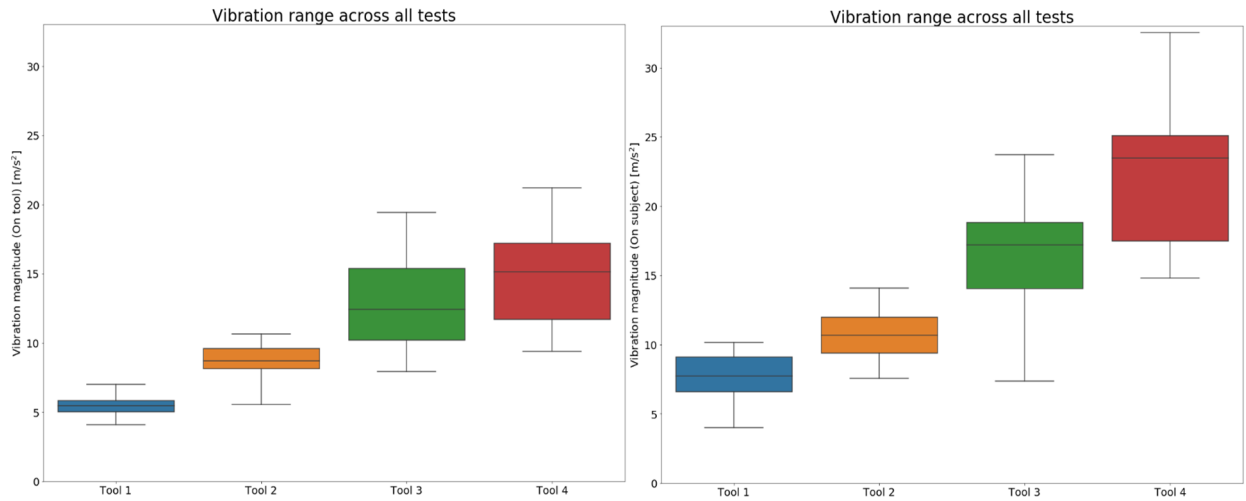
Figure 3: Inter-operator vibration distributions for all tests, expressed in the form of boxplots for each of the tools used in the experiment. To the left, the vibration values obtained from the tool handle. On the right, the same results obtained using a wearable device.

4.2 Effect of posture on vibration magnitude

The obtained results were analysed to determine how a change in working posture affects the vibration levels that affect the operators. The distribution of vibration magnitudes, categorised by tool and posture, is illustrated in Figure 4.
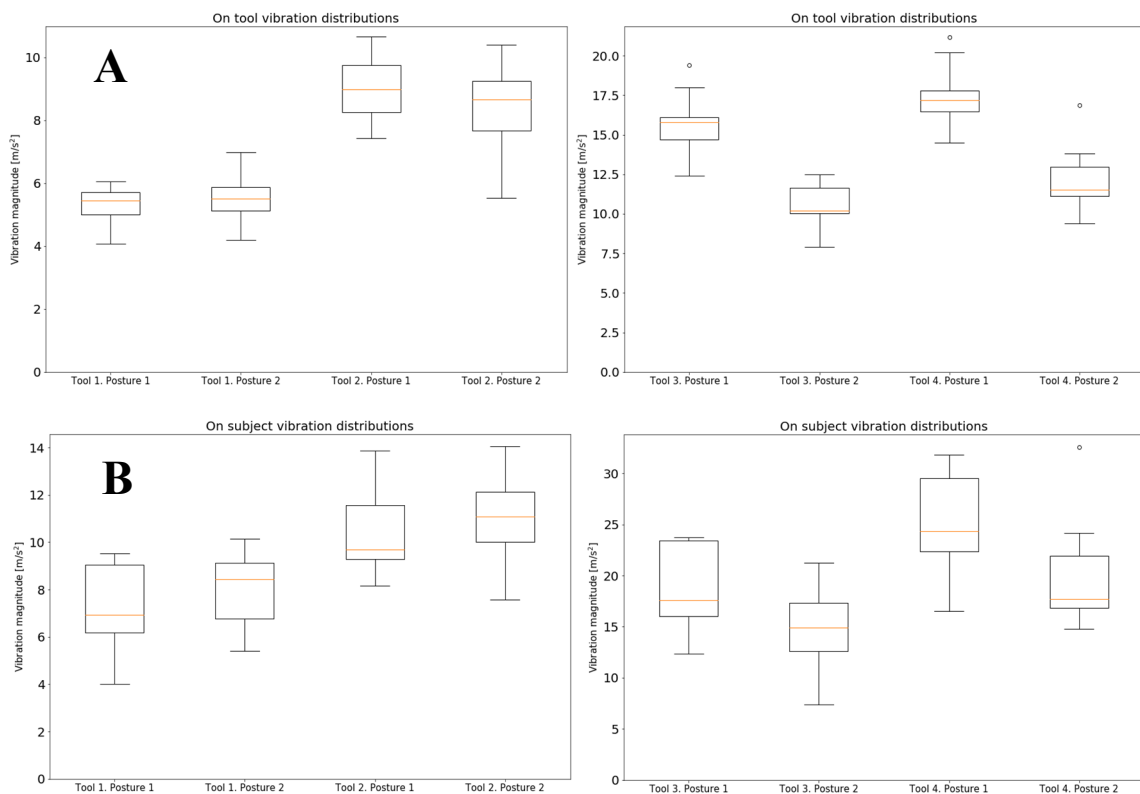
Figure 4: Vibration magnitude distributions for each of the tools and operator postures, as measured (A) on the tool handle and (B) on the subject wrist.

When comparing the vibration magnitudes for each of the postures, some effects become evident. The first consideration is that, for a given tool, there are significant changes in the vibrations produced depending on the operator posture. Moreover, both measuring techniques are capable of

detecting these changes in vibration magnitude. These findings reinforce the ideas included in Annex D of ISO5349-1 and challenge the validity of a single magnitude value for accurate risk assessment of the operators. Existing research (Maeda and Shibata, 2008, 2007) studying the effect of posture on human physiological response to vibration is consistent with these results, and found that operator posture can translate into changes in hand-transmitted vibration.

A second interesting result concerns the specific direction of change with the posture. For tools 1 and 2, lighter and easier to use, the transition between a downward posture (posture 1) and a horizontal posture (posture 2) translates into an increase in the vibration generated by the tool. The exception of on-tool measurements for tool 2 will be discussed in the following section. In contrast to this trend, the heavier tools 3 and 4 show an inverse pattern. The transition between the downward posture and the horizontal posture translates into a decrease in the measured vibration. The significance of this finding lies in the fact that the interaction between posture and vibration is not unique or easily predictable. This is relevant in the eyes of the investigators as it will preclude any attempt to account for posture effects when basing any risk assessment on a fixed vibration value.

Finally, it is interesting to study how these changes in vibration magnitude translate into the work exposure of an operator. When considering the changes in vibration magnitude due to posture, as measured on the subject, the change from the vertical to the horizontal posture translates into a -4.6% change in the time required to achieve an A(8) level of $2.5m/s^2$ for Tool 1, and +14.4% for Tool 2. While these may not heavily alter acceptable work period for an operator, when observing the heavier tools and the same change in posture, the time required to reach an A(8) level of $2.5m/s^2$ is reduced by -53.8% with tool 3 and -50.8% for tool 4, reducing the potential work performance of an operator by more than half. The presented changes in operation time have been calculated based on On Tool magnitude values, but very similar results are obtained when considering On Subject measurements. These significant results, which are illustrated in Figure 5, reveal that accurate knowledge of the effects of posture on operator exposure to vibration can be crucial both in ensuring operator health and maximising worker productivity.
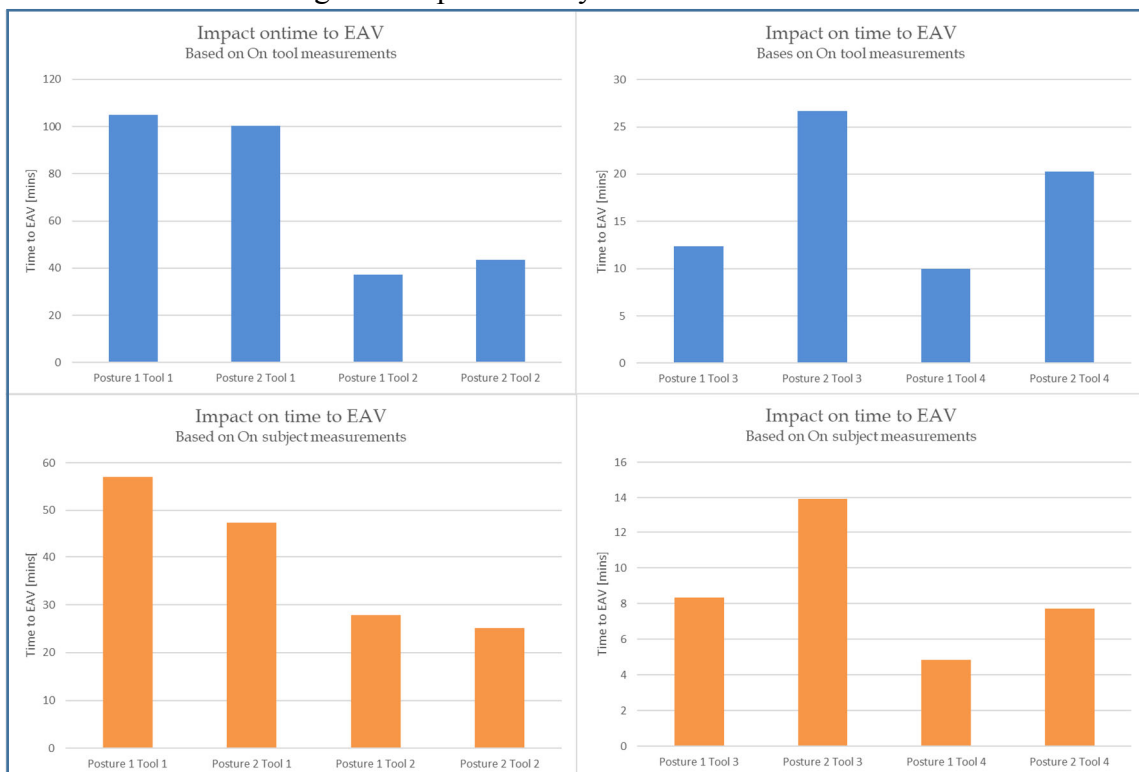
Figure 5: Changes in work time to EAV when considering different tools and both On Tool and On Subject measured vibration magnitudes

4.3 Posture effects on human physiological response

In this study, the human response to vibration is assessed through testing of the temporary threshold shift (TTS) of the vibrotactile perception threshold (VPT). This test has for decades been established as a method to determine the energy absorbed by the operator and to diagnose the risk for long-term neurological damage (Malinskaya et al., 1964; Radziukevich, 1969).

The vibration magnitude measurements for each tool/posture combination were compared against the obtained TTS after their respective tests, and are detailed in Figure 6.
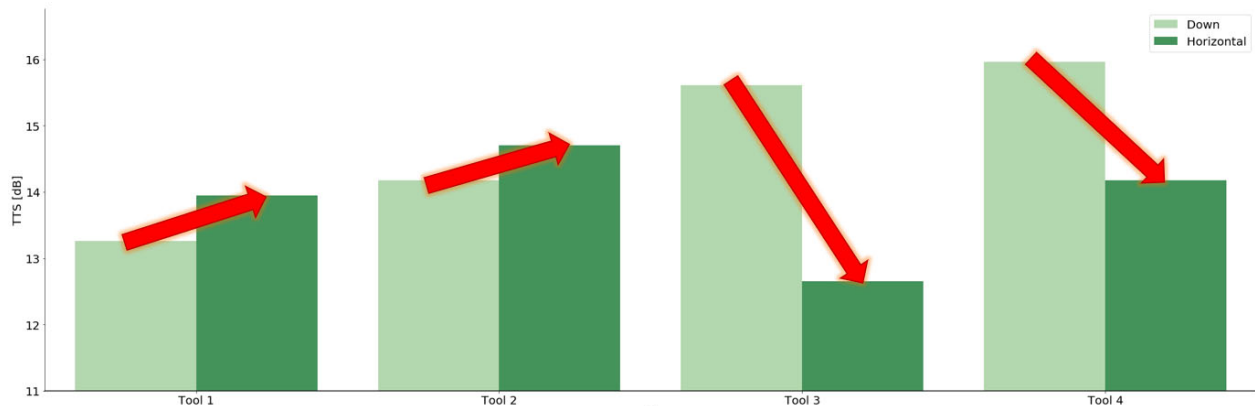
Figure 6: TTS measurements (mean) across the different test configurations.

These results evidence a high degree of correlation with the vibration measurements discussed in previous sections. Firstly, significant differences in human response can be observed when transitioning between postures. This indicates that the observed differences in vibration are representative of the physiological effects these vibrations have on the subject, confirming the effect of posture in the risk of HAVS development.

Secondly, the trends revealed in human response match the observation made at a vibration level. For tools 1 and 2, a change from a downward (posture 1) to a horizontal (posture 2) position increases the vibration levels received by the operator. A notable exception lies in the vibration emitted by tool 2, which in the case of on tool measurements failed to capture the trend, unlike on subject measurements. Conversely, in tools 3 and 4 the opposite trend is present, with reduced vibration exposure when transitioning between postures. Again, this finding is significant as it precludes the ability to predict the effect of posture without specific assessment but does validate the use of real time vibration assessment as an effective indicator of risk.

4.4 Validity of on-tool and on-subject vibration measurement to capture posture effects

Considering that the transfer function included in the wearable device was originally designed to correlate with ISO-5349 measurements due to existing human research being based on this standard, it is expected for both techniques to yield similar results. Figure 7 confirms this tight relationship between both sets of results. However, it can be observed that while the correlation between both results in Posture 1 is very high (Pearson's correlation coefficient = 0.92), this relationship becomes more spread when considering Posture 2 (Pearson's correlation coefficient = 0.74). It is argued that in a simpler position like the vertical posture, in which the transmission of vibration from the tool to the hand-arm system is likely to be affected by less factors, both measurements are expected to yield similar conclusions. However, these results may vary when moving to a horizontal position, more complex to execute and offering a less direct transmission from the tool to the hand-arm system. In this case, as shown by the posture transition in Tool 2, the on-tool measurements may not accurately capture the trends observed in TTS tests and therefore the correlation with on-subject measurements could decrease.
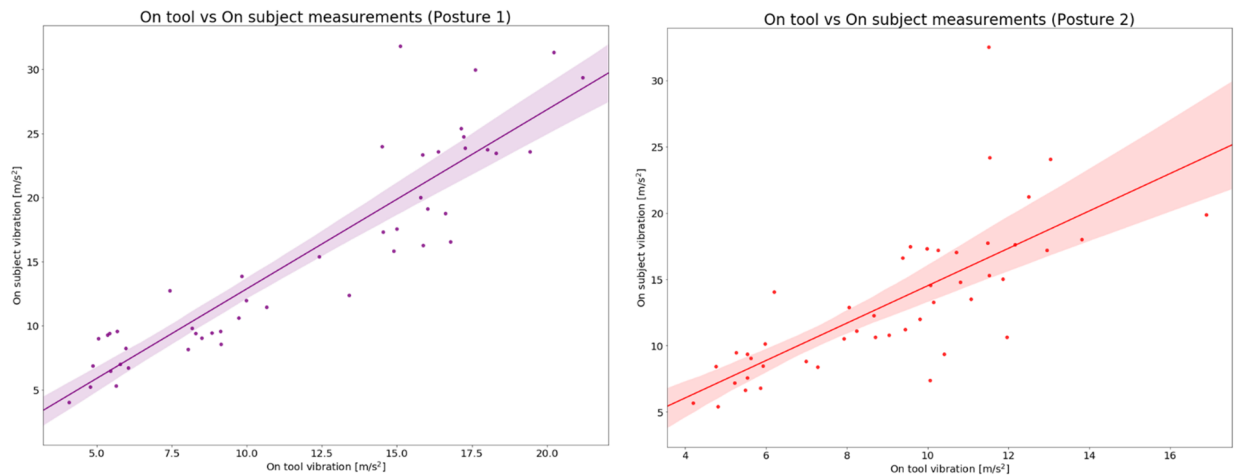
Figure 7: Comparison between the on-tool and on-subject measurements for each of the tests, for both postures.

When comparing both sets of results against their corresponding TTS measurements, results for human response in the form of TTS of the VPT seem to mirror the detected changes in vibration emission. When both sets of results are represented together, in Figure 8, the relationship becomes clear.
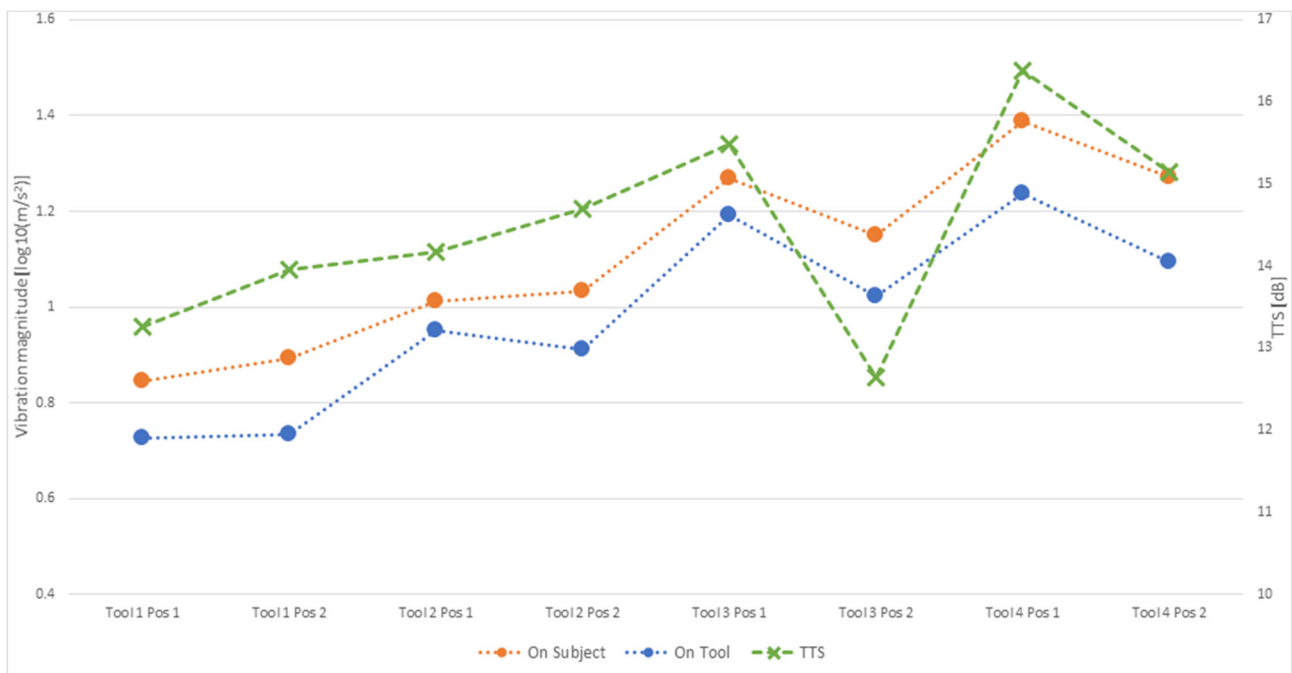

Figure 8: Mean TTS measurements (green) across the different test configurations, represented together with their respective vibration magnitude measurements, obtained on the tool (blue) and on the subject (orange).

The figure illustrates how the trend in human response to vibration are accurately predicted by both vibration magnitude measurements. The overall pattern is represented by a high coefficient of determination between TTS and vibration magnitude, with 0.70 for on-tool measurements and 0.71 for on-subject measurements. It must be noted that tool 3 was exceptionally challenging to handle for the operators in a horizontal position (posture 2), due to its weight distribution. If this result (Posture 2 in Tool 3) was removed from the analysis, the coefficients of determination rise to 0.94 and 0.96,

respectively. This result confirms the effectiveness of both vibration measurement technologies for the assessment of potential risk for the operator.

The observed posture effects, both in terms of vibration magnitude and TTS for each pair of postures, are similar in terms of TTS and vibration magnitude. An exception can be found in tool 2, in which the transition from a downward to a horizontal position translates into an increase in vibration exposure, as measured by TTS. While measurements on the subject accurately capture this effect, the vibration measurements on the tool would have indicated the opposite trend.

5   CONCLUSION

The presented study offers a deeper insight into the effects of body posture on the vibration exposure of power tool operators in a typical civil engineering environment and illustrates the relative significance of certain factors listed within Annex D of ISO 5349-1 which are not typically captured in risk assessments. Correlation between the relative changes in assessed vibration and human response in each posture demonstrates that the change to assessed vibration is not merely an artefact arising from the different posture but does in fact have consequences for the risk faced by the individual.

As data from the study demonstrated, effects of posture change are not uniform across tools or posture. This is considered highly significant in the context of the current approach to managing risk from vibration in the workplace as these findings challenge the idea of a robust risk assessment using a formula of a fixed vibration magnitude and exposure time. The study highlighted that posture could affect the estimated safe time of working for the heavier tools by a factor of two.

A more detailed analysis of the relationship between findings from this study and the physiology of specific subjects would also be beneficial as the authors recognise the link between physiology and the ability to maintain certain postures more or less easily for certain subjects.

The ability of the modern wearable device to directly track vibration exposure transmitted to the operator in real time and its positive correlation with human response offers a promising avenue for improvement whereby risk might be managed on an individual level or at least risk assessments more widely informed through a more extended period of data gathering and from a wider cohort of operators. While the study has also demonstrated the ability of the current on tool methodology for vibration assessment to capture some of these effects the authors feel it is import to recognise that this form of measurement is rarely performed in the real worksite for both practical and economic reasons.

Further research will be necessary to characterise the effects of the other factors present in the real work environment, with the final aim of creating a model capable of offering an assessment of HAVS risk with the maximum accuracy.

6 REFERENCES

British Standards Institution, 2013. Mechanical vibration. Guideline for the assessment of exposure to hand-transmitted vibration using available information including that provided by manufacturers of machinery (No. 15350). Comite Europeen de Normalisation.

Harada, N., Griffin, M.J., 1991. Factors influencing vibration sense thresholds used to assess occupational exposures to hand transmitted vibration. Occup. Environ. Med. 48, 185–192. https://doi.org/10.1136/oem.48.3.185

International Organization for Standardization, 2011. ISO 20345:2011 [WWW Document]. ISO 203452011. URL https://www.iso.org/standard/51036.html (accessed 6.6.19).

International Organization for Standardization, 2005. ISO 8041:2005 [WWW Document]. ISO 80412005. URL http://www.iso.org/cms/render/live/en/sites/isoorg/contents/data/standard/03/01/30145.html (accessed 6.6.19).

International Organization for Standardization, 2001a. ISO 5349-1:2001 [WWW Document]. ISO 5349-12001. URL http://www.iso.org/cms/render/live/en/sites/isoorg/contents/data/standard/03/23/32355.html (accessed 6.6.19).

International Organization for Standardization, 2001b. ISO 5349-2:2001 [WWW Document]. ISO 5349-22001. URL https://www.iso.org/standard/27511.html (accessed 6.6.19).

International Organization for Standardization, I., 2001. ISO 13091-1:2001, Mechanical vibration -- Vibrotactile perception thresholds for the assessment of nerve dysfunction -- Part 1: Methods of measurement at the fingertips. Multiple. Distributed through American National Standards Institute.

Maeda, S., Griffin, M.J., 1993. Temporary threshold shifts in fingertip vibratory sensation from hand-transmitted vibration and repetitive shock. Occup. Environ. Med. 50, 360–367. https://doi.org/10.1136/oem.50.4.360

Maeda, S., Shibata, N., 2008. Temporary threshold shifts (TTS) of fingertip vibrotactile perception thresholds from hand-held tool vibration exposures at working surface. Int. J. Ind. Ergon. 38, 693–696. https://doi.org/10.1016/j.ergon.2007.10.005

Maeda, S., Shibata, N., 2007. Problem of A(8) Evaluation. Presented at the 15th Japan conference on Human Response to Vibration, Japan.

Maeda, S., Taylor, M.D., Anderson, L.C., McLaughlin, J., 2019. Determination of hand-transmitted vibration risk on the human. Int. J. Ind. Ergon. 70, 28–37. https://doi.org/10.1016/j.ergon.2019.01.002

Malinskaya, N.N., Filin, A.P., Shkarinov, L.N., 1964. Problem of occupational hygiene in operating mechanized tools. Vestnik Academy of Medical Science U.S.S.R.

Mansfield, N.J., 2004. Human Response to Vibration. CRC Press.

Radziukevich, T.M., 1969. Interrelationship between temporary and permeanent shifts in the threshold of vibration and pain sensitivity under the effect of local vibration. Gig. Tr. Prof. Zabol. 13, 20–23.

Venkatesan, L., Barlow, S.M., Kieweg, D., 2015. Age- and sex-related changes in vibrotactile sensitivity of hand and face in neurotypical adults. Somatosens. Mot. Res. 32, 44–50. https://doi.org/10.3109/08990220.2014.958216

Yonekawa, Y., Maeda, S., Morioka, M., Kanada, K., Takahashi, Y., 1998. Prediction of TTS for hand intermittent vibration. Ind. Health 36, 191–196.

10 Session 3: HAV 2

Session chair: Chris Oliver

THE EFFECT OF FINGER SIZE ON TEMPERATURE PERCEPTION ON MALES AND FEMALES

Ying Ye
Institute of Sound and Vibration Research
University of Southampton
Southampton, SO17 1BJ
United Kingdom
Y.Ye@soton.ac.uk

Abstract

Temperature threshold testing is a key element of neurological examinations for neuropathy. Temperature thresholds at the fingertips are included as part of a standardized test for quantifying neurological disorders caused by hand-transmitted vibration, as it has been found that vibration at the fingertips can cause loss of neurological sensation.The paper seeks to determine if there is a correlation between finger size and the point at which an individual can detect a change in temperature. A total of 19 healthy volunteers (9 males and 10 females, age range 20-22 years) participated in an experiment which was designed to test the effect of finger diameter on the thermotactile thresholds at hot and cold temperatures. A thermal aesthesiometer was used for the experiment which followed a method of limits process with a baseline temperature of 32.5°C. The subjects placed the distal phalanx of each finger onto the apparatus and responded when they felt a change in temperature. It was found that an increase in diameter, as measured with a ring sizer, resulted in a lower hot threshold and higher cold threshold for thermotactile responses. Gender effects were minimal and dominance had no impact on the findings. Further studies are recommended to explore the effect of initial skin temperature and thermotactile thresholds and more analysis on the difference between each finger will help determine the most accurate choice for future testing. This study concludes that finger size is important and should be considered when assessing temperature thresholds at the fingertip.

1. Introduction

Prolonged occupational exposure to hand-transmitted vibration has been associated with a series of disorders in the vascular, sensorineural, and musculoskeletal structures of the human hand-arm system, collectively called the hand-arm vibration syndrome (HAVS) (Griffin, 1990). Vibration-induced neuropathy in the hand, most often manifested as reduced sensitivity, numbness, pain, tingling or clumsiness in hand movement can reduce work ability and the quality of life (Anonymous, 1995; Brammer et al., 1987; Gemne et al., 1995; Lundborg, 1988). It has been suggested that peripheral sensorineural symptoms may cause more discomfort and disability than vibration-induced vascular disorders, such as white finger, since this latter is episodic (usually triggered by exposure to cold) while sensory disturbances can be persistent and may interfere with life activities including sleep (Lundborg et al., 1990). Currently, there is no gold standard test to diagnose any stage of the sensorineural component of HAVS. However, for the assessment of changes in sensorineural function associated with exposures to hand-transmitted vibration, measurements of thermal thresholds and vibrotactile thresholds have been recommended in the UK (Lindsell and Griffin, 1998).

Human physical interactions are governed by the somatosensory system, the functioning element of the

body responsible for the conscious perception of touch, pain and temperature (Bhatnagar, 2008). Temperature perception is vital to human life, as it provides the body with essential information regarding the surroundings and allows the body to adapt in order to deal with them. Perception of temperature is vital in the hand, as instinctively we use our hands to feel our surroundings initially, and use our fingers to test temperature. It provides the necessary thermal information of an object by touching, warns of danger and informs our perception and understanding of the objects has been touched.

Temperature thresholds at the fingertips are included as part of a standardized test for quantifying neurological disorders caused by hand-transmitted vibration, as it has been found that temperature thresholds are correlated to neurological sensation. Neurological disorders can be identified in a subject who experiences temperature detection difficulties as established by several papers (Griffin, 2008, Brammer et. al, 1987 and Ekenvall et. al, 1986). However, with no real understanding of how a person's finger size could be affecting their ability to perceive these temperature changes, this test for neurological disorders is unlikely to be accurate and may be failing to correctly diagnose some cases where the subject has an extreme finger size. The existing knowledge is insufficient to ensure this test is robust and cannot currently predict a correlation between finger size and thermotactile thresholds. This experiment will provide data to support the diagnosis and allow for the standardized tests to be carried out with more accuracy and less variables to be considered.

Green and Zaharchuk (2001) concluded that 'temperature perception is highly dependent on the stimulus size'. They measured the sensitivities of 1, 2, 4 and 8 segments of a 10.24 cm^2 16-segment array using all possible combinations to stimulate a variety of areas. The results were then compared with each other. This found that averaging the thresholds for all the individual combinations produced a difference of 2.5°C between the single segment, 0.64cm^2, and the largest segment area, 5.12cm, while using only the most sensitive combination produced a difference of only 0.6°C. This indicated that there are some differences in thermo-receptibility when the area of stimulus is changed. Small receptive fields of areas of approximately a few mm2 are found in human skin (Hensel and Iggo, 1971) and these are randomly distributed with warm spots being fewer in number than cold spots (Green and Cruz, 1998). There are 2 -4 cold spots per square centimetre in the finger volar (Strughold and Proz, 1931) compared to 1.6 warm spots per square centimetre (Rein, 1926). Seah (Seah and Griffin, 2010) found evidence that the finger has few warm and cold spots, so it would be logical to conclude that a larger contact area would increase the chance of stimulating a sensitive spot. The evidence from Seah and Griffin's (2010) experiment supported this theory; temperature sensitivity increased with increasing areas of contact at the fingertip.

This paper reports an investigation on the effect of finger size on the perception of hot and cold temperature at the fingertip. The paper seeks to determine if there is a correlation between finger size and the point at which an individual can detect a change in temperature. It was hypothesised that a larger finger diameter will result in a larger contact area with the stimulus, hence temperature thresholds will fall closer to the baseline temperature used.

2. Methods

2.1 Apparatus

An *HVLab* thermal aesthesiometer was used to measure thermotactile thresholds (hot and cold thresholds) via the method of limits (see Table 1). Thresholds were measured on the distal phalanx of the index and little fingers of the right and left hands.

Subjects placed their fingertips so that the centre of the distal phalanx coincided with the centre of the applicator surface. They were instructed to apply a constant finger force of 2 N to the applicator surface, which they monitored using a digital scale located below the applicator. The temperature of the applicator increased or decreased from a reference temperature of 32.5°C at a rate of $1°C.s^{-1}$. Subjects were instructed to press the response button as soon as they perceived a change in temperature (i.e., increase or decrease of temperature). The temperature of the applicator then returned to the reference temperature and was held at 32.5°C for a random interval before the temperature increased or decreased again.

Table 1. Parameters of the *HVLab* Thermal Aesthesiometer and *HVLab* Vibrotactile Perception Meter.

Parameter	Condition
Thermotactile thresholds	
Contact area	Circular, 5.5 cm diameter
Contact surface	Smooth and planar
Psychophysical method	Method of limits
Number of judgements	Six hot or cold
Reference temperature	32.5°C
Rate of change of temperature	1°C/s
Vibrotactile thresholds	
Probe diameter	6 mm
Probe surround gap	2 mm
Contactor surface	Smooth and planar
Psychophysical method	von Békésy
Number of judgements	At least six peaks and troughs
Rate of change of stimulus	3 dB/s
Push force	2 N

Six hot and six cold thresholds were determined. For both thresholds the mean was calculated from the last four judgements. The temperature difference between the hot threshold and the cold threshold, known as the thermal neutral zone, was also calculated on all four fingers.

Figure 1 Images showing the ring sizer in use, shown at position G

To accurately and consistently measure the subjects finger diameter, this experiment utilised an international ring sizer. Ring size is an international reference in determining finger diameter, so is transferrable worldwide. This made it a suitable measurement method. The multi-sizer works in a similar manner to a belt; one end is pushed through a buckle to form a ring shape. This ring is then slipped onto the finger to be measured and adjusted by tightening the strap through the buckle to give a comfortable fit. To provide consistency the measurement was taken at the flexor digitorum sublimis (first knuckle point) and tightened until it was snug, but just loose enough to slip off the finger comfortably. Figure 1 shows the ring sizer at size G which equates to 45.5mm as converted by Goldsmiths (Goldsmiths, 2015).

2.2 Subjects

Nineteen subjects (10 females and 9 males) were recruited from the student population of the University of Southampton. The subjects were healthy and without existing neurological disorders. All participants completed a heath questionnaire and gave their written informed consent to participate in the study prior to participating in the experiment. This assessed their previous exposure to hand injury and provided details of their background. None of the subjects had thresholds that exceeded the accepted range to suggest there would be a healthy response, so all subjects were included in the present research.

All subjects were right handed with the mean age of the patients was 20.9 years (SD: 3.4, range: 18-24 years), their mean stature was 170.6 cm (SD: 8.7, range: 158-188 cm), their mean weight was 66.1 kg (SD: 15.8, range: 51-86 kg), and their mean body mass index (BMI) was 22.6 (SD: 2.7, range: 19.6-25.8).

The subjects were requested to avoid consuming caffeine for 2 hours and alcohol for 12 hours prior to the testing. The experiment was approved by the ethics committee of the University of Southampton (ID 31092).

2.3 Procedure

The experiment was conducted on each distal phalange on both hands of each subject. The diameter was measured at the joint between the distal and middle phalange to ensure a consistent reference for

each subject. The free probe was used at this point to measure the initial finger temperature. Patients sat on a supported chair and were instructed to rest their left forearm on a support block to ensure their comfort. This also helped prevent the subject from moving their fingers during the test, ensuring each experiment was consistent. The other hand was used to hold the remote button which they were to push to record a response when they detected a temperature change. With the left arm in place, the subject could place each finger in turn onto the centre of the stimulus. They were then instructed to apply enough pressure to form a flattening of the fingertip but not to cause discomfort. The subjects then repeated the experiment with the right hand on the stimulus.

For each subject the hot threshold was tested first. The subjects were reminded again after reading the information sheet that the temperature would rise at a constant rate until they detected that a temperature change had occurred. At this point they were to push the button and then instructed to wait until they felt the next rise in temperature. The temperature gently returned to the baseline and held there for three seconds before rising again at the same rate as before. The subjects were not told how long this interval was, instead simply instructed to only respond when they felt an increase in temperature. Following the hot threshold testing, the subjects completed the experiment in reverse for the cold threshold, with the temperature decreasing from the baseline and the subjects recording a response when they felt the decrease.

Subjects attended a single session lasting approximately an hour. The session was broken into three sections each lasting about 20 minutes. The first included the completion of documentation, full brief and measuring and recording finger sizes. The second was the experiment on the left hand, and the third the right hand. There was the opportunity for a break between each section. At the conclusion of the final section a debrief was completed and contact details provided for any future questions.

2.4 <u>Statistical methods</u>

Data analysis was performed using the software package SPSS (version 24.0). The data were summarised with the median as a measure of central tendency and the inter-quartile range (IQR) as a measure of dispersion. Non-parametric tests were employed to analyse the data, which were not normally distributed. The Mann-Whitney U test was used to investigate differences between male and females. The Spearman's ranking test was used to determine the extent of correlation between finger size and hot and cold thresholds. The Wilcoxon test was used to determine the difference between thresholds obtained on different fingers. The criterion for statistical significance was $p<0.05$. The reported p-values have been adjusted for multiple comparisons.

3. Results

The mean finger diameter, as measured between the distal and medial phalange at the knuckle point, and standard deviation of all the subjects tested was 47.70mm (6.87mm). Male subjects had a mean diameter of 49.30mm (standard deviation 7.02mm) and females had a mean of 46.26mm (standard deviation 6.43mm). A significant difference in finger diameter between males and females was found (p=0.001, Mann Whitney-U), in the direction indicating a smaller finger diameter for females as was

expected, but both genders were included for assessing the effect of gender on thermotactile thresholds at the fingertips. The room temperatures were in the range 21-25°C (mean 23.05°, median 24°C).

3.1 Thermotactile thresholds

The median thermotactile threshold for hot temperatures was 37.1°C with an inter quartile range of 35.58- 38.59°C. The maximum threshold reached was 43°C which is below the threshold of 48.5°C, thought to indicate a probable disorder. Male subjects had a mean hot threshold of 37.04°C and females displayed a mean hot threshold of 37.14°C. The cold threshold median for all the subjects was 28.63°C with an inter quartile range of 27.10- 29.73°C. Male subjects had a cold threshold mean of 28.323°C while females had a slightly lower cold threshold mean of 27.94°C. The interquartile range and the total range are displayed in Figure 2. Whilst the mean results were far from the threshold of 20°C which indicates a probable disorder, the lowest threshold recorded was 20.4°C which was very close to this limit. No significant difference between males and females was found at either the hot (p=0.792, Mann Whitney-U) or cold (p=0.185, Mann Whitney-U) thresholds when tested at the 0.05 significance level.

This indicates that a larger finger size has a higher threshold for cold receptors. This correlation was also statistically significant at the 0.01 level (p=0.007, Spearman).
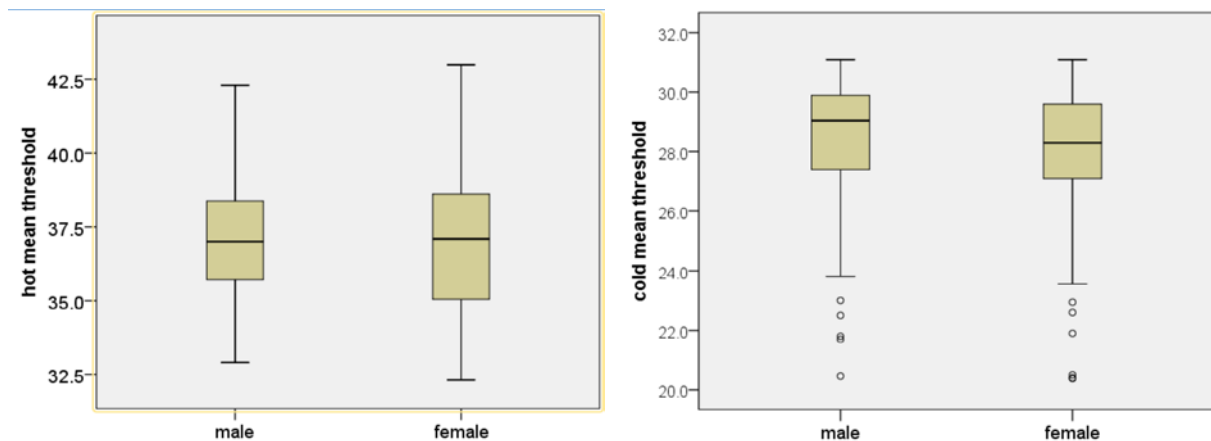
Figure 2 Graphs to present the range, interquartile range, and median values of the hot and cold thresholds of both male and female subjects

3.2 Correlation between thermotactile thresholds and finger size

Figure 3 details all the responses given by subjects for every finger at both the hot and cold thermotactile thresholds across all ten digits. A gentle correlation is seen for both sets of data on the scatter graph. The statistical analysis found a small to moderate negative correlation of the hot threshold which was shown to be statistically significant at the 0.01 level (p=0.001, Spearman). This means that a larger finger diameter resulted in a lower thermotactile threshold at the hot region. There was a small to moderate positive correlation found between the cold thermotactile threshold and the finger diameter.

3.3 Effects of initial skin temperature

During the experiment, initial finger temperature was recorded to determine if this variable impacted the results as suggested by the literature. The range of initial skin temperature was 18.6°C-35.5°C. The median initial temperature for all subjects was 31.20°C, and the interquartile range was 27.55-32.80°C.
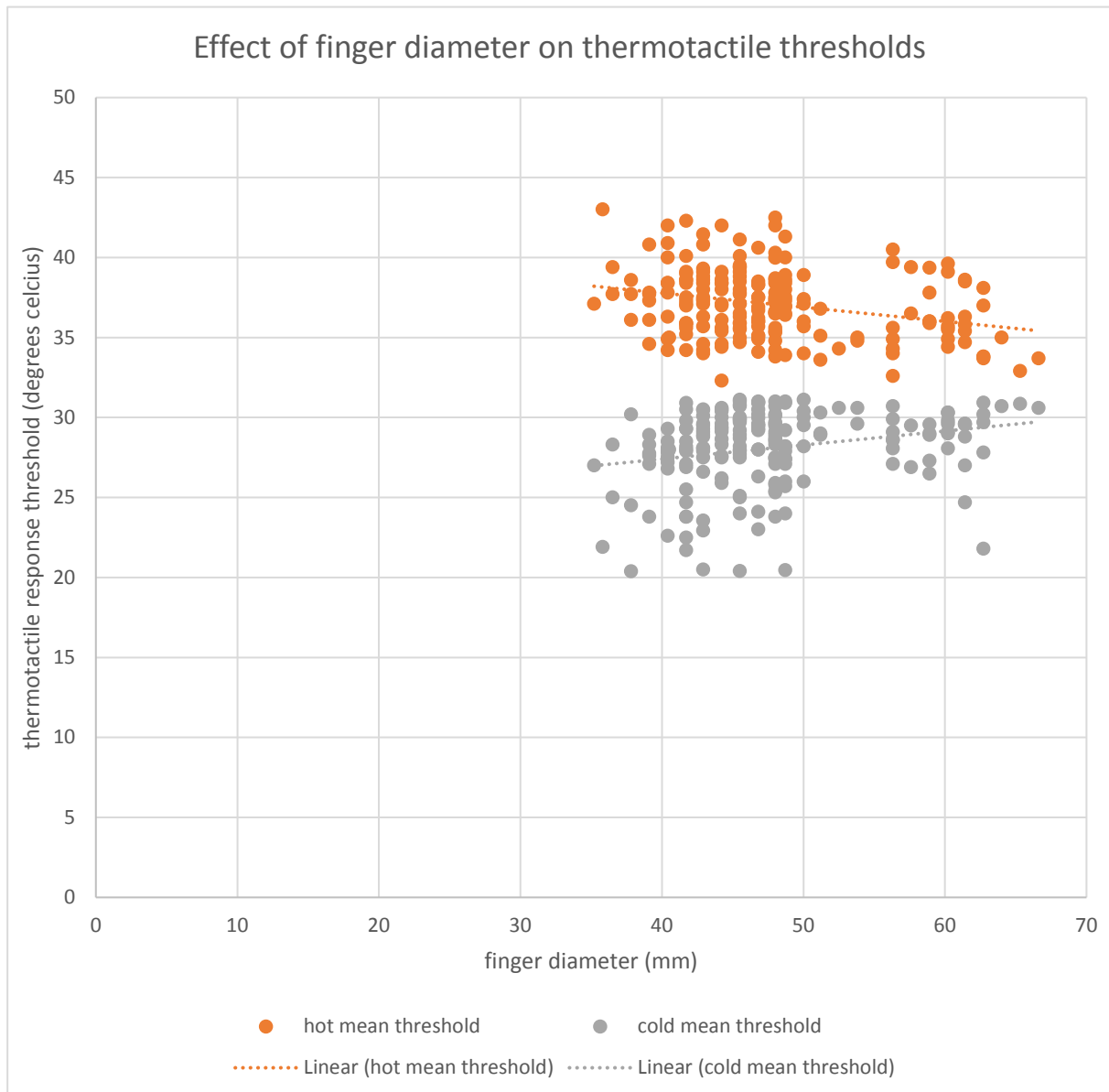
Figure 3 Graph demonstrating the linear correlation between the mean thresholds of each finger of every subject at both the hot and cold thresholds

Males had a higher median initial temperature (32.05°C) than females (30.1°C) which was found to be statistically significant at the 0.01 level (p=0.008, Mann Whitney- U). Figure 4 shows the scatter graph comparing the effect of initial finger temperature on the temperature threshold. It indicates a slight correlation with the hot threshold data, however statistical analysis found there to be no statistical correlation (p=0.845, Spearman). The cold threshold data appears to have a stronger correlation as shown in figure 4. This was found to be just significant at the 0.01 level (p=0.0098, Spearman), thus suggesting that initial temperature may have impacted the results for the cold threshold. No statistical significance was found between the initial finger temperature and the finger diameter (p=0.11, Spearman)
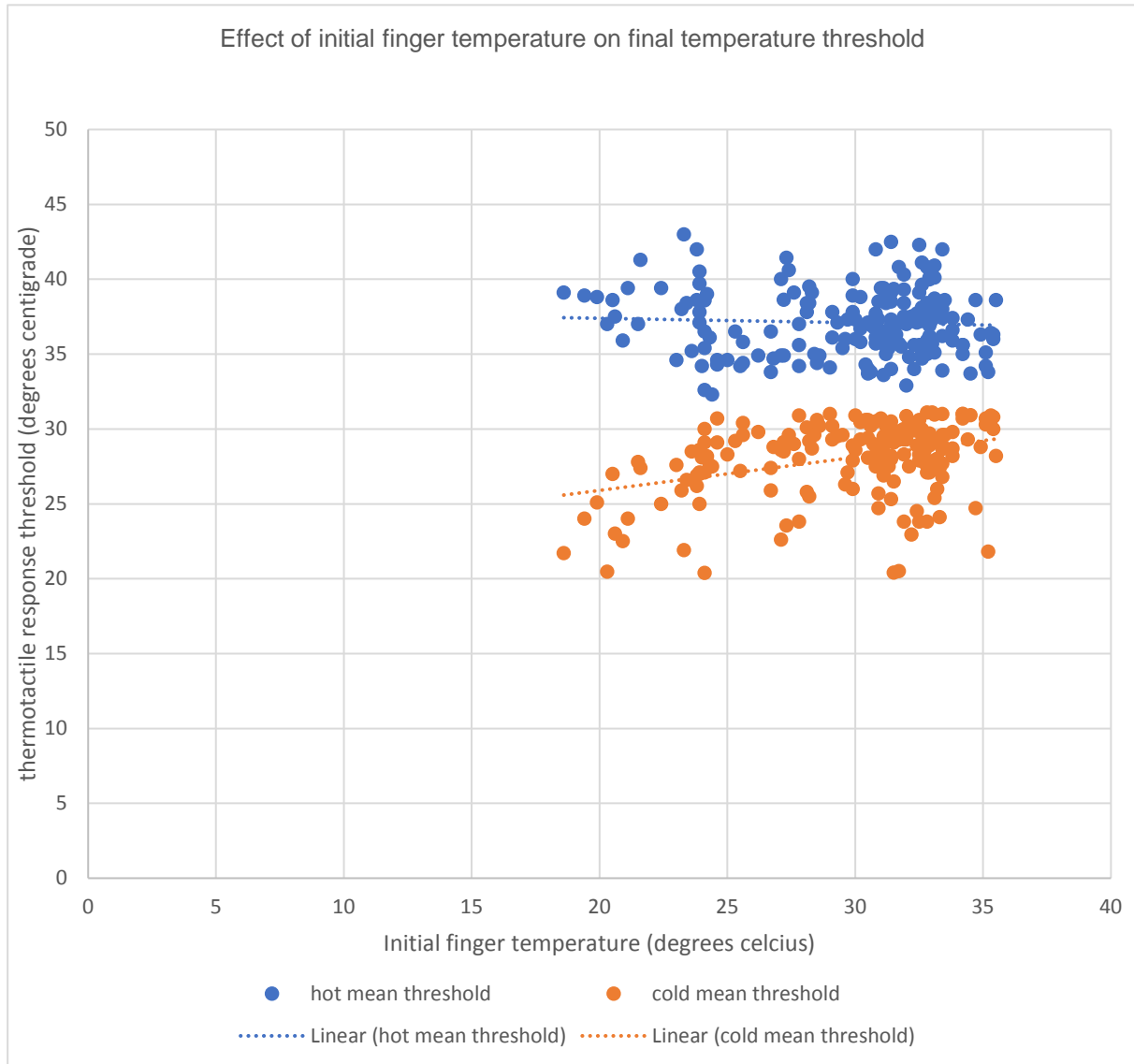
Figure 4 Graph displaying the linear correlations between the initial finger temperatures and the mean thermotactile thresholds for each finger of every subject at both the hot and cold thresholds

4. Discussion

The findings of this paper suggest that a larger finger size in terms of diameter demonstrated a lower hot threshold and higher cold threshold for thermotactile responses. The statistically significant correlations were found when all the data was combined, and tables 1, 2 and 3 present the differences between sub sections of data. Seah and Griffin (2010) found evidence supporting the present study and displayed findings that thermotactile thresholds were lower at hot and higher at cold temperatures when the stimulus area increased. They found that a larger contact area increased the probability of the stimulus exciting a warm or cold spot and the complementary results of this experiment support the hypothesis that a larger finger diameter results in an increase in contact area. Green (Green and Zahrachuk, 2001) used areas which varied by as much as 4.48cm2 showing much greater variance in contact area than the present study in which the standard deviation of finger diameter was just 6.87mm. Yet the findings were broadly similar with that of the present study since small receptive fields of areas

of approximately a few mm2 are found in human skin (Hensel and Iggo, 1971) so the variance in diameter across all subjects would still be valid to form an accurate conclusion.

A larger contact area was found to lower thresholds in many other studies and is usually explained by spatial summation (Kojo and Pertovaara, 1987; Dyck et al., 1993; Hilz et al., 1996; 1998; Lautenbacher et al., 2001;). Hilz et. al (1996; 1998) used the method of limits with a baseline temperature of 32°C, but tested on various site on the forearm, calf and foot and used subjects who were all below the age of 18, thus nervous development may have influenced their findings. The existence of warmth insensitive fields, skin areas with apparent lack of low threshold warm receptors, were also found to influence results (Green and Cruz, 1998; Green and Zaharchuk, 2001) although the present study found no evidence of the existence of these fields.

The analysis of the present data concluded that there were no significant differences between correlation in the left and right hands, or between dominant and non-dominant hands. This is in line with the observation that there were no significant differences between finger size between each hand. No correlations were found between individual digits on either the dominant or non-dominant hands, and only a few subjects found correlations when all ten digits of each subject were compared to one another. Inter-subject analysis would be expected to be the most reliable data as all external factors (age, gender, time, room temperature etc.) were kept consistent, however the range of finger sizes within these sub sections was too small to contribute to an accurate conclusion.

No correlation was found between the initial skin temperature at the finger and the hot threshold thermotactile response however, the cold response was affected by initial temperature. Hagander et. al (1999) also evaluated the effect of local skin temperature on thermal detection thresholds and found a similar conclusion that initial skin temperature had no significant effect on hot thresholds but a minor effect on cold thresholds. However, Hagander et. al (1999) used an initial skin temperature range of 27-37°C compared to the range of 18.6- 35.5°C recorded in the present study. Hagander et. al (1999) also measured the local skin temperature continuously during the experiment unlike the present study which took a reading before each finger was tested. This may have contributed to an inaccurate reading, as the subject placed their finger onto the stimulus after the recording of temperature was made and there may have been enough time for the stimulus to begin to alter that initial temperature before the test began. This may have had had an adverse effect on the findings. Several authors have reported no effect of local skin temperature on thermal detection (Fowler et al., 1987; Sosenko et al., 1989; Gelber et al., 1995) showing that there is a lack of certainty of the effects of initial temperature on thermotactile thresholds, hence this is a factor which should be more closely monitored in the future.

The outcome of this experiment agreed with the initial hypothesis that a larger finger diameter will have thermotactile thresholds that fall closer to the baseline temperature. This was found by analysing the data of all the subjects and supported evidence found in several previous studies showing that an increase in contact area increased the temperature sensitivity (Seah and Griffin, 2008 and Green and Zaharchuk, 2001). In the current paper, a significant correlation between finger diameter and a decrease in hot threshold and an increase in cold threshold was found. However, this paper did not find the same correlations when comparing the digits of a single subject suggesting that the overall correlation was a

trend rather than a causation argument. It should be noted that the difference in finger diameters of a single subject ranged from 16mm- 22.4mm compared to the overall range of 31.4mm, hence likely explaining why a more significant correlation was found overall.

If there were the same number of receptors in each hand, as argued by Parker and Newsome (1998) larger hands would be expected to have presented higher hot thresholds and lower cold thresholds because their larger hands mean they have a lower chance of exciting a temperature receptor within a given area. This was not the case, hence it may follow that receptors numbers increase with area as found in previous studies (Strughold and Proz, 1931; Rein, 1926), however further investigation will be required to argue that conclusion.

5. Conclusions

An increase in finger size as determined by the diameter, results in a lower hot threshold and higher cold threshold for thermotactile responses. There are no differences between the responses of the left and right hand of an individual, regardless of their dominance. Inter-subject variations of thresholds showed no significant difference. It can be concluded that the range of finger sizes of an individual is not great enough to cause a different response at each finger. The difference found in thermotactile thresholds due to different finger diameters confirm the need to control finger size when determining the standardised threshold used to diagnose a neurological disorder.

6. References

Anonymous (1995) Clinical and laboratory diagnostics of neurological disturbances in workers using hand-held vibrating tools. Report from discussions in a working group. In: Gemne G, Brammer AJ, Hagberg M, Lundström R, Nilsson T (eds.) Proceedings of the Stockholm Workshop 94. Hand-arm vibration syndrome: diagnostics and quantitative relationships to exposure. National Institute of Occupational Health, Solna, Sweden, 25–28 May 1994. Arb Hälsa 5:187–194.

Bhatnagar, S., Baltimore, M.D., Philadelphia, P.A., 2008. Somatosensory System. Neuroscience for the Study of Communicative Disorders. 3rd ed. Lippincott: Williams & Wilkins. P.164-184.

Brammer, A.J., Taylor W., Lundborg, G., 1987. Sensorineural stages of the Hand-Arm Vibration Syndrome. *Scandinavian Journal of Work, Environment and Health*. **13**(4), p.279–283.

Dyck, P.J., Zimmerman, I., Gillen, D.A., Johnson, D., Karnes, J.L., O'Brien, P.C., 1993. Cool, warm and heat-pain detection thresholds: Testing methods and inferences about anatomic distribution of receptors. *Neurology*, **43**, p.1500-1508.

Ekenvall, L., Nilsson, B.Y., Gustavsson, P., 1986. Temperature and vibration threshold in vibration syndrome. *British Journal of Industrial Medicine*. **43**, p.825–829.

Fowler, C.J., Carroll, M.B. and Burns, D. 1987. A portable system for measuring cutaneous thresholds for warming and cooling. *Journal of Neurology, Neurosurgery and Psychiatry*. **50**, p.1211-1215.

Gelber, D.A., Pfeifer, M.A. and Broadstone, V.L. 1995. Components of variance for vibratory and thermal thresholds testing in normal and diabetic subjects. *Journal of Diabetes Complications*. **9**, p.170-176.

Gemne G, Brammer AJ, Hagberg M, Lundström R, Nilsson T (eds) (1995) Stockholm Workshop 94. Hand–arm vibration syndrome. Diagnostics and quantitative relationships to exposure. Swedish National Institute for Working Life. Arbete och Hälsa 5:1–213.

Green, B.G. and Cruz, A., 1998. ''Warmth-insensitive fields'': Evidence of sparse and irregular innervation of human skin by the warmth sense. *Somatosensory Motor Research*. **15**(4), p.269–275.

Green, B.G. and Zaharchuk, R., 2001. Spatial variation in sensitivity as a factor in measurements of spatial summation of warmth and cold. *Journal of Somatosensory and Motor Research*, **18** (3), p.181-190.

Griffin MJ (1990) Handbook of human vibration. Academic Press, London.

Griffin MJ (2008) Measurement, evaluation, and assessment of peripheral neurological disorders caused by hand-transmitted vibration. Int Arch Occup Environ Health 81:559–573.

Goldsmiths, 2015. *Getting the right ring size, a Goldsmiths guide.* [online]Available at: www.goldsmiths.co.uk/i/know-your-ring-size (Accessed: 12/02/2018).

Hagander, L.G., Midanib, H.A., Kuskowskib, M.A., Parry, G.J.A., 1999. Quantitative sensory testing: effect of site and skin temperature on thermal thresholds. *Clinical Neurophysiology.* **111,** p.17-22.

Harju, E., 2002. Cold and warmth perception mapped for age, gender and body area. *Journal of Somatosensory and Motor Research*, **19** (1), p.61-75.

Hensel, H. and Iggo, A., 1971. Analysis of cutaneous warm and cold fibres in primates. *Pflügers Archive.* **329**, p.1–10.

Hilz, M.J., Glorius, S.E. and Schweibold, G. 1996. Quantitative thermal perception testing in preschool children*. Muscle Nerve*. **19**, p381-383.

Hilz, M.J., Stemper, B. and Schweibold, G. 1998. Quantitative thermal perception testing in 225 children and juveniles. *Journal of Clinical Neurophysiology.* **15**, p529-534.

Kojo, I. and Pertovaara, A. 1987. The effects of stimulus area and adaptation temperature on warm and heat pain thresholds in man. *International Journal of Neuroscience.* **32**, p.875–880.

Lautenbacher, S., Nielsen, J., Andersen, T., Arendt-Nielsen, L. 2001. Spatial summation of heat pain in males and females. *Somatosensory and Motor Research.* **18**, p.101–105.

Lindsell C, Griffin MJ (1998) Standardised Diagnostic Methods for Assessing Components of the Hand–Arm Vibration Syndrome, CRR 197/1998, Sudbury, Suffolk: HSE Books,1–87.

Lundborg G (1988) Nerve injury and repair. Churchill Livingstone, New York.

Lundborg G, Dahlin LB, Hansson H-A, Kanje M, Necking L-E (1990) Vibration exposure and peripheral nerve fiber damage. J Hand Surg 15A:346–351.

Parker, A.J. and Newsome, W.T., 1998. Sense and the single neuron: Probing the physiology of perception. *Annual Review of Neuroscience.* **21**, p.227–277.

Rein, F.H., 1925. Über die Topographie der Warmemfindung. Beziehungen zwischen Innercation und receptorischen Endorganen. *Z. Biol.,* **82**, p.189-212.

Seah, A.S. and Griffin, M.J., 2010. Thermotactile thresholds at the fingertip: Effect of contact area and contact location. *Somatosensory and Motor Research.* **27**(3), p.82–92.

Sosenko, J.M., Kato, M. and Soto, R. 1989. Determinants of quantitative sensory testing in non-neuropathic individuals. *Electromyography and clinical Neurophysiology.* **29**, p.459-463.

Strughold, H. and Porz, R., 1931. Die Dichte der Kaltpunkte auf der Haut des menschlichen Körpers. *Z. Biol.*, **91**, p.563-571.

The Effect of Grip Force on an Upper Arm under both Continuous and Shock Vibration using the MDOF Model

Hamzah H. Khalil, Jem A. Rongong, Matt J. Carré
University of Sheffield, Department of Mechanical Engineering
Sheffield, S1 3JD United Kingdom
hhkhalil1@sheffield.ac.uk

ABSTRACT

The objective of this study was to analyse the effects of grip force on the upper arm under both continuous and shock vibration. A 5 DOF model was used to simulate the biodynamics response of the system. Measured data from previous studies have been used as parameters for the analytical model. The results show that the responses predicted from the model agree reasonably well with the measured data. The variations in the model parameters under different grip forces are further discussed in view of the biological and mechanical system behaviour. The presented study could be useful for design and assessment of vibration handheld tools.

1   INTRODUCTION

Prolonged exposure to vibration from handheld tools has been linked to vascular, neurological and musculoskeletal disorders, together known as hand arm vibration syndrome (HAVS) (Griffin, 1990). Shock vibration generated from pneumatic handheld tools are used in varies industries. A portion of this impact/shock vibration can be conveyed, absorbed or dissipated by to the upper arm with the working frequencies of the pneumatic actuators being in the range of 10 Hz to 40 Hz. Unfortunately, for workers, the resonances of the human wrist-forearm are in a similar range. To be more specific, the wrist-forearm and upper arm can be effectively excited by frequencies under 40 Hz and 20 Hz respectively (Pan *et al.*, 2018). The biodynamics force (cyclic stress and deformation) is an important factor for evaluating the driving-point biodynamics parameters such as apparent mass and mechanical impedance (Dong, Wu & Welcome, 2005). Thus, enhancing the understanding of the biodynamic response of human hand to both continuous and shock vibration could offer more reliable means to quantify vibration exposures from such tools. There is a substantial potential in assessing and evaluating the exposure of human hand to vibration in analytical studies, but human involvement in the experimental setting may carry health risks due to the unclear nature of human response to vibration (Rakheja *et al.*, 2002). In sum, the understanding of the biodynamics response is essential for a number of reasons, such as simulating the hand-arm system, testing handheld tools or applying vibration isolation to a device (Dong *et al.*, 2007).

2 METHODS

The human hand-arm combination is a complex system that can be simplified by removing the nervous and muscular systems from consideration and representing the system as a mechanical MDOF model, as shown in Figure 1 in which the hand arm model is divided into five components.
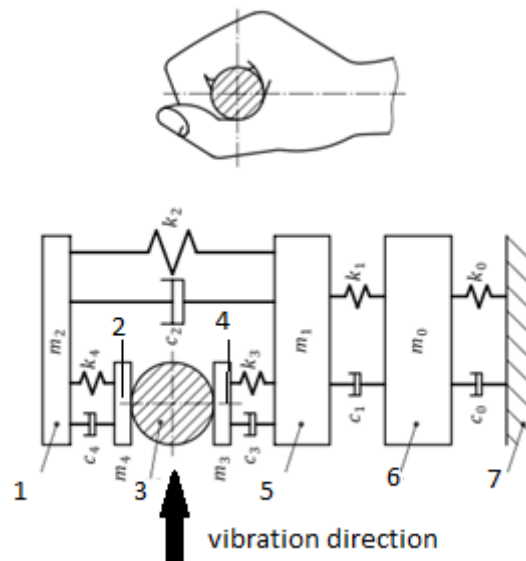
Figure 1: MDOF hand-arm system: 1 – fingers; 2 - finger skin; 3 – handle; 4 - palm skin; 5 - palm-wrist-forearm; 6 - upper arm; 7 - ground (ISO 10068:2012 , 2012)

Table 1: Parameters of 5-DOF system (ISO 10068:2012 , 2012)

Header	Vibration in x direction	Unit
M0 mass of upper arm	0.236	Kg
M1 mass of palm-wrist-forearm	0.3998	Kg
M2 mass of fingers	0.0576	Kg
M3 mass of skin of the palm	0.0205	Kg
M4 mass of skin of the fingers	0.01	Kg
K0 stiffness of upper arm	1000	N/m
K1 stiffness of palm-wrist-forearm	6972	N/m
K2 stiffness of fingers	100	N/m
K3 stiffness of skin of the palm	4000	N/m
K4 stiffness of skin of the fingers	65844	N/m
C0 damping of upper arm	21.8	N*s/m
C1 damping of palm-wrist-forearm	22.1	N*s/m
C2 damping of fingers	69.8	N*s/m
C3 damping of skin of the palm	128.6	N*s/m
C4 damping of skin of the fingers	81.5	N*s/m
f1 undamped natural frequencies	14.1	Hz
f2 undamped natural frequencies	36.9	Hz
f3 undamped natural frequencies	170.3	Hz

Table 1 summarises the parameters of a mechanical model for the 5-DOF of hand-arm system (ISO 10068:2012, 2012). The parameters were measured by coupling a vibrating source to the human hand to find the mechanical impedance, apparent mass and apparent stiffness of the hand-arm system. The direction of vibration was selected to match the direction of vibration of the rig in the Human Interaction group (HIG) lab, which was developed by Almagirby *et al.* (2017). In the 5 DOF dynamic

system, masses, springs and dampers are represented by M, K and C respectively. The equation of motion for a multi-degree-of-freedom system can be represented as:

$$m\ddot{x} + c\dot{x} + kx = F \tag{1}$$

The equation of motion for each mass can be represented as:

$$\ddot{x}_1 = (F - C_2\dot{x}_1 - (C_2 + C_4)\dot{x}_2 - (K_2 + 4)\,x_1 - k_2\,x_2)/M_1 \tag{2}$$

$$\ddot{x}_2 = (- C_1\dot{x}_1 - (C_1 + C_2 + C_3)\dot{x}_2 + C_2\dot{x}_3 - k_1\,x_1 - (k_1 + k_2\,)x_2 + k_2\,x_3)/M_2 \tag{3}$$

$$\ddot{x}_3 = (- C_1\dot{x}_2 - (C_1 + C_0)\dot{x}_3 - k_1\,x_2 - (k_1 + k_0)\,x_3)/M_3 \tag{4}$$

$$\begin{bmatrix} M1 & 0 & 0 \\ 0 & M2 & 0 \\ 0 & 0 & M3 \end{bmatrix} \begin{Bmatrix} \ddot{X} \\ \ddot{x} \\ \ddot{x} \end{Bmatrix} + \begin{bmatrix} C2 + C4 & -C2 & 0 \\ -C2 & C1 + C2 + C3 & -C1 \\ 0 & -C1 & C1 + C0 \end{bmatrix} \begin{Bmatrix} \dot{X} \\ x \\ x \end{Bmatrix} +$$

$$\begin{bmatrix} K2 + K4 & -K2 & 0 \\ -K2 & K1 + K2 + K3 & -K1 \\ 0 & -K1 & K1 + K0 \end{bmatrix} \begin{Bmatrix} X \\ x \\ x \end{Bmatrix} = \begin{Bmatrix} F \\ 0 \\ 0 \end{Bmatrix} \tag{5}$$

$$F = A\cos(w * t) \tag{6}$$

Where A is the amplitude of vibration and w is the driving frequency

$$\dot{y} = A * y + B * F \tag{7}$$

$$A = \begin{bmatrix} 0 & I \\ -K/M & -C/M \end{bmatrix}, B = \begin{bmatrix} 0 \\ F/M \end{bmatrix}, F = \begin{bmatrix} f(t) \\ 0 \end{bmatrix}, y = \begin{bmatrix} x \\ \dot{x} \end{bmatrix} \tag{8}$$

3   RESULTS

The responses of the hand-arm system were obtained using MATLAB and the Ode45 function was used to solve the equations. A sinusoidal signal was applied to the system to simulate continuous and shock with the same frequency and amplitude. Both types of vibration were compared in terms of the effect of grip force on the transmissibility of the upper arm.
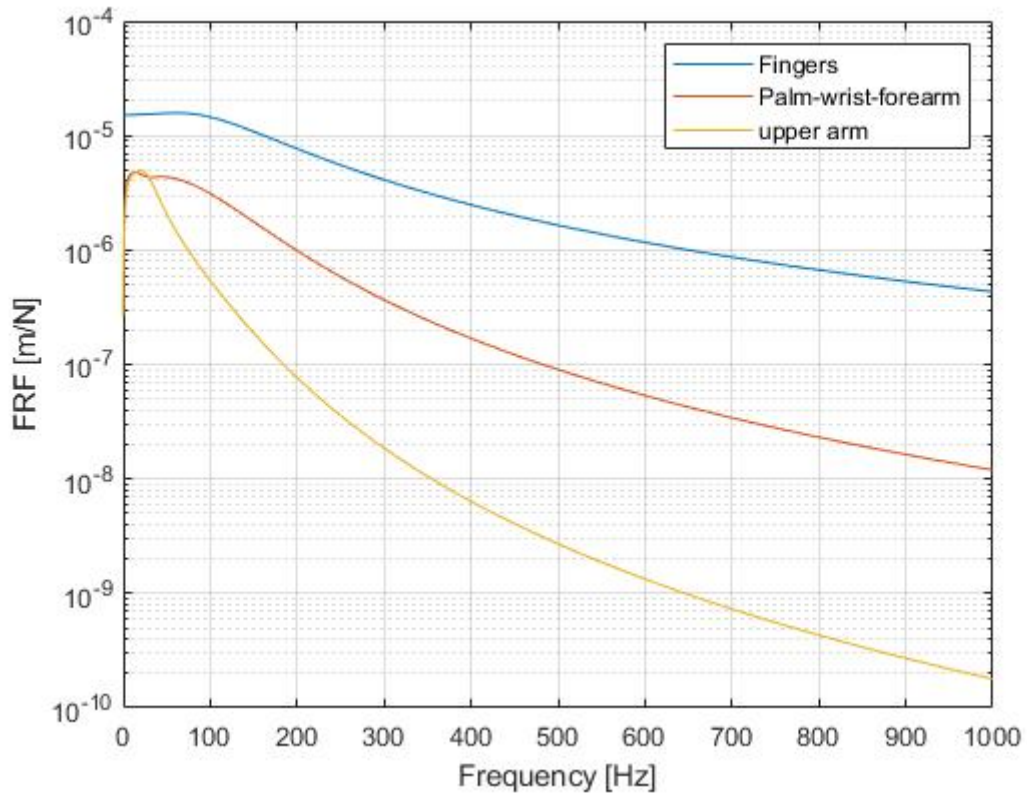
Figure 2: Frequency response function
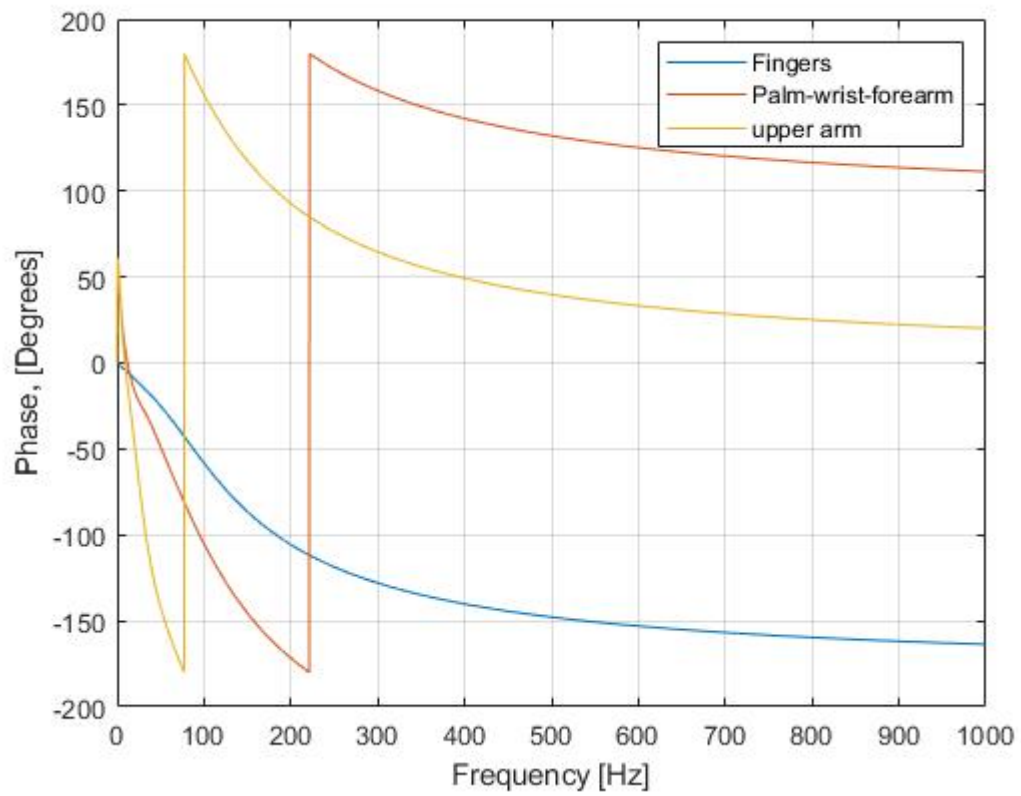
Figure 3: Phase response
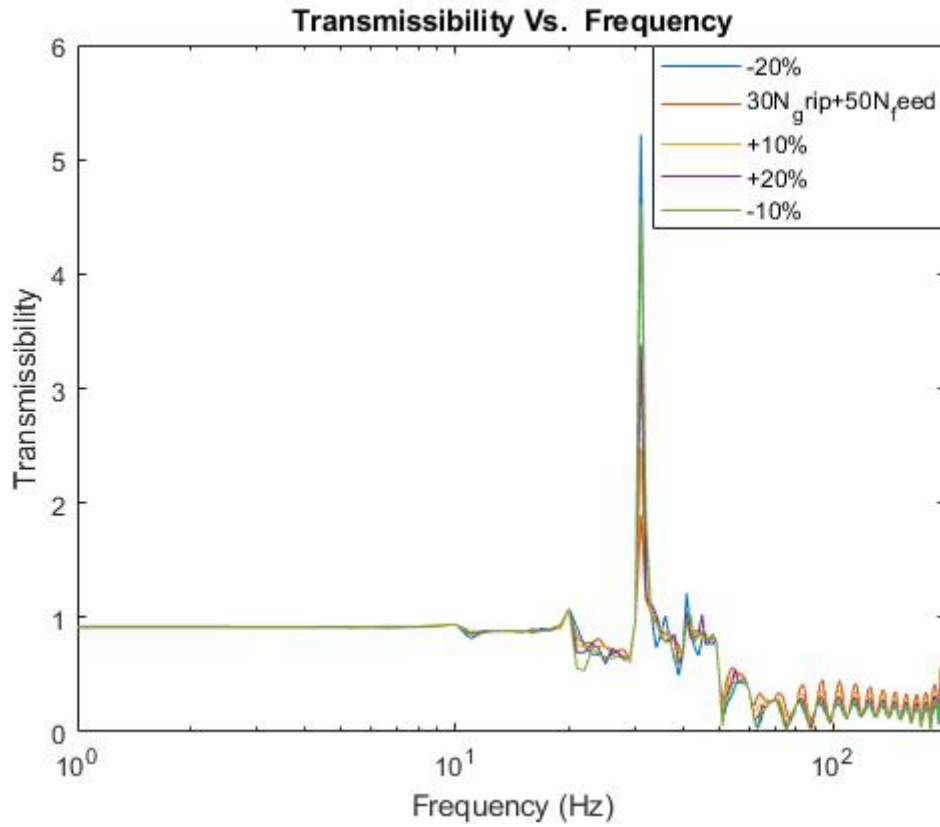
Figure 4: Transmissibility of the upper arm with different grip force for shock vibration
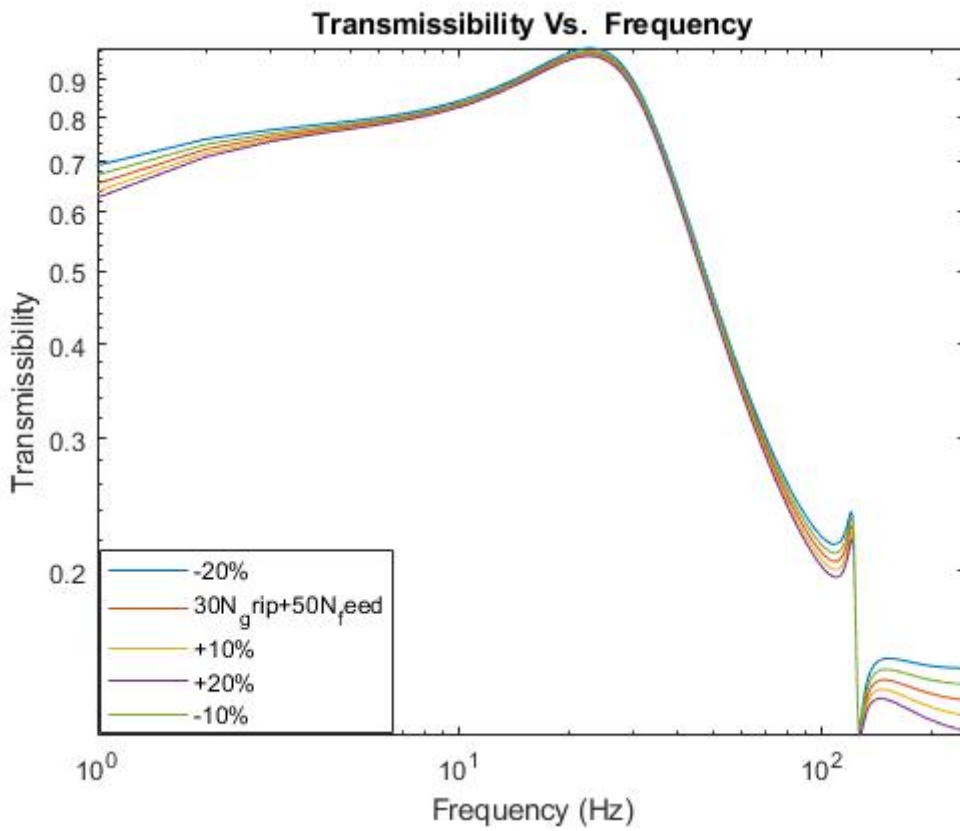
Figure 5: Transmissibility of the upper arm with different grip force for continuous vibration
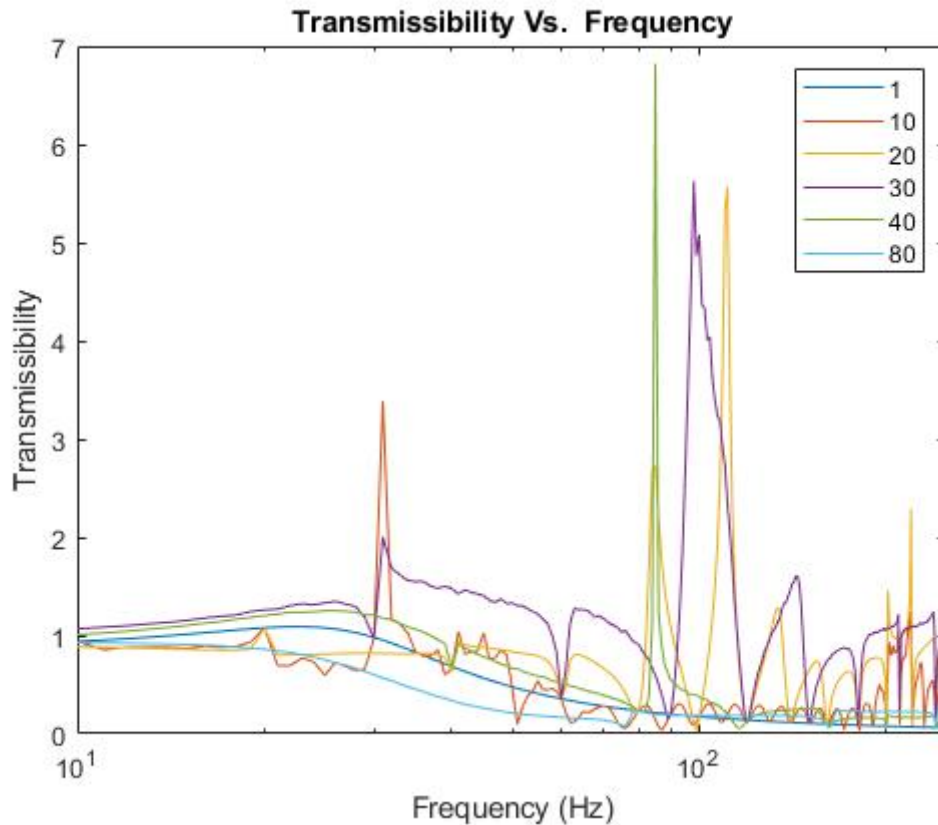
Figure 6: Transmissibility of the upper arm with different repetition rate for shock vibration

The frequency response function in Figure 2 shows no significant peak for the fingers. However, natural frequencies can be estimated from Figure 3. A possible explanation for this might be the high damping characteristics of human hand. As the frequency increases, the displacement of the system (fingers, palm-wrist-forearm and upper arm) decreases in a linear pattern. Therefore, displacement depends more on change in frequencies rather than excitation force.

Figures 4 and 5 shows a comparison between the transmissibility of the system under the same excitation force with the same corresponding data in Table 1 and illustrates that continuous vibration behaves similarly to shock vibration. Figure 6 illustrates the effect of repetition rate on transmissibility of the upper arm whereby the highest and the lowest reputation rate show the least transmissibility and the repetition rates of 10, 20 and 30 show higher transmissibility.

4 DISCUSSION AND CONCLUSION

The hand-arm biodynamic response to vibration has been investigated computationally using 5-DOF models of hand-arm system. Analyses of this model were achieved to observe the deflection patterns in the system and the transmissibility in the upper arm. The fingers, palm-wrist-forearm and the upper-arm show different deflection patterns, and the general pattern of transmissibility under continuous and shock vibrations shown in Figures 4 and 5 suggests that the change in grip force is a minor factor in the transmissibility in the upper arm. However, the repetition rate is an important factor in the transmissibility of vibration in the upper arm. This can be related to the fact that the resonance of the upper arm ranges from 7 to 12 Hz (Xu *et al.*, 2017).

Since displacement decreases when an excitation signal is applied at high frequency, frequencies lower than 10 Hz exhibit large deflection patterns even though this frequency range is not covered in the frequency weighting detailed in ISO 5349-1:2001(ISO 5349-1:2001). Very high frequencies, which are also not covered in ISO 5349-1:2001, show very low deflection patterns and acceleration; however, epidemiological studies contradict this finding (BOVENZI, 2012). Therefore, estimating the health risks from exposure to vibration with very low frequencies (shocks) or very high frequencies by the traditional means (e.g. ISO standards) may not be sufficient.

An extended version of the ISO weighing has been introduced which includes frequencies up to 10,000 Hz to assess the risk of vascular disorders based on epidemiological studies (ISO/TR 18570, 2017). That said, much uncertainty still exists about the human hand response to vibration. Reduction in finger blood flow, energy of vibration and transmissibility and the relationship between them could provide better understanding to this phenomena (Dong, Wu and Welcome, 2005; Ye *et al.*, 2014). Indeed, coupling the biodynamics system with handheld tools could be fruitful for frequencies covered by ISO 5349-1:2001 (8-1250 Hz) (Dong *et al.*, 2018). In addition, higher order systems could produce better estimation of the biodynamic response. This is due to the continuity and the complexity of the human hand-arm system (Rakheja *et al.*, 2002).

The upper arm can only be excited by lower frequencies (lower than 15 Hz), a finding consistent with the conclusion of Reynolds *et al.* which sets the upper limit at 25 Hz (Reynolds *et al.*, 1978). It should be noted that the system has a very high damping characteristic which can dissipate large amount of energy from exposure (Rakheja *et al.*, 2002). This may complicate the mechanical modelling of hand-arm systems (Rakheja *et al.*, 2002). Moreover, the grip force of the hand and muscles contractions in the upper hand could be factors that make the operators more prone to health risks. As future avenues of study, further experiments and analysis must be done to correlate the findings with more variables such as posture, hand force and magnitude of vibration to provide more accurate results.

REFERENCES

Almagirby, A., Carré, M. J. and Rongong, J. A. (2017) 'A new methodology for measuring the vibration transmission from handle to finger whilst gripping', *International Journal of Industrial Ergonomics*, 58, pp. 55–61. doi: 10.1016/j.ergon.2017.02.011.

Bovenzi, M. (2012). Epidemiological Evidence for New Frequency Weightings of Hand-Transmitted Vibration. *Industrial Health*, 50(5), pp.377-387.

Reynolds D. D. (1978) 'Hand-arm vibration: a review of 3 years' research pp. 99–128. (30 pages, 45 figures, 3 tables, 33 references)', *Journal of Sound and Vibration*, 61(4), p. 619. doi: 10.1016/0022-460X(78)90463-7.

Dong, R. G. *et al.* (2007) 'Modeling of biodynamic responses distributed at the fingers and the palm of the human hand-arm system', *Journal of Biomechanics*, 40(10), pp. 2335–2340. doi: 10.1016/j.jbiomech.2006.10.031.

Dong, R. G. *et al.* (2018) 'A model for simulating vibration responses of grinding machine-workpiece-hand-arm systems', *Journal of Sound and Vibration*. Elsevier Ltd, 431, pp. 276–294. doi: 10.1016/j.jsv.2018.06.008.

Dong, R. G., Wu, J. Z. and Welcome, D. E. (2005) 'Recent advances in biodynamics of human hand-arm system.', *Industrial health*, 43(3), pp. 449–71. doi: 10.2486/indhealth.43.449.

Griffin, M. J. (1990) *Handbook of Human Vibration*.

ISO/TR 18570 (no date) *Mechanical vibration — Measurement and evaluation of human exposure to hand transmitted vibration — Supplementary method for assessing risk of vascular disorders*.

ISO 5349-1:2001 (2001) *Mechanical vibration – measurement and evaluation of human exposure to hand-transmitted vibration, part 1: general requirements. Geneva: ISO*.

Pan, D. *et al.* (2018) 'The relationships between hand coupling force and vibration biodynamic responses of the hand-arm system', *Ergonomics*. Taylor & Francis, 61(6), pp. 818–830. doi: 10.1080/00140139.2017.1398843.

ISO 10068:2012 (2012) 'BSI Standards Publication Mechanical vibration and shock — Mechanical impedance of the human hand-arm system at the driving point'.

Rakheja, S. *et al.* (2002) 'Comparison of biodynamic models of the human hand-arm system for applications to hand-held power tools', *Journal of Sound and Vibration*, 249(1), pp. 55–82. doi: 10.1006/jsvi.2001.3831.

Xu, X. S. *et al.* (2017) 'Vibrations transmitted from human hands to upper arm, shoulder, back, neck, and head', *International Journal of Industrial Ergonomics*. Elsevier B.V, 62, pp. 1–12. doi: 10.1016/j.ergon.2016.07.001.

Ye, Y. *et al.* (2014) 'Association between vasoconstriction during and following exposure to hand-transmitted vibration', *International Archives of Occupational and Environmental Health*, 87(1), pp. 41–49. doi: 10.1007/s00420-012-0836-7.

Comparison of hand-arm vibration emissions of battery powered tools and tools of other power sources

Antonia Hawker
Health and Safety Executive
Buxton, SK17 9JN
antonia.hawker@hse.gov.uk

ABSTRACT

Recent improvements in battery technology have meant that battery-powered tools are becoming more common in the workplace. The Health and Safety Executive (HSE) investigated the likely impact on the hand-arm vibration exposures of workers using battery-powered hand-held power tools. HSE worked with manufacturers to identify six different types of machine most commonly used in industry and for each of these obtained comparable battery-powered and alternative traditionally-powered versions (combustion-engine, pneumatic or electric). Each machine type underwent a series of tests, which replicated typical real use. Testing took place at manufacturer's test facilities and at the HSE's laboratory. The vibration total values for comparable machines were assessed to determine whether the battery-powered tool, in general, produced lower or higher emissions than equivalent alternatively powered version of the same tool. The battery-powered chain-saws and impact wrenches tested produced lower vibration total values than the equivalent alternatively-powered tools. This was not observed for the cut-off saws, reciprocating saws, angle grinders or drills; in these cases, either there was no consistent relationship between vibration emission data and tool power source or the data depended on the activity and inserted tool used. Overall, the data shows that for the tools tested, it is not possible to advise employers that battery-powered tools are in all cases a low-vibration alternative option. HSE guidance for users of hand-held power tools – regardless of how they are powered – remains unchanged; find the tools that are suitable for the job and then avoid those with unnecessarily high vibration.

1   INTRODUCTION

Use of battery-powered hand-held tools is an example of emerging technology. HSE needed to collect evidence relating to the likely impact of this new technology on the hand-arm vibration exposures of tool users; to ensure that an opportunity to reduce vibration exposures is not missed or that the potential for higher vibration exposure does not go unnoticed until such time as the consequences to health become apparent. Battery powered machines are particularly attractive to industries such as grounds maintenance, construction and motor vehicle repair, where their portability can simplify the undertaking of site work. As the technology improves, wider use in other industries can be expected. Some manufacturers are suggesting that the use of battery-powered machines is advantageous for reduction of both noise and vibration exposures. Instruction manuals quote figures that suggest considerable reductions in the emission values for these machines.

The work reported here is aimed at understanding whether there are consistent differences in vibration total values between battery powered and alternatively powered tools and to enable HSE to provide appropriate guidance on the use of these machines.

The aim of this work is to evaluate whether there is a difference in vibration emissions from battery powered tools and equivalent alternatively powered tools.

2 METHOD

2.1 Identification of machines tested

Six machine types were chosen for investigation. These were machines that are commonly used in industry, as identified by tool manufacturers and HSE inspectors, and known to represent a substantial vibration risk. These were:

- chain-saws;

- cut-off saws;

- combi-drills;

- reciprocating saws;

- impact drivers/wrenches;

- angle grinders.

For each machine type identified, HSE worked with a manufacturer to identify from their range of commercially available products equivalent tools to test.

2.2 Test procedure

For each machine identified, vibration emissions were measured during controlled tests designed to simulate in-use tasks. The test procedures were specific to each tool type and are discussed in section 2.4. For the battery powered tools, all batteries started the tests fully charged. Measurements were made on both manufacturers' premises and at the HSE Science and Research Centre. Operators consisted of professional tool operators and HSE scientists trained in tool use. The resultant data was used to establish whether battery powered tools have lower vibration emissions and therefore lower vibration exposures for tool users.

2.3 Hand-arm vibration measurements

Simultaneous triaxial vibration measurements were made at both hand positions (front and rear) where appropriate. For each position, three Brüel & Kjær (B&K) type 4393 accelerometers (unless otherwise stated) were bolted onto a custom-made aluminium mounting block. The block was then attached to the machine with a nylon cable tie, which was fitted using a tensioning gun. The measurement location was chosen to be as close as possible to the centre of the operator's gripping zone without interfering unduly with the operator's grip during normal machine use. The three transducers at each hand position measured acceleration in three orthogonal directions simultaneously, in accordance with BS EN ISO 5349-1: 2001[1]. The total mass of the mounting assembly at each hand position was approximately 18 grams. Measurements were made according to BS EN ISO 5349-2:2001+A1:2015[2]. The data presented in this paper is for the handle with highest vibration unless otherwise stated.

The signals from the accelerometers were amplified using B&K Nexus amplifiers and analysed using a B&K multi-channel real-time frequency analyser. Vibration was measured in unweighted one-third octave bands. The one-third octave band data were then frequency-weighted in accordance with BS EN ISO 8041-1:2017[3] and the vibration total values calculated. The vibration total value is a single frequency-weighted value, obtained from the root-sum-of-squares of the three individual axes, which represents the vibration entering the operator's hand at the measurement location.

Prior to starting testing, each channel of the measurement system was checked using a B&K type 4294 vibration calibrator, which applies a 160 Hz sinusoidal calibration signal with a magnitude of 10 m/s² to accelerometer.

2.4 Operating conditions

For each machine category, matched pairs of machines were selected so that they were as far as possible the same, with the exception of the power source. For most tool types this was difficult and in practice there were differences in other characteristics such as weight and speed. Each pair of machines was operated by the same set of operators, using the same consumables on the same test materials. Tool operators were used in accordance with manufacturers' instructions.

2.4.1 Chain-saws

Two battery-powered and two petrol-powered chain-saws of equivalent rated power and weight were tested under up to three different operating conditions; cross cutting, snedding and tree service. For all tests the tools were used at maximum speed. During cross cutting, the chain-saw was used to make vertical cuts through a horizontal oak log that was placed on a saw-horse. During snedding, the chain-saw was used to strip branches off a horizontally positioned tree or log. The tree service test was similar to snedding, but involved using the chain-saw to cut the branches off an upright rather than horizontal tree. Each tool was operated by three different operators during the tests. Each operator made four cuts during the cross cutting tests, two cuts during the tree service tests and three cuts during the snedding tests. The measurement durations varied according to the chain-saw power source and the operating condition. One pair of chain-saws was used for cross-cutting and snedding; another pair were used for the tree service tests.

2.4.2 Cut-off saws

One battery-powered and two petrol-powered cut-off saws were tested. The battery-powered cut-off saw was the largest and most powerful battery-powered version that was available to buy at the time of testing, however it was not as powerful as either of the petrol-powered saws. Each saw was tested by three different operators who each used the tool to make three cuts through paving slabs with dimensions 600x600x50 mm. Each cut was made through the entire depth of the slab and took approximately 15 seconds with the petrol saw and approximately 25 seconds with the battery saw. The same consumables were used as provided with the tools when purchased.

2.4.3 Drills

Two battery-powered and two corded (electric) drills of equivalent rated power were tested drilling holes into a concrete block with dimensions 440x220x95 mm and a 5 mm thick mild steel plate. Two combi-hammer drills were used, one mains-powered and one battery-powered, to drill holes vertically downwards into the concrete block. Hammer drills were also used, one mains-powered and one battery-powered, to drill holes horizontally into a vertical metal plate using a 6 mm drill bit. The tools were fitted with the drill bits recommended by the manufacturer for concrete or metal. Each tool was tested by three different operators doing three repeat measurements, with each measurement consisting of drilling 4 holes.

2.4.4 Reciprocating saws

One battery-powered and one corded (electric) reciprocating saw of equivalent rated power were tested cutting both chipboard and wooden beams. Both types of workpiece were rigidly clamped to a solid table. The dimensions of the chipboard were 500x600x38 mm; the wooden beam 100x100x500

mm. Cuts were made into each workpiece 250 mm from the clamp; each cut was 30 mm apart. Three different operators tested each saw making four cuts into each workpiece.

2.4.5 Impact wrenches

The data for impact wrenches was collected during the course of controlled operations in the training centre of a major vehicle manufacturer. Five battery powered tools and five pneumatic tools were tested. The test involved completing eight tightenings in a 20 second measurement period on bespoke metal training boards developed by the vehicle manufacturer.

2.4.6 Angle grinders

Three pairs of battery-powered and corded (electric) angle grinders of equivalent rated power were tested. The sizes of the paired angle grinders were 115 mm, 125 mm and 230 mm, which represent the most commonly used machines. The angle grinders were tested cutting stone, and cutting and grinding metal. The 115 mm and 125 mm grinders were tested cutting stone both with the manufacturer's recommended on-board dust extraction system and indoors in a dust extraction booth without the on-board extraction system. The 230 mm angle grinders were not used with the manufacturer's extraction hood as they were too large for it to fit. A limestone block was placed on a solid work bench. A carpet on the bench, beneath the limestone stopped the block moving during the tests. The tests using metal were performed outside. For the cutting task, a metal plank was used which initially had dimensions of 800x1050x60 mm. Cuts were made 10 mm apart across the width of the plank. For the grinding task, a 40 cm square of metal approximately 1 cm thick was used. Three different operators tested each angle grinder, cutting and/or grinding each test material; measurements were averaged over 16 seconds. Five repeat measurements were made for each test. Operators were instructed to use the tool in the same way for each measurement. All the angle grinders tested can be used with standard or anti-vibration side-handles; the tools were all tested with standard side handles.

3   RESULTS

Figures 1 to 9 show vibration total values determined for the tools tested during simulated real use operations. Each figure compares the data obtained for the battery powered tool and the equivalent alternative powered versions. For each figure the vibration emissions values taken from the manufacturer's instructions are plotted (where available) with error bar showing the K value added to the emission value.

Data for each tool has been combined from different operators and with repeat measurements to provide a mean and standard deviation.
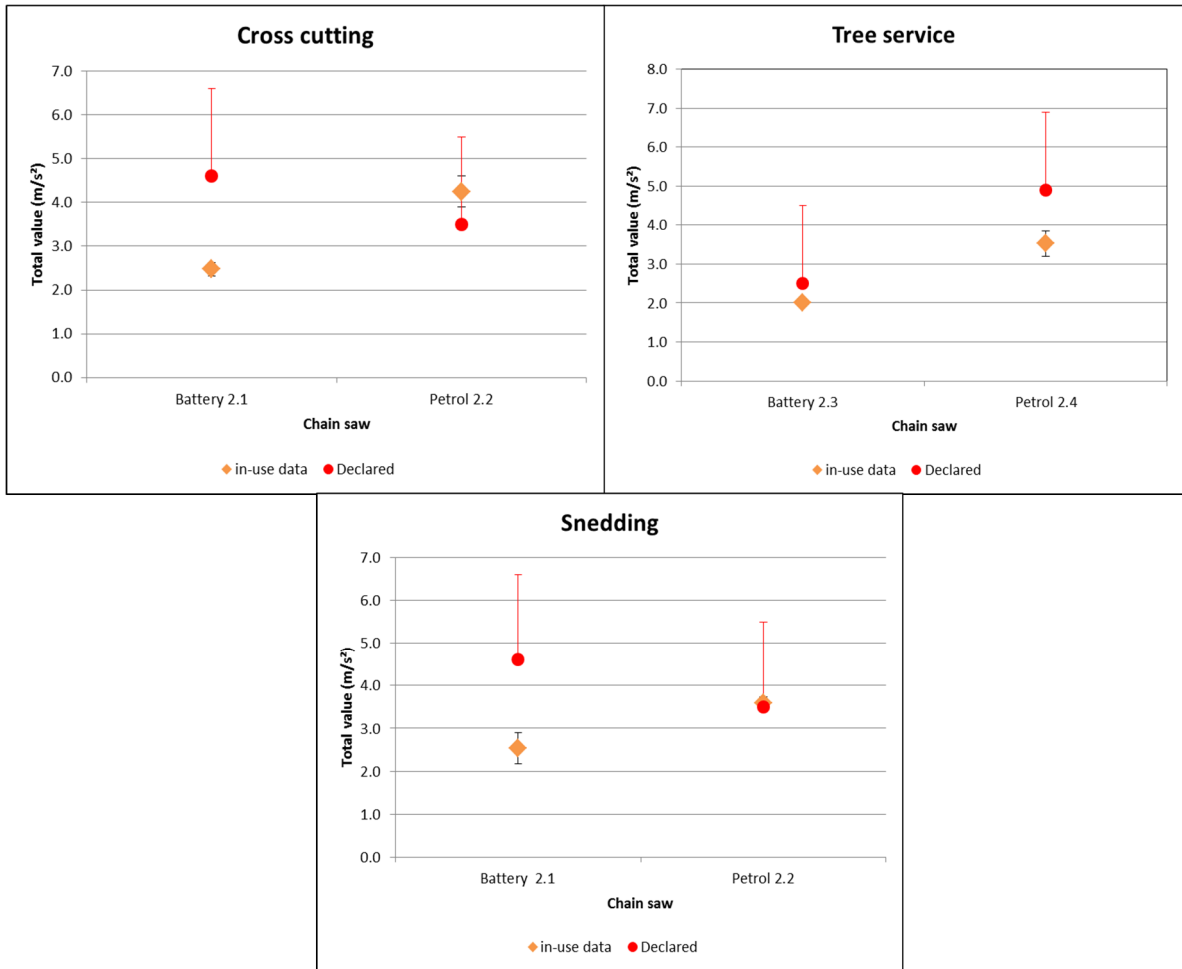
Figure 1 Measured vibration emission data for chain-saws
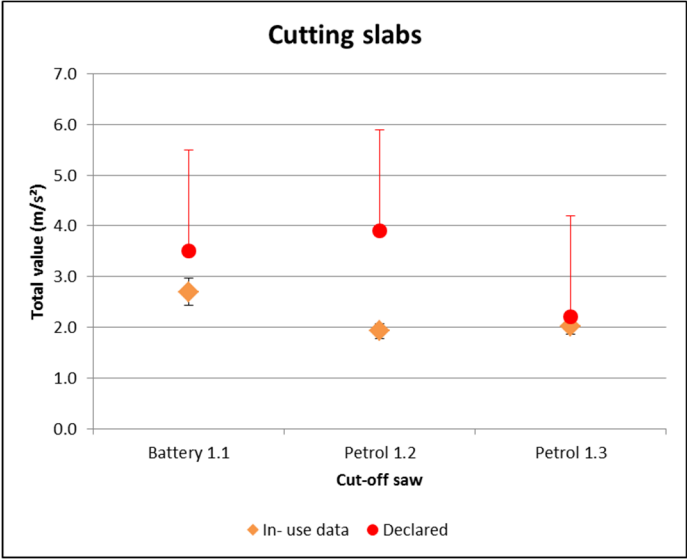
Figure 2 Measured vibration emission for cut-off saws
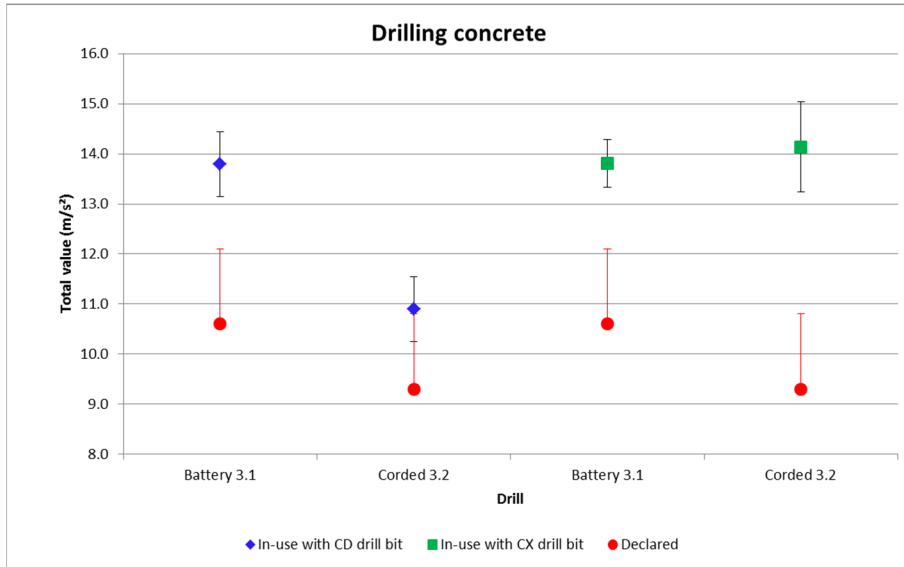
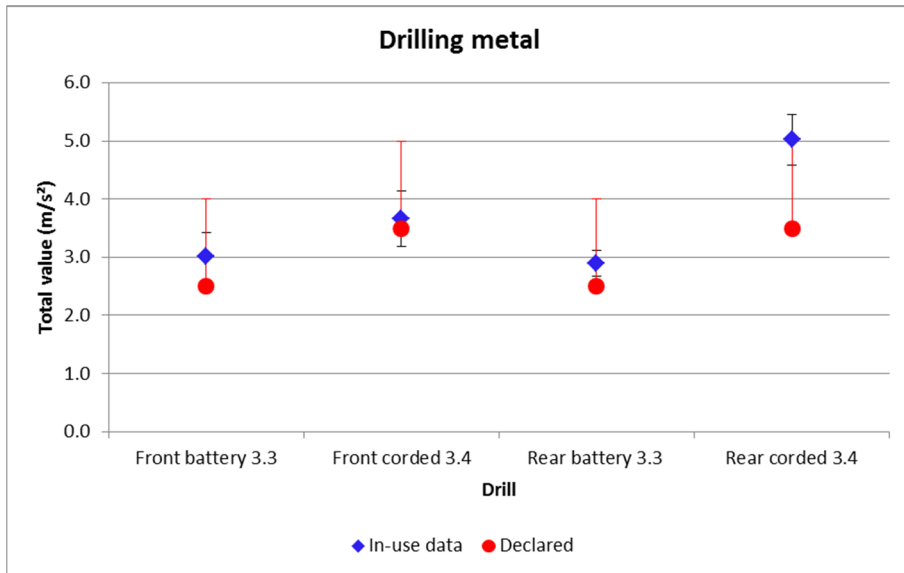Figure 3 Measured vibration emission for drilling concrete.

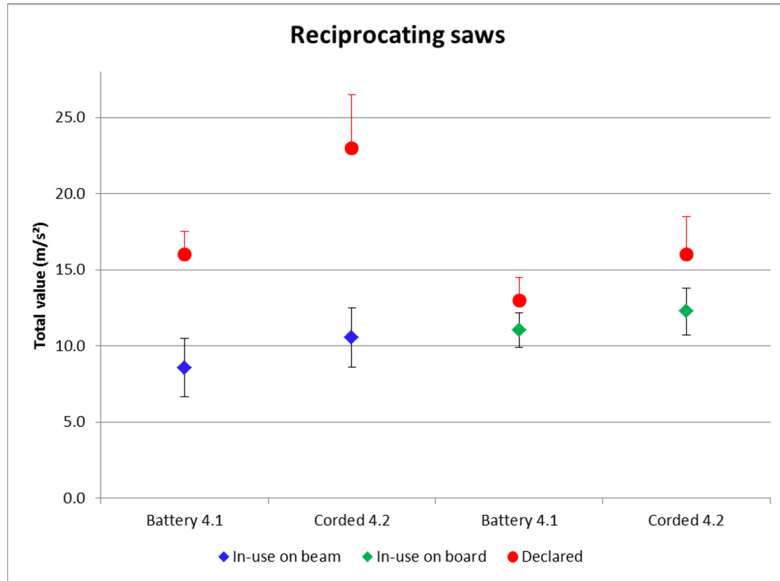Figure 4 Measured vibration emission for drilling metal.

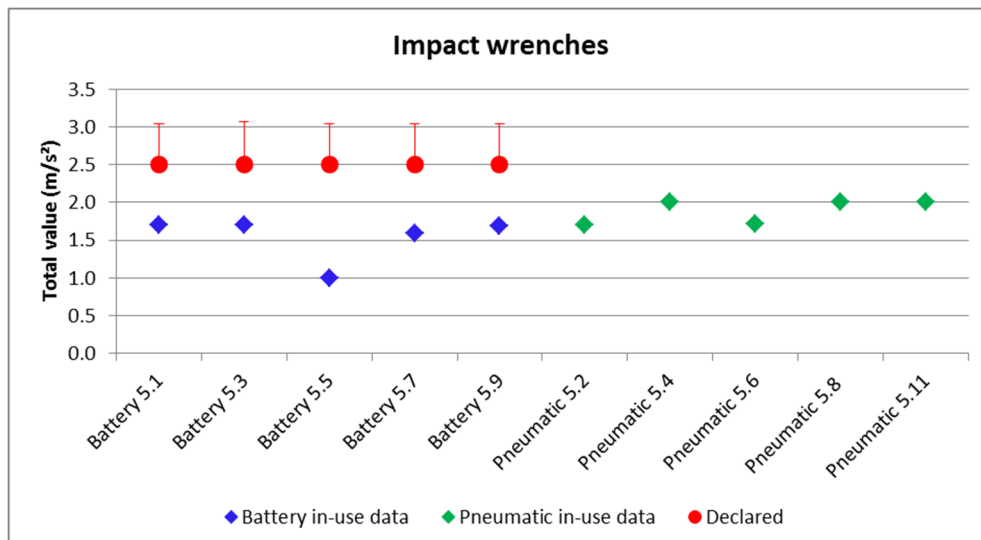Figure 5 Measured vibration emission for reciprocating saws.

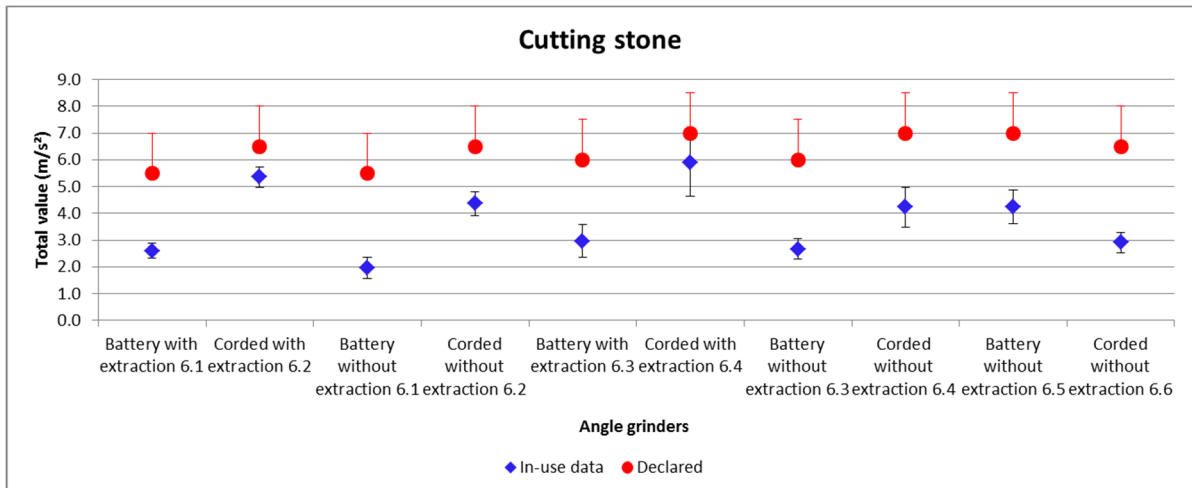Figure 6 Measured vibration emission for impact wrenches.

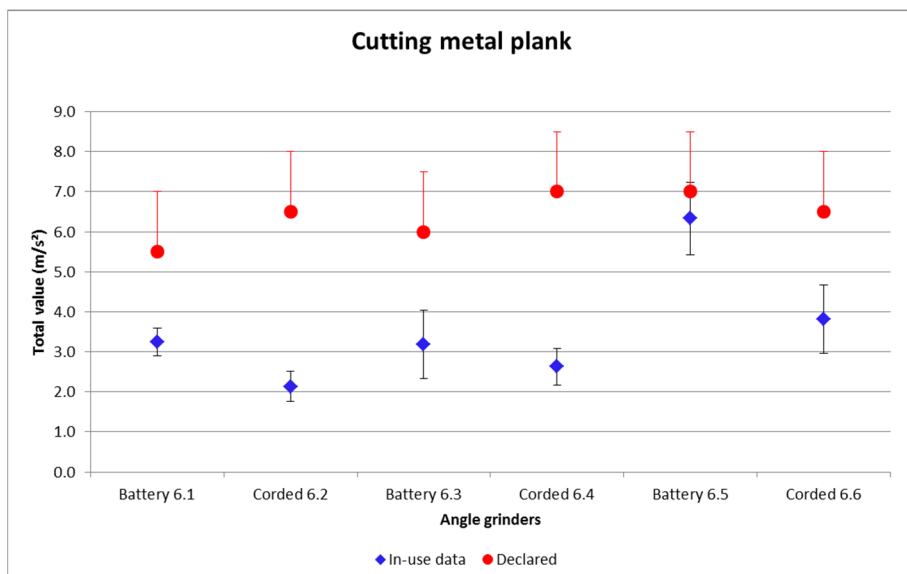Figure 7 Measured vibration emission for cutting stone with angle grinders.

Figure 8 Measured vibration emission for cutting a metal plank with an angle grinder.
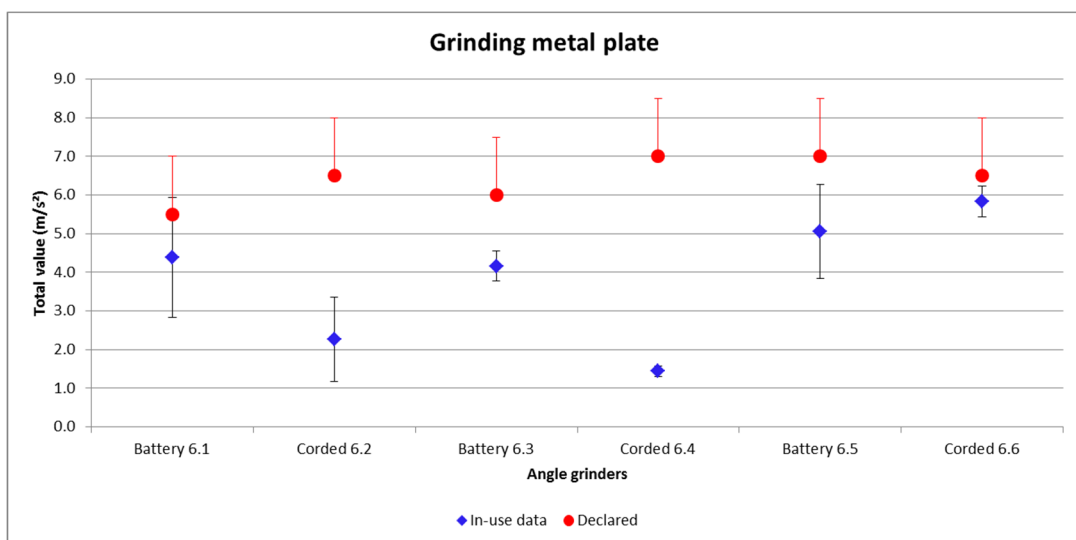
Figure 9 Measured vibration emission for grinding a metal plank with an angle grinder

4   DISCUSSION

For each tool various performance characteristics are discussed. These were characteristics which were considered when choosing equivalent tools.

4.1   Chain-saws

Table 1 shows selected performance data for the four chain-saws tested, as provided in the manufacturer's instruction manual.

Table 1 Manufacturer's technical data - chain-saws

Machine ID	Engine type	Engine size/ battery voltage	Weight bar and chain (kg)	Bar length (inches)	Maximum chain speed (m/s)
2.1	Battery	36 V battery	2.9[a]	14	18.8
2.2	Petrol	35.2 cc	4.3	14	24.8
2.3	Battery	36 V battery	2.7[a]	12	16.1
2.4	Petrol	23.6 cc	2.6	12	22.5
[a]Weight without battery, bar and chain					

The two combustion chain-saws had higher maximum chain speed than either of the battery-powered ones. Figure 1 shows that the vibration emissions for both the battery-powered machines were lower than those measured for the roughly equivalent petrol-powered chain-saw doing the same activity. The petrol-powered chain-saws produced higher vibration emission values than the roughly equivalent battery-powered tools for all operating conditions. For snedding, the battery-powered tool produced 2.5 ± 0.4 m/s² compared to 3.6 ± 0.2 m/s² for the petrol-powered tool. For cross cutting the battery-powered tool produced 2.5 ± 0.2 m/s² compared to the petrol-powered tool which produced 4.2 ± 0.4 m/s².

4.2   Cut-off saws

Table 2 shows selected performance data for the three cut off saws tested, as provided in the manufacturer's instruction manual.

Table 2 Manufacturer's technical data – cut-off saws

Machine ID	Engine type	Weight (kg)	Wheel diameter (mm)	Max spindle speed	Idle speed	Engine power
1.1	Battery	3.9[a]	230	6650 rpm	n/a	n/a
1.2	Combustion	9.9[b]	300	4880 rpm	2600 rpm	3.2 kW at 9000 rpm
1.3	Combustion	10.0[b]	300	4985 rpm	2500 rpm	3.9 kW at 9300 rpm
[a] Weight without battery and wheel with water connection						
[b] Weight without wheel and with electronic water control						

The maximum spindle speed for the petrol driven cut-off saws was lower than the battery-powered saw and consequently produced a lower vibration emission as seen in Figure 2; 2.0 ± 0.2 m/s² compared to 2.7 ± 0.3 m/s².

4.3 Combi-drills

4.3.1 Drilling concrete

Table 3 contains selected performance data for the two drills tested drilling into concrete, as taken from the manufacturer's instruction manual.

Table 3 Manufacturer's technical data - drilling concrete

Machine ID	Engine type	Weight (kg)	Impact rate	Single impact energy
3.1	Battery 36 V	5.1	4500 impacts/min	3.6 J
3.2	Mains 240 V	4.2	4500 impacts/min	3.6 J

Both drills were compatible with two different drill bits, the CX and the CD bits. The CD drill bit is a dust extraction drill bit. It is hollow and connects to a dust extraction system. The CX drill bit is solid. Figure 3 shows that while the in-use vibration emissions were lower for the electric drill compared with the battery-powered drill when used with the dust extraction drill bit, they were higher when the tools were used with the solid CX drill bit. The reason for this result is not clear.

4.3.2 Drilling metal

Table 4 shows selected performance data for the two drills tested drilling into metal, as taken from the manufacturer's instruction manual.

Table 4 Manufacturer's technical data – drilling metal

Machine ID	Engine type	Weight of body (kg)	Rotational speed (RPM)
3.3	Battery 22 V	1.9	220/550/1250/2150
3.4	Mains 240 V	2.4	1200/3300

Table 4 shows the rpm information for the two machines used; they have several gear settings resulting in more than one rotational speed option. The maximum rotational speed of the battery-powered machine is lower than that of the mains-powered machine. During testing all tools were run at maximum speed.

Figure 4 shows that when drilling through a 5 mm mild steel plate, lower vibration emissions were measured on both the front and rear handles of the battery-powered machine compared with the electric.

When drilling metal, it can be seen (Figure 4) that the vibration was higher for the mains-powered machine. As these machines were set to the same rotational speed for drilling metal, should a duty holder wish to purchase machines of lower vibration for drilling the metal, the battery-powered machine should be considered.

4.4 Reciprocating saws

Table 5 shows selected performance data for the two reciprocating saws tested, as taken from the manufacturer's instruction manual.

Table 5 Manufacturer's technical data – reciprocating saws

Machine ID	Engine type	Power / Battery Voltage	Weight (kg)	Stroke (mm)	Speed
4.1	Battery	36 V	4.4	32	2850 strokes/minute
4.2	Mains	900 W	3.5	32	2700 strokes/minute

Figure 5 shows that the battery-powered reciprocating saws produced lower vibration emissions than the electric tools during tests on both test pieces. On the wooden beam the emission values 8.6 ± 1.9 m/s² for the battery-powered tool compared to 11.6 ± 2.3 m/s² for the electric tool; on chipboard the vibration emissions were 11.0 ± 1.2 m/s² compared to 13.0 ± 2.4 m/s².

4.5 Impact wrenches

The data displayed in Figure 6 was provided by a vehicle manufacturer hosting testing. Declared vibration emission data were only available for the battery-powered machines as the pneumatic machines tested are no longer available to purchase. Figure 6 shows that the in-use vibration emissions were comparable for the battery-powered and electric impact wrenches.

4.6 Angle grinders

Table 6 shows selected performance data for the six angle grinders tested, as taken from the manufacturer's instruction manual.

Table 6 Manufacturer's technical data – angle grinders.

Machine ID	Inserted tool size	Engine Type	Power/Battery Voltage	Net weight (kg)	Rotational speed (rpm)
6.1	115 mm	Battery	18 V	2.4-3.1	3000-8500
6.2	115 mm	Mains	1100 W	2.4-2.8	11000
6.3	125 mm	Battery	18 V	2.4-3.1	3000-8500
6.4	125 mm	Mains	1100 W	2.5-3.6	11000
6.5	230 mm	Battery	2 x 18 V	5.2-8.0	6000
6.6	230 mm	Mains	2000 W	5.8-8.16	6600

Figure 7 shows that for the 115 mm and 125 mm angle grinders, the battery-powered tools produced lower vibration emissions than the equivalent electric versions. The 115 mm and the 125 mm angle grinders were tested with and without a dust extraction hood when cutting limestone; the dust extraction hood was not big enough for the 230 mm grinders. The results suggested that the in-use vibration emissions are slightly higher with dust extraction hood than without for both battery and electric grinders; the difference was approximately 1 m/s². However, when using the grinders with the hood, it was difficult to see where the wheel was cutting so the cuts were less consistent and not as deep, which may have influenced the measured vibration emission values.

Figures 8 and 9 show that when cutting and grinding metal, the 115 mm and 125 mm battery-powered machines produced higher vibration emission values compared to the equivalent electric grinders. This was not observed with the 230 mm grinder; the battery version produced higher vibrations when cutting metal and lower vibrations when grinding metal compared to the electric 230 mm grinder. Again, the reason for these differences is not clear from this study.

When using the battery-powered angle grinders to grind metal, the measured vibration emissions decrease as the battery ran down until the machine completely stopped; the vibration value dropped by approximately 3 m/s² as shown in Table 7. The battery was starting to run down for Tests 1 and 2; a fully charged battery used for Test 3 showed a marked increase in the measured vibration when using the tool to grind metal. The data from Tests 1 and 2 were not included in the mean displayed in Figure 9. The average of the 5 tests was taken from Test 3 to Test 7.

Table 7 Comparison of vibration emission data for tool 6.5

Machine ID	Test number	Test conditions	Vibration total value m/s²	
			Front	**Rear**
6.5	1	Cutting metal	1.86	2.93
6.5	2	Cutting metal	1.72	2.55
6.5	3	Cutting metal	4.78	5.60
6.5	4	Cutting metal	5.25	7.14
6.5	5	Cutting metal	4.36	5.73
6.5	6	Cutting metal	4.58	6.49
6.5	7	Cutting metal	4.70	7.09

4.7   Impact of battery-powered machines on in-use vibration emissions

Table 8 summarises the findings of this study, identifying the power sources that produce lower vibration emissions during simulated real use operations. The impact wrenches are not included in Table 8 as the vibration emissions for the battery-powered and pneumatic versions were comparable.

Whilst the results of this study show that battery-powered machines do provide a lower vibration option for some tool types, they may not be the most appropriate machine to use. The range of available combustion engines (petrol), pneumatic and mains powered machines tends to include models with higher power than the battery-powered versions which are likely to be more efficient (faster) at completing a wider range of typical real use tasks.

The battery-powered versions of smaller hand-held tools, such as impact wrenches and drills, which are used for tasks that require manoeuvrability, may benefit from not having to rely on an external power source with the associated trailing cables. For some of these machines the differences in vibration emissions between the battery and alternatively powered machines was small. The differences found for wrenches and drills were similar in magnitude to the variabilities found due to the workpieces and tool bits.

Table 8 Summary showing the power sources that give the lowest vibration emissions

Tool ID	Description	Power source	Activity	Lowest vibration
1.1	Cut-off saw	Battery	Cutting slabs	
1.2	Cut-off saw	Petrol	Cutting slabs	Petrol 1.2
1.3	Cut-off saw	Petrol	Cutting slabs	
2.1	Chain-saw	Battery	Cross cutting	
2.2	Chain-saw	Petrol	Cross cutting	Battery 2.1
2.3	Chain-saw	Battery	Tree service	
2.4	Chain-saw	Petrol	Tree service	Battery 2.3
2.1	Chain-saw	Battery	Snedding	
2.2	Chain-saw	Petrol	Snedding	Battery 2.1
3.1	Drill with CD bit	Battery	Drilling concrete	
3.2	Drill with CD bit	Mains	Drilling concrete	Mains 3.2
3.1	Drill with CX bit	Battery	Drilling concrete	
3.2	Drill with CX bit	Mains	Drilling concrete	Battery 3.1
3.3	Drill with 6mm bit	Battery	Drilling metal	
3.4	Drill with 6mm bit	Mains	Drilling metal	Battery 3.3
4.1	Reciprocating saw	Battery	On beam	
4.2	Reciprocating saw	Mains	On beam	Battery 4.1
4.1	Reciprocating saw	Battery	On board	
4.2	Reciprocating saw	Mains	On board	Battery 4.1
6.1	115 mm angle grinder	Battery	Cutting limestone	Battery 6.1

Tool ID	Description	Power source	Activity	Lowest vibration
6.2	115 mm angle grinder	Mains	Cutting limestone	
6.3	125 mm angle grinder	Battery	Cutting limestone	Battery 6.3
6.4	125 mm angle grinder	Mains	Cutting limestone	
6.5	230 mm angle grinder	Battery	Cutting limestone	Mains 6.6
6.6	230 mm angle grinder	Mains	Cutting limestone	
6.1	115 mm angle grinder	Battery	Cutting metal	Mains 6.2
6.2	115 mm angle grinder	Mains	Cutting metal	
6.3	125 mm angle grinder	Battery	Cutting metal	Mains 6.4
6.4	125 mm angle grinder	Mains	Cutting metal	
6.5	230 mm angle grinder	Battery	Cutting metal	Mains 6.6
6.6	230 mm angle grinder	Mains	Cutting metal	
6.1	115 mm angle grinder	Battery	Grinding metal	Mains 6.2
6.2	115 mm angle grinder	Mains	Grinding metal	
6.3	125 mm angle grinder	Battery	Grinding metal	Mains 6.4
6.4	125 mm angle grinder	Mains	Grinding metal	
6.5	230 mm angle grinder	Battery	Grinding metal	Battery 6.5
6.6	230 mm angle grinder	Mains	Grinding metal	

4.8 Comparison of in-use and manufacturers' declared vibration emissions

In general the declared emissions were comparable to, or higher than, the measured in-use vibration emissions, with the exception of using the combi-drills to drill concrete. A trend can also be seen in much of the data, for example a higher measured value also has a higher declared value. This information could be used to identify low vibration versions of tools.

5 CONCLUSION

For the machine categories investigated in this study, there was no consistent relationship between battery-powered machines and their alternative powered equivalents in terms of vibration emissions. For some machines, such as chain-saws, the battery-powered machines all produced lower vibration emissions than the comparative petrol or mains-powered versions. For other machine types, the relationship was less clear and depended on factors such as the material being processed.

It was not possible for all the tool types tested to find equivalent machines that were identical in all aspects other than power source. There were differences in speed, body shape, weight and power, which can reasonably be expected to affect the vibration emissions as well as the overall suitability of the machine for a job.

For most of the machines tested there was a difference between the HSE measure values and the manufacturer's declared vibration emissions. There are differences in the standard tests for different power sources using the same machine; differences in the declared vibration emissions of machines with different power sources therefore do not necessarily reflect a difference in the vibration hazard presented to the user. The manufacturer's declared emission data could be used identify low vibration versions.

This research has shown that HSE's advice regarding tool selection should not be modified and therefore remains unchanged: selection on the basis of vibration should be made from a shortlist of tools that have already been shown to be well suited to the work[5]. This shortlist may include battery-powered tools that provide a credible low vibration alternative depending on the tool type and the application.

6   REFERENCES

1.   BS EN ISO 5349-1:2001 Mechanical vibration. Measurement and evaluation of human exposure to hand-transmitted vibration. General requirements.
2.   BS EN ISO 5349-2:2001+A1:2015: Mechanical vibration. Measurement and evaluation of human exposure to hand-transmitted vibration. Practical guidance for measurement at the workplace.
3.   BS EN ISO 8041-1:2017: Human response to vibration. Measuring instrumentation. General purpose vibration meters.
4.   BS EN ISO 11681-1:2011: Machinery for forestry. Portable chain-saw safety requirements and testing. Chain-saws for forest service.
5.   Control of Vibration at Work Regulations 2005. http://www.hse.gov.uk/pUbns/priced/l140.pdf (accessed August 2019).

Competitive mountain bike racing: a study of rider hand-arm vibration exposure

Mark D. Taylor [1], Lewis A. Kirkwood [2], Lesley A. Ingram[2], Eva Malone[2], Geraint D. Florida-James[2]

[1]Edinburgh Napier University
School of Engineering & the Built Environment, 10 Colinton Road,
Edinburgh, EH10 5DT
m.taylor@napier.ac.uk
[2]Edinburgh Napier University, School of Applied Sciences, 9 Sighthill Court,
Edinburgh, EH11 4BN
l.kirkwood@napier.ac.uk, l.ingram@napier.ac.uk,
e.malone@napier.ac.uk, g.florida-james@napier.ac.uk

ABSTRACT

Limited information is available regarding the hand-arm vibration (HAV) exposure for professional off-road cyclists. Previous research has suggested that commuting and recreational cyclists are at risk of exceeding exposure limit values (ELV) in a single ride. Therefore, further investigation of HAV exposure in competitive mountain biking is warranted. Exposure data (A(8) (ms^{-2})) were obtained for national level mountain bike enduro competitions. Hand-arm vibration exposure was assessed using a tri-axial accelerometer recording at a frequency of 3.2 kHz mounted on the handlebars. Frequency weighting and band limiting filters were applied in accordance with BS EN ISO 5349-1. The data presented shows that HAV exposure during one day of competitive enduro mountain bike racing exceeds ELV (mean race exposure = 5.84 ms^{-2}, minimum = 5.47ms^{-2}, maximum = 6.61ms^{-2}) and is greater than the HAV exposure observed in recreational cycling. This suggests that further work is required to determine exposure reduction associated with changes in equipment, technique and international racing events in professional athletes.

1   INTRODUCTION

Exposure to hand-arm vibration in the workplace is tightly controlled due to evidence linking excessive exposure to musculoskeletal, neuromuscular, vascular and other types of pathologies. Hand-arm vibration syndrome (HAVS) is a recognised industrial disease induced by excessive exposure to vibration through occupational tasks involving vibrating machinery [1]. HAVS is a progressive and irreversible condition comprising a range of disorders affecting the peripheral circulatory system, peripheral nervous system and muscular skeletal system of the hand and arm. Therefore, the ability to predict a rate of progression of HAVS and take timely preventative action through exposure reduction or complete elimination of hazardous exposure is highly desirable. Despite strict enforcement of vibration exposure guidelines in the work place, professional sports have received less attention despite evidence of potentially harmful vibration exposure. However, vibration data has been considered in relation to overuse injury prevention in sports [2]. There have also been significant competitive wins where increased performance has been associated with vibration management. These include Gilbert Duclos-Lassalle's Paris-Roubaix win in 1992 and more recently, Peter Sagan's win at the same race in 2018. Both bicycles were fitted with shock absorbing

devices in the front fork designed to reduce vibration transferred to the handlebar induced from the cobbles encountered throughout this race.

Previous research has assessed the relative difference of bicycle components on the vibration induced in the hands and body of cyclists. Lépine *et al.* [3] assessed the relative contribution of vibration through measurement in three locations. These included the vibration transmitted through the handlebars, saddle and brake hoods. Results showed that the handlebar and fork were the main contributors of vibration induced at the hands, whilst the frame and wheels were the main components associated with vibration induced at the buttocks of the cyclist [3]. Gomes and Savionek [4] conducted hand-arm vibration exposure assessment on a range of pavement surfaces including asphalt, precast concrete and interlocking concrete blocks. Using an accelerometer attached to the handle bars, they determined the daily vibration exposure using a two-hour duration to represent the average time of a commuter cyclist's journey. Terrain was shown to be a key factor of vibration exposure with interlocking concrete blocks presenting significantly higher values than asphalt or precast concrete. Parkin and Eugenie Sainte [5] provided a study of comfort and health factors including the nature of vibration from riding in different circumstances in the City of London. Several cyclists reported having discomfort or pain after cycling, proposed to be related to vibration exposure during cycling, inappropriate body position while cycling or a combination of both factors [6].

Munera *et al.* [7] summarised the different standards and guidelines associated with the evaluation of vibration and exposure limits whilst cycling. Focussing on performance athletes, they considered the application of European Directive 2002/44/EC (EC 2002) in defining the limits of exposure and action 'triggers' for safe exposure management in sport with particular reference to the exposure action value (EAV; 2.5 ms^{-2}) and the exposure limit value (ELV; 5.0 ms^{-2}). In a limited number of studies on road cycling, harmful levels of hand-arm vibration have been reported when riding on cobbled surfaces where exposure limit values (ELV) values are exceeded in less than 20 minutes [8, 9, 10]. This is particularly concerning as riders competing in races such as the Paris-Roubaix spend ~90 minutes riding on cobblestones and are therefore subjected to harmful levels of hand-arm vibration.

Despite the broad range of research concerning road or commuter cycling, to the authors' knowledge, there has been no attention given to the hand-arm and hand-transmitted vibration that mountain bike enduro athletes are exposed to. Additionally, studies that have explored magnitude of vibration experienced by downhill [11] and cross-country riders [12, 13] were limited by the fact that they did not meet the analysis requirements of hand-arm vibration exposure in compliance with of the international standard BS EN ISO 5349-1:2001. In particular, there has been limited attention to measurement of the appropriate frequency range and the application of the appropriate weighting filters within the previous work.

Enduro mountain bike races are composed of a series of timed, predominantly downhill race stages on challenging downhill terrain linked by non-competitive, primarily uphill, transition sections (Enduro World Series 2018). The physiological demands of elite enduro competition requires a large aerobic capacity with intermittent anaerobic contribution coupled with the ability to navigate technical terrain at high speed [14, 15]. This latter study also demonstrated that faster riders experienced greater vibration exposure values (r.m.s. ms^{-2}) over the duration of an international enduro race stage, though no detailed vibration analysis was presented. The extreme terrain, high velocities and prolonged duration warrant further investigation of hand-arm vibration in enduro mountain bike competition.

2 EXPERIMENTAL METHOD

2.1 Test participants

Two male elite enduro athletes (athlete no. 1 age = 24 years; athlete no. 2 age = 31 years) who were either currently or recently professional athletes and previously placed in the top ten overall

positions at an Enduro World Series race were recruited for this study. Ethical approval for this study was granted by the Edinburgh Napier University ethics committee in accordance with the World Medical Association Declaration of Helsinki (World Medical Association 2001). Written and verbal consent was obtained from both participants prior to commencement of data collection.

2.2   Track and bicycle details

Vibration exposure data was collected during two national level enduro races: (i) a round of the Scottish Enduro Series (SES) and (ii) the British Enduro Championship Race from the same year (BC). Elevation and distance profiles of each race event are provided in Figures 1 and 2. Data concerning the elevation, distances covered and gradients for the BC and SES stages are provided in Tables 1 and 2. The athletes rode their own bicycles (all size large) which were set up to personal preference as detailed in Table 3. Athlete 1 (A1) rode a bicycle with 584mm outer diameter rims (650b) front and rear in both events while athlete 2 (A2) rode a 650b bicycle during SES and a bicycle with 622mm outer diameter rims (29er) front and rear during BC. The SES race consisted of five race stages over a distance of 33.8km with a total elevation gain of 1579m. The BC race consisted of six race stages within a 52.2km course featuring 1493m elevation gain.
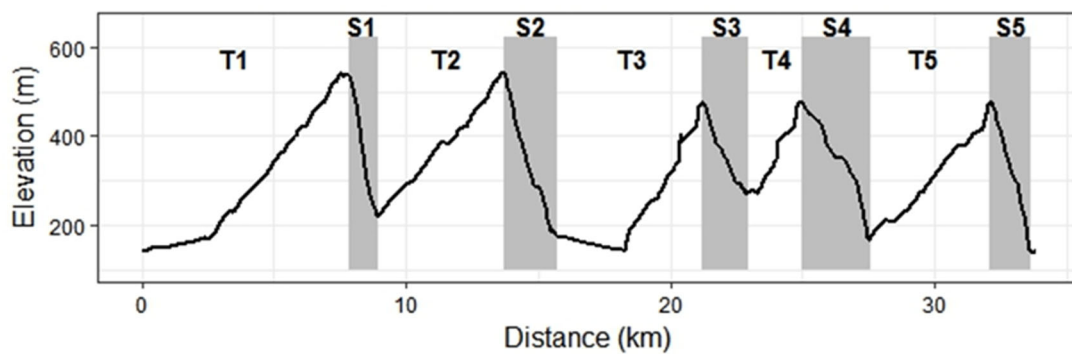
Figure 1: SES stage summary showing transitions, stages and elevation.

Table 1: Distance, elevation and gradient of SES race event.

Section	Distance (km)	ΔElevation (m)	Gradient (%)
Course total	33.8	1579	-
Stage 1	1.12	-297	-26.5
Stage 2	1.05	-221	-21.1
Stage 3	1.58	-198	-12.6
Stage 4	2.52	-308	-12.2
Stage 5	1.43	-331	-23.1
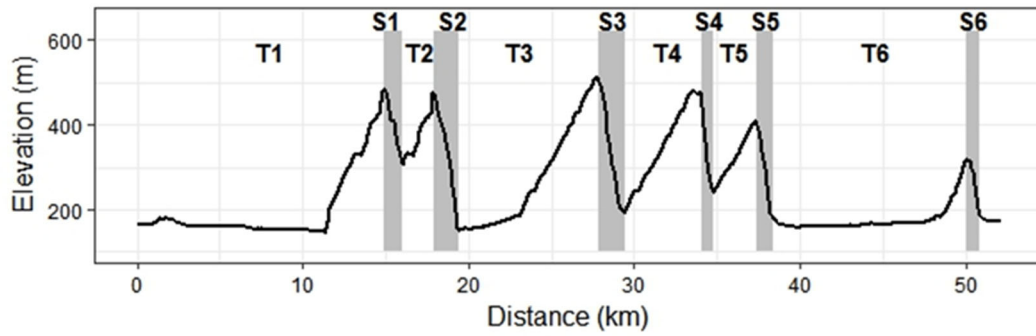
Figure 2: BC stage summary showing transitions, stages and elevation.

Table 2: Summary of distance, elevation and gradient for BC event.

Section	Distance (km)	Elevation (m)	Gradient (%)
Course total	52.2	1493	-
Stage 1	0.99	-157	-15.9
Stage 2	1.38	-298	-21.5
Stage 3	1.40	-292	-20.9
Stage 4	0.72	-215	-29.9
Stage 5	0.76	-153	-20.2
Stage 6	0.60	-114	-19.1

Table 3: Details of participant bicycle components and set-up.

	Scottish Enduro Series		British Championships	
Participant	1	2	1	2
Height (cm)	181	182.3	181	182.3
Total mass (kg)	78.9	80.4	77.5	81.5
Bike mass (kg)	15.2	15.5	14.8	15.9
Total cycling mass (kg)	94.1	95.9	92.3	97.4
Tyre pressure (front/rear; psi)	22/27	18/20	22/26	20/20
Fork pressure (psi)	75	77	75	70
Fork suspension travel (mm)	170	160	170	160
Wheelsize	650b	650b	650b	29
Frame	Ibis Mojo HD4	Ibis Mojo HD4	Ibis Mojo HD4	Ibis RipMo
Fork	Fox 36	Fox 36	Fox 36	Fox 36

Shock	Fox Float X2	Fox Float X2	Fox Float X2	Fox Float X2
Handlebars	Joystick Analog Carbon	Joystick Analog Carbon	Joystick Analog Carbon	Joystick Analog Carbon
Stem	Joystick Analog 50mm	Joystick Analog 50mm	Joystick Analog 50mm	Joystick Analog 50mm

2.3   Accelerometer and mounting positions

A proprietary three-axis accelerometer and data logger (Axivity AX-3) was selected as a robust and compact measurement device with suitable overall dimensions and data storage capability. The device sample rate was 3.2 kHz with a range of ±16g.

It is essential that human vibration exposure is quantified by the vibration conditions at the interface between the environment and the human body: not by the vibration at any other arbitrary position on the body or in the vibration environment [16]. However, due to the need to avoid potential interference with the riders hand grip and control ergonomics under racing conditions, a compact, lightweight and generic handle bar mount adaptor was utilised. Due to the low mass of the combined mount and accelerometer (26.432g < 5% of the handle bar, refer to BS EN ISO 5349-2:2001, Clause 6.1.5), it was deemed not to affect the vibration characteristics of the handlebars. The accelerometer mount was positioned in close proximity to the handlebar grip. The bespoke accelerometer mount was constructed from a stereolithography file using a 3D printer (Makerbot Replicator 2) and was printed from acrylonitrile butadiene styrene (ABS) thermoplastic polymer. Figure 3 shows the adaptor dimensions. Figure 4 shows the position of the accelerometer mount on the handlebar.
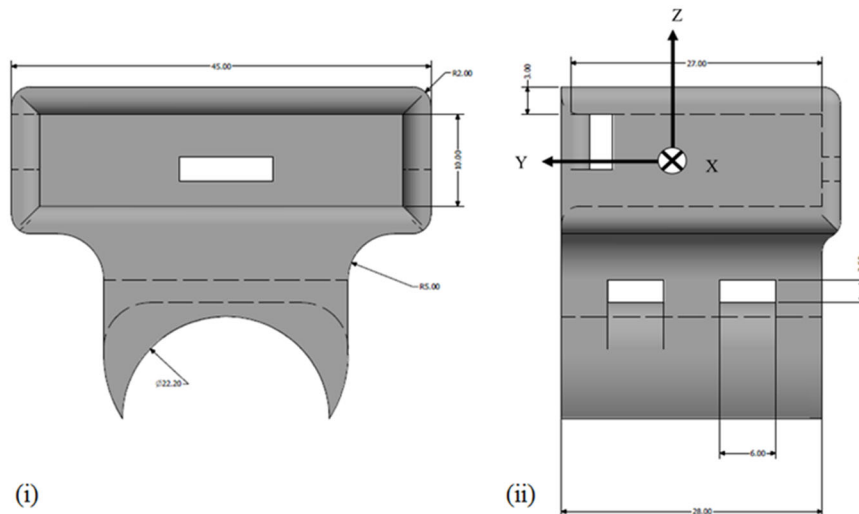
Figure 3: (i) Front and (ii) end elevation of handle bar accelerometer mount showing apertures for fixing ties and orientation of measurement axes.
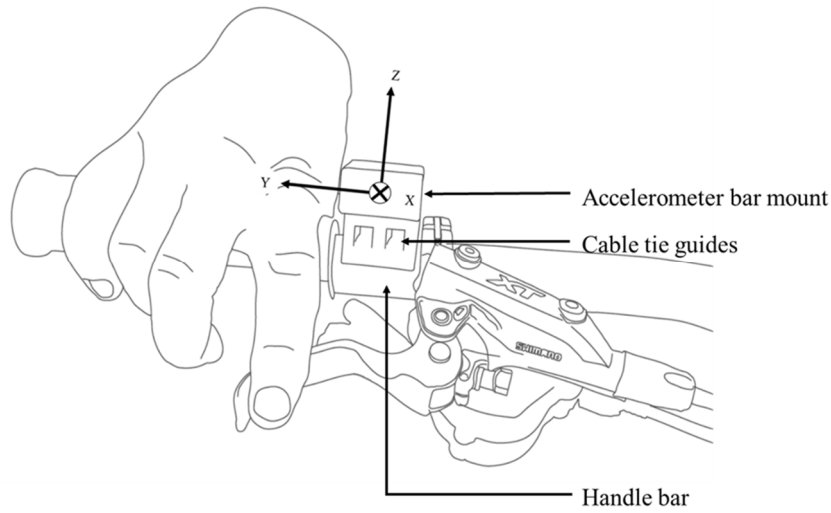
Figure 4: *In-situ* handle bar accelerometer mount showing proximity to hand grip.

2.4   Signal processing and analysis

Digital signal processing was undertaken using Matlab 2018b. Toolbox add-ons included the Control System Toolbox (Version 10.2), Digital Signal Toolbox (Version 9.4) and Signal Processing Toolbox (Version 7.4). Digital filters (W_h) were constructed in accordance with ISO 5349 [17] (BSI 2001) using continuous time transfer functions. The current research considers the application of European Directive 2002/44/EC to mountain bike enduro race events. Therefore, daily vibration exposure is considered in the present study with reference to the exposure action value (EAV = 2.5 ms^{-2}) and the exposure limit value (ELV = 5.0 ms^{-2}).

Each racing stage of the race was considered as a discrete operation and as a partial vibration exposure ($A_i(8)$). Transition stages were not included in the present analysis. However, despite riders not racing, these stages may also contribute to additional partial vibration exposure over the duration of the race. The r.m.s. acceleration values (Equation 1) were calculated for each rider on each race stage (Scottish Enduro Series, Stage 1-5 and British Championship Stage 1-6).

The r.m.s. acceleration value was calculated using:

$$a_{hv} = \sqrt{a_{hwx}^2 + a_{hwy}^2 + a_{hwz}^2}$$

(1)

where a_{hv} is the total vibration value (frequency-weighted acceleration sum), a_{hwx}, a_{hwy} and ah_{wz} are the single axes acceleration values for the axes denoted x, y and z.

Amplitude analysis was conducted using the mean value, standard deviation, root-mean-square (r.m.s.) and root-mean-quad (r.m.q.). For the time series sampled for a period of time, Ts, at fs samples per second with a total of N samples data values x(i), where i = 1 to N, the mean value (x′) is calculated as:

$$x' = \frac{1}{N} \sum_{i=1}^{i=N} x(i)$$

(2)

The standard deviation is calculated as:

$$\sigma = \left\{ \frac{1}{N} \sum_{i=1}^{i=N} [x(i) - x']^2 \right\}^{1/2}$$

(3)

The root-mean-square (r.m.s.) value, is calculated as:

$$r.m.s. = \left[\frac{1}{N} \sum x^2(i) \right]^{1/2}$$

(4)

The root mean quad (*r.m.q.*) considers the *r.m.s.* acceleration raised to the fourth power and ensures that consideration is given to the peaks in the acceleration levels. The authors propose the use of the r.m.q., alternatively known as the vibration dose value (VDV) and commonly used in whole body vibration analyses, as an indicator of the peak vibrations (or shock) experienced by the rider. The root-mean-quad is calculated as:

$$r.m.q. = \left[\frac{1}{N} \sum x^4(i) \right]^{1/4}$$

(5)

The exposure time for each stage was calculated in accordance with the official event times provided by the race organiser. The partial exposure time for each race stage (Equation 2) was then combined to calculate the 8-hour energy equivalent vibration total value (Equation 3). This value can then be considered to be the race vibration exposure value. To facilitate comparison between the different stages and evaluate the individual contribution, each stage was considered as a partial stage vibration exposure calculated as:

$$A_{i,stage}(8) = a_{hvi} \sqrt{\frac{T_i}{T_0}}$$

(6)

The race exposure (considering racing stages only) has been calculated in the similar manner to the calculation of a daily vibration (BSI 2015) considering the summation of the partial exposure values as:

$$A_{race}(8) = \sqrt{\sum_{i=1}^{n} A_i^2(8)}$$

(7)

The daily vibration exposure for the rider would include all race stages, transition stages and all riding throughout the entire day. Due to the data storage requirements of recording a rider's entire daily vibration exposure, race stage vibration exposure has been considered for the present study. Frequency-weighted partial vibration exposure values (r.m.s., ms^{-2}) are calculated by applying the W_h weighting filter (BSI 2001). The human sensitivity to vibration depends on (i) the frequency, (ii) the direction of vibration, both translational and rotational and (iii) the posture of the human (Giubilato & Petrone 2012). Frequency weighting curves consider these aspects of human sensitivity. The frequency-weighting and band-limiting filter reflected the assumed importance of the different frequencies in causing injury to the hand and arms. Band-limiting high-pass and low-pass filters are used to restrict the measured value of vibration frequencies. These filters were realised using digital

methods and applied using a Matlab 2018b programme. The characteristics of the W_h filter are provided in Annex A of BS EN 5349-1:2001 (BSI 2001).

3   RESULTS

The athletes successfully finished both race events and provided complete data sets. Both athletes finished in the top 10 overall positions at both race events, highlighting the elite status of these athletes. The athletes provided permission for these details to be included as it is realised that they could potentially be identifiable from these data. Details of overall race and individual stage performance are provided in Table 4.

Table 4: Time and mean speed for each stage.

Stage	Time (s)		Mean speed (km.h^{-1})	
Participant	1	2	1	2
SES Overall	1282.8	1319.0	21.61	21.02
SES 1	195.47	202.27	20.63	19.93
SES 2	266.35	273.32	14.19	13.83
SES 3	259.95	270.20	21.88	21.05
SES 4	455.26	485.55	19.93	18.68
SES 5	233.33	245.58	22.06	20.96
BC Overall	928.5	1041.0	22.68	20.23
BC 1	138.90	159.91	25.66	22.29
BC 2	186.80	214.58	26.60	23.15
BC 3	242.17	266.98	20.81	18.88
BC 4	141.11	158.21	18.37	16.38
BC 5	127.44	140.44	21.47	19.48
BC 6	92.08	100.84	23.46	21.42

Table 5 provides the overall stage time (*r.m.s*). vibration exposure for the duration of the stage including the mean (x'), standard deviation (σ), root-mean-quad (*r.m.q.*) and partial vibration exposure ($A_{i,stage}$ *(8)*). The race vibration exposure for both athletes in both the British Championship and Enduro Series races was in excess of the ELV (5.0 ms^{-2}) in accordance with EC Directive 2002/44/EC.

Both athletes experienced lower vibration exposure at BC compared to SES. The faster rider (A1) also presented larger stage and overall race vibration exposure values throughout both races and all stages with the exception of BC stage 2. The greatest race vibration exposure value was experienced by A1 at SES ($A_{race}(8) = 6.97$ ms^{-2}) while the lowest vibration exposure was A2 at BC ($A_{race}(8) = 5.47$ ms^{-2}). Figure 5 and Figure 6 show the time domain data for the maximum and minimum partial vibration (stage) exposures. Figure 5 shows a peak value of the total vibration (frequency-weighted acceleration sum) of 144.14 ms^{-2}. Figure 6 shows a peak value of the total vibration (a_{hv}) of 126.15 ms^{-2}. Interestingly, the r.m.q. results for BC A1 Stage 2 show that the course has more peak acceleration values despite the r.m.s. value being lower than the other stages in the race. Furthermore, BC Stage 6 also shows a considerable amount of shock impacts with high VDV of 37.12 ms$^{-1.75}$ in comparison with the other stages in race.

Table 5: Summary of vibration analysis results from British championship (BC) and Scottish Enduro Series (SES). S = stage, A1 = athlete 1, A2 = athlete 2.

Athlete/ race		t (s)	x' (ms^{-2})	σ (ms^{-2})	*r.m.s.* (ms^{-2})	*r.m.q.* (ms$^{-1.75}$)	$A_i(8)$ (ms^{-2})	$A_i^2(8)$ (ms^{-2})
A1 BC	S1	138.90	27.05	17.73	32.34	42.35	2.25	5.04
	S2	186.80	21.87	18.32	30.61	43.18	2.46	6.08
	S3	242.17	25.82	17.51	31.20	41.38	2.86	8.18
	S4	141.11	26.61	17.51	31.85	41.55	2.23	4.97
	S5	127.44	26.72	17.19	31.77	41.29	2.11	4.47
	S6	92.08	26.48	17.25	31.60	41.07	1.79	3.19
Total race		-	-	-	-	-	-	**5.65**
A2 BC	S1	159.91	23.28	15.55	27.99	36.85	2.09	4.35
	S2	214.58	25.51	17.16	30.75	40.38	2.65	7.04
	S3	266.98	23.22	16.10	28.25	37.76	2.72	7.40
	S4	158.21	23.62	15.71	28.37	37.46	2.10	4.42
	S5	140.44	23.78	15.73	28.51	37.15	1.99	3.96
	S6	100.84	23.37	15.54	28.06	37.12	1.66	2.76
Total race		-	-	-	-	-	-	**5.47**
A1 SES	S1	195.47	26.24	17.87	31.75	41.79	2.62	6.84
	S2	266.35	23.56	16.52	28.77	38.98	2.77	7.66
	S3	259.95	27.75	18.59	33.40	43.57	3.17	10.07
	S4	455.26	24.79	16.35	29.69	39.18	3.17	10.03
	S5	233.33	27.38	19.20	33.44	44.43	3.01	9.06
Total race		-	-	-	-	-	-	**6.61**
A2 SES	S1	202.27	22.86	15.87	27.83	36.99	2.33	5.44
	S2	273.32	20.42	14.16	24.85	33.37	2.42	5.86
	S3	270.20	22.99	15.32	27.63	36.20	2.68	7.16
	S4	485.55	20.58	13.44	24.58	32.30	2.62	6.87
	S5	245.58	23.08	15.66	27.89	36.85	2.58	6.63
Total race		-	-	-	-	-	-	**5.65**
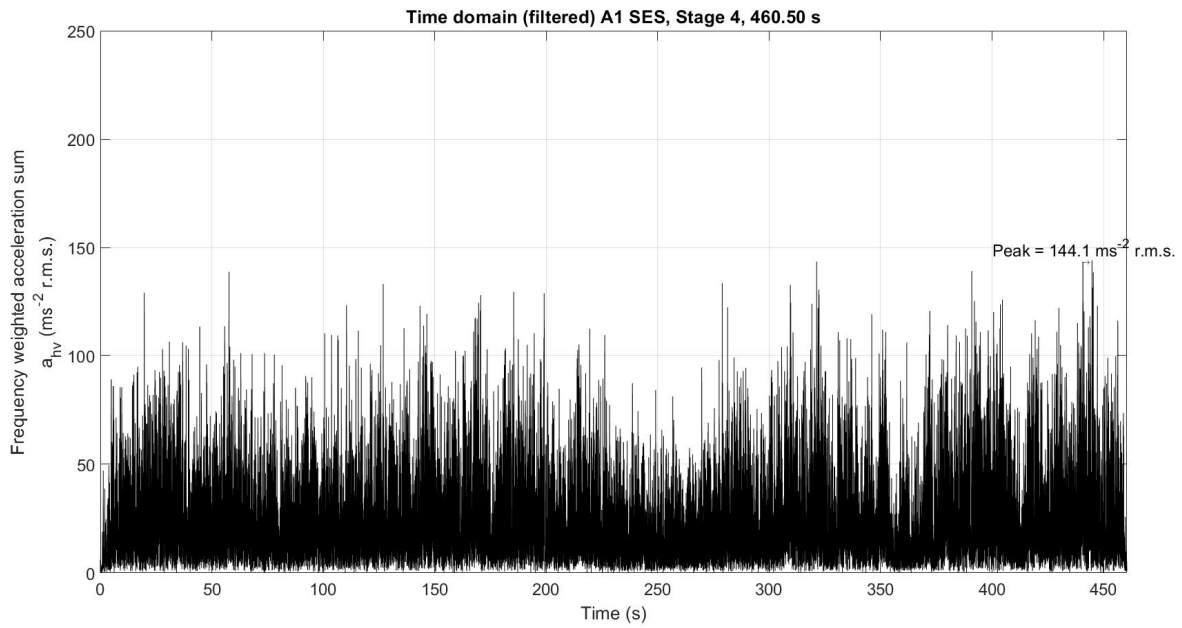
Figure 5: Time domain data showing maximum partial vibration exposure (A(8) = 3.87 ms^{-2}, SES A1, Stage 4).
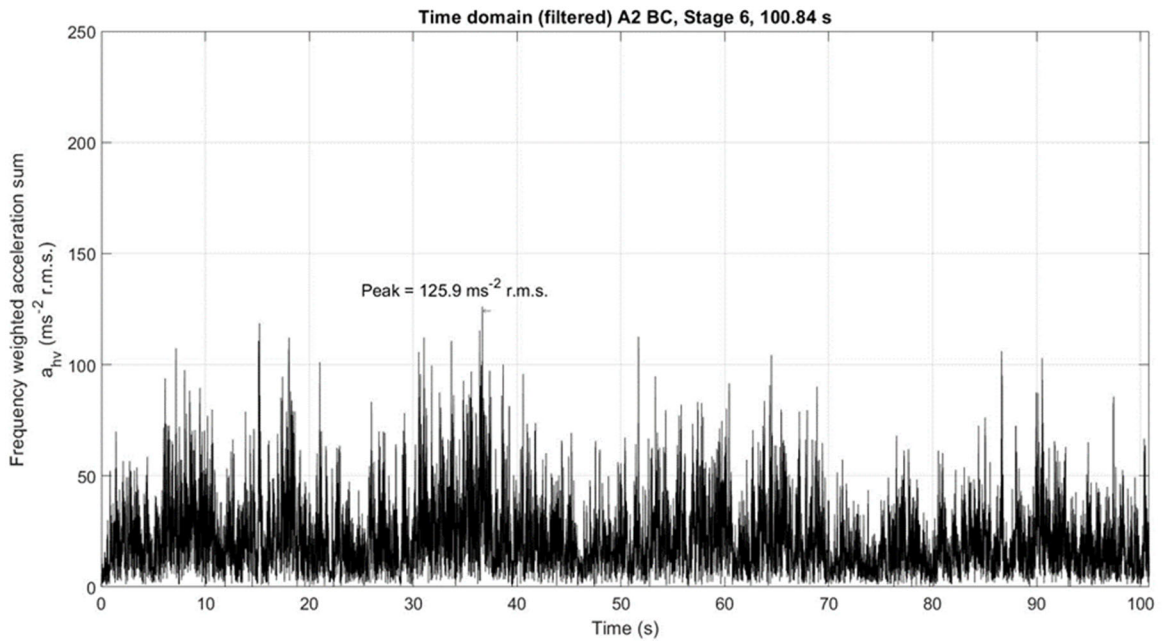
Figure 6: Time domain data minimum partial stage vibration exposure (A_i(8) = 1.66 ms^{-2}, BC A2, Stage 6).

Figure 7 and Figure 8 show the frequency domain data for the two stages in the SES and BC races. The race stage (A1, SES, Stage 4) with the higher partial stage vibration exposure shows a reduced magnitude of vibration in comparison with the lower partial stage vibration exposure (A2, BS, Stage 5). Power spectral density has been used to compare the power in each of the example vibration signals.

Frequency domain (filtered) A1 SES, Stage 4, 460.50 s
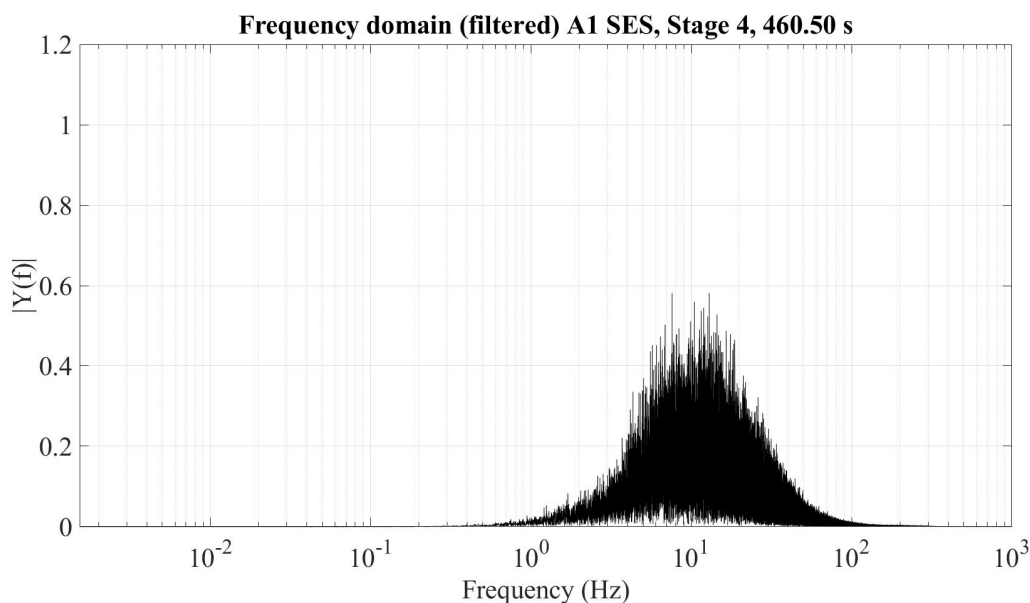
Figure 7: Frequency domain data showing the dominant frequencies and magnitudes (SES A1, Stage 4).

Frequency domain (filtered) A2 BC, Stage 6, 100.84 s
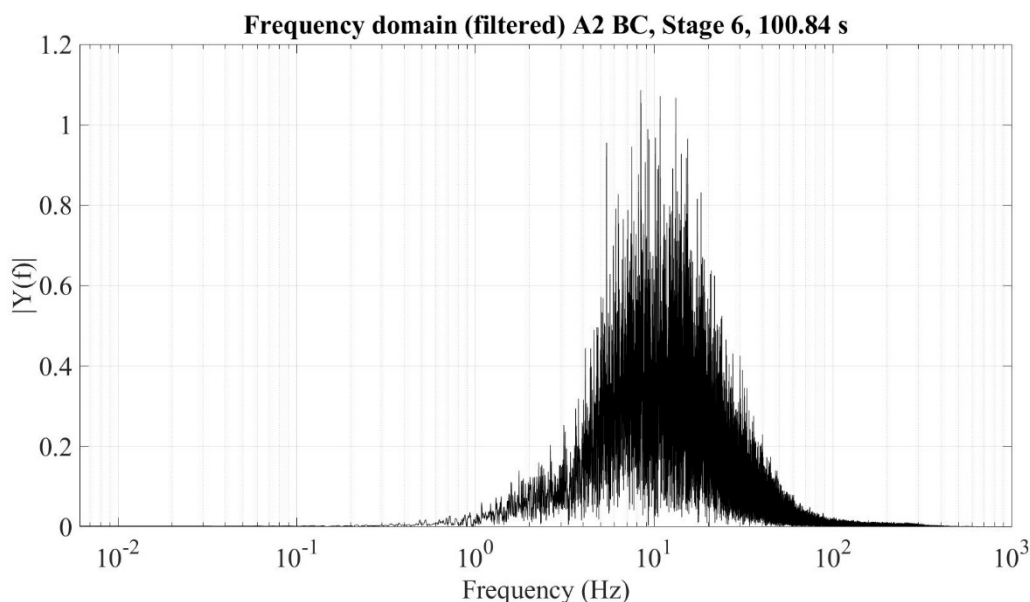
Figure 8: Frequency domain data showing the dominant frequencies and magnitudes (BC A2, Stage 6).

The power spectral analysis are shown in Figure 9 and 10 for the British Championship Stage 6. They show how power of the vibration signal is distributed over frequency by constructing a power spectral density. Figure 9 shows the spectral analysis for rider A1 on Stage 6 (t = 92.08 s). Considering the power from 6.3 Hz to 1259 Hz, the total power in the vibration was 22.33 dBHz. Considering a range of 6 Hz to 80 Hz, the total power in the vibration 22.29 dBHz. Three peak frequencies were identified at 18.75 Hz (-9.23 dBHz), 31.25 Hz (-9.30 dBHz) and 50 Hz (-21.25 dBHz). Figure 10 shows the spectral analysis for rider A2 on Stage 6 (t = 100.84 s). Considering the power from 6.3 Hz to 1259 Hz, the total power in the vibration was 21.13 dBHz. Considering a range of 6 Hz to 80 Hz, the total power in the vibration 21.10 dBHz. A peak frequency was identified at 37.50 Hz (-12.82 dBHz). Power spectral analysis may provide insights into the performance of the suspension and rider in relation to monitoring power and peak frequencies. These may contribute to assessing the overall physical impact of the stage (or race) on the hand-arm system and provide understanding of how vibration analysis may contribute to reducing the potential for harm and

improving performance. Monitoring hand-arm vibration exposure may contribute to a riders' ability to sustain competitive performance.
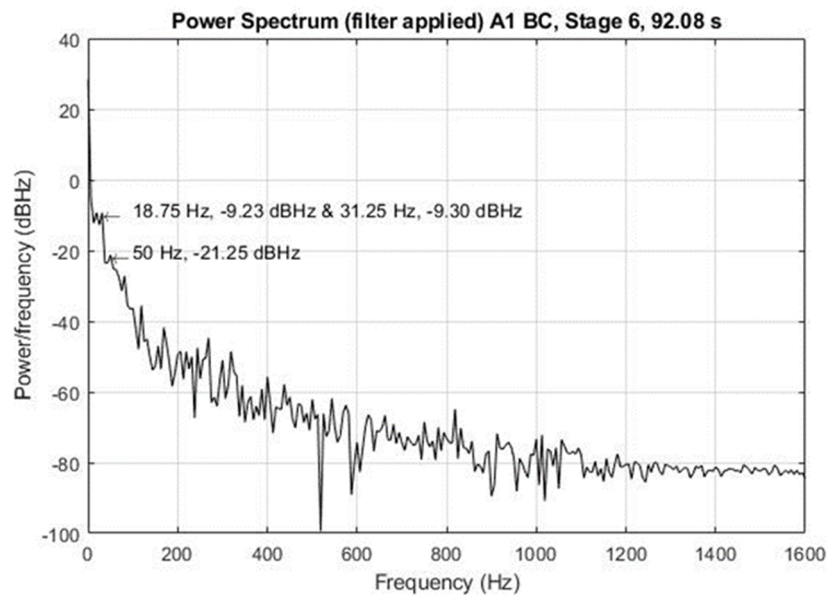
Figure 9: Power spectral analysis for SES A1, Stage 4.
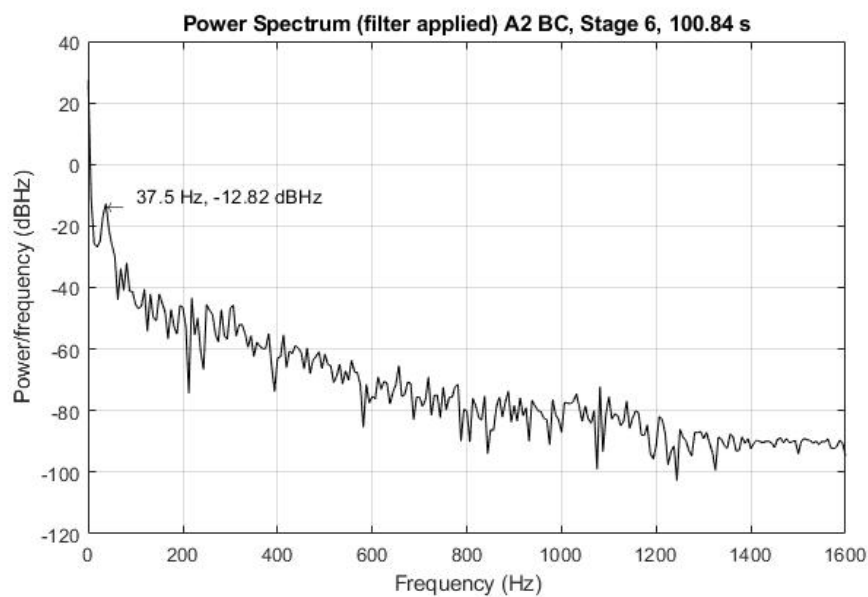
Figure 10: Power spectral analysis for BC A2, Stage 6.

4 DISCUSSION

The results presented in this study suggest that elite enduro mountain bike athletes are exposed to potentially harmful levels of hand-arm vibration during the race stages of an enduro event. As the total race vibration exposure (A(8)) is exceeded at each event for both athletes, prolonged or repeated exposure to such levels of vibration could potentially lead to the development of vibration related pathologies such as ulnar nerve compression or HAVS. Under the control of vibration at work regulations adopted in industrial sectors, employers have an obligation to ensure they take immediate action to reduce exposure to below the limit value. Furthermore, they should introduce a programme of controls or new equipment to eliminate risk, or to reduce exposure to as low as reasonably practicable.

As the competitive season spans March to November and athletes potentially train on similar terrain at similar velocities it appears that prolonged exposure is a likely scenario, however more work is required to investigate this suggestion. The findings of this paper are aligned with those of Duc *et al.* [18] who showed that ELV for hand arm vibration was exceeded during a cobbled road cycling event. However, the vibration exposure values presented here are significantly greater than those observed in cycling on a range of surfaces on a commuting bicycle. This suggests that mountain bike athletes are at an increased risk of exposure to potentially harmful levels of hand arm vibration, particularly when taking a longer-term view of chronic exposure.

As the addition of vibration to cycling at fixed power output reduces time to exhaustion and increases oxygen uptake [19, 20], these findings suggest that vibration exposure is a key component of physiological workload during elite enduro mountain bike racing. The findings presented here also support previous work suggesting that faster riders encounter greater exposure to hand arm vibration. The only exception observed in this study is the lower partial vibration exposure reported by the faster rider during BS stage 2. The cause of this result is not clear, though may be related to line choice, mechanical malfunction or rider error. Prolonged vibration exposure reduces motor output during maximal voluntary contractions and further reduces endurance of maximal isometric contraction [21]. Therefore, the data presented here may also offer an explanation for previous findings of ~30% reductions in grip strength during downhill mountain biking dependant on the number of impacts experienced by the rider on the day before [22]. This may have negative implications for performance both by reducing the riders grip on the handlebar which may result in loss of control and reduced ability to operate the brakes. Effective braking is an essential component of performance, as shown by experienced riders producing more braking power for shorter periods of time than inexperienced riders [23, 24]. Therefore, it is likely that reductions in grip strength due to vibration may compromise this ability meaning the athlete has to reduce velocity during the technical terrain typically associated with race stages in enduro, resulting in reduced performance and potentially resulting in what is commonly called '*arm pump*' by mountain bike racers. The stage with the highest partial vibration exposure returned vibration amplitude values lower than those of the stage featuring the lowest partial vibration exposure. This suggests that the cumulative effect of accelerations caused by smaller impacts such as braking bumps has a larger contribution to vibration exposure than accelerations caused by larger impacts such as jumps and drop offs. This may be influenced by equipment set up such as suspension setting or tyre pressure. Accordingly, athletes often experiencing '*arm pump*' may benefit from utilising equipment settings aiming to improve the damping of accelerations induced by smaller impacts. Unfortunately, little information is available regarding the optimisation of bicycle equipment to reduce vibration exposure to the rider, thus further research is warranted to potentially improve performance. Overall, it appears than employing strategies to mitigate vibration exposure during enduro mountain biking will benefit performance.

Previous studies have shown different components, frames and tyre pressure to have different vibration transmission properties. Therefore, further work is required to explore the vibration transmission of different components with the aim to find means to reduce vibration exposure in mountain biking. Additionally, due to the rising popularity of mountain biking as a recreational sport, future studies should assess the vibration exposure in recreational settings. Many of the vibration exposure values for the race stages analysed here exceed the EAV level suggesting further investigation in downhill mountain biking (one timed race run) are warranted. Furthermore, the races analysed in the present study have a shorter duration (~16-25 minutes overall) when compared to EWS events (up to 60 minutes for winning rider) thus suggesting further investigation is required to measure vibration exposure during international competition.

5   CONCLUSIONS

In conclusion, elite enduro mountain bike athletes are exposed to potentially harmful vibration exposure during race stages at national enduro events. Further work is required to explore the extent of potential long-term health effects and the influence of vibration exposure on performance,

physiological load and recovery from racing and training in enduro mountain biking. Consideration must be given to the reduction in exposure from the use of appropriately specified components. Furthermore, it may be advisable to monitor hand-arm and human transmitted vibration exposure during training and competition. Monitoring hand-arm vibration exposure during training sessions may offer greater insight to rider fatigue and further contribute to improved event performance.

6   ACKNOWLEDGEMENTS

REFERENCES

[1] Bovenzi, M. (1998) Exposure-response relationship in the hand-arm vibration syndrome: An overview of current epidemiology research. *International Archives of Occupational and Environmental Health*, 71 (8): 509–519.

[2] Spörri, J., Kröll, J., Fasel, B., Aminian, K., & Müller, E. (2017) The use of body worn sensors for detecting the vibrations acting on the lower back in alpine ski racing. *Frontiers in Physiology*, 8: 1–9.

[3] Lépine, J., Champoux, Y., & Drouet, J-M. (2015) The relative contribution of road bicycle components on vibration induced to the cyclist. *Sports Engineering* 18 (2): 79–91.

[4] Gomes, H.M., & Savionek, D. (2014) Measurement and evaluation of human exposure to vibration transmitted to hand-arm system during leisure cyclist activity. *Revista Brasileira de Engenharia Biomedica*, 30 (4): 291–300.

[5] Parkin. J., & Eugenie Sainte, C. (2014) The impact of vibration on comfort and bodily stress while cycling. In *46th Annual Universities Transport Research Group Conference*. Newcastle University, 6th-8th January.

[6] Capitani, D. & Beer, S. (2002) Handlebar palsy – a compression syndrome of the deep terminal (motor) branch of the ulnar nerve in biking. *Journal of Neurology*, 249 (10): 1441-1445.

[7] Munera M., Chiementin X, Crequy S, & Bertucci W (2014) Physical risk associated with vibration at cycling. *Mechanics & Industry* 15 (6): 535–540.

[8] Chiementin X., Rigaut M, Crequy S, Bolaers F, & Bertucci W (2013) Hand-arm vibration in cycling. *Journal of Vibration and Control*, 19 (16): 2551–2560.

[9] Duc S, Puel F, & Bertucci W (2016) Vibration exposure on cobbles sectors during ParisRoubaix. In *Science and Cycling*.5(2) 19-20, Caen, France.

[10] Taylor M.D., Edgar A., & Raine M. (2018) Scottish cycling pavement assessment using hand-arm vibration exposure. *Proceedings of the Institution of Civil Engineers Infrastructure Asset Management* 6(2), 86-101.

[11] Hurst, H.T., Swarén, M., Hébert-Losier, K., Ericsson, F., Sinclair, J., Atkins, S., & Holmberg, H.-C. (2013) GPS-Based Evaluation of Activity Profiles in Elite Downhill Mountain Biking and the Influence of Course Type. *Journal of Science and Cycling*, 2 (1): 25-32.

[12] Macdermid, P.W., Fink. P.W., & Stannard, S.R. (2014) Transference of 3D accelerations during cross country mountain biking. *Journal of Biomechanics*, 47 (8): 1829–1837.

[13] Macdermid, P.W., Miller, M.C., Macdermid FM, & Fink PW (2015) Tyre Volume and Pressure Effects on Impact Attenuation during Mountain Bike Riding. *Shock and Vibration*, 1–10.

[14] Hassenfratz, C., Ravier, G., & Grappe, F. (2012) Etude des responses mechaniques et physiologiques en Enduro VTT. Seminaires Des Entraineures et Cadres Techniques Du Cyclisme.

[15] Kirkwood, L.A., Ingram, L.A., Cunningham, J., Malone, E., & Geraint, D. (2017) Physiological characteristics and performance in elite vs non-elite enduro mountain biking. *Journal Of Science & Cycling* 6 (2), 13–21.

[16] Griffin, M.J. (1990) *Handbook of Human Vibration*. Cambridge, USA: Academic Press.

[17] BSI (2001) BS EN ISO 5349-1:2001. Mechanical vibration — Measurement and evaluation of human exposure to hand-transmitted vibration.

[18] Duc, S., Puel, F., & Bertucci, W. (2016) Vibration exposure on cobbles sectors during ParisRoubaix. In *Science and Cycling*. 5(2), 19-20

[19] Rønnestad BR, Moen M, Gunnerød S, & Øfsteng S (2018) Adding vibration to high-intensity intervals increase time at high oxygen uptake in well-trained cyclists. *Scandinavian Journal of Medicine & Science in Sports*.

[20] Samuelson, B., Jorfeldt, L., & Ahlborg, B. (1989a) Influence of Vibration on Work Performance during Ergometer Cycling. *Upsala Journal of Medical Sciences* 94 (1), 73–79.

[21] Samuelson, B., Jorfeldt, L., & Ahlborg, B. (1989b) Influence of vibration on endurance of maximal isometric contraction. *Clinical Physiology* 9, 21-25.

[22] Florida-James, G., Ball, C., & Westbury, T. (2010) Demands of DH mountain biking. In *World Science in Cycling* (Invited symposium Vol. 1). Edinburgh, UK.

[23] Lopes B, & McCormack, L. (2017) *Mastering mountain bike skills* (3rd Edition). Leeds, UK: Human Kinetics.

[24] Miller, M.C., Fink, P.W., Macdermid, P.W., Allen, D., & Stannard, S.R. (2018) Braking and performance characteristics of experienced and inexperienced mountain bikers navigating an isolated off-road turn using a brake power meter. International Journal of Performance Analysis in Sport, 1–12.

11 Session 4: WBV 1

Session chair: Peter Johnson

Exposure to Acute Whole Body Vibration of Three Different Frequencies: Physiological and Physical Changes in the Elderly

**MH Mahbub[1], Keiichi Hiroshige[2], Ryosuke Hase[1], Natsu Yamaguchi[1],
Noriaki Harada[3], Tsuyoshi Tanabe[1]**

[1]Yamaguchi University Graduate School of Medicine, 1-1-1 Minami-Kogushi, Ube, Yamaguchi, 755-8505, Japan
hossain@yamaguchi-u.ac.jp, hase@umin.ac.jp, natsu@yamaguchi-u.ac.jp, tanabe@yamaguchi-u.ac.jp

[2]Kyushu Nutrition Welfare University, 1-5-1 Kuzuhara-Takamatsu, Kokuraminami-ku, Kitakyushu, Fukuoka, 800-0298, Japan
hiroshige@knwu.ac.jp

[3]Junshin Gakuen University, 1-1-1 Chikushigaoka, Minami-ku, Fukuoka, 815-8510, Japan
harada@yamaguchi-u.ac.jp

ABSTRACT

We attempted to ascertain the specific patterns of changes in peripheral circulation and vibrotactile perception, autonomic nervous activity (ANA) and balance from acute exposure of apparently healthy elderly subjects to whole-body vibration (WBV). Thirty subjects were randomly exposed to WBV (vertical, side-alternating; three bouts of 1 min with 1 min interval between bouts) at 15, 20 and 25 Hz with corresponding A(8) values of 0.76, 1.12 and 1.41 m/s^2 r.m.s., respectively, and to control condition (0 Hz). Skin blood flow (SBF), skin temperature (ST), vibrotactile perception threshold (VPT) of feet and heart rate variability (HRV) were measured and balance tests were performed before and during and/or after exposure. Relative to the corresponding control condition, SBF and VPT increased significantly under all 3 WBV exposure conditions ($P < 0.05$-0.001) with greater responses under higher frequencies of vibration which were comparable at 20 and 25 Hz. On the other hand, exposure to WBV did not produce any significant change in ST, HRV or balance tests. Therefore, WBV of 20 Hz with a magnitude within the recommended exposure limit can be used effectively in inducing improvements in peripheral SBF without causing any negative effects on the ANA among the elderly; however, improvements in balance may require chronic or long-term exposure or exposure to WBV of different frequencies and/or magnitudes.

INTRODUCTION

Ageing is associated with autonomic and endothelial dysfunction and impaired peripheral circulation which may lead to greater susceptibility and severity in macrovascular and microvascular impairments of the extremities and also delayed wound healing or impaired healing of chronic wounds like pressure injuries or diabetic ulcers posing increased risk for mortality or morbidity among the elderly (Mayfield et al. 2001; Tew et al. 2012). On the other hand, approximately 30% of adults over the age of 65 suffer from falls every year, majority of which are thought to be caused by ageing-related impairments in gait, balance and postural control (Era et al. 2006; Shaffer and Harrison 2007). Falls among the elderly is a major public health concern as being the leading cause of fractures, serious soft tissue injuries, head trauma or other trauma-related

morbidity, mortality and hospital admissions among them (Rizzo et al.1998). Therefore, to preserve the health and well-being of the elderly, non-invasive and easy-to-conduct interventions with the potential to improve or restore peripheral circulation, balance and postural control would be highly beneficial clinically to such populations.

In recent years, the training or treatment intervention using controlled exposure to whole body vibration (WBV) has shown the potential to increase peripheral circulation, balance and postural control among the elderly. However, the findings reported in the exiting literature on the patterns of responses in human peripheral circulation and changes in balance among older adults seem inconsistent and inconclusive (Mahbub et al. 2019; Lam et al. 2018; Merriman and Jackson 2009). The situation has been complicated by the fact that a number of such studies investigating the effects of WBV on peripheral circulation and balance used a vibration protocol that consisted of passive vibration, or combined the vibration exposure condition with simultaneous exercise training making the differentiation of the sole contribution of active WBV on such responses uncertain (Lohman et al. 2011 and 2012; Orr 2015). The situation has been made worse by the fact that a number of those studies exposed human subjects to relatively high magnitudes of vibration exceeding the limit recommended by the International Standard, ISO 2631-1 (1997) and EU Directive 2002/44/EU (2002) (Mahbub et al. 2019) for such exposure. Above all, useful or optimum vibration parameters like frequency, acceleration and amplitude for intervention with WBV have not yet been established making the application of WBV into practices difficult.

Previous studies have suggested significant effects of exposure to vibration on the autonomic nervous activity which might cause enhanced sympathetic activation and/or exaggerated vasoconstriction with vibration-induced decreases in peripheral circulation (Eger et al. 2014; Murata et al. 1997; Thompson et al. 2010). On the other hand, body balance has a close relationship with the sensitivity of plantar cutaneous mechanoreceptors, and ageing-related deterioration in such sensitivity and associated proprioception are thought to be important contributors to the impairments in postural balance among the elderly (Era et al. 2006; Kennedy and Inglis 2002; Meyer et al. 2004; Perry 2006). Theoretically, an intervention modality with exposure to WBV is desirable that would be able to enhance peripheral circulation without significant alterations or preferably with modulations in the autonomic nervous activity and improve balance without an increase (indicating a decrease in plantar sensitivity) or preferably with a reduction (indicating an increase in plantar sensitivity) in the mechanoreceptor perception thresholds of exposed individuals. However, to our knowledge, no study has been conducted with the measurements of responses in peripheral circulation, autonomic nervous activity, plantar cutaneous mechanoreceptor perception and balance and functional mobility from controlled exposure to WBV in the same elderly subjects with consideration of the exposure limit specified in the relevant international standards.

Considering the above-mentioned issues and controversies, the purpose of the current study was to examine the acute effects of short-time active WBV-only intervention of three different frequencies on leg skin blood flow (SBF) and skin temperature (ST), heart rate variability (HRV), plantar cutaneous vibrotactile perception threshold (VPT), and balance and functional mobility, among the healthy elderly subjects with the vibration intensities defined according to the ISO 2631-1 (1997).

SUBJECTS AND METHODS

Subjects and measurements The study protocol was approved by the relevant institutional review board of Yamaguchi University School of Medicine. Fifteen male (Age: median, 73.0 years; IQR, 10.0 years. BMI: median, 25.7 kg/m^2; IQR, 3.2 kg/m^2) and 15 female (Age: median, 71.0 years; IQR, 6.0 years. BMI: median, 22.6 kg/m^2; IQR, 5.0 kg/m^2) elderly subjects were enrolled in this study. They received a detailed oral explanation of the study protocol, participated in a
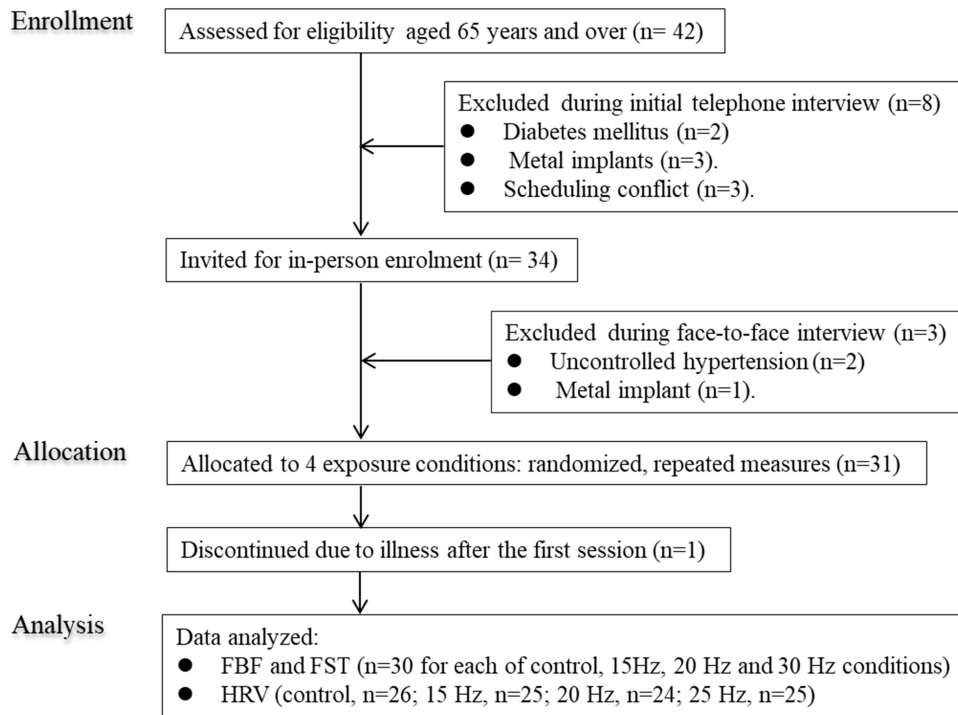
Figure 1 Flowchart of current study participants.

familiarization session, and provided written informed consent to participate in this study. Flowchart of the current study participants has been depicted in figure 1. The subjects were instructed to refrain from eating and drinking tea or coffee for at least 3 h and smoking, alcohol drinking and strenuous physical activity for at least 12 h prior to the beginning of the test. They entered the experiment room after voiding. Participants undergoing antihypertensive drugs were asked to adhere to their current treatment regimens during the study period. The subjects were instructed to wear light indoor clothing (two each for the upper and lower parts of the body) in the laboratory, and regular socks and shoes.

Experimental design During each session, the tests/measurements were performed in the sequence as shown in figure 2. Upon arrival, a subject underwent acclimatization for a period of 20 min in the first experiment room (room temperature maintained at 24±1°C) seated comfortably on a height-adjustable chair without physiological or psychological stress. After acclimatization, upper arm blood pressure was recorded by a validated digital oscillometric blood pressure device (HEM-705IT, Omron Healthcare, Kyoto, Japan). Then the following balance and mobility tests were performed in a random order: one leg stance (OLS) test with eyes open and closed – time interval from the beginning till the end of the test was recorded; parallel walk (PW) test – a score of +1 was given for foot placement on any of the two lines 6 m long and 20 cm apart, and +2 if any foot was placed outside the line or the subject attempted to grasp the experimenter who moved in close proximity to the participant during the test; timed up and go (TUG) test – the time interval from

HRV, heart rate variability; SBF, skin blood flow; ST, skin temperature; VPT, vibrotactile perception threshold.
§SBF was measured immediately after the cessation of exposure which corresponds to the beginning of the rest period following each bout of exposure.

Figure 2 Schematic for the experimental protocol and the sequence of different measurements in a single session.

participants' buttocks leaving the seat of a chair and touching it again after completion of a walk at a fast but safe speed for a distance of 3 m and turning around clockwise; and 30-s chair stand (CS-30) test – the number of complete repetitions comprising standing up and sitting down. All tests were performed twice. For each applicable test, the same standard armless chair was used by all subjects. Subjects performed two trials of each set of tests and the tests were presented in a random order. One min (2 min after the CS-30 test) of rest was allowed between tests with a rest period of approximately 30 s (2 min for the CS-30 test) between trials within the same test when the participants were allowed to sit on a chair except the OLS test. A higher score denoted a better performance for assessment with OLS and CS-30 tests; for the PW and TUG tests - a higher score indicated a worse performance.

At the end of balance tests, the subject moved to the next temperature-controlled experiment room where he/she seated comfortably on a height-adjustable chair with the trouser rolled up to a level between the knees and heels and the socks taken off. The electrodes for the measurements of HRV were attached to the forearms and the sensors of the thermistor were attached to the dorsal surface of the middle of left foot with adhesive tape. Then the subject underwent acclimatization to the room temperature (maintained at $25.0 \pm 0.5°C$) for a period of 15 min. At the end of acclimatization period, while seated, the baseline measurements of HRV were recorded for 5 min which was followed by baseline measurements of VPT of the right foot. For VPT measurements, the subjects sat comfortably upright with their eyes open, right hand on the right thigh and the left hand holding the switch of the VPT device, left foot rested on the wooden floor and the right foot rested on a level with the vibrating probe (fixed at a height of about 4 cm above the floor). VPT was measured by the same researcher following the protocol mentioned in the international standard ISO 13091-1 (2001), randomly at three locations of the right foot: plantar aspect of the hallux, the heel, and the base of the little toe, at the test frequency of 31.5 Hz.

After completion of the measurements of VPT, the subject was asked to stand in complete upright posture, looking forward, on the rectangular platform of the side-alternating vibration device while lightly grasping the rails of the platform with the hands. After a rest period of 3 min, baseline SBF of the right foot was recorded twice at an interval of 1 min. Following this, the participant stood with bent knees at an angle of about 30° (considering a full knee extension of 0°) and positioned the feet at a distance of 10.5 cm from the centre of the platform to the midline of the heels. After the above measurements, all the subjects underwent an intervention consisting of any of the four exposure conditions/sessions which were performed randomly approximately at the same time on four different days separated by at least 24 h (Table 1).

The peak-to-peak displacement of the vibrating platform was 4 mm. The 5-min intervention protocol consisted of three bouts of 1 min of exposure separated by an interval of 1 min between the bouts. Just after the cessation of each bout of exposure, the subjects were asked to stand up quickly but smoothly and the measurements of SBF were performed. The subjects maintained the upright posture during 2 intervals of 1 min each between the bouts. After the completion of intervention, the participants maintained the upright position for further 1 min which was followed by measurement of after-exposure SBF. Then the subjects were seated again on the chair and measurements of VPT were conducted. ST was continuously recorded from the dorsum of left foot at each min before, during and after intervention. After this, the subjects moved to the other experimental room to

Table 1 Experimental design of the study showing the intervention including four different exposure conditions

Condition	Frequency (Hz)	Peak-to-peak amplitude (mm)	Peak acceleration Unweighted ($m s^{-2}$)	Peak acceleration (ms^{-2} r.m.s.) Frequency-weighted	A(8)
1 (Control)	0	–	–	–	–
2 (WBV)	15	4	17.75	9.64	0.76
3 (WBV)	20	4	31.56	14.19	1.12
4 (WBV)	25	4	49.3	17.59	1.41

A(8): 8-h energy-equivalent frequency-weighted acceleration.

undergo the balance tests following which the experimental session ended.

Equipment WBV was produced using a commercially available side-alternating vibration device (Galileo 900, Novotec Medical GmbH, Pforzheim, Germany). Foot ST and room temperature was measured by using digital thermistors (SZL-64, Technol seven, Japan) connected to a scanner (X115, Technol seven, Japan) and high accurate data logger (K730, Technol seven, Japan). SBF was recorded from a circular target area of same size (260 pixels) proximal to the metatarsophalangeal joints, by the non-contact commercially available Laser Speckle Flowgraphy system (LSFG-ANW, Softcare Co., LTD., Fukuoka, Japan) with the recording unit (which incorporated a charge coupled device camera of 600×480 pixels) attached to the movable arm of a stand fixed on the floor and positioned 19 cm above the right foot of the subject at an angle of 20°. HRV data were recorded using a portable battery-operated heart rate device (CheckMyHeart, DailyCare BioMedical, Inc., Taiwan) connected via electrode cables with self-adhesive disposable Ag/AgCl circular (diameter 2 cm) surface electrodes (Bioload SDC-H, GE Healthcare, Japan) placed on the ventral side of subject's forearms. VPT (m/s^2) was measured by a commercially available Vibrotactile Perception Meter, VPM (HVLab, University of Southampton, UK). The test locations and test frequencies were randomized for each participant.

Data processing For the balance and mobility tests, the results were calculated as the average of two trials. For the HRV data, visual inspection for any noise or ectopic beats were performed using the HRV analysis software (DailyCare BioMedical, Inc., Taiwan). Then using the fast-Fourier-transformation (FFT), the following components (in milliseconds squared) were calculated for the detrended values of regular R-R interval data: 1) high-frequency power (HF, 0.15 to 0.40 Hz), 2) low-frequency power (LF, 0.04 to 0.15 Hz), and 3) LF/HF (the ratio of low-to high-frequency power). The values of HF and LF were normalized as follows: (1) normalized HF or HFnu = HF ÷ (total power - VLF); and (2) normalized LF or LFnu = LF ÷ (total power - VLF), where VLF indicates very low frequency power (between 0.003 to 0.04 Hz) of HRV. The data extracted for the real exposure period (total 3 min during 3 bouts of exposure) were used in the analysis. The values of SBF and ST measured at same time points at baseline (average of 2 measurements before intervention), during intervention (3 time-points collected at the end of each bout of exposure) and after intervention were used in the analysis.

Statistical analyses The continuous variables are shown as the median and interquartile range (IQR) in the text, tables and figures of this study. The data were analyzed using Wilcoxon signed-ranks test for two-related samples and Friedman test for k-related samples. Statistical analysis was performed with statistical software package SPSS version 22 for Windows (SPSS Inc., Chicago, IL, USA). Statistical significance was considered at a two-sided P-value of <0.05.

RESULTS

The values of SBF before, during (3 time points) and after exposure for each of the four exposure conditions are presented in figure 3. As observed, the baseline/before-intervention values of SBF did not differ significantly between the four exposure conditions (P > 0.05). In contrast, during intervention, compared to the corresponding values under the control condition, the SBF increased significantly under all 3 vibration exposure conditions at all 3 time points (P < 0.001). Compared to the corresponding values under 15 Hz condition, the SBF showed significantly higher values at all 3 time points under both 20 Hz and 25 Hz conditions (P < 0.01 to 0.001). Also, at three time points during exposure, the increased SBF differed significantly between the latter two conditions (P < 0.05 to 0.005). On the other hand, after cessation of intervention, compared to the values under control and 15 Hz conditions, the SBF remained significantly elevated under both 20 Hz (P < 0.05 to 0.001) and 25 Hz (P < 0.005 to 0.001) exposure conditions whereas the increased SBF did not differ significantly between the latter two exposure conditions.
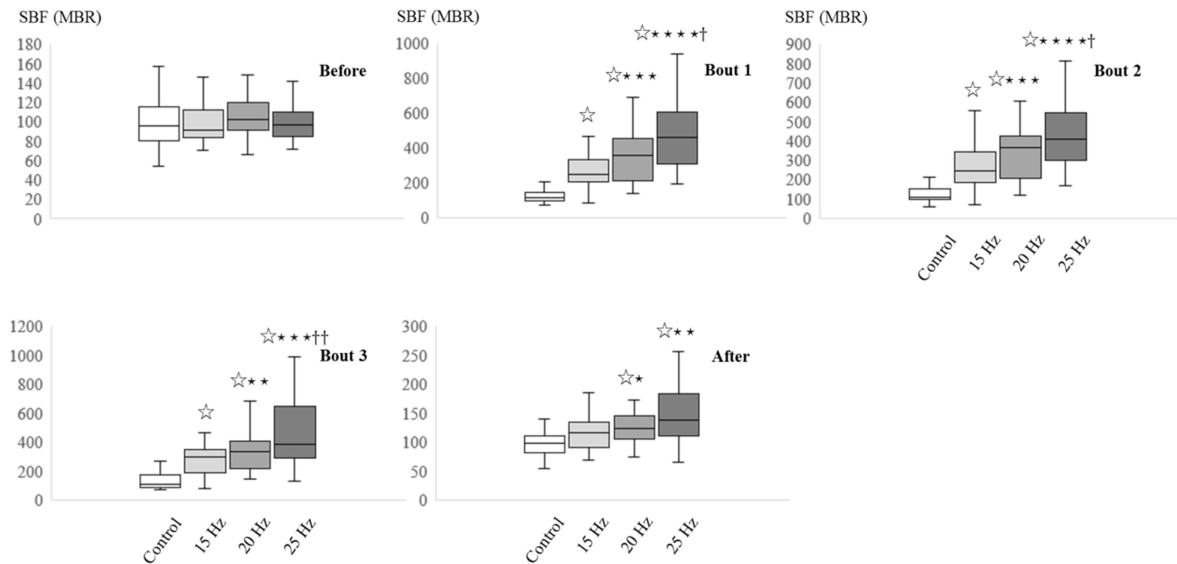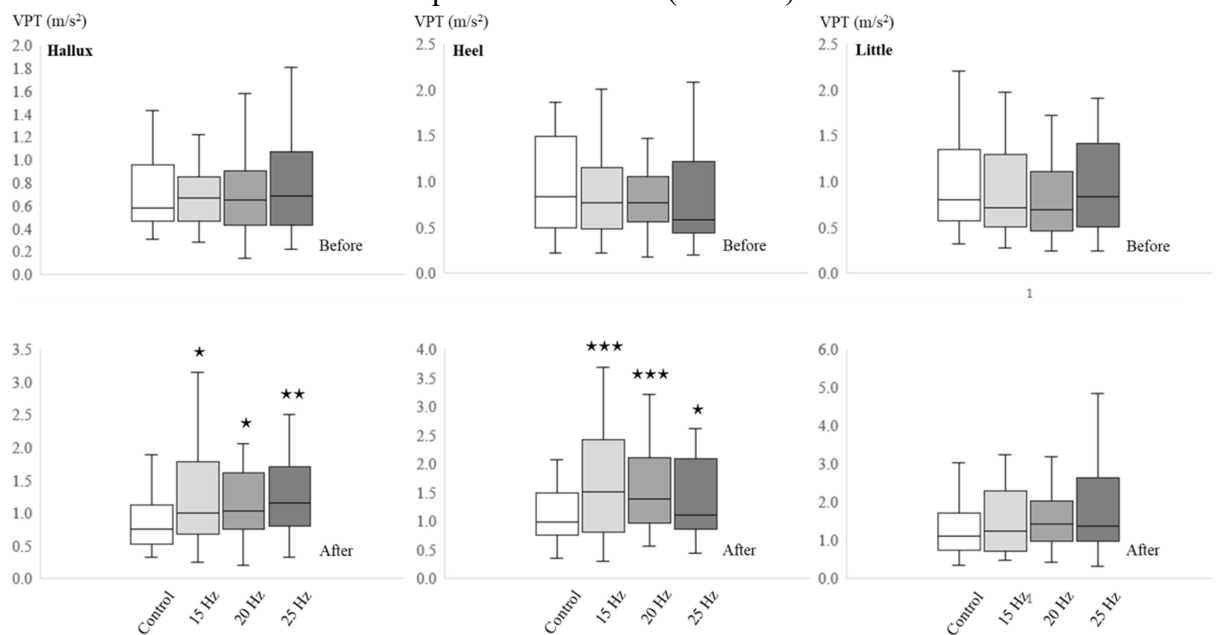
Figure 3 Boxplots displaying median with 25th and 75th percentile values of SBF (MBR) under different exposure conditions obtained before, during (bouts 1, 2 and 3) and after exposure. Significantly different from the corresponding control values: ☆P < 0.001. Significantly different from the corresponding values under 15 Hz: ****P < 0.001, ***P < 0.005, **P < 0.01, *P < 0.05. Significantly different from the corresponding values under 20 Hz: ††P < 0.005, †P < 0.05. The P-values were derived by applying the Wilcoxon signed ranks test with adjustments for multiple comparisons by Bonferroni corrections as necessary.

As shown in table 2, no significant difference in ST could be revealed when the values under four exposure conditions were compared before, during and after intervention (P > 0.05).

When the values for different components of HRV (LFnu, HFnu or LF/HF) were compared between four exposure conditions, the values did not show any significant difference before and during intervention (P > 0.05) (Table 3).

Table 2 Median and IQR values of ST (°C) under different exposure conditions obtained before, during and after intervention

Measurement time-points	Control		15 Hz		20 Hz		25 Hz	
	Median	IQR	Median	IQR	Median	IQR	Median	IQR
Before	29.9	1.9	29.8	1.4	29.9	1.5	29.8	1.9
Bout 1	29.8	2.2	29.7	1.5	29.8	1.7	29.6	1.8
Bout 2	29.8	2.1	29.8	1.6	29.7	1.6	29.5	1.8
Bout3	29.7	2.2	29.7	1.8	29.6	1.6	29.8	1.8
After	29.6	2.1	29.8	1.8	29.6	1.6	30.0	2.0

Table 3 Median and IQR values of three components of HRV before and during intervention under four exposure conditions

HRV component	Before/during intervention	Control		15 Hz		20 Hz		25 Hz	
		Median	IQR	Median	IQR	Median	IQR	Median	IQR
HFnu	Before	42.8	27.7	37.8	27.2	42.5	23.9	42.9	38.2
	During	39.3	30.9	37.4	23.9	30.1	20.3	40.4	30.9
LFnu	Before	57.3	27.7	62.2	27.2	57.5	23.9	57.1	38.2
	During	60.7	31.4	62.6	23.9	69.9	20.3	59.6	30.9
LF/HF	Before	1.3	1.7	1.7	1.9	1.4	1.5	1.4	2.8
	During	1.5	1.6	1.7	1.5	2.3	1.9	1.5	2.2

HF, high frequency (nu); LF, low frequency (nu).

The values of VPT obtained before and after intervention at three test locations of right plantar foot are shown in figure 4. As observed, comparison between the before-intervention values at all test locations did not reveal any significant difference between those values (P > 0.05). After intervention, compared to the corresponding control values, the values of VPT increased significantly at the hallux and heel. However, when the multiple comparisons were made between the values under 15 Hz, 20 Hz and 25 Hz exposure conditions, no significant differences could be revealed (P > 0.05). On the other hand, after intervention values of VPT did not differ significantly at the little finger (P > 0.05).

The effects of intervention on balance and mobility tests were assessed by OLS test (eyes open and closed), PW test, TUG test, and CS-30 test. The before-exposure values did not differ significantly between the four exposure conditions for any of the tests (P > 0.05) (Table 4). Also, no WBV-induced improvements in those tests were evident from comparison of the corresponding values of different tests between different exposure conditions (P > 0.05).

Figure 4 Boxplots displaying median with 25th and 75th percentile values of VPT (m/s^2) under different exposure conditions obtained before and after exposure measured at hallux, heel and little finger of right plantar foot. Significantly different from the corresponding control values: ***P<0.005, **P<0.01, *P<0.05. The P-values were derived by applying the Wilcoxon signed ranks test with adjustments for multiple comparisons by Bonferroni corrections as necessary.

Table 4 Median and IQR values of balance and mobility tests under different exposure conditions obtained before and after intervention under four different exposure conditions

Test	Before/After	Control		15 Hz		20 Hz		25 Hz	
		Median	IQR	Median	IQR	Median	IQR	Median	IQR
OLS, eyes open (s)	Before	37.1	29.5	43.4	17.0	38.5	24.9	38.8	26.1
	After	35.8	19.7	43.1	20.0	41.7	25.3	44.5	22.5
OLS, eyes closed (s)	Before	3.8	5.0	2.7	2.2	3.6	1.8	3.0	1.7
	After	3.4	3.0	3.1	2.5	4.0	4.2	3.5	3.4
PW (total score)	Before	1.0	1.5	1.3	2.1	0.8	2.1	0.5	2.1
	After	1.3	1.3	1.0	2.0	0.5	1.5	1.3	2.5
TUG (s)	Before	6.4	1.2	6.4	1.4	6.4	1.2	6.4	1.0
	After	6.5	1.4	6.6	1.4	6.5	0.9	6.5	1.1
CS-30 (repetitions)	Before	17.5	5.8	18.0	6.6	18.3	6.0	18.5	5.8
	After	18.0	6.3	18.8	6.1	17.8	6.0	19.0	6.9

OLS, one leg stance test; PW, parallel walk test; TUG, timed up and go test; CS-30, 30-s chair stand test.

DISCUSSION

Intervention with exposure to WBV can be a safe and simple intervention especially for the elderly who may be passive or physically weak, with limited mobility or physical disability, and unable to perform conventional active or high impact physical exercise or with contraindications to aerobic exercise (Brooke-Wavell and Mansfield 2009). For the purpose of increasing peripheral circulation and/or balance by exposure to WBV, safe and effective vibration parameters like frequency, amplitude, acceleration etc have not yet been established which make the application of WBV into practices difficult. In the current study, we examined the effects of acute exposure to WBV of different frequencies but with the same amplitude on the responses in peripheral circulation, autonomic nervous activity, plantar cutaneous sensitivity and balance in the elderly. We used a knee flexion angle of 30° during exposure to minimize the transmission of rotational vibration to the head. Furthermore, we used an intermittent exposure protocol with 3 min of cumulative WBV exposure considering the possible muscle fatigue from such exposure (Abercromby et al. 2007) and the exposure limit recommended by ISO 2631-1 (1997).

In a recent systematic review, we observed that acute exposure of various groups of populations to WBV at frequencies below 30 Hz with a relatively low value of A(8) demonstrated a consistent increase in peripheral circulation with greater responses at the higher frequencies (Mahbub et al. 2019). On the other hand, occupational exposure to WBV with the dominant frequency range of 28 Hz and 40 Hz has been reported to cause impairments in peripheral circulation and associated symptoms among workers exposed to vibration (Eger et al. 2014). Considering all these, in our study we decided to use the vibration frequencies of 15 Hz, 20 Hz and 25 Hz with different vibration magnitudes but with the same peak-to-peak displacement. The International Standard ISO 2631-1 (1997) suggests that subjects should not be exposed to high levels of vibration during experiments involving human exposure to vibration and shock. According to the EU Directive 2002/44/EU (2002), people regularly exposed to WBV in their occupations should not be exposed to the vibration level exceeding an A(8) value of 1.15 m/s^2 rms. Griffin (2004) mentioned that for exposures between 1 min and 10 min (the exposure period commonly being used for exposure to devices producing WBV), the upper boundary of the caution zone is assumed to be at the frequency-weighted acceleration of 6.0 m/s^2 r.m.s. and the lower boundary at 3.0 m/s^2 rms. In line with these, we exposed subjects to WBV to relatively lower frequencies and magnitudes of vibration. In this study, using the same feet position on the vibration platform and same amplitude of vibration for all three frequencies led to the generation of a level of vibration magnitude at 25 Hz that exceeded the recommended A(8) value. However, we believe, subjects' posture on the platform with flexed knees caused partial reduction of the mechanical energy of WBV transmitted to the body through the feet (Abercromby et al. 2007).

In our study, WBV generated at 20 and 25 Hz caused an increase in SBF both during and after the exposure and the responses under these two conditions were significantly greater than that observed under the 15 Hz exposure condition. Our findings are comparable with those of Lythgo et al. (2009) who exposed young healthy subjects to acute intermittent WBV (frequency, 5 Hz to 30 Hz; amplitude, 2.5 and 4.5 mm) generated by a side-alternating vibration platform and observed an increase in blood flow of the femoral artery with greater increases at 30 Hz exposure frequency. Also, Johnson et al. (2014; vibration type, side-alternating; frequency, 26 Hz; amplitude, 3 mm) reported an increase in leg SBF following exposure to acute intermittent WBV. However, in all those studies, the peak vibration magnitude largely exceeded the recommended value and the applications of such high levels of WBV into practice are questionable (Mahbub et al. 2019). In contrast, our findings contradict the findings of Lohman et al. (2011 and 2012) who did not observe such improvements in peripheral circulation from exposure to active WBV. However, this might have been caused by the fact that these studies used a comparatively high vibration frequency (50 Hz) with a high vibration magnitude. On the other hand, the same group of researchers found a significant increase in SBF while using a relatively lower vibration frequency (30 Hz) with a lower magnitude of WBV (Lohman et al. 2007). As observed, the increase in SBF was significantly

greater under the condition of 25 Hz than that at 20 Hz, but the responses did not appear to be different between these two exposure conditions after exposure. However, the fact that the peak vibration magnitude exceeded the recommended safe exposure limit at 25 Hz and SBF remained elevated even after cessation of exposure to WBV at 20 Hz, these provide the evidence for the efficacy and practical applicability of exposure to WBV at 20 Hz as a simple, safe and feasible non-invasive modality for increasing SBF of the lower extremity in the elderly.

In our study, no significant change in ST was observed under any condition during or after exposure to WBV which are in line with the similar findings observed by Menendez et al. (2015) and Robbins et al. (2014). The exact mechanisms underlying such discrepant responses in SBF and ST cannot be explained from the current study findings. However, a possible explanation behind such observations may be the fact that we measured ST at the dorsal (nonglabrous/hairy) skin which is thermally more stable as it lacks arteriovenous anastomoses and less responsive to external stimuli than the glabrous skin (Romanovsky 2014; Shepherd 1963). Also, it might be possible that local temperature-sensitive mechanisms mediating limb tissue perfusion were probably not affected by the parameters of vibration used in this study (Chiesa et al. 2015).

Ageing is associated with reduced HRV and the latter has been found to be associated with the development of cardiovascular adverse outcomes including hypertension, coronary artery disease, myocardial infarction, and chronic heart failure etc (Reardon and Malik 1996; Routledge et al. 2010). On the other hand, HRV properties can be greatly affected by afferent feedbacks resulting from vibration-induced stimulation of plantar cutaneous mechanoreceptors with the possibility of negative impacts on the autonomic nervous function (Jiao et al. 2004; Pyykkö et al. 1994). Therefore, a WBV intervention modality should not have any negative effects on the ANA and thereby cause any stress to the cardiovascular system. As observed in this study, WBV intervention did not have any significant effects at any frequency on the HRV indicating that any additional cardiovascular stress caused by different frequencies and magnitudes used in this study was minimal. Our findings are in line with those of Rittweger et al. (2000) who observed that even if performed to exhaustion, cardiovascular effects of vibration exercise are mild. Figueroa et al. (2012) reported that WBV suppresses sympathovagal balance (LFnu/HFnu) due to a concurrent decrease in sympathetic (LFnu) and increase in cardiovagal (HFnu) modulation from WBV training.

Among the skin mechanoreceptors, the Meissner corpuscles respond to mechanical stimuli produced at frequencies between 30-50 Hz (Purves et al. 2001). Therefore, in the literature, vibration exposure frequencies like 31.5 Hz have been suggested for investigation of vibrotactile perception mediated by the Meissner corpuscles (ISO 13091-1). The frequencies of WBV used in this study (15-30 Hz) would have stimulated the Meissner corpuscles. Therefore, in this study, we investigated VPT at the test frequency of 31.5 Hz. The results show significant decline in cutaneous sensitivity at hallux and heel of the sole of the foot. But in this study, the aforementioned effects did not seem to have a direct influence on balance and mobility as exposure to WBV did not produce any significant change in balance and mobility tests. The findings of the previous studies investigating the effects of WBV on balance and functional mobility in older adults are conflicting. For example, Ko et al. (2017) observed improved postural control from such exposure in middle aged and elderly healthy individuals. In contrast, Lam et al. (2018) in a recent randomized controlled trial observed a lack of significant effect of WBV on balance and functional mobility in the elderly with mild or moderate dementia. In future studies, it would be interesting to investigate the WBV-induced changes in balance and mobility from long-term exposure to WBV at various exposure frequencies with magnitudes considering the recommended limit for such exposure.

CONCLUSION

Acute exposure to WBV with a vibration frequency of 20 Hz and peak-to-peak displacement of 4 mm producing an A(8) value that is within the ISO-recommended limit appears to be able to induce improvements in peripheral SBF without exerting any negative effects on the autonomic nervous activity in the elderly. However, no improvements in balance and mobility among the

elderly were observed from exposure to WBV of three different frequencies used in this study with the same peak-to-peak displacement for all frequencies. Future studies should investigate the changes in balance and mobility among the subjects from long-term exposure to WBV of different frequencies, amplitudes or magnitudes considering the recommended limit for such exposure.

ACKNOWLEDGMENT

CONFLICT OF INTEREST

The authors declare no conflict of interest.

REFERENCES

Abercromby AF, Amonette WE, Layne CS, McFarlin BK, Hinman MR, Paloski WH, "Vibration exposure and biodynamic responses during whole-body vibration training", Med Sci Sports Exerc, 39(10), 1794-800 (2007)

Brooke-Wavell K, Mansfield NJ, "Risks and benefits of whole body vibration training in older people", Age Ageing, 38(3), 254-55 (2009)

Chiesa ST, Trangmar SJ, González-Alonso J, "Temperature and blood flow distribution in the human leg during passive heat stress", J Appl Physiol 120(9), 1047-58 (1985)

Eger T, Thompson A, Leduc M, Krajnak K, Goggins K, Godwin A, House R, "Vibration induced white-feet: overview and field study of vibration exposure and reported symptoms in workers", Work, 47(1), 101-10 (2014)

Era P, Sainio P, Koskinen S, Haavisto P, Vaara M, Aromaa A, "Postural balance in a random sample of 7,979 subjects aged 30 years and over", Gerontology, 52(4), 204-13 (2006)

European Union, "Directive 2002/44/EC of the European Parliament and of the Council of 25 June 2002 on the minimum health and safety requirements regarding the exposure of workers to the risks arising from physical agents (vibration)", Official Journal of the European Communities, L177, 13-9, 2002

Figueroa A, Gil R, Wong A, Hooshmand S, Park SY, Vicil F, Sanchez-Gonzalez MA, "Whole-body vibration training reduces arterial stiffness, blood pressure and sympathovagal balance in young overweight/obese women", Hypertens Res, 35(6), 667-72 (2012)

Griffin MJ, "Minimum health and safety requirements for workers exposed to hand-transmitted vibration and whole-body vibration in the European Union; a review", Occup Environ Med, 61, 387-97 (2004)

Inglis JT, Kennedy PM, Wells C, Chua R, "The role of cutaneous receptors in the foot", Adv Exp Med Biol, 508, 111-7 (2002)

International Organization for Standardization, "Mechanical vibration – vibrotactile perception thresholds for the assessment of nerve dysfunction- Part 1: Methods of measurement at the fingertips", International Standard, ISO 13091-1, Geneva, Switzerland, 2001

International Organization for Standardization, "Mechanical vibration and shock – Evaluation of human exposure to whole-body vibration - Part 1: General requirements", International Standard, ISO 2631–1, Geneva, Switzerland, 1997

Jiao K, Li Z, Chen M, Wang C, Qi S, "Effect of different vibration frequencies on heart rate variability and driving fatigue in healthy drivers", Int Arch Occup Environ Health, 77(3), 205-12 (2004)

Johnson PK, Feland JB, Johnson AW, Mack GW, Mitchell UH, "Effect of whole body vibration on skin blood flow and nitric oxide production", J Diabetes Sci Technol, 8 (4), 889-94 (2014)

Kennedy PM, Inglis JT, "Distribution and behaviour of glabrous cutaneous receptors in the human foot sole", J Physiol, 538(Pt 3), 995-1002 (2002)

Ko MC, Wu LS, Lee S, Wang CC, Lee PF, Tseng CY, Ho CC, "Whole-body vibration training improves balance control and sit-to-stand performance among middle-aged and older adults: a pilot randomized controlled trial", Eur Rev Aging Phys Act, 14, 11 (2017)]

Lam FMH, Liao LR, Kwok TCY, Pang MYC, "Effects of adding whole-body vibration to routine day activity program on physical functioning in elderly with mild or moderate dementia: a randomized controlled trial", Int J Geriatr Psychiatry, 33(1), 21-30 (2018)

Lohman EB 3rd, Bains GS, Lohman T, DeLeon M, Petrofsky JS, "A comparison of the effect of a variety of thermal and vibratory modalities on skin temperature and blood flow in healthy volunteers", Med Sci Monit, 17, MT72-81 (2011)

Lohman EB 3rd, Petrofsky JS, Maloney-Hinds C, Betts-Schwab H, Thorpe D, "The effect of whole body vibration on lower extremity skin blood flow in normal subjects", Med Sci Monit, 13(2), CR71-76 (2007)

Lohman EB 3rd, Sackiriyas KS, Bains GS, Calandra G, Lobo C, Nakhro D, Malthankar G, Paul S, "A comparison of whole body vibration and moist heat on lower extremity skin temperature and skin blood flow in healthy older individuals", Med Sci Monit, 18, CR415-24 (2012)

Lythgo N, Eser P, de Groot P, Galea M, "Whole-body vibration dosage alters leg blood flow", Clin Physiol Funct Imaging, 29(1), 53-9 (2009)

Mahbub MH, Hiroshige K, Yamaguchi N, Hase R, Harada N, Tanabe T, "A systematic review of studies investigating the effects of controlled whole-body vibration intervention on peripheral circulation", Clin Physiol Funct Imaging (2019) (Epub ahead of print)

Mayfield JA, Caps MT, Reiber GE, Maynard C, Czerniecki JM, Sangeorzan BJ, "Trends in peripheral vascular procedures in the Veterans Health Administration, 1989-1998", J Rehabil Res Dev, 38(3), 347-56 (2001)

Menéndez H, Martín-Hernández J, Ferrero C, Figueroa A, Herrero AJ, Marín PJ, "Influence of isolated or simultaneous application of electromyostimulation and vibration on leg blood flow", Eur J Appl Physiol, 115(8), 1747-55 (2015)

Merriman H, Jackson K, "The effects of whole-body vibration training in aging adults: a systematic review", J Geriatr Phys Ther, 32(3), 134-45 (2009)

Meyer PF, Oddsson LI, De Luca CJ, "The role of plantar cutaneous sensation in unperturbed stance", Exp Brain Res, 156(4), 505-12 (2004)

Murata K, Araki S, Okajima F, Nakao M, Suwa K, Matsunaga C, "Effects of occupational use of vibrating tools in the autonomic, central and peripheral nervous system", Int Arch Occup Environ Health, 70 (2), 94-100 (1997)

Orr R, "The effect of whole body vibration exposure on balance and functional mobility in older adults: a systematic review and meta-analysis", Maturitas, 80(4), 342-58 (2015)

Perry SD, "Evaluation of age-related plantar-surface insensitivity and onset age of advanced insensitivity in older adults using vibratory and touch sensation tests", Neurosci Lett, 392(1-2), 62-7 (2006)

Purves D, Augustine GJ, Fitzpatrick D, "Mechanoreceptors specialized to receive tactile information", In: Neuroscience, 2nd ed, Sunderland (MA), Sinauer Associates (2001)

Pyykkö I, Färkkilä M, Inaba R, Starck J, Pekkarinen J, "Effect of hand-arm vibration on inner ear and cardiac functions in man", Nagoya J Med Sci, 57(Suppl), 113-9 (1994)

Reardon M, Malik M, "Changes in heart rate variability with age", Pacing Clin Electro-physiol, 19(11 Pt 2), 1863-6 (1996)

Rizzo JA, Friedkin R, Williams CS, Nabors J, Acampora D, Tinetti ME, "Health care utilization and costs in a Medicare population by fall status", Med Care, 36(8), 1174-88 (1998)

Robbins D, Yoganathan P, Goss-Sampson M, "The influence of whole body vibration on the central and peripheral cardiovascular system", Clin Physiol Funct Imaging, 34(5), 364-9 (2014)

Rittweger J, Beller G, Felsenberg D, "Acute physiological effects of exhaustive whole-body vibration exercise in man", Clin Physiol, 20(2), 134-42 (2000)

Romanovsky AA, "Skin temperature: its role in thermoregulation", Acta Physiol (Oxf) 210(3), 498-507 (2014)

Routledge FS, Campbell TS, McFetridge-Durdle JA, Bacon SL, "Improvements in heart rate variability with exercise therapy", Can J Cardiol, 26(6), 303-12 (2010)

Shaffer SW, Harrison AL, "Aging of the somatosensory system: a translational perspective", Phys Ther, 87(2), 193-207 (2007)

Shepherd JT, "Physiology of the circulation in human limbs in health and disease". Saunders, Philadelphia, pp 12-15, 1963

Tew GA, Saxton JM, Hodges GJ, "Exercise training and the control of skin blood flow in older adults", J Nutr Health Aging, 16(3), 237-41 (2012)

Thompson A, House R, Krajnak K, Eger T, "Vibration white foot: A case report", Occup Med (Lond), 60(7), 572-4 (2010)

Next-generation cars, secondary activities, and sitting configurations: In-line transmission of vertical vibration at seat cushion

Francesco D'Amore and Yi Qiu
Institute of Sound and Vibration Research, University of Southampton
Southampton SO17 1BJ, United Kingdom
F.DAmore@soton.ac.uk, Y.Qiu@soton.ac.uk

ABSTRACT

Next-generation cars will be electric, connected, autonomous, and shared. Aboard, primary activities such as driving or travelling will coexist with secondary activities such as (self-) entertaining, socialising, relaxing, sleeping, working, and eating. Although secondary activities have already been identified, related seating issues have only been touched. A three-factor mixed-design laboratory experimental study was conducted to test whether the concept of 'sitting configuration' (introduced and defined in this paper) is appropriate to characterise the seat–occupant system as a whole. Specifically, investigated were main effects and interaction effects of (biological) sex, vibration magnitude, and sitting configuration on in-line transmission of vertical vibration at seat cushion. With the Six-Axis Motion Simulator of the University of Southampton, six men and six women occupying a production reclining car seat were subjected to four vibration magnitudes in four sitting configurations corresponding to four pairs of primary and secondary activities. Transmissibility and coherence functions were calculated from acceleration measurements. An ANOVA model of first-resonance frequency of transmissibility showed an appreciable main effect of both vibration magnitude ($F(2.21, 22.11) = 369.54$, $p < 0.001$, $\eta^2 = 0.28$, $\eta_P^2 = 0.97$, $\eta_G^2 = 0.54$) and sitting configuration ($F(1.98, 19.80) = 82.27$, $p < 0.001$, $\eta^2 = 0.48$, $\eta_P^2 = 0.89$, $\eta_G^2 = 0.67$) but failed to show an appreciable main effect of sex ($F(1, 10) < 0.001$, $p > 0.99$, $\eta^2 < 0.001$, $\eta_P^2 = 0.001$, $\eta_G^2 < 0.001$) and any appreciable interaction effects ($p > 0.99$, $\eta^2 \leq 0.004$, $\eta_P^2 \leq 0.12$, $\eta_G^2 \leq 0.02$). Results suggest that the concept of sitting configuration is appropriate to characterise the seat–occupant system as a whole. Ultimately, in design and development of seats for next-generation cars, secondary activities and corresponding sitting configurations should be taken into consideration to optimise not only functionality, but also comfort and protection (and related affective/emotional attributes).

1   INTRODUCTION

The world of road transport has been rapidly metamorphosing in recent years. Indeed, both major advances and new challenges are expected within the automotive industry [1]. The four keywords of next-generation cars are *electrification*, *connection*, *automation*, and *sharing* [2]. It is still a matter of discussion whether such innovations will prove truly disruptive and revolutionary or just incremental and evolutionary [3]; in fact, it is even unclear whether they will be welcomed or not by the public [4]. However, at the very least, an automotive paradigm shift is a plausible development.

Should electric, connected, autonomous, and shared cars hit the road, important behavioural changes would spread amongst users [5]. Being more often passengers than drivers, users of next-generation cars might engage not only in *primary activities* such as *travelling* or *driving*, but also in *secondary activities* such as (*self-) entertaining*, *socialising*, *relaxing*, *sleeping*, *working*, and *eating* [6, 7, 8, 9, 10, 11, 12, 13]. In a similar automotive-industry scenario, when it comes to customer

expectations and related product requirements, performance is likely to be outweighed not only by functionality, but also by comfort and protection (and related affective/emotional attributes [14]). In other words, *human factors and ergonomics (HFE)* is likely to become key.

We may know 'what' people will be doing in next-generation cars, and yet we do not know 'how'. To date, the (transport) HFE community has addressed the topic mainly within the *organisational* branch (*traffic management* [15] and *traffic safety* [16]) and the *cognitive* branch (*situational awareness* [17] and *human-machine interaction* [18]). Indeed, apart from *motion sickness* [19, 20], researchers have not probed deep into the *physical* branch (*comfort* and *protection*). In particular, *seating issues* specific to next-generation cars remain relatively unexplored from a 'static' point of view (*occupant packaging* [21, 22, 23, 24]) and barely approached from a 'dynamic' point of view (*vehicle safety* [25] and *human vibration* [26, 27, 28]).

As regards (whole-body) human vibration, many laboratory experimental studies have been designed to investigate *objective responses of seated human body to motion environment* [29, 30]. On the one hand, working closer to the 'basic' end of the basic–applied research continuum, investigators in *biodynamics* have used rigid or semirigid laboratory seats to characterise the occupant alone (mainly in terms of *apparent mass* [31, 32, 33]). On the other hand, working closer to the 'applied' end of the basic–applied research continuum, investigators in *seating dynamics* have used deformable factory seats to characterise both the seat alone (mainly in terms of *dynamic stiffness* [34, 35, 36]) and the seat–occupant system as a whole (mainly in terms of *transmissibility* [35, 37]). However, in many cases, attention has been paid to effects of specific factors considered in isolation. The most popular has been perhaps severity of motion environment (usually characterised in terms of *vibration magnitude*), which has shown unequivocal nonlinear effects [38, 39]. Other favourites are *seat-back reclination* [40], *footrest configuration* [41, 42], and *demographic and anthropometric characteristics* [43]; amongst these, only seat-back reclination has shown clear and consistent effects.

Now, three considerations are in order. First, although in real-life scenarios both seat-back reclination and footrest configuration contribute to determining the *overall arrangement of the seat–occupant system*, they have rarely been subjected to simultaneous experimental manipulation. Second, although women represent approximately half of the population, experimental studies have recurrently used samples composed only of men, and, if not, they have just sporadically included *(biological) sex* [1] as a factor. Third, although main effects are typically superseded by interaction effects (and, in turn, lower-order interaction effects are typically superseded by higher-order interaction effects), *interaction effects* of any kind have scarcely been investigated.

To meet habitability needs of next-generation cars, important advances in car interiors and specifically in car seats are to be pursued with targeted applied research. After adopting a conceptual framework in which the seat–occupant system is regarded as a whole [26], the natural step forward is deploying operational tools that facilitate addressing practical issues. Following this line of thought, the concept of *sitting configuration* is introduced and defined in this paper as *"activity-related overall arrangement of the seat–occupant system specified by position, orientation, body posture, body support, and body restraint"*.

In light of the above, a *laboratory experimental study* was conducted to test whether the concept of sitting configuration is appropriate to characterise the seat–occupant system as a whole. In particular, three *research questions* were formulated. On objective seat–occupant responses to motion environment, besides the well-known main effect of vibration magnitude:

- Is there an appreciable main effect of sitting configuration?
- Is there an appreciable main effect of sex?
- Are there any appreciable interaction effects between sex, vibration magnitude, and sitting configuration?

In what follows, objective seat–occupant responses to motion environment are related to *in-line transmission of vertical vibration at seat cushion*.

---

[1] Within the context of this study, biologically rather than culturally determined characteristics are of interest. Accordingly, in this paper, the term 'sex' is used instead of the term 'gender'.

2   METHOD

Considering findings of published studies, four *sitting configurations* were identified and characterised, both qualitatively and quantitatively, to match one pair of primary activities [44, 45, 46, 47, 48, 49, 50, 51, 52, 53, 54, 55, 56, 57] and three pairs of secondary activities [8, 22, 23, 24, 58, 59, 60]. Sitting configurations, shown in **Figure 1**, were labelled *(self-) entertaining/socialising (ES)*, *relaxing/sleeping (RS)*, *travelling/driving (TD)*, and *working/eating (WE)*. Qualitative characteristics of sitting configurations are shown in **Table 1**.

Figure 1 Sitting configurations. **Top left:** (self-) entertaining/socialising (ES). **Top right:** relaxing/sleeping (RS). **Bottom left:** travelling/driving (TD). **Bottom right:** working/eating (WE).

Table 1 Qualitative characteristics of sitting configurations

	ES	RS	TD	WE
Body posture	crouched	zero-gravity	regular	upright
Seat-back reclination	medium–high	high	medium–low	low
Footrest horizontal position	far	far	far	near
Footrest vertical position	high	medium–low	medium–high	low
Footrest inclination	high	medium	medium–high	zero

Four whole-body mechanical vibrations were used as *excitations/stimuli*. They were designed to perform an appropriate frequency-domain characterisation in the widest possible portion of the frequency band of interest for road-transport applications involving exposure to whole-body mechanical vibration (but not motion sickness) [29, 30]. In particular, chosen excitations/stimuli were intended to represent 'baseline' conditions with 'simple' direction, 'well-behaved' waveform, 'wide' frequency band, 'relatively modest' severity, and 'sufficiently long' duration. Even if it seems reasonable to expect passengers travelling aboard next-generation cars to be exposed to more complex motion environments [27, 28], baseline conditions were preferred to facilitate not only performing an appropriate frequency-domain characterisation, but also referencing to previous studies. Characteristics of excitations/stimuli are shown in **Table 2**.

Table 2 Characteristics of excitations/stimuli

Type	whole-body mechanical vibration
Direction	'vertical' (z-axis of laboratory geocentric coordinate system)
Waveform	low-crest-factor stationary pseudorandom with pseudo-white-noise power spectral density
Frequency band	between 0.5 Hz and 50 Hz
Severity [a]	{0.28 m·s^{-2}, 0.45 m·s^{-2}, 0.71 m·s^{-2}, 1.12 m·s^{-2}}
Duration	60 s
[a] Severity is expressed in terms of root-mean-square value of W_k-weighted acceleration [61] (approximately equal to root-mean-square value of W_b-weighted acceleration [62]).	

Since the four excitations/stimuli differed only in severity, they were characterised in terms of *vibration magnitude*. In principle, vibration magnitude is a continuous quantity (whose four chosen values are equally spaced on a logarithmic scale). However, for the purposes of this study, it was conveniently considered as an (ordinal) categorical quantity assuming four values labelled *0d28w*, *0d45w*, *0d71w*, and *1d12w*. In terms of approximate indications of likely reactions, these four vibration magnitudes correspond respectively to the four verbal descriptors 'not uncomfortable', 'a little uncomfortable', 'fairly uncomfortable', and 'uncomfortable' [61, 62]. The four vibration magnitudes were chosen to cover the range of severity that may be expected in road-transport applications involving next-generation cars. The use of four values was decided to allow capturing possible non-monotonic trends with some detail.

2.1 Participants

This study was approved by the Faculty Ethics Committee of Engineering and the Environment at the University of Southampton (ERGO II submission reference 41143). A *sample* of 'adult' and 'healthy' men and women was selected amongst students and staff members of the University of Southampton to represent the target population of users of next-generation cars. To be regarded as 'adult', participants had to be eighteen years old or more. To be regarded as 'healthy' without further medical advice, participants had to be fit to travel in public transport without assistance and to accept the stress of a normal day's work, did not have to be suffering any serious illness or injury, did not have to be under medical treatment or suffering disability affecting their daily life, and did not have to have certain conditions (active disease of the respiratory system, active disease of the digestive system, active disease of the cardiovascular system, active disease of the genitourinary system, active disease of the musculoskeletal system, active or chronic disease or disorder of the nervous system, mental health problems, recent trauma, recent surgical procedures, prosthesis, pregnancy, and breastfeeding). For the formal assessment of eligibility, a health questionnaire was designed in compliance with International Standard ISO 13090-1:1998 [63].

Neither random nor systematic sampling plan was implemented, but equal numbers of men and women were sought to obtain *two independent groups* of the same size. The intended total *sample size* of *twelve participants* (*six men* and *six women*) was chosen, in the wake of the psychophysical

tradition [64], with the aim of detecting 'large' effect sizes. Fourteen potential participants were reached haphazardly, either through direct approach (five men and four women) or through advertisement (one man and four women), and were preliminarily screened. Two directly approached women were excluded (one because of a refusal to participate and the other because of a scheduling conflict). Twelve potential participants (six men and six women) were formally assessed for eligibility and were recruited. They gave their informed consent to participate and received a reimbursement payment. Personal data collected or created about participants were pseudonymised and managed confidentially in compliance with the Data Protection Policy of the University of Southampton as well as with the Data Protection Act 2018 (for the purposes of which the University of Southampton is the data controller).

Major *demographic and anthropometric characteristics* of the two independent groups were as follows. The *male group* had age with median 28 y and interquartile range 3 y, body mass (weight) with median 78.6 kg and interquartile range 14.2 kg, stature (body height) with median 1797 mm and interquartile range 37 mm, and body mass index with median 23.8 kg·m^{-2} and interquartile range 2.8 kg·m^{-2}. The *female group* had age with median 30 y and interquartile range 9 y, body mass (weight) with median 67.7 kg and interquartile range 11.0 kg, stature (body height) with median 1666 mm and interquartile range 57 mm, and body mass index with median 23.6 kg·m^{-2} and interquartile range 5.2 kg·m^{-2}.

2.2   Measures

Objective seat–occupant responses to motion environment were measured within a laboratory experiment. Measurements of *rectilinear components of acceleration* were performed, by means of measuring instrumentation complying with International Standard ISO 8041-1:2017 [65], in the three perpendicular directions of each of *two coordinate systems*. The $\{x_t, y_t, z_t\}$ coordinate system was located at the *vibration table*, whereas the $\{x_c, y_c, z_c\}$ coordinate system was located at *the interface between seat cushion and occupant buttocks*. Experimental arrangement and coordinate systems are shown in **Figure 2**.

Figure 2 Experimental arrangement and coordinate systems. $\{x_t, y_t, z_t\}$: coordinate system at vibration table. $\{x_c, y_c, z_c\}$: coordinate system at interface between seat cushion and occupant buttocks.

At the seat–occupant interface, the non-zero value of the cushion angle led to the adoption of a *basicentric biodynamic coordinate system* [66]. Hence, unlike the axes of the $\{x_t, y_t, z_t\}$ coordinate system, the axes of the $\{x_c, y_c, z_c\}$ coordinate system were not exactly parallel to those of the geocentric coordinate system of the laboratory (having z-axis lying in the direction of the earth's gravity). The $\{x_c, y_c, z_c\}$ coordinate system seemed appropriate on the reasonable assumption that

psychophysiological responses to vibration depend on motion components in the directions of the axes of biodynamic rather than geocentric coordinate systems [61, 62]. However, considering the parallelism tolerances specified in International Standard ISO 2631-1:1997 [61] and in British Standard BS 6841:1987 [62] (respectively up to 20° and up to 15°), the z_t axis and the z_c axis could be considered in-line to a first approximation.

The seat–occupant system had a longitudinal plane of symmetry passing through the centreline of the seat and coinciding with the sagittal plane of the occupant; besides, the excitations/stimuli were one-directional and vertical. Accordingly, relevant measurements of acceleration were in the directions z_t, x_c, and z_c; nevertheless, for verification purposes, they were also performed in the directions x_t, y_t, and y_c. In what follows, only the $\{z_t, z_c\}$ *input–output pair* is considered; this implies regarding the seat–occupant system as a single-input single-output (SISO) dynamic system.

For each test, *two response functions* and *one response variable* were obtained from the input acceleration in the direction z_t and from the output acceleration in the direction z_c. The response functions were the $\{z_t, z_c\}$ *transmissibility function* (complex-valued function) and the corresponding $\{z_t, z_c\}$ *coherence function* (real-valued function), both defined in International Standard ISO 2041:2018 [67]. For subsequent analyses, the complex-valued transmissibility function was decomposed into modulus and argument (also known as amplitude and phase angle respectively). Calculations of transmissibility function and coherence function were performed, as described in International Standard ISO 18431-1:2005 [68], starting from estimated power spectral density and cross-spectral density of input and output accelerations. In particular, the transmissibility function was calculated as a frequency-response function of the first type. For its theoretical and practical importance, *first-resonance frequency* of $\{z_t, z_c\}$ transmissibility function (real-valued scalar) was chosen as response variable for statistical analysis.

2.3 Research Design

Implemented was a *(balanced) three-factor mixed design* with *one two-level between-group factor* (*sex*) and *two four-level within-group factors* (*vibration magnitude* and *sitting configuration*). Accordingly, each of the six participants within each of the two independent groups received *sixteen treatments*. An effort was made to adopt all the three fundamental principles of experimental design attributed to the British statistician and geneticist Ronald Aylmer Fisher (1890–1962): replication, blocking, and randomisation. To control random measurement error and improve measurement precision, *replication* was systematically implemented: namely, each of the sixteen treatments was replicated three times with each of the twelve participants to obtain thirty-six tests per treatment. To control the effect of nuisance factors and improve statistical power, *blocking* was implemented at two levels: namely, independent groups were used as blocks with respect to between-group factor and participants were used as blocks with respect to within-group factors and replicate. To control systematic measurement error and improve measurement trueness, *randomisation* was completely implemented with respect to within-group factors and replicate: namely, a different random test sequence was used for the forty-eight tests of each participant.

For inferential statistical analysis, a *three-way mixed-design univariate analysis of variance (ANOVA)* was used. The *(nil) null hypothesis* was that experimental manipulation of sex, vibration magnitude, and sitting configuration had neither appreciable main effects nor appreciable interaction effects. Despite requiring more restrictive assumptions than those required by semiparametric and nonparametric counterparts, a parametric technique was preferred because of the greater statistical power; the legitimacy of this choice was assessed a posteriori by verifying the assumption of normality for the model residuals.

These authors are aware of the criticism of the procedure of *null hypothesis statistical significance testing* [69]. In fact, controversies about statistical inference are perennial. At a higher level, epistemological discussions about paradigms (frequentist vs Bayesian) [70], frameworks (parameter estimation vs hypothesis testing) [71], and even approaches within the same framework (Fisher's vs Neyman–Pearson's hypothesis testing) [72] have persisted for decades. At a lower level,

the old frequentist dilemma between parametric and nonparametric techniques [73] has been flanked by a more recent debate about possible parametric substitutes for ANOVA [74, 75]. Pragmatically, a classic well-attested technique allowing the analysis of three-way interactions with a relatively easy implementation was deemed appropriate for the purposes of this study. However, considering both the many well-founded reservations about the procedure of null hypothesis statistical significance testing [69] and the latest recommendations of the American Statistical Association (ASA) [76], no declarations of 'statistical significance' are made in this paper. Instead, assessments of 'practical significance' of effects are made by complementing p-values with numerical measures of *effect size* (eta-squared η^2, partial eta-squared η_P^2, and generalised eta-squared η_G^2) [2] and point estimates with graphical representations of *interval estimates* (confidence intervals at 95 % confidence level). In this paper, to avoid using the worn word 'significant' altogether, an effect deemed practically significant is qualified as 'appreciable'.

2.4   Experimental Manipulations

The *vibration generator system* (Six-Axis Motion Simulator of the University of Southampton) was composed of a hydraulic vibration generator with table and a digital control system. In order to reproduce realistic seat–occupant interactions, used was a *production reclining car seat* (NHK left-outboard front-row passenger seat for right-hand-drive Subaru Outback) rigidly mounted on the vibration table. A *four-piece configurable footrest* made of wood and carpet (handcrafted at the University of Southampton) was mounted on the vibration table in front of the seat.

Target acceleration signals for the four excitations/stimuli were generated in MATLAB software environment (version 8.5.1.959712) by means of the HVLab Human Response to Vibration Toolbox (version 2.0). The corresponding *drive displacement signals* were obtained through an iterative 'equalisation' process by means of the vibration generator system.

All *acceleration measurements* were performed according to International Standard ISO 10326-1:2016 [78]. At vibration table, used were three uniaxial accelerometers (Silicon Design 2260-005). At the interface between seat cushion and occupant buttocks, used was one special-purpose triaxial accelerometer (HVLab SITpad-3-10g). The instrumented seat is shown in **Figure 3**.

Figure 3 Instrumented seat. **Left:** front view. **Right:** side view.

---

[2] Interpretations of measures of effect size against arbitrary benchmarks are not recommended; accordingly, they are not provided in this paper. In principle, one can use eta-squared η^2 for comparisons of effects within a single study, partial eta-squared η_P^2 for power analyses and for comparisons of effects across studies with the same research design, and generalised eta-squared η_G^2 for meta-analyses and for comparisons of effects across studies with different research design [77].

Acquisition of acceleration signals was performed in MATLAB software environment via the HVLab Human Response to Vibration Toolbox at a sampling rate of 512 $S \cdot s^{-1}$. The multichannel data acquisition system was composed of a multifunction I/O device (National Instruments NI USB6211) and of a signal conditioning system, which in turn was composed of two eight-channel mobile Micro Analog 2 enclosures (Fylde FE-MM8), two power supply modules (Fylde FE-810-BPS DC), six two-channel bridge transducer amplifier modules (Fylde FE-366-TA), and two auto-zero modules (Fylde FE-366-AZ).

The forty-eight tests of each participant were performed at the University of Southampton within *two sessions* held on two different days, each including twenty-four tests and lasting between 2.5 h and 3 h. The long duration of each session was due to the randomisation with respect to sitting configuration, which required long breaks between consecutive tests. Within these breaks, seat-back reclination and footrest configuration would be adjusted by using respectively an inclinometer and a set of reference stickers on the vibration table. Special care was taken to ensure that sitting configurations were reproduced consistently across different tests, both with the same participant and with different participants. Each sitting configuration was visually checked and documented photographically with each participant.

In accordance with the approved *research protocol*, participants had their demographic data collected and their anthropometric data measured at the beginning of their first session. Before actual tests of each of their two sessions, participants read an instruction sheet and received preliminary training for a duration of 5 min. Before each test, participants were secured with a safety harness and were given ready access to an emergency stop control. Within each test, participants were exposed to an excitation/stimulus for a duration of 60 s whilst sitting relaxed but unmoving. As expected, participants did not suffer from motion sickness nor other malaise throughout their sessions.

3   RESULTS

Data processing was performed in MATLAB software environment at a frequency resolution of 0.25 Hz. *Statistical analysis* was performed in RStudio integrated development environment for R (version 1.2.5019) running against R software environment (version 3.6.1) [79]. There were no missing data nor deleted cases. Median and interquartile range of the response variable (first-resonance frequency of $\{z_t, z_c\}$ transmissibility) calculated across all tests were respectively 4.5 Hz and 1 Hz.

The *data set* used for inferential statistical analysis was composed of median values of the response variable calculated across all three replicates of each treatment with each participant. The corresponding interquartile range values were generally less than the frequency resolution value of 0.25 Hz. For each treatment with each participant, such interquartile range values provide numerical information about intra-participant variability. The data set was deemed robust enough to allow abstaining from further detection and treatment of outliers.

Graphical summaries of *frequency-domain analysis* for the response functions are provided in **Figure 4** and **Figure 5**, which show Bode plots and coherence plots of grand-median response functions ($\{z_t, z_c\}$ transmissibility modulus, $\{z_t, z_c\}$ transmissibility argument, and $\{z_t, z_c\}$ coherence) calculated across all thirty-six tests per treatment. Bode plots and coherence plots shown in **Figure 4** and **Figure 5** are equivalent, but they are parameterised and arranged differently for convenience.
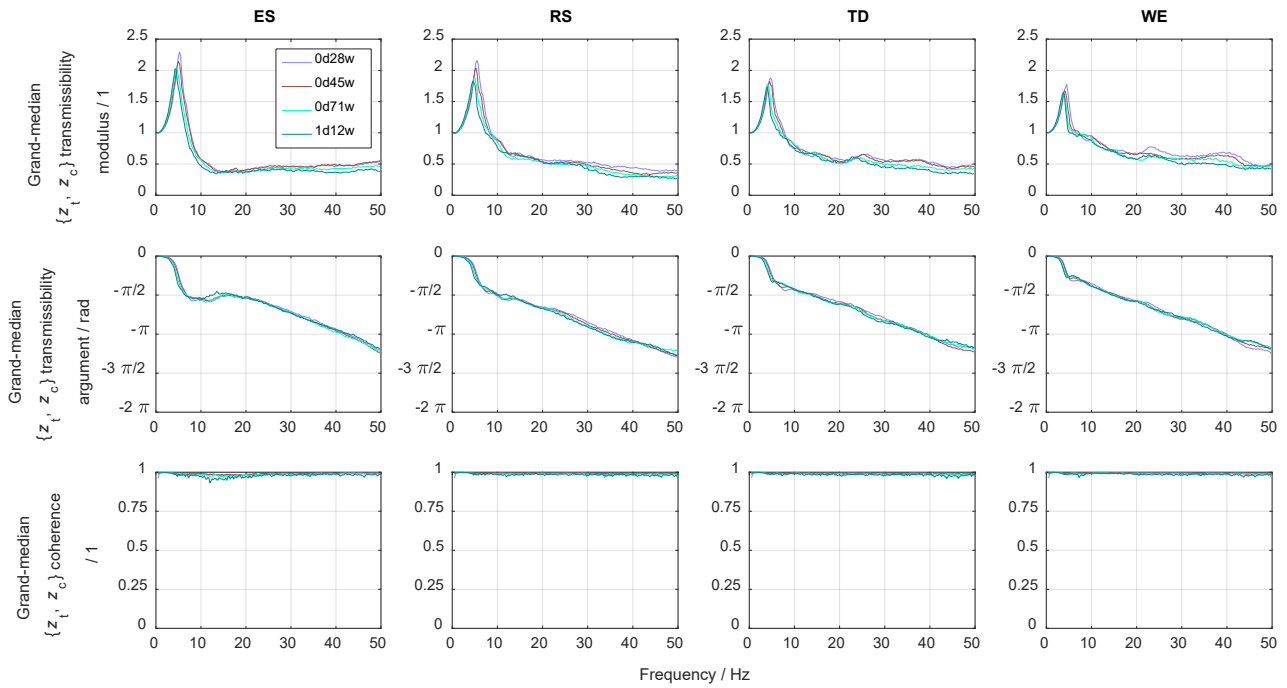
Figure 4 Bode plots and coherence plots of grand-median response functions ($\{z_t, z_c\}$ transmissibility modulus, $\{z_t, z_c\}$ transmissibility argument, and $\{z_t, z_c\}$ coherence) calculated across all thirty-six tests per treatment. Total sample: twelve participants (six men and six women). Vibration magnitude levels: {0d28w, 0d45w, 0d71w, 1d12w}. Sitting configuration levels: {ES, RS, TD, WE}. **Top row:** grand-median $\{z_t, z_c\}$ transmissibility modulus vs frequency. **Middle row:** grand-median $\{z_t, z_c\}$ transmissibility argument vs frequency. **Bottom row:** grand-median $\{z_t, z_c\}$ coherence vs frequency. (All graphs parameterised on vibration magnitude and arranged in columns by sitting configuration).
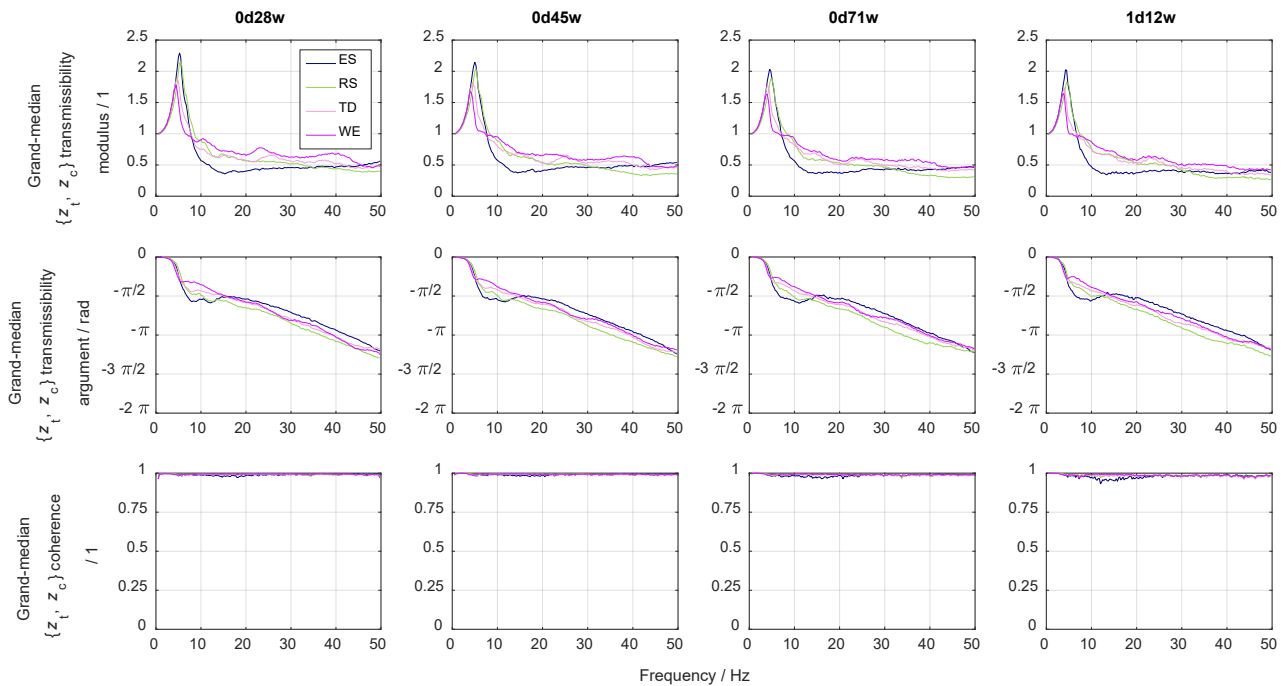
Figure 5 Bode plots and coherence plots of grand-median response functions ($\{z_t, z_c\}$ transmissibility modulus, $\{z_t, z_c\}$ transmissibility argument, and $\{z_t, z_c\}$ coherence) calculated across all thirty-six tests per treatment. Total sample: twelve participants (six men and six women). Vibration magnitude levels: {0d28w, 0d45w, 0d71w, 1d12w}. Sitting configuration levels: {ES, RS, TD, WE}. **Top row:** grand-median $\{z_t, z_c\}$ transmissibility modulus vs frequency. **Middle row:** grand-median $\{z_t, z_c\}$ transmissibility argument vs frequency. **Bottom row:** grand-median $\{z_t, z_c\}$ coherence vs frequency. (All graphs parameterised on sitting configuration and arranged in columns by vibration magnitude).

Graphical summaries of *descriptive statistical analysis* for the response variable are provided in **Figure 6**, which shows box plots of median response variable (first-resonance frequency of $\{z_t, z_c\}$ transmissibility) calculated across all three replicates. For each treatment with each independent group, such box plots provide graphical information about inter-participant variability. The bottom line of each box (lower hinge) corresponds to the lower quartile (also known as first quartile and coinciding with the 25th percentile). The middle line of each box corresponds to the median (also knowns as second quartile and coinciding with the 50th percentile). The top line of each box (upper hinge) corresponds to the upper quartile (also known as third quartile and coinciding with the 75th percentile). The difference between upper quartile and lower quartile is the interquartile range. The lower whisker extends from the lower hinge to the minimum value at or above the lower fence (value situated 1.5 times the interquartile range below the lower quartile). The upper whisker extends from the upper hinge to the maximum value at or below the upper fence (value situated 1.5 times the interquartile range above the upper quartile). Values beyond the lower fence and the upper fence are marked separately. Box plots shown on the left side and of the right side of **Figure 6** are equivalent, but they are parameterised and arranged differently for convenience.
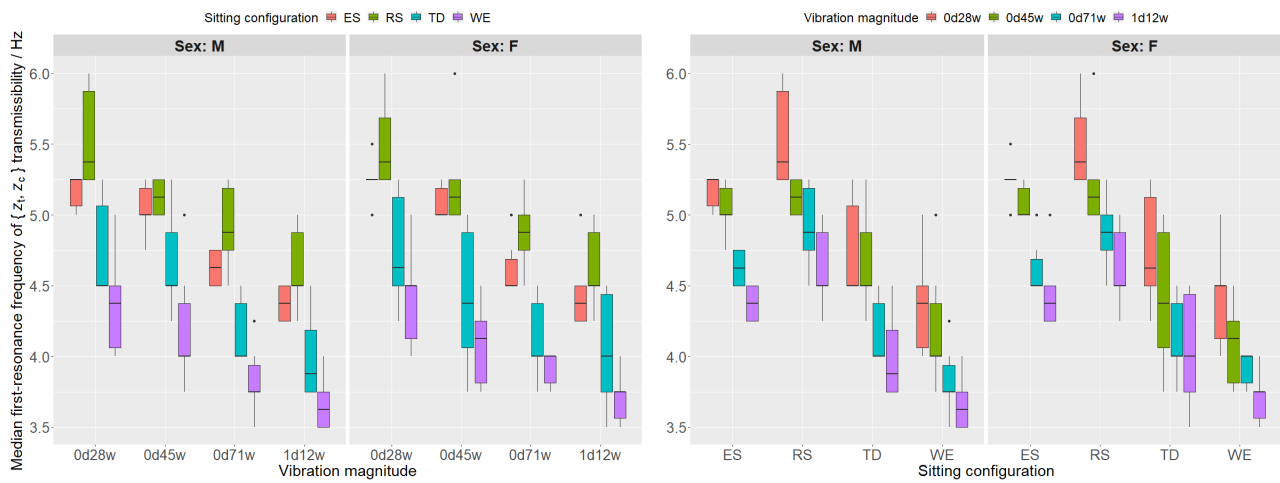
Figure 6 Box plots of median response variable (first-resonance frequency of $\{z_t, z_c\}$ transmissibility) calculated across all three replicates. Independent groups: male group (six participants) and female group (six participants). Sex levels: $\{M, F\}$. Vibration magnitude levels: $\{0d28w, 0d45w, 0d71w, 1d12w\}$. Sitting configuration levels: $\{ES, RS, TD, WE\}$. **Left:** median first-resonance frequency of $\{z_t, z_c\}$ transmissibility vs vibration magnitude (graphs parameterised on sitting configuration and arranged in columns by sex). **Right:** median first-resonance frequency of $\{z_t, z_c\}$ transmissibility vs sitting configuration (graphs parameterised on vibration magnitude and arranged in columns by sex).

A *three-way mixed-design univariate ANOVA model* of the response variable was fit by using the R package afex (version 0.25-1) [80]. To protect against possible violations of the sphericity assumption, conservative Greenhouse–Geisser corrections were applied to eligible statistical degrees of freedom. To mitigate the multiple-comparisons problem inherent in multiway ANOVA [81], *p*-values were adjusted using the Holm–Bonferroni method. The normality assumption for the model residuals was verified by means of diagnostic plots; the histogram of residuals, the residual–fitted plot, and the quantile–quantile plot of residuals indicated no obvious deviation from normality.

The ANOVA model of the response variable showed an appreciable main effect of both vibration magnitude ($F(2.21, 22.11) = 369.54$, $p < 0.001$, $\eta^2 = 0.28$, $\eta_P^2 = 0.97$, $\eta_G^2 = 0.54$) and sitting configuration ($F(1.98, 19.80) = 82.27$, $p < 0.001$, $\eta^2 = 0.48$, $\eta_P^2 = 0.89$, $\eta_G^2 = 0.67$) but failed to show an appreciable main effect of sex ($F(1, 10) < 0.001$, $p > 0.99$, $\eta^2 < 0.001$, $\eta_P^2 = 0.001$, $\eta_G^2 < 0.001$) and any appreciable interaction effects ($p > 0.99$, $\eta^2 \leq 0.004$, $\eta_P^2 \leq 0.12$, $\eta_G^2 \leq 0.02$). Graphical summaries of *inferential statistical analysis* for the response variable are provided in **Figure 7**, which shows three-way interaction-effect plots of ANOVA model of response variable (first-resonance

frequency of $\{z_t, z_c\}$ transmissibility) with confidence-interval error bars at confidence level 95 % (not usable for comparisons across different levels of the between-group factor sex) [3]. Interaction-effect plots shown on the left side and of the right side of **Figure 7** are equivalent, but they are parameterised and arranged differently for convenience.
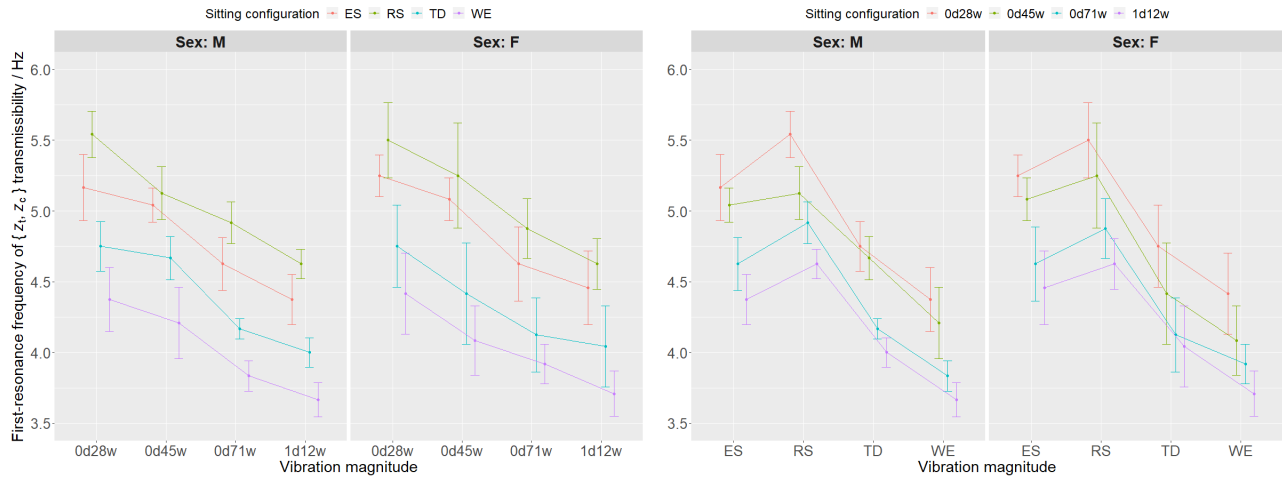
Figure 7 Three-way interaction-effect plots of ANOVA model of response variable (first-resonance frequency of $\{z_t, z_c\}$ transmissibility) with confidence-interval error bars at confidence level 95 % (not usable for comparisons across different levels of the between-group factor sex). Independent groups: male group (six participants) and female group (six participants). Sex levels: {M, F}. Vibration magnitude levels: {0d28w, 0d45w, 0d71w, 1d12w}. Sitting configuration levels: {ES, RS, TD, WE}. **Left:** first-resonance frequency of $\{z_t, z_c\}$ transmissibility vs vibration magnitude (graphs parameterised on sitting configuration and arranged in columns by sex, data points horizontally offset for clarity). **Right:** first-resonance frequency of $\{z_t, z_c\}$ transmissibility vs sitting configuration (graphs parameterised on vibration magnitude and arranged in columns by sex, data points horizontally offset for clarity).

4   DISCUSSION

In almost static conditions, near zero frequency, *transmissibility functions* are almost real-valued; in particular, modulus is almost equal to unity (by virtue of input and output axes being almost parallel), and argument is almost null (by virtue of input and output accelerations being in phase). Within the low end of the frequency band of interest, a one-degree-of-freedom-like first resonance is identifiable by means of a prominent peak in modulus and a corresponding drop in argument.

As can be seen in **Figure 4**, transmissibility functions are affected by vibration magnitude in terms of *shifting* and *scaling*. Indeed, with increasing vibration magnitude, a decrease both in first-resonance frequency of transmissibility and in first-resonance value of transmissibility modulus is observed. This nonlinear *softening effect*, well known from previous studies [38, 39], occurs not only locally, but also across the whole frequency band of interest; in particular, with increasing vibration magnitude, both transmissibility modulus curves and (less markedly) transmissibility argument curves shift to the left and scale down.

As can be seen in **Figure 5**, transmissibility functions are affected by sitting configuration in terms of *shaping*. Indeed, different behaviours can be observed at the two ends of the frequency band of interest; this allows identifying two *end zones* and one separating *transition zone*. The frequency

---

[3] It is worth emphasising that, when used for comparisons, overlapping confidence-interval error bars at confidence level $1 - \alpha$ do not preclude a 'statistically significant' difference between the means at a 'significance level' less than or equal to α. In fact, non-overlapping confidence-interval error bars at confidence level $1 - \alpha$ imply a 'statistically significant' difference between the means at a 'significance level' distinctly less than α [82].

boundaries of the three zones and the overall shape of transmissibility modulus and argument curves depend on the sitting configuration. By inspection, the transition zone appears to have lower bound approximately at the first-resonance frequency (having median value 4.5 Hz and interquartile range 1 Hz across all tests) and upper bound approximately at a frequency between 14 Hz and 16 Hz. In accordance with previously reported results, it can be hypothesised that response functions are controlled in the low-end zone by seat-back reclination [40] and in the high-end zone by footrest horizontal and vertical position [41, 42]. In turn, these parameters may exert their influence by affecting loading distribution and contact area at the interface between seat cushion and occupant buttocks and, through the latter, by affecting dynamic stiffness of the seat [34, 35, 36] and apparent mass of the occupant [31, 32]. In terms of the reference items defined in Surface Vehicle Recommended Practice SAE J1100:2009-11 [83], the most important role is probably played in the low-end zone by A40 (torso angle) and in the high-end zone by the difference between A57 (thigh angle) and A27 (cushion angle).

For all treatments, *coherence* is high across the whole frequency band of interest, which proves the *input–output relation* to be *linear* and *noiseless*. Nevertheless, with increasing vibration magnitude, a slight decrease in coherence can be observed across the whole frequency band of interest; this can be explained by the contact at the interface between seat cushion and occupant buttocks becoming less stable. In particular, approximately between 5 Hz and 25 Hz, coherence takes slightly (but consistently) lower values for the ES sitting configuration; this can be interpreted as an effect of *occupant (involuntary) muscular activity*, which is a confounder in the adopted research design.

Median and interquartile range of the *response variable* calculated across all tests (respectively 4.5 Hz and 1 Hz) are in agreement with previous observations [37]. Main effects and interaction effects of the three considered factors on the response variable offer a varied picture. On the one hand, whilst an *appreciable main effect of vibration magnitude* is unsurprising [38, 39], an *appreciable main effect of sitting configuration* is a new finding, which suggests that the concept of sitting configuration is appropriate to characterise the seat–occupant system as a whole. On the other hand, whilst *failure to observe an appreciable main effect of sex* is consistent with previous inconclusive observations [33, 42, 43], *failure to observe any appreciable interaction effects* cannot be compared with known previous findings; however, if confirmed by further studies, it will have relevant implications in product design and development.

5   CONCLUSION

This study allowed showing that the concept of sitting configuration is appropriate to characterise the seat–occupant system as a whole. Indeed, at least as regards in-line transmission of vertical vibration at seat cushion, possible sitting configurations for secondary activities in next-generation cars are associated with different objective seat–occupant responses to motion environment. Ultimately, in design and development of seats for next-generation cars, secondary activities and corresponding sitting configurations should be taken into consideration to optimise not only functionality, but also comfort and protection (and related affective/emotional attributes). In order to generalise these findings to the target population of users of next-generation cars, the main technical limitation of this study is the sample size. Future investigations should consider more realistic motion environments as well as a wider range of response functions and response variables. The effects of different seat designs should also be investigated.

ACKNOWLEDGEMENTS

REFERENCES

[1] Kaas, H.-W., Mohr, D., Gao, P., Müller, N., Wee, D., Hensley, R., Guan, M., Möller, T., Eckhard, G., Bray, G., Beiker, S., Brotschi, A., and Kohler, D. (2016) *Automotive revolution. Perspective towards 2030. How the convergence of disruptive technology-driven trends could transform the auto industry*. McKinsey & Company.

[2] McKerracher, C., Orlandi, I., Wilshire, M., Tryggestead, C., Bouton, S., Mohr, D., Knupfer, S., Hannon, E., Ramkumar, S., Morden, E., Ramanathan, S., Nijssen, J.T., and Möller, T. (2016) *An integrated perspective on the future of mobility*. McKinsey & Company.

[3] Jiang, T., Petrovic, S., Ayyer, U., Tolani, A., and Husain, S. (2015) Self-driving cars: Disruptive or incremental? *Applied Innovation Review,* 1, 3–22.

[4] Nordhoff, S., De Winter, J., Kyriakidis, M., Van Arem, B., and Happee, R. (2018) Acceptance of driverless vehicles: Results from a large cross-national questionnaire study. *Journal of Advanced Transportation,* 2018, 1–22.

[5] Trommer, S., Kolarova, V., Fraedrich, E., Kröger, L., Kickhöfer, B., Kuhnimhof, T., Lenz, B., and Phleps, P. (2016) *Autonomous driving: The impact of vehicle automation on mobility behaviour*. Munich, Germany: Institute for Mobility Research.

[6] Pettersson, I. and Karlsson, I.C.M.-A. (2015) Setting the stage for autonomous cars: A pilot study of future autonomous driving experiences. *IET Intelligent Transport Systems,* 9 (7), 694–701.

[7] Pfleging, B. and Schmidt, A. (2015) (Non-) driving-related activities in the car: Defining driver activities for manual and automated driving. Paper presented at Workshop on Experiencing Autonomous Vehicles: Crossing the Boundaries between a Drive and a Ride at CHI 2015, Seoul, South Korea, 18–23 April 2015.

[8] Ive, H.P., Sirkin, D., Miller, D., Li, J., and Ju, W. (2015) "Don't make me turn this seat around!": Driver and passenger activities and positions in autonomous cars IN: Burnett, G., Pfleging, B., Kun, A., Meschtscherjakov, A., and Fröhlich, P. (eds.) *7th International Conference on Automotive User Interfaces and Interactive Vehicular Applications (AutomotiveUI 2015)*, University of Nottingham, Nottingham, United Kingdom, 1–3 September 2015. New York, New York, United States of America: Association for Computing Machinery, 50–55.

[9] Pfleging, B., Rang, M., and Broy, N. (2016) Investigating user needs for non-driving-related activities during automated driving IN: Häkkila, J. and Ojala, T. (eds.) *15th International Conference on Mobile and Ubiquitous Multimedia (MUM 2016)*, Rovaniemi, Finland, 12–15 December 2016. New York, New York, United States of America: Association for Computing Machinery, 91–99.

[10] Jorlöv, S., Bohman, K., and Larsson, A. (2017) Seating positions and activities in highly automated cars. A qualitative study of future automated driving scenarios IN: *2017 International Research Council on the Biomechanics of Injury (IRCOBI) Conference*, Antwerp, Belgium, 13–15 September 2017. Zurich, Switzerland: International Research Council on Biomechanics of Injury.

[11] Hecht, T., Darlagiannis, E., and Bengler, K. (2019) Non-driving related activities in automated driving. An online survey investigating user needs IN: Ahram, T., Karwowski, W., Pickl, S., and Taiar, R. (eds.) *2nd International Conference on Human Systems Engineering and Design (IHSED2019): Future Trends and Applications*, Universität der Bundeswehr München, Munich, Germany, 16–18 September 2019. Cham, Switzerland: Springer, 182–188.

[12] Östling, M. and Larsson, A. (2019) Occupant activities and sitting positions in automated vehicles in China and Sweden. Paper presented at 26th International Technical Conference on the Enhanced Safety of Vehicles (ESV), Eindhoven, Netherlands, 10–13 June 2019.

[13] Fitzen, F., Reimann, J., Amereller, M. and Paetzold, K. (2019) Quantitative characterisation for non-driving-related activities in automated vehicles IN: *22nd International Conference on Engineering Design (ICED19)*, Delft, Netherlands, 5–8 August 2019. Cambridge, United Kingdom: Cambridge University Press, 2893–2900.

[14] Tanoue, C., Ishizaka, K., and Nagamachi, M. (1997) Kansei engineering. A study on perception of vehicle interior image. *International Journal of Industrial Ergonomics*, 19 (2), 115–128.

[15] Wagner, P. (2016) Traffic control and traffic management in a transportation system with autonomous vehicles IN: Maurer, M., Gerdes, J.C., Lenz, B., and Winner, H. (eds.) *Autonomous driving: Technical, legal and social aspects*. Berlin, Germany: Springer, 301–316.

[16] Linkov, V., Zámečník, P., Havlíčková, D., and Pai, C.-W. (2019) Human factors in the cybersecurity of autonomous vehicles: Trends in current research. *Frontiers in Psychology,* 10, 1–7.

[17] Petersen, L., Robert, L., Yang, X.J., and Tilbury, D. (2019) Situational awareness, driver's trust in automated driving systems and secondary task performance. *SAE International Journal of Connected and Automated Vehicles,* 2 (2), 129–141.

[18] Burnett, G., Large, D.R., and Salanitri, D. (2019) *How will drivers interact with vehicles of the future?* London, United Kingdom: RAC Foundation.

[19] Sivak, M. and Schoettle, B. (2015) *Motion sickness in self-driving vehicles.* Ann Arbor, Michigan, United States of America: The University of Michigan Sustainable Worldwide Transportation, UMTRI-2015-12.

[20] Diels, C. and Bos, J.E. (2016) Self-driving carsickness. *Applied Ergonomics,* 53, 374–382.

[21] Reed, M. (2018) Applicability of occupant packaging and interior ergonomics tools to highly automated vehicles. *SAE Technical Paper Series,* 2018-01-0845, 1–7.

[22] Parida, S., Mallavarapu, S., Franz, M., and Abanteriba, S. (2018) A literature review of seating and body angles for non-driving secondary activities in autonomous driving vehicles IN: Stanton, N. (ed.) *AHFE 2018 International Conference on Human Factors in Transportation*, Loews Sapphire Falls Resort at Universal Studios, Orlando, Florida, United States of America, 21–25 July, 2018. Cham, Switzerland: Springer, 398–409.

[23] Parida, S., Mallavarapu, S., Abanteriba, S., Franz, M., and Gruener, W. (2019) User-centered-design approach to evaluate the user acceptance of seating postures for autonomous driving secondary activities in a passenger vehicle IN: Ahram, T., Karwowski, W., and Taiar, R. (eds.) *1st International Conference on Human Systems Engineering and Design (IHSED2018). Future Trends and Applications*, CHU-Université de Reims Champagne-Ardenne, Reims, France, 25–27 October 2018. Cham, Switzerland: Springer, 28–33.

[24] Parida, S., Mallavarapu, S., Abanteriba, S., Franz, M., and Gruener, W. (2019) Seating postures for autonomous driving secondary activities IN: Chen, Y.-W., Zimmermann, A., Howlett, R.J., and Jain, L.C. (eds.) *KES International conferences on Innovation in Medicine and Healthcare (KES-InMed-19) and Intelligent Interactive Multimedia Systems and Services (KES-IIMSS-19)*, Saint Julian's, Malta, 17–19 June 2019. Singapore: Springer, 423–434.

[25] Boin, M. (2018) Occupant protection in alternative seating position. Paper presented at 15th German LS-DYNA Forum 2018, Bamberg, Germany, 15–17 October 2018.

[26] D'Amore, F. and Qiu, Y. (2017) Whole-body oscillatory motion and road-transport innovations: A human-factors-and-ergonomics perspective within a ride-quality framework IN: Zioupos, P. (ed.) *52nd UK Conference on Human Responses to Vibration (UK HRV 2017)*, Sudbury House, Faringdon, United Kingdom, 5–6 September 2017. Shrivenham, United Kingdom: Cranfield University Press, 1–4.

[27] Burkhard, G., Vos, S., Munzinger, N., Enders, E., and Schramm, D. (2018) Requirements on driving dynamics in autonomous driving with regard to motion and comfort IN: Bargende, M., Reuss, H.-C., and Wiedemann, J. (eds.) *18th Stuttgart International Symposium. Automotive and Engine Technology*, Stuttgart, Germany, 13–14 March 2018. Wiesbaden: Springer, 683–697.

[28] Enders, E., Burkhard, G., Fent, F., Lienkamp, M., and Schramm, D. (2019) Objectification methods for ride comfort. Comparison of conventional methods and proposal of a new method for automated driving conditions. *Forschung im Ingenieurwesen*, 1–14.

[29] Griffin, M.J. (1990) *Handbook of human vibration*. London, United Kingdom: Academic Press.

[30] Mansfield, N.J. (2005) *Human response to vibration*. Boca Raton, Florida, United States of America: CRC Press.

[31] Toward, M.G.R. and Griffin, M.J. (2009) Apparent mass of the human body in the vertical direction: Effect of seat backrest. *Journal of Sound and Vibration,* 327 (3–5), 657–669.

[32] Toward, M.G.R. and Griffin, M.J. (2010) Apparent mass of the human body in the vertical direction: Effect of a footrest and a steering wheel. *Journal of Sound and Vibration,* 329 (9), 1586–1596.

[33] Toward, M.G.R. and Griffin, M.J. (2011) Apparent mass of the human body in the vertical direction: Inter-subject variability. *Journal of Sound and Vibration,* 330 (4), 827–841.

[34] Wei, L. and Griffin, M.J. (1997) The influence of contact area, vibration magnitude and static force on the dynamic stiffness of polyurethane seat foam. Paper presented at 32nd UK Conference on Human Responses to Vibration (UK HRV 1997), Chilworth Manor, Southampton, United Kingdom, 17–19 September 1997.

[35] Wei, L. (2000) *Predicting transmissibility of car seats from the seat impedance and the apparent mass of the human body*, Doctoral Thesis, University of Southampton, United Kingdom.

[36] Zhang, X., Qiu, Y., and Griffin, M.J. (2013) Static and dynamic stiffness of the cushion of a car seat. Paper presented at 48th UK Conference on Human Responses to Vibration (UK HRV 2013), Sunningdale Park, Ascot, United Kingdom, 16–18 September 2013.

[37] Zhang, X., Qiu, Y., and Griffin, M.J. (2012) Transmission of vertical floor vibration to various locations on a car seat. Paper presented at 47th UK Conference on Human Responses to Vibration (UK HRV 2012), Chilworth Manor, Southampton, United Kingdom, 17–19 September 2012.

[38] Mansfield, N.J. and Griffin, M.J. (2000) Non-linearities in apparent mass and transmissibility during exposure to whole-body vertical vibration. *Journal of Biomechanics,* 33 (8), 933–941.

[39] Tufano, S. and Griffin, M.J. (2013) Nonlinearity in the vertical transmissibility of seating: the role of the human body apparent mass and seat dynamic stiffness. *Vehicle System Dynamics,* 51 (1), 122–138.

[40] Houghton, T.J.C. (2003) The effect of backrest inclination on the transmission of vertical vibration through an automotive seat. Paper presented at 38th UK Conference on Human Responses to Vibration (UK HRV 2003), Institute of Naval Medicine, Gosport, United Kingdom, 17–19 September 2003.

[41] Fairley, T.E. (1986) *Predicting the dynamic performance of seats*, Doctoral Thesis, University of Southampton, United Kingdom.

[42] Corbridge, C., Griffin, M.J., and Harborough, P.R. (1989) Seat dynamics and passenger comfort. *Proceedings of the Institution of Mechanical Engineers, Part F: Journal of Rail and Rapid Transit,* 203 (1), 57–64.

[43] Toward, M.G.R. and Griffin, M.J. (2011) The transmission of vertical vibration through seats: Influence of the characteristics of the human body. *Journal of Sound and Vibration,* 330 (26), 6526–6543.

[44] Picard, F. and Wisner, A. (1961) How can the physiologist contribute to the improvement of automobile seats. *SAE Technical Paper Series,* 610176, 1–21.

[45] Rebiffé, R. (1969) Le siège du conducteur: son adaptation aux exigences fonctionnelles et anthropométriques. *Ergonomics,* 12 (2), 246–261.

[46] Babbs, F.W. (1979) A design layout method for relating seating to the occupant and vehicle. *Ergonomics,* 22 (2), 227–234.

[47] Tilley, A.R. (1993) *The measure of man and woman*. New York, New York, United States of America: Henry Dreyfuss Associates.

[48] Porter, J.M. and Gyi, D.E. (1998) Exploring the optimum posture for driver comfort. *International Journal of Vehicle Design,* 19 (3), 255–266.

[49] Harrison, D.D., Harrison, S.O., Croft, A.C., Harrison, D.E., and Troyanovich, S.J. (2000) Sitting biomechanics, Part II: Optimal car driver's seat and optimal driver's spinal model. *Journal of Manipulative and Physiological Therapeutics,* 23 (1), 37–47.

[50] Park, S.J., Kim, C.-B., Kim, C.J., and Lee, J.W. (2000) Comfortable driving postures for Koreans. *International Journal of Industrial Ergonomics,* 26 (4), 489–497.

[51] Andreoni, G., Santambrogio, G.C., Rabuffetti, M., and Pedotti, A. (2002) Method for the analysis of posture and interface pressure of car drivers. *Applied Ergonomics,* 33 (6), 511–522.

[52] Reed, M.P., Manary, M.A., Flannagan, C.A.C., and Schneider, L.W. (2002) A statistical method for predicting automobile driving posture. *Human Factors,* 44 (4), 557–568.

[53] Vogt, C., Mergl, C., and Bubb, H. (2005) Interior layout design of passenger vehicles with RAMSIS. *Human Factors and Ergonomics in Manufacturing & Service Industries,* 15 (2), 197–212.

[54] Hanson, L., Sperling, L., and Akselsson, R. (2006) Preferred car driving posture using 3-D information. *International Journal of Vehicle Design,* 42 (1-2), 154–169.

[55] Kyung, G. and Nussbaum, M.A. (2009) Specifying comfortable driving postures for ergonomic design and evaluation of the driver workspace using digital human models. *Ergonomics,* 52 (8), 939–953.

[56] Schmidt, S., Amereller, M., Franz, M., Kaiser, R., and Schwirtz, A. (2014) A literature review on optimum and preferred joint angles in automotive sitting posture. *Applied Ergonomics,* 45 (2, Part B), 247–260.

[57] Peng, J., Wang, X., and Denninger, L. (2017) Ranges of the least uncomfortable joint angles for assessing automotive driving posture. *Applied Ergonomics,* 61, 12–21.

[58] Keegan, J.J. (1964) The medical problem of lumbar spine flattening in automobile seats. *SAE Technical Paper Series,* 640788, 57–66.

[59] Kamp, I., Kilincsoy, Ü., and Vink, P. (2011) Chosen postures during specific sitting activities. *Ergonomics,* 54 (11), 1029–1042.

[60] Reed, M.P., Ebert, S.M., and Jones, M.L.H. (2019) Posture and belt fit in reclined passenger seats. *Traffic Injury Prevention,* 20 (S1), S38–S42.

[61] International Organization for Standardization (1997) *ISO 2631-1:1997: Mechanical vibration and shock. Evaluation of human exposure to whole-body vibration. Part 1: General requirements*. Geneva, Switzerland: International Organization for Standardization.

[62] British Standards Institution (1987) *BS 6841:1987: Guide to measurement and evaluation of human exposure to whole-body mechanical vibration and repeated shock*. London, United Kingdom: British Standards Institution.

[63] International Organization for Standardization (1998) *ISO 13090-1:1998: Mechanical vibration and shock. Guidance on safety aspects of tests and experiments with people. Part 1: Exposure to whole-body mechanical vibration and repeated shock*. Geneva, Switzerland: International Organization for Standardization.

[64] Rouder, J.N. and Haaf, J.M. (2018) Power, dominance, and constraint: A note on the appeal of different design traditions. *Advances in Methods and Practices in Psychological Science,* 1 (1), 19–26.

[65] International Organization for Standardization (2017) *ISO 8041-1:2017: Human response to vibration. Measuring instrumentation. Part 1: General purpose vibration meters*. Geneva, Switzerland: International Organization for Standardization.

[66] International Organization for Standardization (1997) *ISO 8727:1997: Mechanical vibration and shock. Human exposure. Biodynamic coordinate systems*. Geneva, Switzerland: International Organization for Standardization.

[67] International Organization for Standardization (2018) *ISO 2041:2018: Mechanical vibration, shock and condition monitoring. Vocabulary*. Geneva, Switzerland: International Organization for Standardization.

[68] International Organization for Standardization (2005) *ISO 18431-1:2005: Mechanical vibration and shock. Signal processing. Part 1: General introduction*. Geneva, Switzerland: International Organization for Standardization.

[69] Nickerson, R.S. (2000) Null hypothesis significance testing. A review of an old and continuing controversy. *Psychological methods,* 5 (2), 241–301.

[70] Kass, R.E. (2011) Statistical inference: The big picture. *Statistical Science,* 26 (1), 1–9.

[71] Woodson, M.I.C.E. (1969) Parameter estimation vs. hypothesis testing. *Philosophy of Science,* 36 (2), 203–204.

[72] Lehmann, E.L. (1993) The Fisher, Neyman–Pearson theories of testing hypotheses. One theory or two? *Journal of the American Statistical Association,* 88 (424), 1242–1249.

[73] Koch, G.G., Amara, I.A., Stokes, M.E., and Gillings, D.B. (1980) Some views on parametric and non-parametric analysis for repeated measurements and selected bibliography. *International Statistical Review,* 48 (3), 249–265.

[74] Gelman, A. (2005) Analysis of variance. Why it is more important than ever. *The Annals of Statistics,* 33 (1), 1–53.

[75] McCulloch, C.E. (2005) Repeated measures ANOVA, R.I.P.? *CHANCE,* 18 (3), 29–33.

[76] Wasserstein, R.L., Schirm, A.L., and Lazar, N.A. (2019) Moving to a world beyond "$p < 0.05$". *The American Statistician,* 73 (S1), 1–19.

[77] Lakens, D. (2013) Calculating and reporting effect sizes to facilitate cumulative science. A practical primer for *t*-tests and ANOVAs. *Frontiers in Psychology,* 4 (863), 1–12.

[78] International Organization for Standardization (2016) *ISO 10326-1:2016: Mechanical vibration. Laboratory method for evaluating vehicle seat vibration. Part 1: Basic requirements*. Geneva, Switzerland: International Organization for Standardization.

[79] R Core Team (2019) R: A language and environment for statistical computing. Vienna, Austria: R Foundation for Statistical Computing.

[80] Singmann, H., Bolker, B., Westfall, J., Aust, F., and Ben-Shachar, M.S. (2019) afex. Analysis of factorial experiments. R package, 0.25-1 ed.

[81] Cramer, A.O.J., Van Ravenzwaaij, D., Matzke, D., Steingroever, H., Wetzels, R., Grasman, R.P.P.P., Waldorp, L.J., and Wagenmakers, E.-J. (2016) Hidden multiplicity in exploratory multiway ANOVA: Prevalence and remedies. *Psychonomic Bulletin & Review,* 23 (2), 640–647.

[82] Belia, S., Fidler, F., Williams, J., and Cumming, G. (2005) Researchers misunderstand confidence intervals and standard error bars. *Psychological Methods,* 10 (4), 389–396.

[83] SAE International (2009) *SAE J1100:2009-11: Motor vehicle dimensions.* Warrendale, Pennsylvania, United States of America: SAE International.

The Prediction of the Vehicle Occupant Discomfort using Transfer Matrix Method

Jianchun Yao [1], Mohammad Fard [2]
School of Engineering, RMIT University
PO Box 71, Bundoora, 3083, VIC, Australia
Author.jianchun.yao@student.rmit.edu.au, Author.mohammad.fard@rmit.edu.au

Kazuhito Kato [3]
NHK SPRING CO., LTD.,
3-10 Fukuura Kanazawa-ku, Yokohama, 236-0004, Japan
Author.kazuhito.kato@nhkspg.co.jp

ABSTRACT

Predicting the vibration discomfort of a vehicle occupant is still challenging. This is due to the non-linear dynamics of the human body and the seat foam as well as the complex coupling between the vehicle floor and the seat. In this paper, a method is developed to predict the vibration transmission to occupant body by combining the transfer matrices of sub-systems including vehicle body, automotive seat, seat foam, and seated human body which are obtained from either physical test or Finite Element model. The structural dynamics of the vehicle body is modelled as a frequency response matrix from measurements at each seat mounting in different orientations. The dynamics of seated occupant body and seat foam are derived from physical tests as a transmissibility matrix. Moreover, the structural dynamics of the occupied automotive seat frame is presented as a transmissibility matrix. The developed prediction method is validated through the comparison of the predicted frequency response functions with the measured values. The results suggest the developed method provided an accurate prediction of the vibration transmitted to a vehicle occupant in a frequency below 100 Hz. This method can be used to assess the vibration discomfort of the vehicle occupants.

1   INTRODUCTION

The vibration discomfort of the seated occupant can be evaluated using the accelerations measured at the contacts between the seated occupant body and seat surface. The dynamic response of the seat and the ride discomfort of the occupant are affected by the non-linear dynamics of the human body (Mansfield and Griffin, 2000, Nawayseh and Griffin, 2003, Qiu and Griffin, 2011, Lo et al., 2013, Kim et al., 2017) and the interactions between the seat and vehicle floor (Griffin, 1996, Qiu and Griffin, 2003) . In the previous studies (Siefert et al., 2008, Grujicic et al., 2009, Zhou and Qiu, 2015, Zhang et al., 2015), several coupled occupant body-seat models have been developed to predict the vibration transmissibilities of the seat when coupled to the occupant body. However, the FE model of the occupant body are complex to develop and can be costly to run, calibrate, and optimise (Zhang et al., 2015).

The vibration performance of automotive seats is usually evaluated without consideration of the structural dynamics of the vehicle body. When the resonant frequencies of the seat are close to the resonance frequencies of the vehicle body, it is likely to provide a poor occupant ride comfort (Fard, 2011). In the design of an automotive seat for ride comfort, the structural dynamics of the seat and the vehicle body coupled system is required. However, when either the finite element models of

the vehicle body or the occupant body is not available, the prediction of the occupant vibration comfort may not be performed with enough accuracy.

In a study of the transmission of vibration between the vehicle body and seat, the seat base, vehicle floor section around the seat mounting points are often assumed to be a rigid body (Qiu and Griffin, 2005). The motions of a rigid seat base can be defined as a complex multi-axial motion which consists of three translational motions (fore-aft, lateral, and vertical) and three rotational motions (roll, pitch, and yaw). Several vehicle body-seat coupled models (Silveira et al., 2014, Zhou and Qiu, 2015) have been developed to predict and improve the vibration discomfort of the vehicle occupant, where the structural dynamics of the vehicle body and the seat frame are represented using spring and mass systems. However, early studies (Qiu and Griffin, 2005, Yao et al., 2017) suggested that the seat base does not always perform as a rigid body, especially at a high frequency. To accurately predict the seat vibration when coupled to the vehicle body, it is required to model the non-rigid motion of the seat base at the seat mounting points. There are a few studies about the combined vehicle-seat-occupant model in predicting vibration transmission to the occupant (Zhou and Qiu, 2015). Therefore, a method to accurately predict the vibration transmission from the vehicle body to the seated occupant is required.

This paper aims to develop a modelling approach to accurately predict the transmission of vehicle body vibration to the seated occupant by combining the vibration transfer matrices of sub-systems. The sub-systems can be sources from the physical tests or from the Finite Element models. The structural dynamics of the vehicle body is characterized and represented using the transfer matrix which is between the multi-axial vibration levels at seat mounting (S/MTG) points and the force input at the shock absorber (S/ABS) mounts. The structural dynamics of the seat is modelled as a transfer matrix between the vibrations at the different points of the seat frame and the S/MTG points. The dynamics of the seated occupant body plus the foam are characterized from a physical test and modelled as a transmissibility matrix between the vibration at the occupant-to-foam contact points and the different points of the seat frame acceleration inputs. To validate the developed modelling method, the predicted results are compared with analytical and experimental values.

2   METHOD

The vehicle body vibration caused by the road input is transmitted to the automotive seat via the seat mounting points. The vibration of the seat frame is then transmitted to the seated occupant body through the seat foam. The structural dynamics of the vehicle body is modelled as a single-input and multi-output (SIMO) system. The excitation input of the vehicle body system is the vertical forces applied at the shock absorber mounts, and the outputs of the vehicle body are at S/MTG points in six-axis translational and rotational orientations. The structural dynamics of the seat is represented using a multi-input and multi-output (MIMO) model between the different points on the seat frame and the S/MTG points. The dynamics of the occupant body plus the seat foam are derived from the physical test as a matrix of transmissibilities between the occupant-to-foam contact points and the several points on the seat frame. By combining the sub-systems, the vibration transmission from the vehicle body to the seated occupant is represented by the combination of several transfer matrices, as shown in Figure. 1.
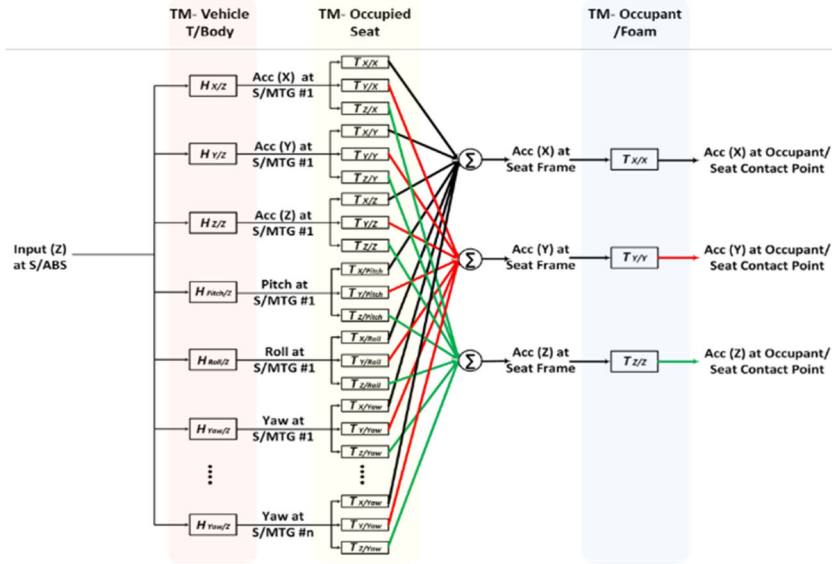
Figure 1: Schematic illustration of the model developed to represent the vibration transmission from the vertical force input applied at the shock absorber mounting points of the vehicle body to the acceleration outputs at the occupant-to-seat contact point, where n is the number of the seat mounting (S/MTG) points.

2.1 Prediction of Vehicle Seat Frame Vibration in Occupied Condition

At a seat mounting point, the interaction between two sub-systems (the vehicle body and the seat frame) is shown in Figure. 2, where $F_{S/ABS}$ is the force input applied at the S/ABS mounts, and $a_{S/Frame}$ is the acceleration responses obtained at a point of the seat frame.
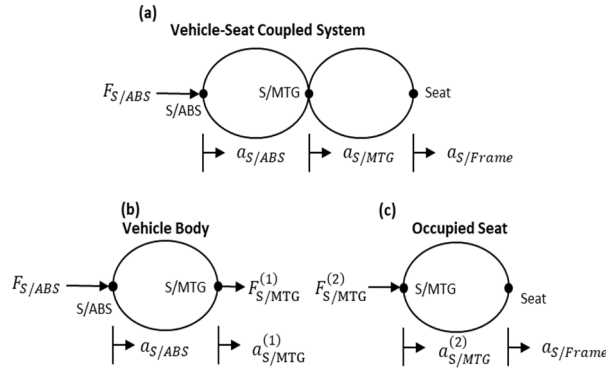
Figure 2: Schematic illustration of the sub-structure synthesis of the vehicle body and the seat frame system at a single seat mounting point: (a) vehicle body-seat coupled system, (b) vehicle body, and (c) seat

The vibration transfer function as a function of frequency was used to represents the structural dynamics of the vehicle body and the seat frame. The vibration transfer function of the vehicle body, $H_{Vehicle}$ which is between the acceleration of S/MTG points $a_{S/MTG}^{(1)}$ at the vehicle floor and the force input at the rear S/ABS mounting points of the vehicle body is defined as Eq. (1). The acceleration transmissibility of the seat T_{Seat} which is between the acceleration response at the point of the seat frame and the acceleration input $a_{S/MTG}^{(2)}$ at S/MTG points is described as Eq. (2).

$$H_{Vehicle} = \frac{a_{S/MTG}^{(1)}}{F_{S/ABS}} \tag{1}$$

$$T_{\text{Seat}} = \frac{a_{\text{S/Frame}}}{F_{S/MTG}^{(2)}} * \frac{F_{S/MTG}^{(2)}}{a_{S/MTG}^{(2)}} = \frac{a_{\text{S/Frame}}}{a_{S/MTG}^{(2)}} \qquad (2)$$

Considering the equilibrium of forces at the connecting point between two sub-systems, the force at S/MTG points, $F_{S/MTG}^{(1)}$ obtained on the vehicle floor and the reaction force $F_{S/MTG}^{(2)}$ obtained on the seat are equal in magnitude but opposite in direction. The seat mounting point acceleration $a_{S/MTG}^{(1)}$ on the floor is the same as the seat mounting point acceleration responses $a_{S/MTG}^{(2)}$ on the point of the seat frame, as the below equations show.

$$F_{S/MTG}^{(1)} = -F_{S/MTG}^{(2)} \qquad (3)$$

$$a_{S/MTG}^{(1)} = a_{S/MTG}^{(2)} \qquad (4)$$

The transfer function between the acceleration response at the point of the seat frame and the force input at S/ABS mounts is obtained mathematically as:

$$H_{Vehicle-Seat} = \frac{a_{\text{S/Frame}}}{F_{S/ABS}} = H_{Vehicle} * T_{Seat} \qquad (5)$$

Hence, the vibration transfer matrix of the vehicle body-seat coupled system which is between the acceleration at the point of the seat frame and the force input at S/ABS mounts of the vehicle body is computed by multiplication of the transfer matrix of the vehicle body and the transmissibility matrix of the seat frame, defined in Eq. (6):

$$[H_{Vehicle-Seat}] = [H_{Vehicle}] * [T_{Seat}] \qquad (6)$$

The transfer matrix of the vehicle body and the seat coupled system which defined as Eq. (7) is consist of the frequency response functions between the acceleration responses at a point on the seat frame and the vertical excitation input at the S/ABS mounts of the vehicle body.

$$[H_{Vehicle-Seat}] = \begin{bmatrix} H_{X_{Seat}/Z_{S/ABS}} \\ H_{Y_{Seat}/Z_{S/ABS}} \\ H_{Z_{Seat}/Z_{S/ABS}} \end{bmatrix}^{T} \qquad (7)$$

The vibration transfer matrices of the vehicle body, defined as Eq. (8) is consists of the Frequency Response Functions (FRF) which are between the translational and the rotational acceleration outputs at the seat mounting points and the vertical force input at the S/ABS mounts in a frequency range of 0-100 Hz. These frequency response functions of the vehicle body are obtained from the vehicle body FE model.

$$[H_{Vehicle}] = \begin{bmatrix} H_{X_{S/MTG\#1}/Z_{S/ABS}} \\ H_{Y_{S/MTG\#1}/Z_{S/ABS}} \\ H_{Z_{S/MTG\#1}/Z_{S/ABS}} \\ H_{RX_{S/MTG\#1}/Z_{S/ABS}} \\ H_{RY_{S/MTG\#1}/Z_{S/ABS}} \\ H_{RZ_{S/MTG\#1}/Z_{S/ABS}} \\ \vdots \\ H_{Z_{S/MTG\#n}/Z_{S/ABS}} \end{bmatrix}^{T} \qquad (8)$$

The transmissibility matrix of the seat frame is expressed as Eq. (9). The seat transfer matrix is made up of a group of acceleration transmissibility values. Each one is between the acceleration

responses at the point on the seat frame and the acceleration input at a single seat mounting point in a frequency range of 0 to 100 Hz. The transmissibilities of the seat frame are obtained from the seat frame FE model.

$$[T_{Seat}] = \begin{bmatrix} T_{X/X_{S/MTG\#1}} & T_{Y/X_{S/MTG\#1}} & T_{Z/X_{S/MTG\#1}} \\ T_{X/Y_{S/MTG\#1}} & T_{Y/Y_{S/MTG\#1}} & T_{Z/Y_{S/MTG\#1}} \\ T_{X/Z_{S/MTG\#1}} & T_{Y/Z_{S/MTG\#1}} & T_{Z/Z_{S/MTG\#1}} \\ T_{X/RX_{S/MTG\#1}} & T_{Y/RX_{S/MTG\#1}} & T_{Z/RX_{S/MTG\#1}} \\ T_{X/RY_{S/MTG\#1}} & T_{Y/RY_{S/MTG\#1}} & T_{Z/RY_{S/MTG\#1}} \\ T_{X/RZ_{S/MTG\#1}} & T_{Y/RZ_{S/MTG\#1}} & T_{Z/RZ_{S/MTG\#1}} \\ \vdots & \vdots & \vdots \\ T_{X/RZ_{S/MTG\#n}} & T_{Y/RZ_{S/MTG\#n}} & T_{Z/RZ_{S/MTG\#n}} \end{bmatrix} \tag{9}$$

2.2 Prediction of Vibration at Occupant-to-Seat Contact Point for Evaluation Discomfort

According to the ISO 2631-1 (1993), the vibration discomfort of the occupant is generally assessed and evaluated using the accelerations measured at the contacts between the seated occupant body and seat surface. The vibration transmitted to the occupant body through the seat cushion, the seatback and the occupant feet (Basri and Griffin, 2012, Kim et al., 2017). Here, the transmission of vibration to the occupant body are considered at four points on the seat cushion foam and four points on the seatback foam. The sub-structural synthesis of two sub-systems (the occupant-seat foam system and the seat frame) at a connecting point on the seat frame is schematically shown in Figure. 3, where $F_{S/MTG}$ is the force excitation inputs to the coupled system at the seat mounting points
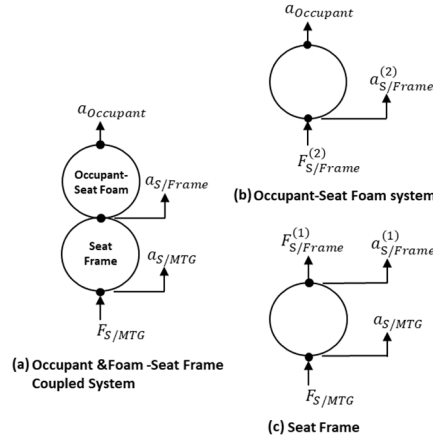
Figure 3: Schematic illustration of the sub-structure synthesis of the occupant body and seat foam system and the seat frame system: (a) the occupant-seat coupled system, (b) the occupant-seat foam system, and (c) the seat frame.

The acceleration transmissibility is used to represent the structural dynamics of the seat frame and the dynamics of occupant-seat foam system. The transmissibility of the seat frame T_{Seat} between the accelerations at different points of the seat frame and the input at a S/MTG point is defined in Eq. (10). The transmissibility of the occupant-foam system $T_{Occupant}$ which is between the accelerations at the occupant-to-foam contact point and the input at the seat frame is expressed as Eq. (11).

$$T_{Seat} = \frac{a^{(1)}_{S/Frame}}{a_{S/MTG}} \tag{10}$$

$$T_{Occupant} = \frac{a_{Occupant}}{F^{(2)}_{S/Frame}} * \frac{F^{(2)}_{S/Frame}}{a^{(2)}_{S/Frame}} = \frac{a_{Occupant}}{a^{(2)}_{S/Frame}} \tag{11}$$

, where $a_{S/MTG}$ and $a^{(1)}_{S/Frame}$ are the acceleration measured at the front left seat mounting point and at the acceleration measured at seat foam-frame connecting points on the seat frame, respectively. $a_{Occupant}$ is the acceleration response measured at the occupant-to-foam contact point; $F^{(1)}_{S/Frame}$ and $F^{(2)}_{S/Frame}$ is the action force and the reaction force which are acting at the seat foam-frame connecting point. Due to a force equilibrium condition, the action force and the reaction force at the foam-frame connection points are equal in magnitude but opposite in direction. Considered the geometric compatibility, the accelerations measured at the foam-frame connecting point $a^{(1)}_{S/Frame}$ and $a^{(2)}_{S/Frame}$ are same in magnitude and direction.

$$F^{(1)}_{S/Frame} = -F^{(2)}_{S/Frame} \tag{12}$$

$$a^{(1)}_{S/Frame} = a^{(2)}_{S/Frame} \tag{13}$$

Therefore, the transmissibility of the whole system between the response at the occupant-to-foam contact point and the input at the S/MTG point is given as:

$$T_{Seat-Occupant} = \frac{a_{Occupant}}{a_{S/MTG}} = T_{Seat} * T_{Occupant} \tag{14}$$

Finally, the vibration transfer matrix of the seat-occupant body coupled system is computed by multiplication of the transmissibility matrix of the seat frame and the transmissibility matrix of occupant- seat foam system, defined in Eq. (15).

$$[T_{Seat-Occupant}] = [T_{Seat}] * [T_{Occupant-Foam}] \tag{15}$$

, where the transmissibility matrix of the seat-occupant body coupled system, defined in Eq. 16 is consist of three acceleration transmissibilities between the seat-to-occupant contact point and the S/MTG point. The transmissibility matrix of the seat frame and the transmissibilities matrix of the occupant-foam system are given in Eq. (17) and Eq. (18), respectively.

$$[T_{Seat-Occupant}] = \begin{bmatrix} T_{X_{Occupant\#I}/X_{S/MTG}} \\ T_{Y_{Occupant\#I}/Y_{S/MTG}} \\ T_{Z_{Occupant\#I}/Z_{S/MTG}} \end{bmatrix}^T \tag{16}$$

$$[T_{Seat}] = \begin{bmatrix} T_{X_{Seat\#P1}/X_{S/MTG}} \\ T_{Y_{Seat\#P1}/Y_{S/MTG}} \\ T_{Z_{Seat\#P1}/Z_{S/MTG}} \end{bmatrix}^T \tag{17}$$

$$[H_{Occupant-Foam}] = \begin{bmatrix} T_{X_{Occupant\#I}/X_{Seat\#P1}} & 0 & 0 \\ 0 & T_{Y_{Occupant\#I}/Y_{Seat\#P1}} & 0 \\ 0 & 0 & T_{Z_{Occupant\#I}/Z_{Seat\#P1}} \end{bmatrix} \tag{18}$$

The transmissibility matrix of the seat frame is between the acceleration at a seat-foam connecting point and input at the S/MTG point. The transmissibility matrix of occupant-seat foam system is between the multi-axial accelerations at an occupant-to-foam contact point and the inputs at the nearby seat-foam connect point, as shown in Figure. 4.

2.3   Characterisation of Dynamics of Occupant-Seat Foam System

The dynamics of the occupant body plus the seat foam system are derived from the seat dynamics test and modelled as an acceleration transmissibility matrix between the different points of the seat frame and the occupant-to-foam contact points. The experiment was conducted on a multi-axis shaker platform. The uncorrelated Gaussian random vibration with flat constant-bandwidth acceleration spectrum of 1.5 m/s^2 r.m.s. in three translational directions over a frequency range of 0.5-100 Hz was applied to the seat. During the experiment, the accelerations at the front left S/MTG point was recorded by a tri-axial accelerometer (PCB 356A03). Following Ittianuwat et al. (2017) configuration of seat surface measurement location, the tri-axial accelerometers (PCB 356A03) are attached to the eight measurement points located on seat frame and eight occupant-to-foam contact points located on the seat surface to record the accelerations at the measurement point on the seat frame and the occupant-to-foam contact points, shown in Figure. 4.
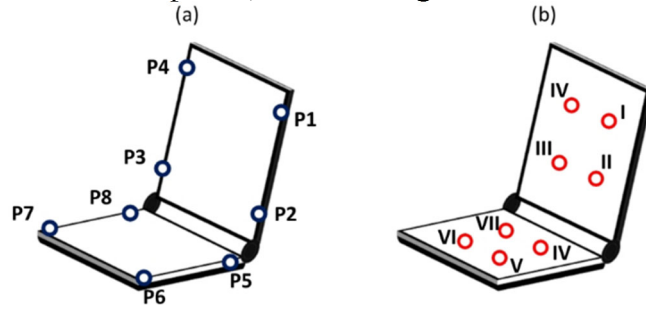
Figure 4: Measurement locations on: (a) the seat frame, (b) occupant-to-foam contact points on the seat surface. To obtain the accelerations at the contact points between the seated occupant body and the seat surface, eight tri-axial accelerometers were attached to the seat surface following Ittianuwat et al. (2017) configuration of seat surface measurement location.

The acceleration transmissibilities between a measurement point on the seat frame and the nearby occupant-to-foam contact points are calculated using the cross-spectral density function method. The transmissibility of the occupant body and the seat foam system is defined as a complex ratio between the cross-spectrum density of input and output acceleration $G_{io}(f)$, and the power spectrum density of input acceleration $G_{ii}(f)$. The coherencies between the input and the output accelerations $\gamma_{io}^2(f)$ is calculated using Eq. (20).

$$T(f) = \frac{G_{io}(f)}{G_{ii}(f)} \tag{19}$$

$$\gamma_{io}^2(f) = \frac{\left| G_{io}(f) \right|^2}{G_{ii}(f) G_{oo}(f)} \tag{20}$$

, where $G_{oo}(f)$ is the power spectrum density of the output acceleration.

3   RESULTS AND DISCUSSION

The developed model is validated by comparing the frequency response functions of the vehicle body-seat coupled system that derived from the model and the vehicle body FE model and the acceleration transmissibility between the occupant-to-foam contact points and the front left S/MTG point that obtained from the model and the seat dynamics test.

3.1   Vehicle Seat Frame Vibration in Occupied Condition

The magnitude and the phase of the predicted frequency response functions of the vehicle seat that obtain from the developed model are compared with the values obtained from the vehicle body FE model, shown in Figure. 5 and Figure. 6. The excitation input of the frequency response functions is a pair of vertical force input applied at the rear shock absorber mounting points of the vehicle. The output of the FRF shown in Figure. 5 is considered at a measurement point (measurement point P1 shown in Figure. 4) on the top of the seatback frame. The output of the FRF shown in Figure. 6 is obtained from a point (measurement point P7 shown in Figure. 4) located at the seat cushion frame. In the comparison of magnitude and phase of the FRFs, the predicted results show a close agreement with the values obtained from the vehicle body FE model in a frequency range of 0 to 100 Hz. The results show that the developed prediction approach provided a good estimation of the seat frame vibration when coupled to the vehicle body.
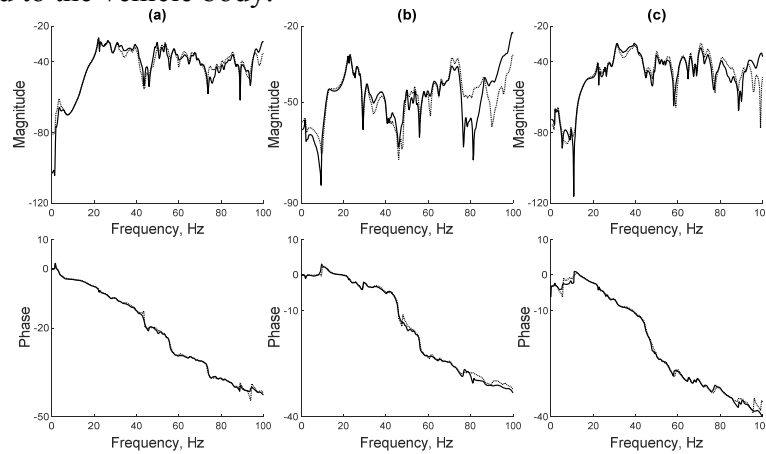
Figure 5: Frequency Response Functions in (a) fore-and-aft cross-axis frequency response functions from S/ABS mounts of vehicle body to the point, P1 at the top of seatback frame; (b) lateral cross-axis frequency response function from S/ABS mounts of vehicle body to the point, P1 at seatback frame; (c) vertical in-line frequency response function from S/ABS mounts of vehicle body to the point, P1 at seatback frame (—, values obtained from vehicle trimmed body FE model; ······, predicted value that obtained from the developed model).
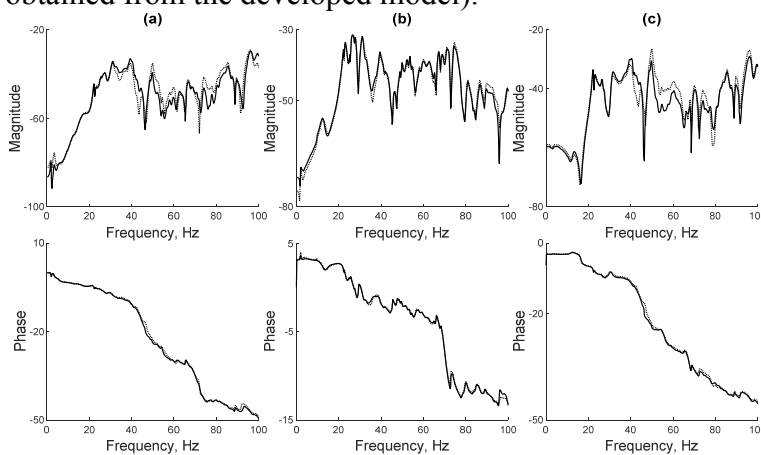
Figure 6: Frequency Response Functions in (a) fore-and-aft cross-axis frequency response function from S/ABS mounts of vehicle body to the point at the point, P7 at seat cushion frame; (b) lateral cross-axis frequency response function from S/ABS mounts of vehicle body to the point, P7 at seat cushion frame; (c) vertical in-line frequency response function from S/ABS mounts of vehicle body to the point, P7 at seat cushion frame (—, values obtained from vehicle trimmed body FE model; ······, predicted value that obtained from the developed model).

3.2   Vibration at Occupied-to-Seat Contact Points

The magnitude and the phase of the predicted transmissibilities between the accelerations at the occupant-to-foam contact points and the acceleration inputs at the front left S/MTG point are compared to the measured value from the seat dynamics test, shown in Fig 7 and 8. The inputs of the transmissibilities are the translational accelerations at the front left seat mounting point. The output of the transmissibilities shown in Figure. 7 is considered at four contact points between the seatback surface and the occupant body. The output of the transmissibilities shown in Figure. 8 is obtained from four contact point between the seat cushion surface and the occupant body. The configuration of measurement points located at the seat surface is presented in the Figure. 4. In the comparison of the magnitude and phase of the transmissibilities at the occupant-to-foam contact points on the seatback surface shown in Figure. 7, the predicted transmissibilities are reasonable correlated to the measured values in a frequency below 100 Hz, although some difference can be seen at the fore-and-aft in-line transmissibilities and the lateral in-line transmissibilities in a frequency range of 50-100 Hz. In Figure. 8, the predicted in-line transmissibilities between the accelerations at the occupant-to-cushion foam contact points show a close agreement with the measured values in a frequency range of 0- 100 Hz. The results show that the developed modelling approach provided a reasonable estimation of the vehicle vibration transmission to the seated occupant.
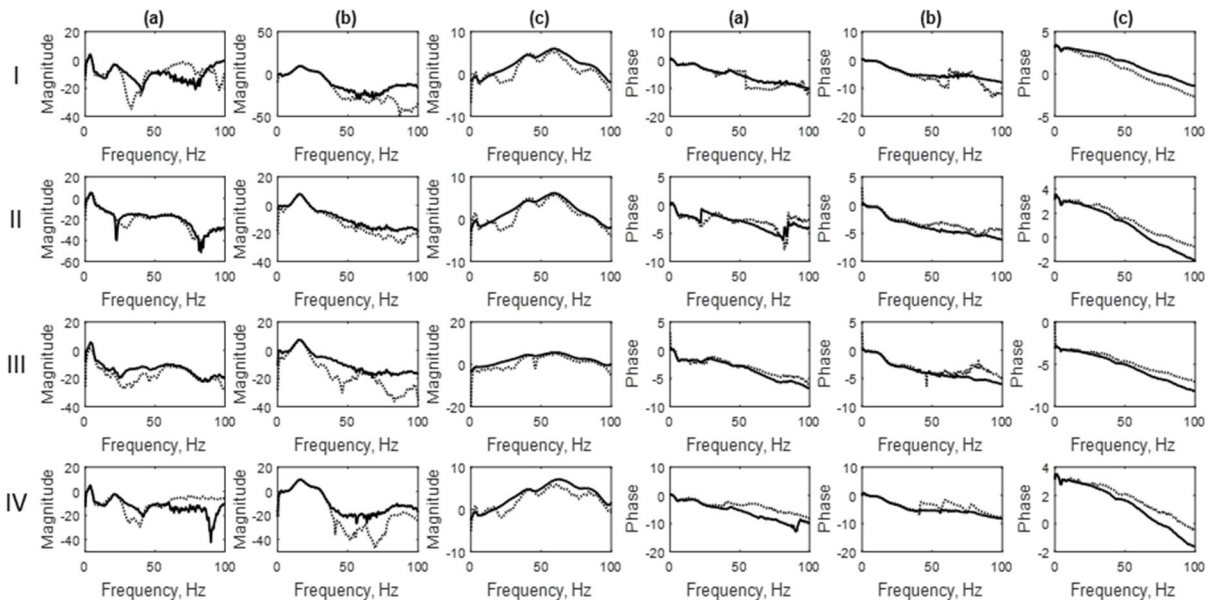
Figure 7: Transmissibilities in: (a) fore-and-aft in-line transmissibilities from the S/MTG point to the occupant-to-seatback foam contact point; (b) lateral in-line transmissibilities from the S/MTG point to the occupant-to-seatback foam contact point; (c) vertical in-line transmissibilities from the S/MTG point to the occupant-to-seatback foam contact (—, values obtained from seat dynamics test; ······, predicted values obtained from the developed model). The configuration of the measurement location is shown in Figure. 4.
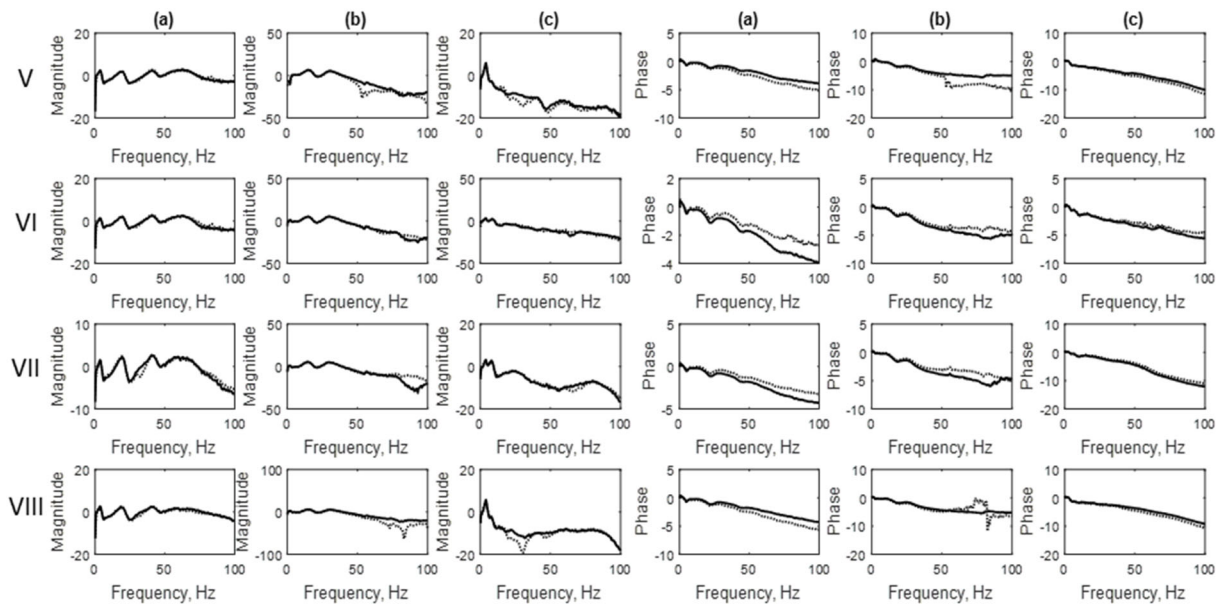
Figure 8: Transmissibilities in: (a) fore-and-aft in-line transmissibilities from the S/MTG point to the occupant-to-cushion foam contact point; (b) lateral in-line transmissibilities from the S/MTG point to the occupant-to-cushion foam contact point; (c) vertical in-line transmissibilities from the S/MTG point to the occupant-to-cushion foam contact point (—, values obtained from seat dynamics test; ······, predicted values obtained from the developed model). The configuration of the measurement location is shown in Figure. 4.

4   CONCLUSION

In this paper, a modelling approach has been developed to accurately predict the transmission of the vehicle body vibration to the occupant. The model is developed based on transfer matrix method which consists of the vehicle body, the seat, and the occupant body sub-systems. Each transfer matrix sub-system can be obtained from the experimental or analytical (FE model) models. Here, the structural dynamics of the vehicle body and the seat frame are obtained from finite element models, and the dynamics of the seated occupant body plus the seat foam are characterized from physical tests. The predicted frequency response functions on the seat frame are compared with the values obtained from the validated vehicle body FE model. The vibration transmissibilities between the occupant-to-foam contact points at the seat surface are compared with the corresponding physical data. The results show that the developed method provides a good estimation of the vibration transmission from the vehicle body to the occupant. This study can be used to predict the transmission of the vibration to the occupant body in the multi-axial orientations and hence can be extended to estimate the occupant vibration discomfort level.

REFERENCES

Basri, B. and Griffin, M. J. (2012) Equivalent comfort contours for vertical seat vibration: effect of vibration magnitude and backrest inclination, Ergonomics, 55(8), 909-922.

Fard, M. (2011) Structural dynamics characterization of the vehicle seat for NVH performance analysis, SAE paper, 501, 2011.

Griffin, M. J. (1996) Handbook of human vibration, London: Academic press.

Grujicic, M., Pandurangan, B., Arakere, G., Bell, W. C., He, T. and Xie, X. (2009) Seat-cushion and soft-tissue material modeling and a finite element investigation of the seating comfort for passenger-vehicle occupants, Materials & Design, 30(10), 4273-4285.

International Organisation for Standardisation (1993) Mechanical Vibration and Shock - Evaluation of Human Exposure to Whole-body Vibration – Part 1: General Requirements, ISO 2631–1

Ittianuwat, R., Fard, M. and Kato, K. (2017) Evaluation of seatback vibration based on ISO 2631-1 (1997) standard method: The influence of vehicle seat structural resonance, Ergonomics, 60(1), 82-92.

Kim, E., Fard, M. and Kato, K. (2017) Characterisation of the human-seat coupling in response to vibration, Ergonomics, 60(8), 1085-1100.

Lo, L., Fard, M., Subic, A. and Jazar, R. (2013) Structural dynamic characterization of a vehicle seat coupled with human occupant, Journal of Sound and Vibration, 332(4), 1141-1152.

Mansfield, N. J. and Griffin, M. J. (2000) Non-linearities in apparent mass and transmissibility during exposure to whole-body vertical vibration, Journal of Biomechanics, 33(8), 933-941.

Nawayseh, N. and Griffin, M. (2003) Non-linear dual-axis biodynamic response to vertical whole-body vibration, Journal of Sound and Vibration, 268(3), 503-523.

Qiu, Y. and Griffin, M. (2011) Biodynamic Response of the Seated Human Body to Single-axis and Dual-axis Vibration: Effect of Backrest and Non-linearity.

Qiu, Y. and Griffin, M. J. (2003) Transmission of fore–aft vibration to a car seat using field tests and laboratory simulation, Journal of Sound and Vibration, 264(1), 135-155.

Qiu, Y. and Griffin, M. J. (2005) Transmission of roll, pitch and yaw vibration to the backrest of a seat supported on a non-rigid car floor, Journal of Sound and Vibration, 288(4), 1197-1222.

Siefert, A., Pankoke, S. and Wölfel, H.-P. (2008) Virtual optimisation of car passenger seats: Simulation of static and dynamic effects on drivers' seating comfort, International Journal of Industrial Ergonomics, 38(5), 410-424.

Silveira, M., Pontes Jr, B. R. and Balthazar, J. M. (2014) Use of nonlinear asymmetrical shock absorber to improve comfort on passenger vehicles, Journal of Sound and Vibration, 333(7), 2114-2129.

Yao, J., Fard, M. and Kato, K. (2017) Analysis of Transmission of Vehicle Floor Vibration into the Seat, in Sakakibara, H., ed. 25th Japan Conference on Human Response to Vibration, Nagoya, Japan, 13 Sept 2017, Japan: Nagoya University 65-75.

Zhang, X., Qiu, Y. and Griffin, M. J. (2015) Developing a simplified finite element model of a car seat with occupant for predicting vibration transmissibility in the vertical direction, Ergonomics, 58(7), 1220-1231.

Zhou, H. and Qiu, Y. (2015) A simple mathematical model of a vehicle with seat and occupant for studying the effect of vehicle dynamic parameters on ride comfort, 50th United Kingdom Conference on Human Responses to Vibration, Southampton, England, 9 - 10 September.

Reduction of occupants' low-frequency motion
to improve automotive seat comfort

Kazuhito KATO, Kousuke SUZUKI, Chikanori HONDA and Masashi OHYAMA
NHK Spring Co., LTD.
3-10 Fukuura, Kanazawa-ku, 236-0004 Yokohama, Japan
kazuhito.kato@nhkspg.co.jp, kou.suzuki@nhkspg.co.jp

ABSTRACT

In this study, we focused on two ride comfort phenomena relating to low-frequency motion. One is human body instability, which means the leaning of the pelvis and torso during cornering. The other is lateral human body shaking, which means the phenomenon of the occupant body shaken by the low-frequency roll vibrations of the vehicle body, and lateral and roll motion in antiphase are generated to head and thorax, and there is a trade-off between them.

For the reduction of lateral human body shaking, we optimised backrest bolster height and separation to minimise the transmission of excitation force from the seat to occupant upper body. For reducing driver body instability, we optimised cushion bolster shape/rigidity to enable thigh to exert greater muscular force as drivers maintain their postures by active muscular responses during cornering. For passengers, we increased cushion pad rigidity/damping capable of moderating the roll motion of pelvis passively and providing greater support to thorax for the reduction of passenger body instability.

The results of the laboratory and field studies showed that the prototype seat we developed achieved a significant reduction of the two phenomena simultaneously for both drivers and passengers

1   INTRODUCTION

Human body instability and lateral human body shaking are the two major ride comfort phenomena manifested by motor vehicle occupants during driving (Figure 1), and correspond to the primary and secondary lateral vibration modes for occupant bodies (Kanke *et al.*, 2007). "Human body instability" means the leaning of the pelvis and torso to one side during vehicle cornering or lane changing operation, which often causes physical fatigue to the occupants due to necessary muscular effort to keep their postures upright and also mental fatigue of having to maneuver a difficult driving situation safely. To moderate human body instability, vehicles are fitted with cushion bolsters and backrest bolsters on the front seats (Yamada *et al.*, 2016). On the other hand "lateral human body shaking" means the phenomenon of the occupant body shaken by the roll vibrations of the vehicle body responding to road surface roughness, and is accompanied by a feeling of ride discomfort due mainly to the lateral swaying of the head and the pressing of thorax against the backrest and may also be accompanied by mental fatigue of having to pass the oncoming vehicles safely on rough-surface roads. As an approach to the reduction of lateral human body shakes being the shielding of occupants against excitation force from the seats, it is regarded important not to excessively restrain the occupants in the seats (Kawano *et al.*, 2017). So human body instability and lateral human body shaking are ride comfort phenomena having a trade-off relationship.

Employed as test vehicles in the present study were SUVs which are known to generate greater lateral human body shakes. Using these vehicles, occupant body behavior mechanisms were

examined in relation to human body instability and lateral human body shaking so as to optimize occupant support by the seat and resolve the trade-off problem of the two ride comfort phenomena.
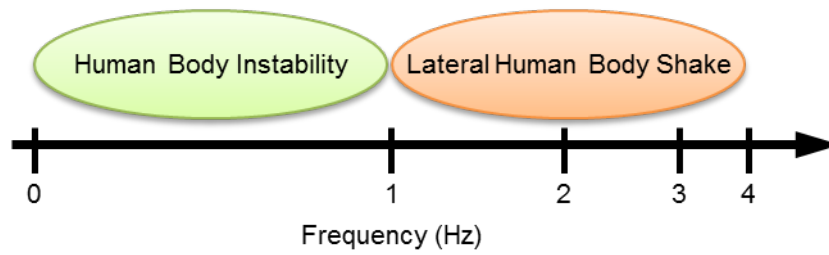
Figure 1: Ride comfort phenomena in low-frequency

2 LOW-FREQUENCY BEHAVIORAL MECHANISMS OF OCCUPANTS

2.1 Human body instability mechanism

Earlier studies have indicated difference in human body instability behavior between driver and passenger (Koike *et al.*, 2013) as illustrated in Figure 2. The driver exhibits active posture control whereby, while pelvis rolls outward, upper body is bent inward by mobilizing flank and thigh muscles (Kato *et al.*, 2014). This is considered to be a series of posture-correcting behaviors for realigning the center of upper thorax with the center of steering wheel in order to continue an accurate steering. In contrast to the driver, the passenger normally exhibits passive posture control whereby, as pelvis rolls outward, upper body also rolls outward while leaning on the backrest, and the head is let projected farther outward. Only when the human body instability is excessively severe or when the support from the seat is insufficient does the passenger tries to hold up posture by reflective muscular responses.
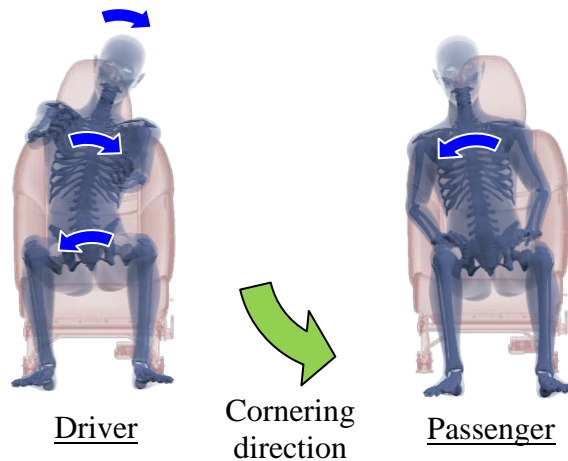
Figure 2: Difference in human body instability behavior between driver and passenger

2.2 Lateral Human body shake mechanism

Unlike human body instability, lateral human body shaking involves body motion too quick for the occupant to control his/her posture (Griffin, 1990) so that both driver and passenger exhibit practically the same lateral body shaking behaviors (Figure 3). In continuous lateral body shaking, accelerations in antiphase are generated to head and thorax.

First step   Second step
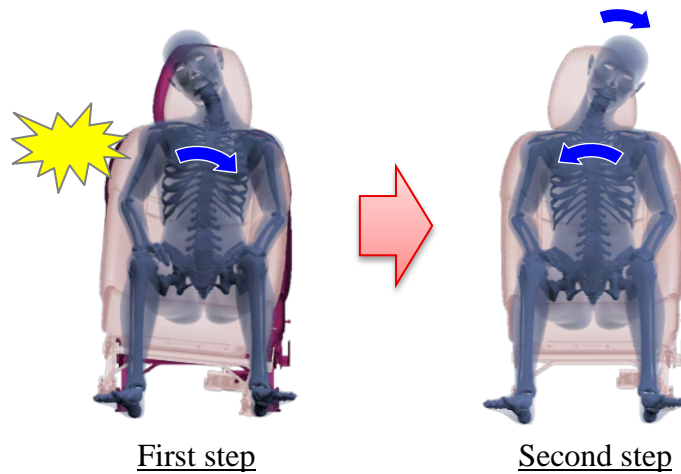
Figure 3: Passenger's behavior in lateral human body shaking

3 MEASURES TO REDUCE HUMAN BODY INSTABILITY AND LATERAL HUMAN BODY SHAKING

3.1 Measures to reduce lateral human body shaking (common to driver and passenger)

For lateral human body shaking whereby both driver and passenger exhibit the same behaviors, it is considered necessary to minimize the transmission of excitation force from the seat to occupant upper body. Assuming that backrest bolster position affects the transmission of excitation force, relations between backrest bolster height/width and excitation force transmission were examined in the present study. Figure 4 shows the effects of the backrest bolster height/width on lateral human body shaking. It was found that higher backrest bolster position increased the transmission of excitation force to the upper thorax, resulting in a greater swaying of the head; lower backrest bolster position resulted in a lateral bending of the thorax and concomitant instabilities in upper-body behavior. As for separation between the pair of backrest bolsters, wider separation caused time lags between thorax shaking and seat shaking, resulting in a hitting of thorax with the backrest bolsters. Narrower separation indicated a direct shaking of the upper body by the seat and a greater swaying of head as the thorax was braced more rigidly by the two side bolsters. It was confirmed that a proper height and separation of backrest bolsters reduced the transmission of excitation force from the seat and moderated head swaying, thus suggesting that optimizing backrest bolster height and separation is an effective way of reducing lateral human body shaking.
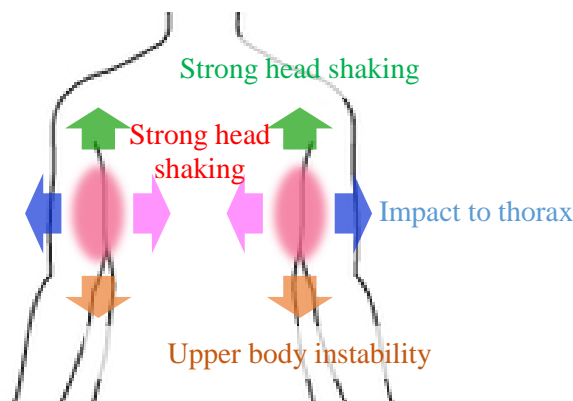
Figure 4: Relation between location of thorax support and lateral human body shaking

3.2 Measures to reduce driver body instability

Since during cornering the driver controls posture by bending torso sideways with the help of flank and thigh muscles (Figure 5), it is considered necessary to hold the upper body upright with the minimum muscular load. In this regard the thigh muscles having a greater force generation capacity can perform body control with a minimum feeling of muscular effort; therefore, it is more advantageous to utilize thigh muscles for the control of driver posture during cornering. So more effective thigh support was explored to enable a greater contribution of the thighs to driver body control during cornering. As shown in Figure 6, it was found that the front part of the thigh--region farther away from the hip joint--was easily pushed back by the cushion bolster while the rear part of the thigh failed to apply sufficient muscular force to the cushion bolster due to the small amount of its displacement. At certain midway points, however, it proved easier for the thigh to keep pressing the cushion bolster and to contribute its muscular force for reducing body instability. Thus, it was confirmed that driver posture can be held as upright as possible during cornering by optimizing cushion bolster shape/rigidity so as to enable thigh to exert greater muscular force.
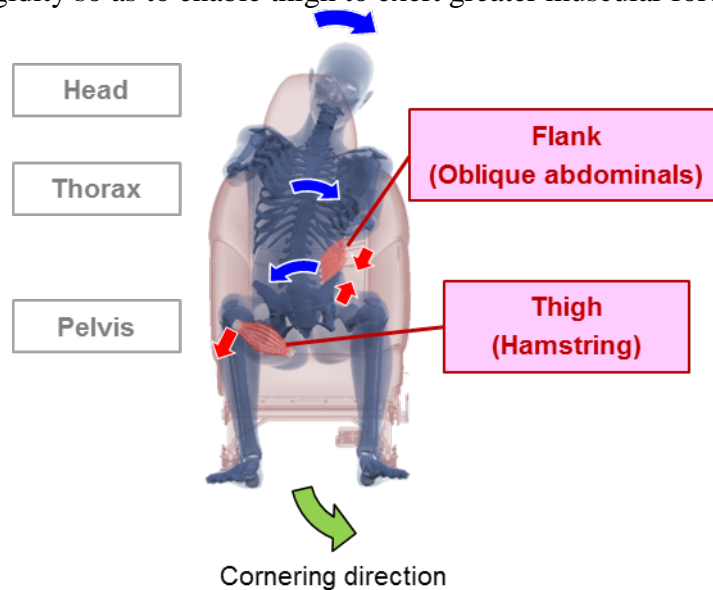
Figure 5: Driver body instability dynamics during cornering
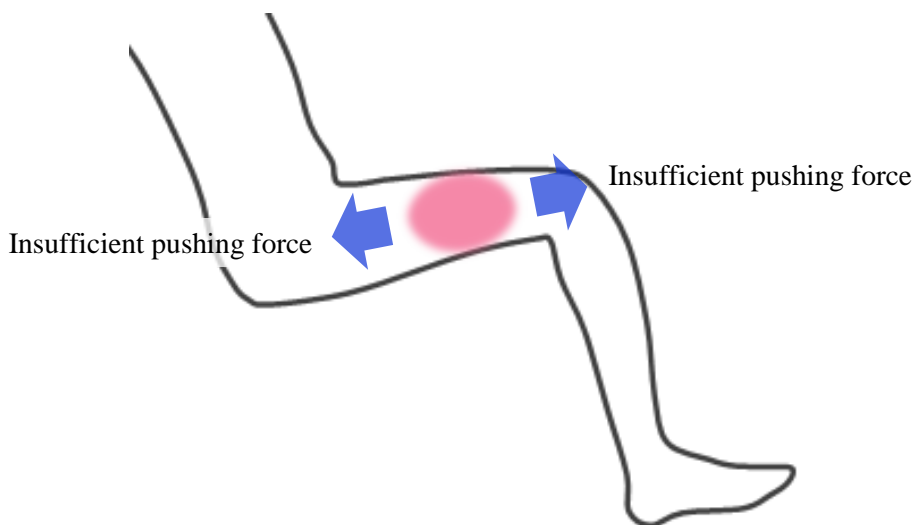
Figure 6: Relation between location of thigh support and subjective pushing force

3.3 Measures to reduce the passenger's body instability

For passengers it is not necessary that posture is corrected by reflectional muscular responses, which suggests a need for cushion bolsters capable of moderating the roll motion of pelvis and providing greater support to thorax for the reduction of passenger body instability. Optimizing the cushion bolster shape and cushion pad rigidity/attenuation was considered to moderate the rolling of pelvis. While thorax support against the passenger's body instability should be provided at the upper part of the backrest bolster, it would be necessary that this support be compatible with the aforementioned support for the reduction of lateral human body shaking. Consequently it was decided that the passenger seat be optimized in such a way that excitation force from the seat would be dampened to reduce body shaking of a large acceleration and a small amplitude and that thorax motion would be restrained at the backrest bolster upper part for body shaking of a small acceleration and a large amplitude.

4 EXPERIMENTAL METHOD

In the present study, both laboratory and field tests were conducted to evaluate human body instability and lateral human body shaking in quantitative terms. Used in the laboratory tests were the pairs of front seats taken from a Japanese-brand small SUV for sale ("Car A"), from a European-brand small SUV with a rated top-class ride comfort ("Car B"), and a pair of developmental seats incorporating the aforementioned improvement measures ("Prototype"). The Car A and Prototype seats were employed in the field tests. The subjects in driver seats were instructed to keep natural or normal posture for steering. The subjects in passenger seats were instructed to be seated and lean fully on the seatback but with some separation between head and headrest. Two male adults of standard body size were employed as subjects and both of them gave their informed consent to participate in the experiment.

4.1 Laboratory tests on human body instability

For the quantitative evaluation of human body instability in a laboratory environment, an experimental apparatus was devised to quasi-statically simulate lateral accelerations in cornering based on the component forces of gravitational accelerations of a seat inclined in the direction of rolling. Each subject was instructed to sit on the experimental seat and wear range-limiting glass to observe closely only a display monitor attached to a jig but not things around the monitor. Shown in the monitor were stationary photo images of a bending road taken from a driver's sitting position. The subject, instructed to simulate actual cornering behavior, performed steering in keeping with the photo images as the seat was inclined. A seat inclination angle of 23.5 degrees to right and left was applied, assuming a component force of 0.4G to the seat and a cornering vehicle speed of 40 km/h. The subjects' behaviors were recorded by a motion capture system. From the results of preliminary tests, the body behaviors of the subjects were evaluated in terms of pelvis roll angle and upper-thorax displacement which were the two parameters indicating a notable correlation with the subjects' sensory evaluations of their body instabilities. These measured values were evaluated in relation to seat inclination. Upper-thorax displacement values nearing zero were considered to indicate that the subject held up his thorax as close as possible to the center of the steering wheel.

4.2 Field tests on human body instability

In the field tests, human body instability was quantitatively evaluated from the measurements of occupants' behaviors and sEMG (surface electromyogram) responses during cornering on an in-plant road, using Car A fitted with Prototype driver and passenger seats. In driver seat the subject actually drove the test vehicle, while merely seated in the passenger seat. As in the laboratory tests,

the subjects' behaviors were recorded by a motion capture system, and their pelvis roll angles and upper-thorax displacements were evaluated quantitatively. Normalized integrated sEMG measurement was also carried out to evaluate the activation of flank (abdominal oblique on inward side) and of thigh (hamstring on outward side) as shown in Figure 7.
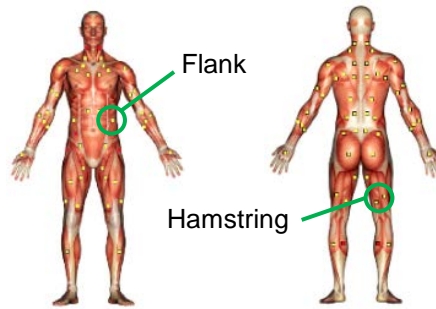
Figure 7: Body locations of sEMGs measurement

4.3 Laboratory tests on lateral human body shaking

A test seat and a footrest jig were fixed on the 1.8m x 1.8m oscillation table of an electric vibration machine with six degrees of freedom (Figure 8). Each subject was seated on the test seat and exposed to artificial vibrations simulating the actual seat vibrations on an uneven road. His body behaviors were recorded by a motion capture system. Since lateral body shaking behaviors had proved identical between driver and passenger, only passenger tests were conducted. As the preliminary tests had found a good correlation between head sway discomfort and head acceleration and between thorax discomfort and upper-thorax acceleration, effective values of head and upper-thorax accelerations were measured.

Figure 8: Laboratory apparatus for lateral human body shaking evaluation

5 EXPERIMENTAL RESULTS

5.1 Results of quantitative evaluation of human body instability

Figure 9 compares the measured values of pelvis roll angle and upper-thorax displacement for the 3 types of seats. Since the measurements obtained from the 2 subjects proved highly similar, data from only one subject were used hereafter in this paper. For pelvis roll angle in both driver and passenger seats, Car B and Prototype proved equally excellent and both clearly better than Car A. For

upper-thorax displacement in driver seats, Prototype recorded a 31% reduction against Car A and a 12% reduction against Car B. Similarly in passenger seats, Prototype showed a 22% cut against Car A and a sharp 33% cut against Car B.
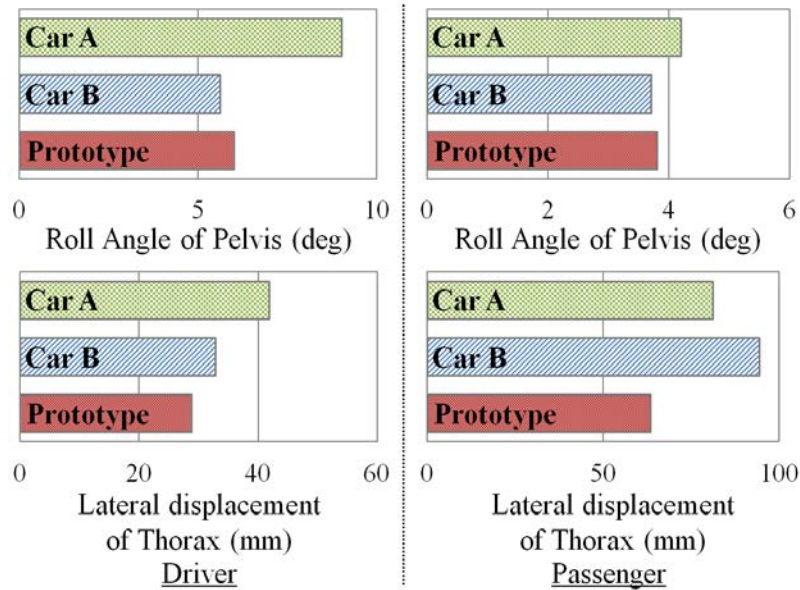
Figure 9: Laboratory test results of human body instability behavior

Figure 10(a) compares the field test results of Car A and Prototype with respect to pelvis roll angle and upper-thorax displacement. For pelvis roll angle, Prototype recorded a 29% reduction against Car A in driver seats and a 21% reduction in passenger seats. For upper-thorax displacement, Prototype failed to show a notable cut against Car A in driver seats; however, Prototype achieved a 21% cut against Car A in passenger seats. Thus the results of both laboratory and field tests indicated greater reductions of pelvis roll angle and upper-thorax displacement by the Prototype seats than by the seats installed in the commercially available vehicles.

Figure 10(b) compares sEMG measurements in driver seats between Car A and Prototype. Prototype indicated a notable 30% reduction in flank muscle effort but a 14% increase in thigh muscle (hamstring) effort against Car A. This is in accord with the general observation that driver posture during cornering is maintained primarily by thigh muscles characterized by a large force generation capacity.

The test results on occupant behaviors and sEMG responses suggest that driver posture during cornering can be best maintained if the seat cushion bolsters are optimized to facilitate thigh muscular effort, which will reduce upper-thorax displacement while also reducing flank muscular load. As for the support of passenger posture, it was confirmed that the improvement of cushion pad rigidity and attenuation proved effective in reducing pelvis roll angle for both drivers and passengers. Furthermore, it is also confirmed that Prototype's optimization of backrest bolster upper part is effective in moderating human body instability as well as lateral human body shaking.
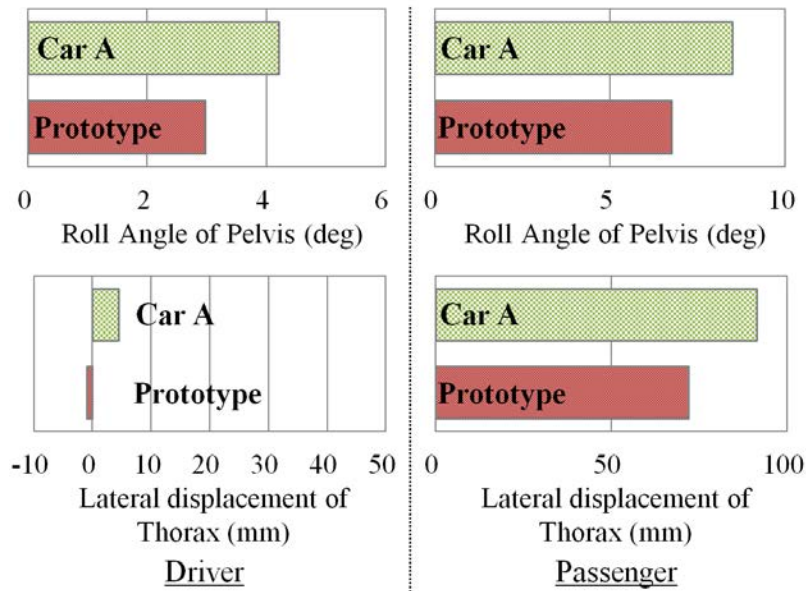
(a) Occupant motion during cornering
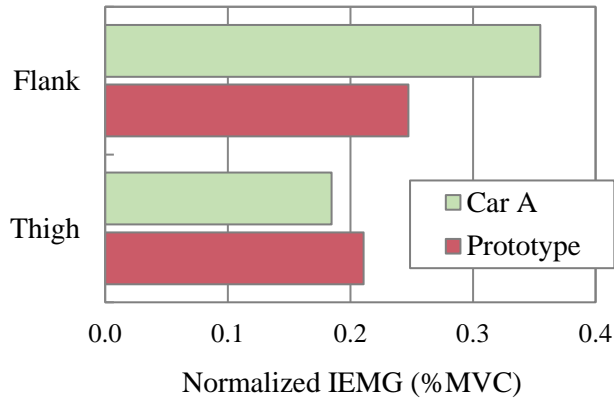
(b) sEMGs measurements of muscle force in driver seats

Figure 10: Field test results of human body instability behavior

5.2 Results of quantitative evaluation of lateral human body shaking

Figure 11 compares the measured values of human body acceleration for the 3 types of seats. For head acceleration in both driver and passenger seats, Car B and Prototype were equally excellent and clearly better than Car A. For thorax acceleration, Prototype recorded the smallest value--22% less than Car A and 14% less than Car B. Since Prototype indicated smaller head and thorax accelerations, which had proved significantly correlative with the subjects' sensory evaluations of their body conditions, Prototype was considered capable of reducing discomfort of head and thorax caused by lateral human body shaking, as its optimized backrest bolsters effectively dampened the transmission of excitation force from the seat.

Quantitative evaluation results indicated that the Prototype exceeded commercially available vehicles in reducing both human body instability and lateral human body shaking. Thus Prototype proved to be a seat capable of dissolving the trade-off relationship between human body instability and lateral human body shaking and also capable of moderating both phenomena simultaneously at high ride comfort levels.
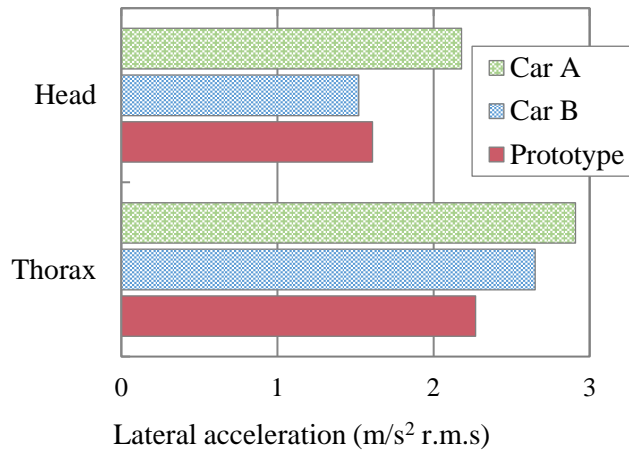
Figure 11: Measured accelerations in laboratory tests on lateral human body shaking

6   DISCUSSION

Focused here is the difference in the measured values of driver upper-thorax displacement between laboratory and field tests in the present study. In the laboratory tests the subjects, instructed to perform steering in a simulated setup, tried to maintain their postures during cornering but their thorax center lost alignment with the steering wheel center. On the other hand in the field tests, the subjects aligned their thorax center with the steering wheel center more accurately.

Two influencing factors may be considered to explain this difference. One is different physical conditions between laboratory and field tests. Because in the laboratory tests the seat was inclined sideways to quasi-statically simulate only the vehicle's lateral accelerations during cornering, the vertical accelerations on the occupant in a seat local coordinate system were smaller in laboratory than field tests. Additionally, test environments were such that the subjects were more strongly prompted to make preparatory behaviors for transition from straight-ahead driving to cornering operation in field tests than in laboratory tests. These differences in vertical acceleration and preparatory driving behavior may have brought difference in the overall behaviors of occupants between laboratory and field tests.

The other influencing factor is different mental conditions induced by laboratory and field tests. While steering error in laboratory tests would not lead to an actual accident in laboratory tests, in field tests steering error may cause an excessive vehicle turning or an actual accident. Due to the above differences in physical and mental conditions, it is likely that subjects become motivated to hold up the upper-thorax center over the steering wheel center more strongly in field tests than in laboratory tests.

7   CONCLUSIONS

The present study was intended to dissolve the trade-off relationship existing between human body instability and lateral human body shaking. For the reduction of human body instability, it was found effective to hold up occupant posture by minimizing pelvis roll motion and by improving support to thorax and thigh. For the reduction of lateral human body shaking, it proved effective to minimize the transmission of excitation force from the seat to the occupant by optimizing backrest bolster shape. As a result the roles of cushion bolsters and backrest bolsters were defined more clearly, and their shapes and characteristics were optimized, achieving the reduction of body instability and lateral body shaking for both drivers and passengers. Hence, the trade-off relationship was dissolved and the two phenomena were moderated at high ride comfort levels.

REFERENCES

Kanke T., Yoshimura T., Tamaoki G., Kato K. and Kitazaki S. (2007) Modeling of vehicle passenger for comfort evaluation, Proceedings of Annual Congress of the Society of Automotive Engineers of Japan, No.138-07, p23-28 (in Japanese)

Yamada K., Motojima H., Kitagawa Y. and Yasuki T. (2016) Investigation of relations between occupant kinematics and supporting by the seat in lane change maneuvers, Proceedings of Annual Congress of the Society of Automotive Engineers of Japan, No.38-16, p941-946 (in Japanese) and Summarized Paper (in English)

Kawano K., Taguchi T., Motohata K., Yasuda E. and Kubota A. (2017) Motion analysis of a passenger in reaction to vehicle sway by varying seat side support, Proceedings of Annual Congress of the Society of Automotive Engineers of Japan, No.174-17, p1644-1650 (in Japanese) and Summarized Paper (in English)

Koike T., Yoshimura T., Tamaoki G. and Kato K. (2013) Vibration behavior of seated human body (Difference between driver and passenger), JSME Dynamics and Design Conference 2013 USB Proceedings, p447-453 (in Japanese)

Kato K., Suzuki K. and Ohyama M. (2014) Stability of vehicle occupant's body during cornering, Proceedings of the 49th United Kingdom Conference on Human Responses to Vibration, USB proceedings

Griffin M.J. (1990) Handbook of Human Vibration, Academic Press, London

12   Session 5: WBV 2

Session chair: Gurmail Paddan

Effect of backrest inclination on the nonlinearity of the apparent mass at the seat pan and backrest during vertical vibration

Weitan Yin[1], Yi Qiu[2]
Human Sciences Group
Institute of Sound and Vibration Research
SO17 1BJ, Southampton, Hampshire
W.Yin@soton.ac.uk

ABSTRACT

Many studies have shown that with the support of an upright backrest, the response of seated human body to the Whole-body Vibration is nonlinear subject to the change of the vibration magnitude. However, although many seats in modern vehicles have inclined backrest, there has been very little study on whether the inclination of backrest could further affect the nonlinearity of human responses to vibration caused by the increase of excitation magnitude. In this study, the in-line (vertical) and cross-axis (fore-aft) apparent masses at the seat pan and backrest were studied with twelve subjects supported by a rigid backrest with three inclination angles (upright, 10° backwards and 20° backwards) adjusted in sequence while exposing to vertical vibration at different magnitudes (0.25, 0.5 and 1.0 ms^{-2} r.m.s.). The results show that the nonlinear behaviour of apparent mass observed when the backrest was upright also existed when the backrest was inclined. It was further found that the effect of the magnitude of excitation on the apparent mass measured at the backrest was influenced by the inclination of the backrest.

1   INTRODUCTION

A comprehensive understanding of the response of the seated human body to the Whole-Body Vibration and the effect of the seat support and excitation magnitude on such response is beneficial to the improvement of the ride comfort. It could allow more effective biodynamic models of human body to be developed, as well as provide more suitable targets for the optimisation of the vehicle- or seat-design, especially in the range of frequency where the human body is most sensitive to the excitation.

The apparent mass of the human body is widely investigated as an indicator of the biodynamic response of the seated or standing human body to the Whole-Body Vibration. The apparent mass can reflect a general dynamic response of the human body, which involves the muscle tension, body mass distribution or the motion of body segments. The trend and peak of the curve of apparent mass reveals the frequency-dependent sensitivity of the human body to the excitation, which is closely related to the effect that Whole-Body Vibration has on the comfort or health of the seated human body. Some factors have been found to have important effect on the resonance frequency or the modulus of the apparent mass to varying degrees, such as the support of the backrest and the magnitude of the excitation.

The presence of the backrest support can affect the response of the seated human body to the vibration in two ways: a backrest reduces the biodynamic activity of the body segments needed to maintain the posture in a vibration environment (Rohlmann et al, 2010), and it transmits extra vibration to the human body at the backrest in addition to the seat pan.

In the case of single-axial vertical excitation, the support of a vertical backrest was found not to have significant effect on the resonance frequency of the vertical apparent mass (at seat pan) or the modulus of the apparent mass (at seat pan) at the resonance, although the peak of the curve showing the median apparent mass of the subjects shifted to a slightly higher frequency with a vertical backrest compared to that measured without backrest (Toward & Griffin, 2009). In another study carried out by Qiu & Griffin (2012), the support of the vertical backrest was found to slightly increase the modulus of apparent mass (at seat pan) at high frequencies.

In real life, the backrest supporting the upper body of the seated occupant may not be well vertical, and the seated occupant may adjust the backrest angle for a better field of vision or more comfort. For example, the backrest of a car seat was reported to have an inclination of 15° in a previous study on the seat transmissibility (Qiu & Griffin, 2003). Studies on the effect of the support of an inclined backrest on the apparent mass are less reported than those on the effect of a vertical backrest. The effect of the backrest inclination on the apparent mass was investigated (Liu, 2017; Toward & Griffin, 2009; Yang & Qiu, 2015). These studies all used random vertical excitation with only one fixed magnitude. It was found that, compared to the support of vertical backrest, the support of an inclined backrest tended to lead to an increase the resonance frequency and a decrease of the modulus of apparent mass at the resonance. However, the change of the resonance frequency due to the change of the backrest inclination was only statistically significant between a few inclination angles. The cross-axis fore-aft apparent mass measured at the seat pan is also affected by the angle of backrest inclination (Yang & Qiu, 2015). A study investigating the effect of backrest inclination on the apparent mass under different magnitudes of vertical vibration has not been seen so far.

Apart from the condition of backrest support, the magnitude of excitation is another important factor that can affect the apparent mass of the seated subject. When the magnitude of excitation in vertical direction increased, the frequency of the primary resonance of the apparent mass in the same direction tends to decrease, and the fore-aft cross-axis apparent mass is also affected (Nawayseh & Griffin, 2003). Such softening behaviour of the apparent mass subject to the increase of the magnitude of excitation has been referred to as the nonlinearity of the apparent mass. The nonlinearity of the apparent mass has been observed in the biodynamic measurements without the support of the backrest (Huang & Griffin, 2008; Qiu & Griffin, 2010; Tufano & Griffin, 2013) and with the support of vertical backrest (Qiu & Griffin, 2012). A study about the nonlinearity of the apparent mass with the support of the inclined backrest and how the nonlinearity may vary when the inclination angle changes, have not been reported so far.

The current ISO standard for the evaluation and assessment of the Whole-Body Vibration for seated occupant suggests to use certain frequency weighting factor for each axis (ISO 2631-1, 1997), which may have not properly reflected the effect of the magnitude of excitation or the angle of backrest inclination on the biodynamic responses. The objective of the study presented in this paper is to investigate the effect of the magnitude of vertical vibration as well as effect of the inclination of the backrest on the nonlinearity of the apparent mass of seated subjects measured at the seat pan and backrest in the vertical and fore-aft directions. It was hypothesised that the nonlinearity of the apparent mass due to the change in excitation magnitude exists with the support of not only upright but also inclined backrests, and that the backrest inclination would influence the effect of excitation magnitude on such nonlinearity.

2   EXPERIMENTAL METHOD

2.1   Apparatus

The experiment was carried out using the 6-axis motion simulator in the Institute of Sound and Vibration Research at the University of Southampton. The simulator is capable of producing vertical displacements up to ± 0.5 m and fore-aft or lateral displacements up to ± 0.25 m. A rigid seat

including a rigid backrest was mounted at the centre of the simulator (Figure 1). The angle of the backrest inclination can be adjusted between 0° and 80° backwards with respect to the upright position. To measure the vertical and fore-aft dynamic forces at the interface between the seat pan and subject, a force plate (Kistler 9281 B) with tri-axial force transducers located at the four corners of the force plate was fixed on the seat pan. The vertical and fore-aft dynamic forces at the interface between the backrest and subject were measured using four tri-axial force transducers (Kistler 9602, with charge amplifier integrated) which were fixed at the at the four corners of the backrest board. The signals from the force plate were amplified using Kistler 5001 charge amplifiers. To measure the acceleration at the interface between the seat (including backrest) and subject, two tri-axial SIT-pads were fixed at the force plate and the backrest, respectively. The experimental study was approved by the Faculty of Engineering and Physical Sciences Ethics Committee at the University of Southampton.

Figure 1: The rigid seat, rigid backrest, force plate at the seat pan, force transducers at the backrest (only the screws securing the transducers are shown) and SIT-pads used in the experiment

2.2   Subjects

Twelve male subjects aged between 22 and 43 years old (with a mean age of 28.75 years old) participated in this experiment, and the weights of the subjects ranged from 57.3 to 93.5 kg (with a mean weight of 75.27 kg). During the experiment, the subjects were asked to sit in an upright relaxed posture (without slouching) against the backrest when the backrest is upright, or sit in a relaxed posture (without slouching) against the backrest when the backrest is inclined. They were asked to rest their hands on the lap and rest their feet on the footrest, so as to have an average thigh contact with the force plate (serving as the seat pan) (Figure 2).

Figure 2: The postures of the subject sitting in the seat with different angles of backrest inclination (from left to right: 0°, 10°, and 20°)

2.3   Stimuli and backrest inclination

The stimuli used in this experiment were three broad-band random vertical excitations over a frequency range between 0.5 and 40 Hz, and the magnitude of each excitation was 0.25, 0.5 and 1.0 ms^{-2} (r.m.s.), respectively. The duration of each of the excitations was 60 seconds. The three vibration signals were generated independently and was mutually uncorrelated.

During the experiment, each subject was exposed to 3 excitations three times, each time under the support of the backrest with a different inclination angle: 1) 0° (upright), 2) 10° backwards, and 3) 20° backwards, making the total number of the excitations that a subject experienced throughout the experiment to be 9. For the experiment with each backrest inclination angle, the order of 3 excitations was randomized.

2.4   Data analysis

The apparent mass is the frequency response function between the dynamic force and the acceleration at the human-seat (or -backrest) interface. In this experiment, the force transducers and SIT-pads at the backrest were mounted in such way that they measured the forces and accelerations normal and parallel to the backrest surface (i.e. in x- and z-axis at the backrest coordinate system). When the backrest was inclined backwards, the surface of the backrest was not perpendicular to the seat pan and floor, making the x- and z-axis of the backrest coordinate system different from those of the coordinate system of the seat pan (Figure 3). The x- and z-axis at the seat pan remained to be the same as those on the floor.
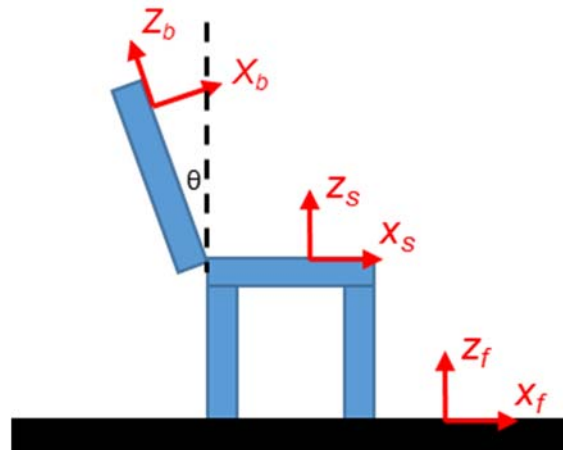
Figure 3: The x- and z-axis of the backrest coordinate system (x_b and z_b), seat coordinate system (x_s and z_s) and floor coordinate system (x_f and z_f) when the backrest was inclined

In this study, when the backrest was inclined, the forces measured in the x- and z-axis of the backrest coordinate system were projected to the x- (or z-) axis in the coordinate system of the floor to calculate the apparent mass at the backrest. When the angle of backrest inclination was θ, the force at the backrest in the x- and z-axis of the floor coordinate system (F_{bx}, F_{bz}) could be calculated as follows:

$$F_{bx} = F_{bxm} \cos\theta - F_{bzm} \sin\theta \tag{1}$$

$$F_{bz} = F_{bxm} \sin\theta + F_{bzm} \cos\theta \tag{2}$$

Where F_{bxm} and F_{bzm} represent the force measured in the x- and z-axis of the backrest coordinate system (as x_b and z_b shown in Figure 3), respectively.

Mass cancellation was performed before the calculation of the apparent mass in the time domain to eliminate the force measured due to the motion of the force plate and SIT-pad at the seat pan, by multiplying the measured acceleration at the seat pan by the mass of the force plate and SIT-pad and then subtracting the product from the measured force in three axes. Similarly, mass cancellation was done on the force measured at the backrest to remove the force due to the motion of the force transducers, backrest board and SIT-pad at the backrest. The force and acceleration were acquired at a sampling rate of 512 samples per second via 100 Hz anti-aliasing filters, and the frequency resolution of the signal processing was 0.25 Hz.

The in-line vertical apparent masses and the cross-axis fore-aft apparent masses at the seat pan and backrest were calculated using a single-input-single-output (SISO) model. If a_z represent the measured vertical acceleration and F_{ij} represent a measured force, then any one of the apparent mass M_{ij} can be calculated as:

$$M_{ij} = \frac{G_{a_z F_{ij}}}{G_{a_z}}$$ (3)

Where $i=s$, b and represents the position of the measured force (at the seat pan and backrest, respectively); $j=x$, z and represents the direction of the measured force (fore-aft and vertical, respectively); G_{azFij} represents the cross-spectra between a_z and F_{ij}; while G_{az} and G_{Fij} represents the auto-spectra of a_z and F_{ij}. If $j=z$, the calculated apparent mass M_{bz} or M_{sz} was the in-line vertical apparent mass, otherwise it was a cross-axis fore-aft apparent mass.

The Friedman two-way analysis of variance was applied in this study to test the effect of the vibration magnitude or the angle of the backrest inclination on the resonance frequency, modulus at the resonance, and the degree of nonlinearity of the apparent masses among the twelve subjects.

3   RESULTS

Figure 4 shows the vertical apparent mass measured at the seat pan under all 9 combinations of conditions (3 backrest inclination angles and 3 magnitudes of excitation) of each subject and the median apparent mass. The vertical apparent masses of different subjects' show an inter-subject variability, but each of the apparent masses exhibits a distinctive principal resonance which is located between 4.5 and 7.5 Hz, regardless of the condition of backrest or excitation. For some of the subjects, other resonances can be identified from the curves, which are less distinct than the principle resonance. For example, apparent masses of some subjects have a secondary resonance in the vicinity of 8 Hz, while some subjects possess apparent masses with a secondary resonance between 12 and 15 Hz.

When the backrest was inclined by 10° or 20°, apparent masses of some subjects had two peaks below 10 Hz with similar modulus (instead of one distinctive peak), one around 5 Hz and another around 8 Hz (Figure 4, the second and third columns).
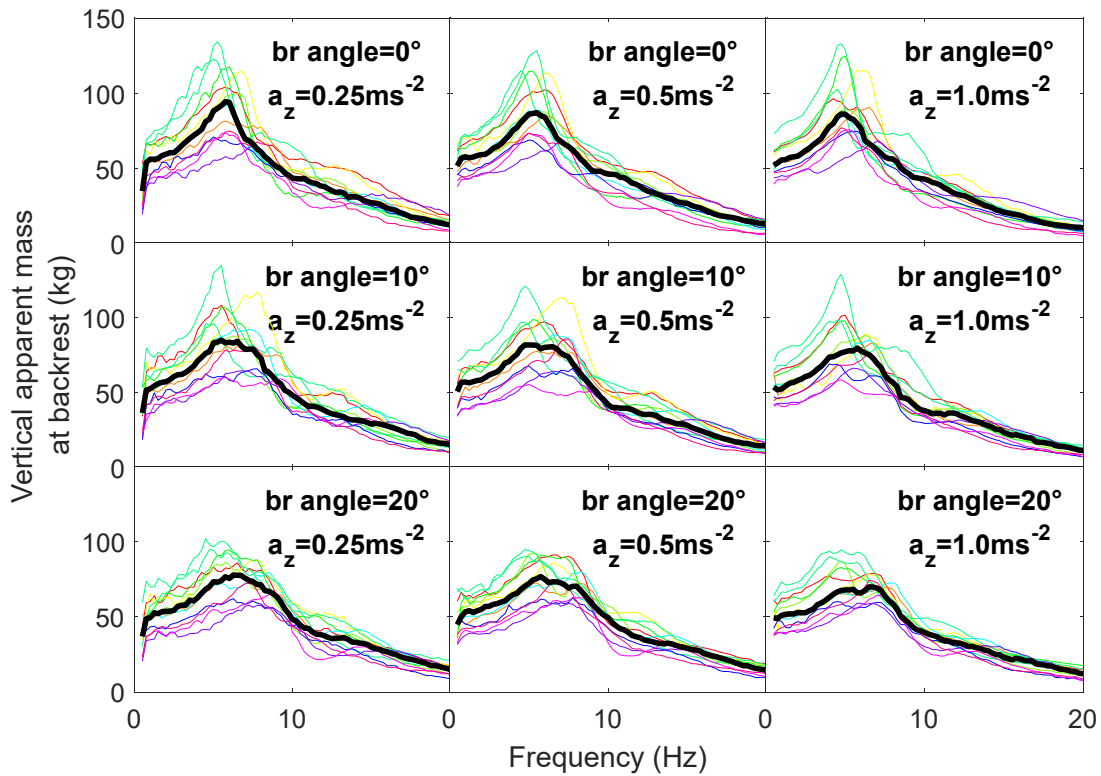
Figure 4: The vertical apparent mass measured at the seat pan under all combinations of conditions (backrest inclination and magnitude of excitation) of 12 subjects (solid black line: median value)

3.1 Effect of the magnitude of excitation on the apparent masses with upright and inclined backrest

In-line vertical apparent mass at the seat pan and backrest

Figure 5 shows the effect of the magnitude of excitation on the in-line vertical apparent mass measured at the seat pan and backrest with three angles of backrest inclination (abbreviated as "br angle"). The magnitude of excitation has some general effects on the resonance of the apparent masses, which can be found with both upright backrest and inclined backrest. The increase of the magnitude of vertical excitation led to a decrease of the primary resonance frequency of the vertical apparent mass at the seat pan (first row of Figure 5) and backrest (second row of Figure 5). Table 1 shows that the statistical significance (*p*-value, Friedman) of the effect of the excitation magnitude on the resonance frequency of the vertical apparent mass at the seat pan was smaller than 0.05 when the backrest was upright or 10° inclined, and marginally greater than 0.05 (*p*=0.064) when the backrest was 20° inclined. For the resonance frequency of the vertical apparent mass at the backrest, the statistical significance was smaller than 0.05 with inclined backrest while much greater than 0.05 (*p*=0.352) when the backrest was upright.

The modulus of apparent mass at the resonance, both at the seat pan and backrest, decreased when the magnitude of excitation increased (Figure 5). The statistical significance of the effect of the magnitude of excitation on the modulus of the apparent mass at the seat pan at the resonance was smaller than 0.05 when the angle of backrest inclination was 0 or 20°. The statistical significance of the effect of excitation magnitude on the modulus of the apparent mass at backrest at the resonance was smaller than 0.05 at all angles of backrest inclination (Table 1). Additionally, it can be found in the second row of Figure 5 that when the angle of backrest inclination increased, the percentage change of the modulus of in-line vertical apparent mass at backrest at the resonance when the magnitudes of excitation changed from 0.25 ms^{-2} (r.m.s.) to 1.0 ms^{-2} (r.m.s.) relative to that modulus at the resonance when the magnitudes of excitation was 0.25 ms^{-2} (r.m.s.) decreased. The actual mean

values of such percentage change (for 12 subjects) were 35.098 % with the upright backrest, 17.516 % with 10° inclined backrest and 6.684 % with 20° inclined backrest.

Furthermore, at frequencies above 7.5 Hz, the modulus of vertical apparent mass both at the seat pan and backrest decreased with the increase of the magnitude of excitation.
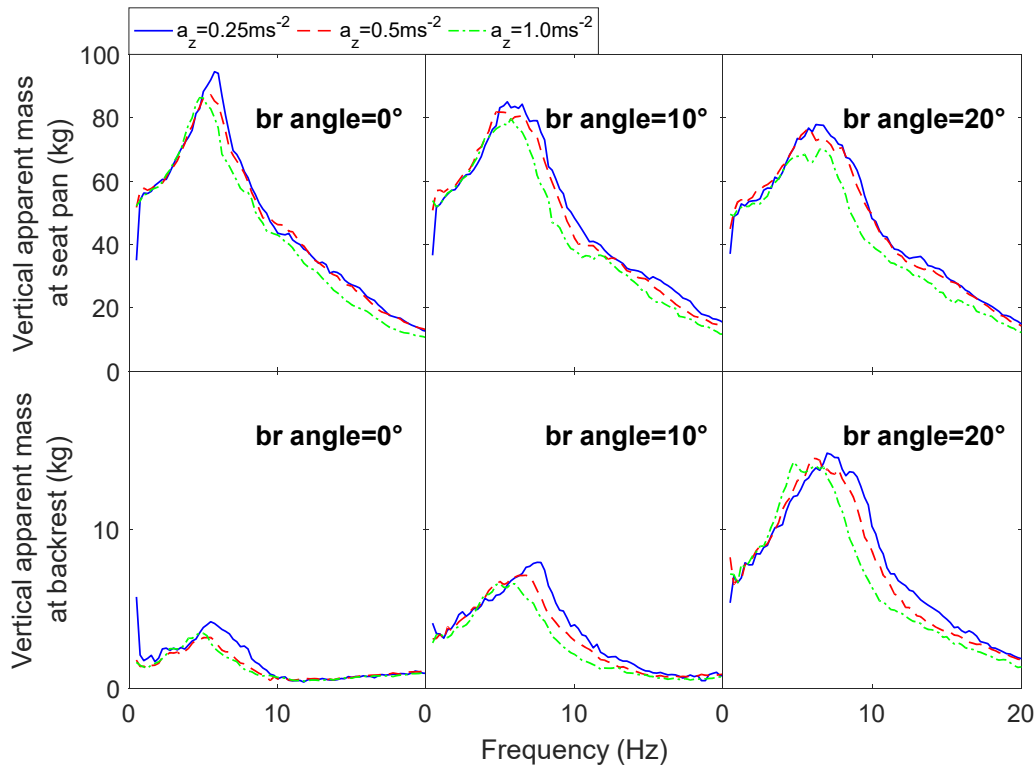
Figure 5: Median in-line vertical apparent mass measured at the seat pan and backrest: effect of the magnitude of excitation

Table 1: Statistical significance (p-value, Friedman) of the effect of the excitation magnitude on the resonance frequency and the modulus of the in-line vertical apparent masses at the seat pan and backrest at the resonance, with different inclination angles of the backrest ("*" highlights cases where $0.01 < p < 0.05$ and "**" highlights cases where $p < 0.01$, sic passim)

The characteristics of the vertical apparent masses associated with the resonance	Backrest inclination angle		
	0°	10°	20°
Resonance frequency of the apparent mass at seat pan	0.031*	0.001**	0.064
Resonance frequency of the apparent mass at backrest	0.352	0.005**	0.004**
Modulus of the apparent mass at seat pan at the resonance	0.046*	0.174	0.017*
Modulus of the apparent mass at backrest at the resonance	0.001**	0.005**	0.004**

Cross-axis fore-aft apparent mass at the seat pan and backrest

The cross-axis fore-aft apparent mass at the seat pan generally exhibits a resonance at around 5 Hz with all backrest conditions, while the resonance frequency of the fore-aft apparent mass at the backrest was located at around 7 Hz (Figure 6). Figure 6 also shows the effect of the magnitude of excitation on the cross-axis fore-aft apparent mass measured at the seat pan and backrest with different angles of backrest inclination.

The increase of the magnitude of vertical excitation led to a decrease of the primary resonance frequencies of the cross-axis fore-aft apparent masses at the seat pan and backrest (Figure 6). Such

effect was significant on the cross-axis fore-aft apparent mass at the seat pan with all angles of backrest inclination ($p<0.01$, Table 2), and was significant on the cross-axis fore-aft apparent mass at the backrest only when the backrest was inclined ($p<0.01$, Table 2). However, the effect of the magnitude of excitation on the modulus of cross-axis fore-aft apparent mass at the seat pan and backrest at the resonance was not significant, regardless of the angle of backrest inclination ($p>0.05$, Table 2).

With the increase of the magnitude of excitation, the modulus of the cross-axis fore-aft apparent masses at the seat pan and backrest below 5 Hz increased (Figure 6), regardless of the angle of backrest inclination.
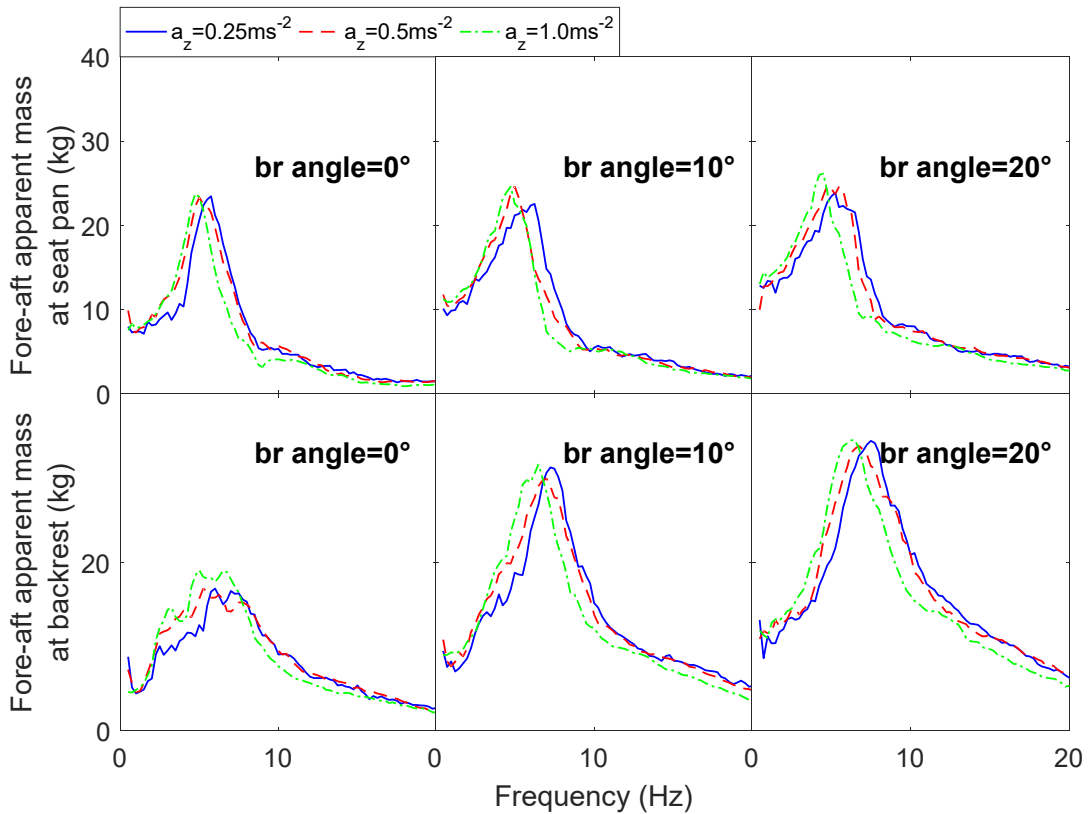
Figure 6: Median cross-axis fore-aft apparent mass measured at the seat pan and backrest: effect of the magnitude of excitation

Table 2: Statistical significance (p-value, Friedman) of the effect of the excitation magnitude on the resonance frequency and the modulus of the cross-axis fore-aft apparent masses at the seat pan and backrest at the resonance, with different inclination angles of the backrest

The characteristics of the fore-aft apparent masses associated with the resonance	Backrest inclination angle		
	0°	10°	20°
Resonance frequency of the apparent mass at seat pan	0.000**	0.000**	0.004**
Resonance frequency of the apparent mass at backrest	0.059	0.001**	0.002**
Modulus of the apparent mass at seat pan at the resonance	0.472	0.339	0.339
Modulus of the apparent mass at backrest at the resonance	0.174	0.717	0.558

3.2 Effect of the backrest inclination on the apparent masses with different excitation magnitudes

In-line vertical apparent mass at the seat pan and backrest

The effect of the angle of backrest inclination on the in-line vertical apparent mass at the seat pan and backrest is shown in Figure 7. The primary resonance frequencies of the apparent masses at the seat pan and backrest increased when the inclination angle increased (Figure 7). However, the effect of increasing the angle of backrest inclination on the primary resonance frequency of vertical apparent mass at the seat pan was not significant ($p>0.05$, Table 4), while for the primary resonance frequency of vertical apparent mass at the backrest, the effect was significant ($p<0.01$, Table 4).

With the increase of the inclination angle, the moduli of the vertical apparent mass at the seat pan at the resonance decreased ($p<0.01$, Table 4), and the modulus of the vertical apparent mass at the backrest at the resonance increased ($p<0.01$, Table 4).
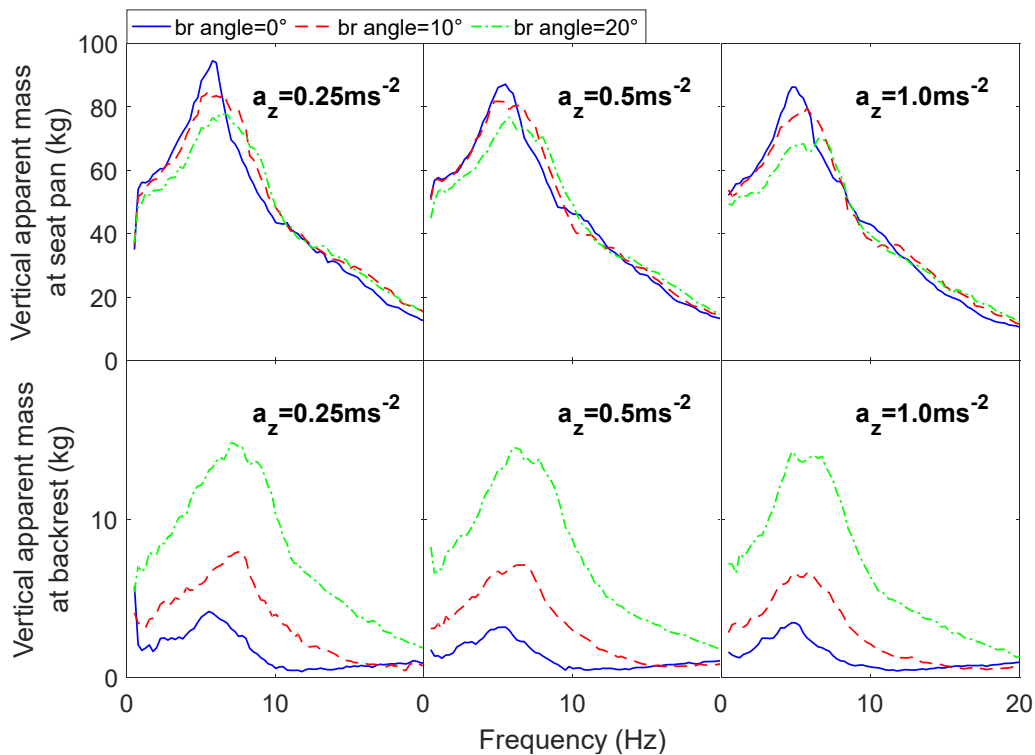
Figure 7: Median in-line vertical apparent mass measured at the seat pan and backrest: effect of the backrest inclination

Table 3: Statistical significance (*p*-value, Friedman) of the effect of the angle of backrest inclination on the resonance frequency and the modulus of the in-line vertical apparent masses at the seat pan and backrest at the resonance, with different magnitudes of excitation

The characteristics of the vertical apparent masses associated with the resonance	Excitation magnitude (r.m.s.)		
	0.25 ms^{-2}	0.5 ms^{-2}	1.0 ms^{-2}
Resonance frequency of the apparent mass at seat pan	0.431	0.301	0.518
Resonance frequency of the apparent mass at backrest	0.000**	0.003**	0.000**
Modulus of the apparent mass at seat pan at the resonance	0.000**	0.002**	0.000**
Modulus of the apparent mass at backrest at the resonance	0.000**	0.000**	0.000**

Cross-axis fore-aft apparent mass at the seat pan and backrest

Figure 8 shows that the increase of the angle of backrest inclination has more evident effect on the cross-axis fore-aft apparent mass at the backrest than that at the seat pan. With the increase of the angle of backrest inclination, the resonance frequency of the cross-axis fore-aft apparent mass at the backrest increased slightly (Figure 8) but significantly ($p<0.05$, Table 5). The modulus of the cross-axis fore-aft apparent mass at the backrest at the resonance increased (Figure 8) significantly ($p<0.01$, Table 5) when the angle of backrest inclination increased.

For the cross-axis fore-aft apparent mass at the seat pan, the increase of the angle of backrest inclination led to a significant ($p<0.01$, Table 5) decrease of the primary resonance frequency only when the magnitude of excitation was 1.0 ms^{-2} (Figure 8 first row, third column). The effect of backrest inclination on the modulus of the cross-axis fore-aft apparent mass at the seat pan at the resonance was not significant with any of the three magnitudes of excitation ($p>0.05$, Table 5). Figure 8 also shows that the modulus of the cross-axis fore-aft apparent mass at the seat pan below 4 Hz increased when the angle of backrest inclination increased with all the three excitations.
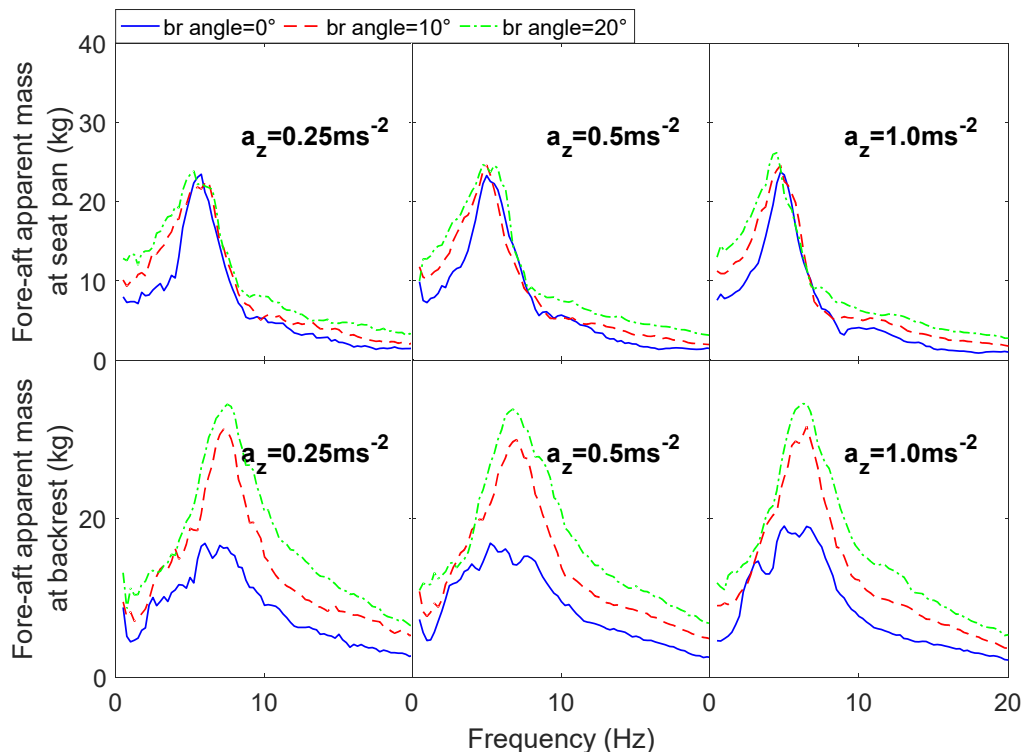
Figure 8: Median cross-axis fore-aft apparent mass measured at the seat pan and backrest: effect of the backrest inclination

Table 4: Statistical significance (*p*-value, Friedman) of the effect of the angle of backrest inclination on the resonance frequency and the modulus of the cross-axis fore-aft apparent masses at the seat pan and backrest at the resonance, with different magnitudes of excitation

The characteristics of the fore-aft apparent masses associated with the resonance	Excitation magnitude (r.m.s.)		
	0.25 ms^{-2}	0.5 ms^{-2}	1.0 ms^{-2}
Resonance frequency of the apparent mass at seat pan	*0.567*	*0.139*	*0.006**
Resonance frequency of the apparent mass at backrest	*0.002**	*0.003**	*0.013*
Modulus of the apparent mass at seat pan at the resonance	*0.920*	*0.264*	*0.339*
Modulus of the apparent mass at backrest at the resonance	*0.002**	*0.000**	*0.000**

4 DISCUSSION

4.1 Effect of the magnitude of excitation on the apparent masses with upright and inclined backrest

With the increase of the magnitude of the vertical excitation, the resonance frequencies of the in-line vertical and cross-axis fore-aft apparent masses measured at the seat pan decreased both when the backrest was upright (which is in consistent with the conclusion by Qiu & Griffin (2012)) and when the backrest was inclined (Figure 5 and 6).

The resonance frequencies of the in-line vertical and cross-axis fore-aft apparent masses measured at the backrest also decreased with the increase of the magnitude of the vertical excitation. However, the effect of the excitation magnitude was significant only when the backrest was inclined (10° and 20°) for both the in-line vertical and cross-axis fore-aft apparent masses at the backrest, and was not significant when the backrest was upright (Figure 5 and 6, Table 1 and 2). The percentage change in the modulus of the vertical backrest apparent mass at the resonance (when the magnitudes of excitation changed from 0.25 ms^{-2} (r.m.s.) to 1.0 ms^{-2} (r.m.s.)) decreased with the increase of the angle of backrest inclination (Figure 5). These results are possibly due to the increased interaction between the human body and the backrest when the backrest was inclined compared with the upright backrest, as a result of the increased upper body mass supported by the backrest.

The moduli of the vertical apparent masses at the resonance decreased with the increase of the excitation at all angles of backrest inclination. Such effect was significant under all conditions except for the apparent mass at the seat pan with 10° inclined backrest. On the other hand, the effect of the excitation magnitude on the modulus of the cross-axis fore-aft apparent masses at the resonance (around 5 Hz for apparent mass at the seat pan and around 7 Hz for apparent mass at backrest) was not significant under all conditions of the backrest inclination (Table 2).

The fact that the increase of the magnitude of vertical excitation had significant effect on the modulus of vertical apparent masses at the resonance but non-significant effect on the modulus of fore-aft apparent masses at the resonance may be related to different vibration modes of the human body. Kitazaki & Griffin (1997) found that when exposed to vertical excitation, the human body exhibited three modes in the frequency range between 4 and 8 Hz: one whole-body mode with both vertical and fore-aft motion at around 5 Hz, one bending mode of the spine with fore-aft motion between 5.5 and 6 Hz, and one mode involving the rotation of the pelvis between 7 and 8 Hz. The bending mode in which the human body performs mainly fore-aft motion (and very little vertical motion) may be related to the non-significant effect of the excitation magnitude on the fore-aft apparent masses.

4.2 Effect of the backrest inclination on the apparent masses with different excitation magnitudes

Figure 7 shows that at low frequency (below 1 Hz) the modulus of the vertical apparent mass at the seat pan decreased with the increase of the backrest inclination while the modulus of the vertical apparent mass at the backrest increased, which may indicate that the body mass supported by the backrest increased (and hence the body mass supported by the seat pan decreased) when the backrest was inclined. At each level of the magnitude of excitation, the angle of the backrest inclination had significant effects on the resonance frequency and the modulus at the resonance of the apparent mass measured at the backrest, for both the in-line vertical and cross-axis fore-aft apparent masses (Figure 7 and 8, Table 3 and 4). The modulus of the vertical apparent mass at the seat pan at the resonance also decreased with high significance (Figure 7, Table 3). Such phenomenon may be explained by the increased body mass supported by the backrest when the backrest was inclined.

The resonance frequency of the vertical apparent mass at the seat pan, however, was not significantly affected by the increase of the angle of the backrest inclination (Figure 7, Table 3), which is in consistent with the results by Yang & Qiu (2015). The resonance frequency of the cross-axis fore-aft apparent mass at the seat pan decreased with the increase of the angle of the backrest inclination significantly only when the magnitude of excitation was 1.0 ms^{-2} (Figure 8, Table 4). This may indicate that when the magnitude of vertical excitation is at a high level (such as 1.0 ms^{-2}), increasing the angle of backrest would make the human body less stiffened in the fore-aft direction compared to that when the magnitude of vertical excitation is at a low level (such as 0.25 ms^{-2}), so as to compensate the increased motion in the fore-aft direction due to the increased interaction between the human body and the backrest when the backrest was inclined.

5   CONCLUSION

In this study, the in-line vertical and cross-axis fore-aft apparent masses at the seat pan and backrest were studied with experiments under single-axis vertical excitation with different magnitudes, and with different inclination angles of the backrest. The results show that when the backrest was inclined, the increase of the magnitude of the vertical excitation led to the decrease of the resonance frequency of the in-line vertical and cross-axis fore-aft apparent masses at the seat pan. This supports the hypothesis that the nonlinearity of apparent mass due to the increase of the excitation magnitude exists both when the backrest is upright and when it is inclined.

The inclination of the backrest was found to further influence the effect of the excitation magnitude on the apparent mass at the backrest. When the backrest was inclined, the effect of the magnitude of excitation on the nonlinearity of the in-line vertical and cross-axis fore-aft apparent masses at the backrest became highly significant in contrast to its non-significant effect when the backrest was upright.

The modulus of the vertical apparent masses at the seat pan and backrest at the resonance changed significantly with the increase of the inclination of the backrest at all levels of the excitation magnitudes.

The results of this study show that interaction effects exist between the magnitude of vertical excitation and the angle of backrest inclination in terms of the biodynamic response of the seated human body, especially for the apparent mass of the human body at the backrest. Hence, when the dynamic performance of a vehicle seat is to be optimized, the effects of both the magnitude of excitation and the inclination of backrest on the nonlinear response of the human body need to be taken into consideration.

REFERENCES

Huang, Y. & Griffin, M. J. (2008) Nonlinear dual-axis biodynamic response of the semi-supine human body during vertical whole-body vibration. *Journal of Sound and Vibration*, 312(1), 296-315.

ISO (1997) ISO 2631-1:1997: Mechanical vibration and shock-Evaluation of human exposure to whole-body vibration-Part 1: General requirements. The International Standard Organization.

Kitazaki, S. & Griffin, M. J. (1997) A modal analysis of whole-body vertical vibration, using a finite element model of the human body. Journal of Sound and Vibration, 200(1), 83-103.

Liu, C. (2017) Localised biodynamic responses of the seated human body during excitation by vertical vibration, PhD Thesis, Institute of Sound and Vibration Research, University of Southampton.

Nawayseh, N. & Griffin, M. J. (2003) Non-linear dual-axis biodynamic response to vertical whole-body vibration. *Journal of Sound and Vibration*, 268(3), 503-523.

Qiu, Y. & Griffin, M. J. (2003) Transmission of fore–aft vibration to a car seat using field tests and laboratory simulation. *Journal of sound and vibration*, 264(1), 135-155.

Qiu, Y. & Griffin, M. J. (2010) Biodynamic responses of the seated human body to single-axis and dual-axis vibration. *Industrial Health*, 48(5), 615-627.

Qiu, Y. & Griffin, M. J. (2012) Biodynamic response of the seated human body to single-axis and dual-axis vibration: Effect of backrest and non-linearity. *Industrial health*, 50(1), 37-51.

Rohlmann, A., Hinz, B., Blüthner, R., Graichen, F. & Bergmann, G. (2010) Loads on a spinal implant measured in vivo during whole-body vibration. *European Spine Journal*, 19(7), 1129-1135.

Toward, M. G. & Griffin, M. J. (2009) Apparent mass of the human body in the vertical direction: Effect of seat backrest. *Journal of Sound and Vibration*, 327(3), 657-669.

Tufano, S. & Griffin, M. J. (2013) Nonlinearity in the vertical transmissibility of seating: the role of the human body apparent mass and seat dynamic stiffness. *Vehicle System Dynamics*, 51(1), 122-138.

Yang, M. & Qiu, Y. (2015) Effect of backrest inclination on apparent mass at the seat and the backrest during vertical whole-body vibration, *50th United Kingdom Conference on Human Responses to Vibration.* University of Southampton, 9 - 10 September.

A wave-by-wave analysis method for assessing marine craft seats intended to isolate repeated shock

Tom Gunston [1]
Finch Consulting
The Nest, Ivanhoe Office Park, Ashby-de-la-Zouch LE65 2AB
Tom.Gunston@finch-consulting.com

Andrew Clarke [2]
Royal National Lifeboat Institution
W Quay Rd, Poole BH15 1HZ
Andrew_Clarke2@rnli.org.uk

ABSTRACT

It is challenging, in practice, to carry out sea trials to assess the performance of seats intended to mitigate the shock and vibration caused by wave impacts. Two key factors are varying and inconsistent sea conditions, and the requirement to minimise shock and vibration exposures of trials personnel. Obtaining a complete set of well-matched data is often impractical and obtaining measurements over a representative distribution of wave impacts, even in relatively consistent conditions, can require measurement for prolonged periods.

This paper describes an alternative *"wave-by-wave"* approach where the performance of a seat is calculated in response to each wave encountered, rather than averaged over a time period including many impacts. Seats can then be compared in terms of their response to similar wave severities, irrespective of when each wave was encountered.

The method is intended to be tolerant of the inconsistent nature of the sea; to extract as much useful information from each period of measurement as possible; to minimise crew shock and vibration exposures; and to present results in a form that allows a Naval Architect to make informed decisions about seat selection and adjustment.

1   BACKGROUND

Shock and vibration exposures in fast boats at sea can, in some operating conditions, be very severe. The motion is often perceived as a sequence of impacts rather than a vibration. A deck acceleration recorded on a planing or semi-planing craft heading into an oncoming sea may be described as a series of wave impact shocks overlaid on an underlying vibration, as shown in Figure 1.
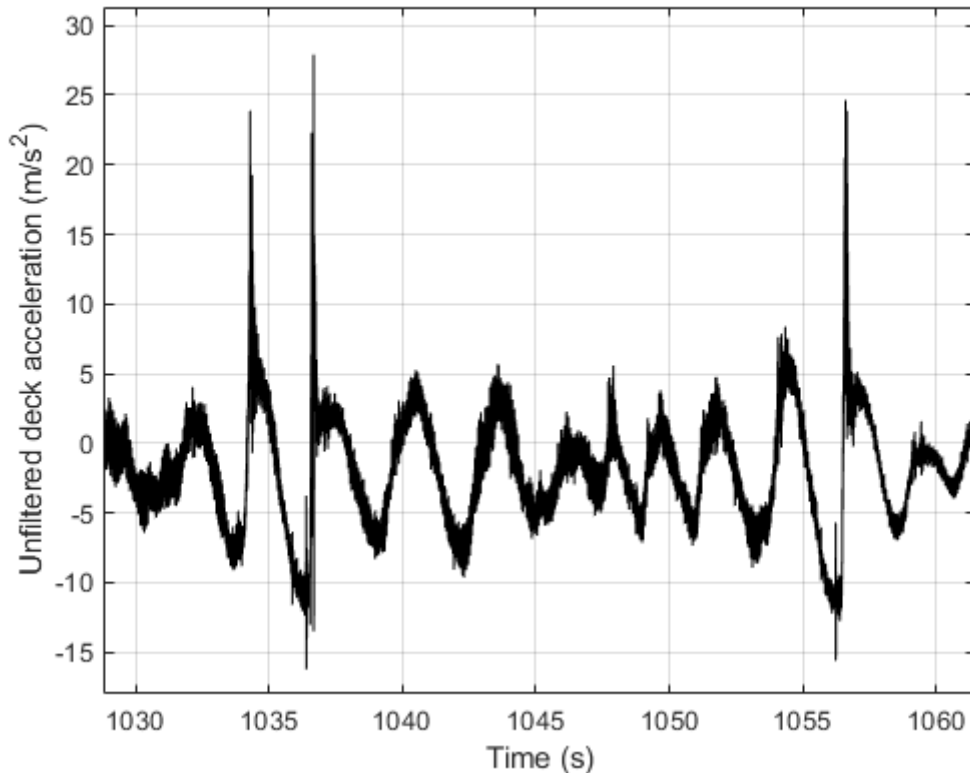
Figure 1 Example unweighted vertical deck acceleration on a semi-planing hull, with three substantial wave impact events

Reducing the risk associated with such exposures requires a holistic approach. Fitting suspension seats is one part of such an approach, but assessment of the suitability of such seats presents a number of challenges.

Assessment of suspension seat performance in a land vehicle may be carried out by running a vehicle over various test surfaces at various speeds and with various seat occupants and then calculating the seat performance for each test run. Standards exist describing this process, for instance ISO 5008 (ISO/TC 23/SC 2, 2002) for agricultural tractor seats.

A similar process can be, and has been, used for sea trials. Unfortunately, in practice, the dataset obtained is often incomplete and indistinct. The test team typically have to commit to operating the boat on a particular day, decided in advance, so are at the mercy of the weather. The test surface on any given day could be milder, or much worse, than the trial requires. The motion experienced on different headings with respect to the prevailing sea can be very different so several test runs may be needed to assess each seat configuration. Even on days when conditions are appropriate, sea conditions vary throughout the day with changes in wind and tide. Sea conditions might be reasonably consistent for short time periods in a given location, but the heights and shapes of consecutive waves will not be identical. Two short duration repeat tests conducted one after the other in the same direction over the same piece of water may result in substantially different overall severities.

Current marine suspension seats are passive vibration isolators, so respond differently to different frequencies of motion. They are extremely non-linear with input magnitude. This results in different stages of operation from semi-friction locked at low magnitudes up to suspension overtravel, involving secondary impact events, at high magnitudes. Figure 2 and Figure 3, from Wu and Griffin (Wu & Griffin, 1996) and Gunston (Gunston, 2002) illustrate some of these behaviours.
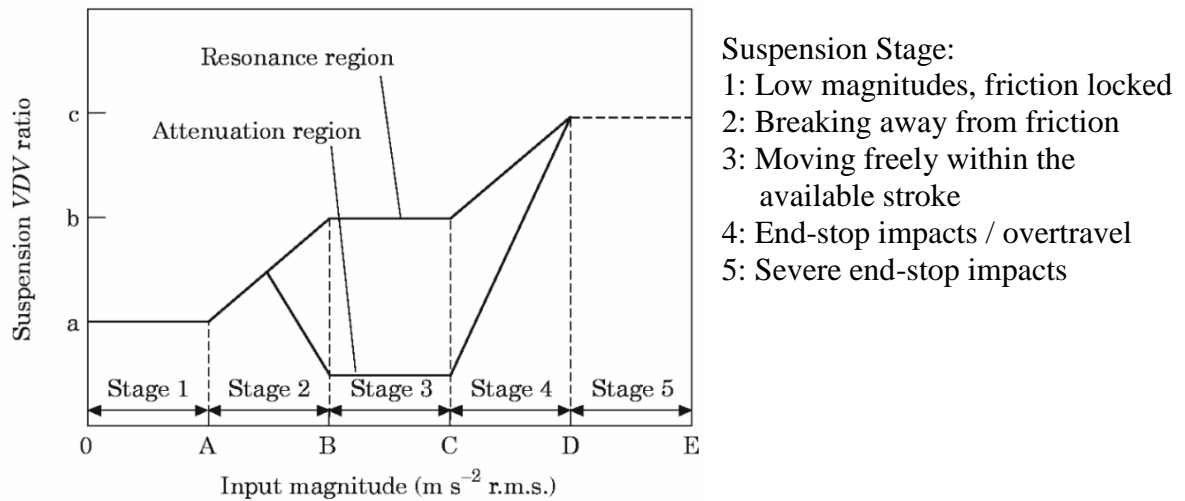
Figure 2 Characterising suspension seat behaviour with magnitude, summarised from Wu and Griffin (1996), the attenuation region refers to response to motions consisting predominantly of frequencies sufficiently high for the suspension to attenuate when moving freely, the resonance region refers to motions with frequencies predominantly in the vicinity of the primary resonance frequency of the seat-person system
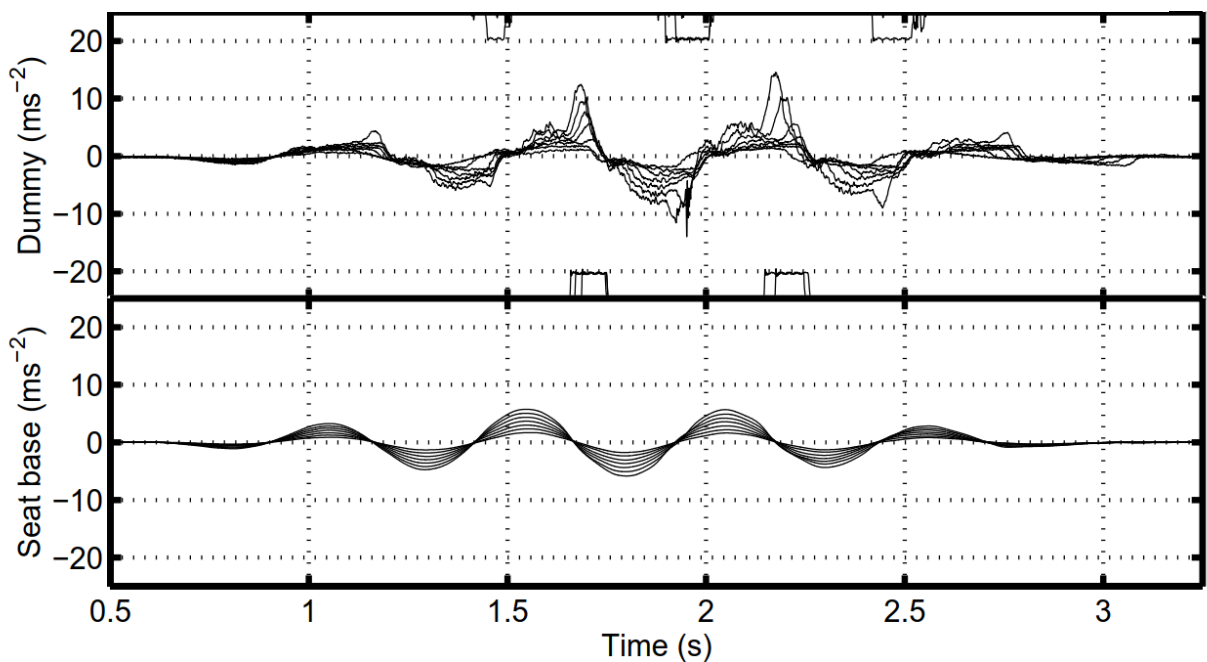
Figure 3 Example response of a suspension seat to seven increasing magnitudes of a windowed sinusoidal motion. Also shown are the signals from microswitches detecting seat end-stop impacts / overtravel events. This example is from Gunston (2002) and uses an earthmover suspension seat tested in the laboratory with a passive anthropodynamic dummy as described by Lewis and Griffin (Lewis & Griffin , 1998).

The seat occupant will also introduce variations in response including intra-subject variability in the impedance of the body, as illustrated by Fairley and Griffin (Fairley & Griffin, 1989) and from passive or active reactions to anticipated inputs, for instance by bracing legs or tensing up before a big wave.

A sea trial of a suspension seat is therefore an attempt to quantify the performance of a highly non-linear mechanical system occupied by an actively varying impedance in response to an input motion that cannot be accurately controlled.

If the purpose of a trial is to compare suspension seats then it is usually necessary to carry out repeated, comparative tests with only two or three seats mounted on the same boat side by side at any time. It can be extremely time consuming to obtain reasonably well-matched conditions for sustained periods over several days.

Depending on the type of boat and the available seat locations, it can also be necessary to swap seat locations. If there is even a slight transverse offset to the centre of mass of the boat, it could fall to one side more often then the other. This would result in varying accelerations for the set of seats. Changing seat locations is often time consuming and requires the boat to be in flat water.

In this study we instead consider the seat response to each wave impact separately. Using this approach, it is possible to assess seat response to mild, moderate and severe wave impacts irrespective of when they occurred during a sea trial.

This approach is intended to obtain as much seat performance data as possible while at the same time making trials more tolerant of changing or inconsistent sea conditions. Both factors help to keep crew vibration exposures as low as possible.

2   THE WAVE-BY-WAVE METHOD

Use of the wave-by-wave method is illustrated using a series of trials conducted in 2018 to compare eight seats under consideration for use in an offshore lifeboat.

The method involves the following steps:

a) measurement of vertical acceleration on, and below, seats in relevant, but not necessarily consistent, sea conditions;
b) data quality check;
c) frequency weighting;
d) identification and extraction of short, 10-second, time history samples involving an impact;
e) calculation of Vibration Dose Values (VDVs) for each 10 second sample;
f) calculation of seat performance ratios, or SEAT values, from the VDVs at the seat base and seat surface;
g) binning SEAT values into groups for comparable conditions and averaging; and
h) comparison of suspension seat performance by inspection of results and by use of statistical methods.

2.1   Acceleration Measurement

Vertical acceleration time histories were recorded at the deck and on the seat surface for an all-weather lifeboat in various operating conditions from sea state 1 to 5 (using the Douglas sea state scale) on seven days between September and December 2018. Seats were occupied by various seat occupants from 65 to 114 kg standing weight. Eight seat variants were assessed, with two or three variants fitted approximately side-by-side at any one time.

Vertical accelerations at the deck and on each seat were measured using 3 single axis, and 3 tri-axial (only logging x and z channels) accelerometers. Seat surface measurements were made using seat pads as described in ISO 10326-1 (ISO/TC 108/SC 4, 2016), although manufactured of a slightly softer material than that specified, and deck accelerometers were positioned directly under each seat. Seat displacement and boat gyration data was also collected but was not used in this analysis. Accelerations were acquired at 5,000 samples per second to a laptop via a Fylde *microanalog* data acquisition system. A typical deck and seat accelerometer layout is shown in Figure 4.
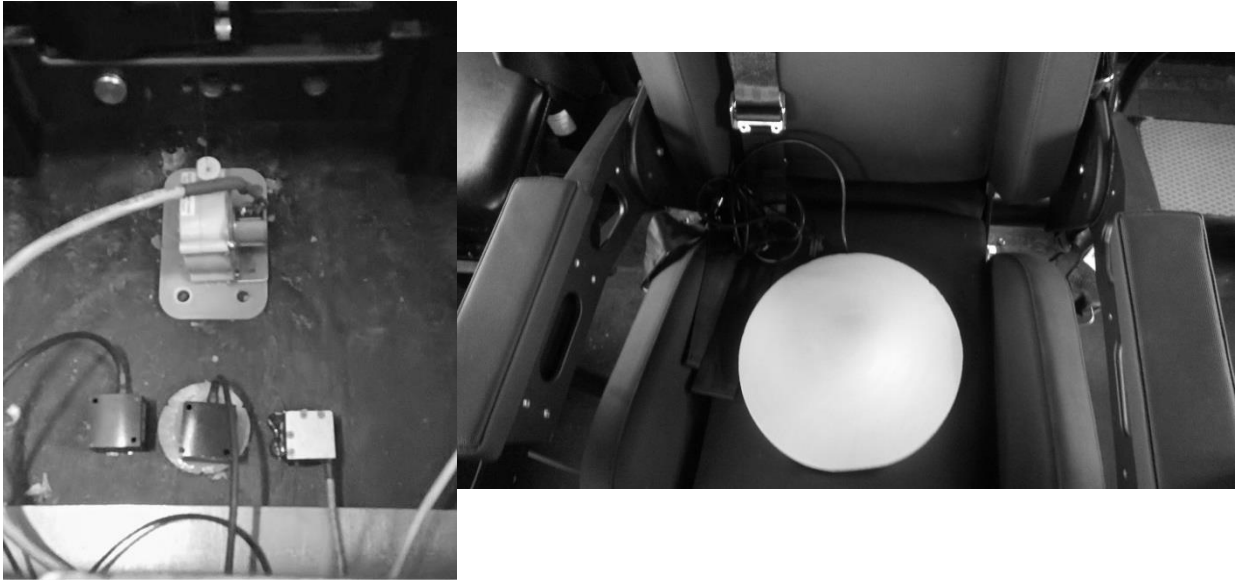
Figure 4 The picture to the left shows a typical deck sensor layout with a 2 tri-axial accelerometer (bottom left), rate gyro (bottom right), and linear string potentiometer (centre back). The image to the right shows the seat pad with the single axis accelerometer mounted inside.

2.2 Inspection and weighting

The acceleration time histories were inspected for measurement artefacts or other data quality issues. No substantial issues were identified.

The time histories were then frequency weighted using the 'Wk' weighting as defined in ISO 2631-1 (1997) (ISO/TC 108/SC 4, 1997). This frequency weighting is used in the calculation of the Vibration Dose Value (Health and Safety Executive, 2005) (British Standards , 2019), and is also used in the calculation of the A(8) method referenced in the 2005 and 2007 UK Regulations on Control of Vibration at Work (HMSO, 2005) (Maritime and Coastguard Agency, 2007).

This weighting is applied to the complete time history, before any consideration of individual impacts. This was considered preferable to applying the weighting to truncated parts of the time history likely to be of similar, or shorter, duration than the impulse response of the Wk weighting filter function.

The option to apply Wk as a zero-phase filter was considered. Wk is based on research techniques that compare the amplitude of different frequencies of motion, so the magnitude of Wk may reasonably be expected to relate to human subjective response. A poor subjective response may suggest motions that a seated human does not wish to experience, which in turn may be indicative of increased potential for injury. The phase response of the weighting, however, is understood by the authors to be a consequence of the requirement to implement this filter in analogue equipment. It can be argued that a zero-phase response is preferable to an arbitrary phase response.

In the authors opinion, however, a zero-phase implementation of Wk is unlikely to be appropriate. Subjective response to shock and vibration is likely to be, in part, a result of the transmission of shock and vibration through the body leading to changes in relative positions and force loadings within the musculoskeletal system. Such mechanical transmission of vibration through the body can be described in terms of both magnitude and phase responses. Phase responses for transmissibility to the lumbar spine in particular seating postures, for instance, have been suggested in some analysis methods including ISO 2631-5:2018 (ISO/TC 108/SC 4, 2018). It is probably appropriate for Wk to have some phase response, but exactly what that should be for a method intended to be a general descriptor of discomfort rather than a predictor of vibration transmission to a specific point, is not clear.

For consistency with previous research, Wk was implemented as defined in ISO 2631-1, including the defined phase response.

Use of part of 'high magnitude' method from ISO 2631-5 was considered. Figure 5 shows the VDV plotted against the Sed (8) value, the latter calculated according to a 2012 draft version of ISO 2631-5, a calculation very similar to the 'high magnitude' method incorporated in the 2018 standard. A total of 96 results are shown from measurements of various durations (typically a matter of minutes) recorded on the deck or the seat of various planing and semi-planing boats operating in various sea conditions, headings, and speeds. The higher magnitude results were generally measurements taken on unmanned flexible decks and involved shocks more severe than a human, if sitting or standing on such a deck, would be expected to experience in practice.

$$y = 0.0905x$$
$$R^2 = 0.988$$

Sed8 2012 (MPa)

1 hour equivalent wk VDV (m/s1.75)
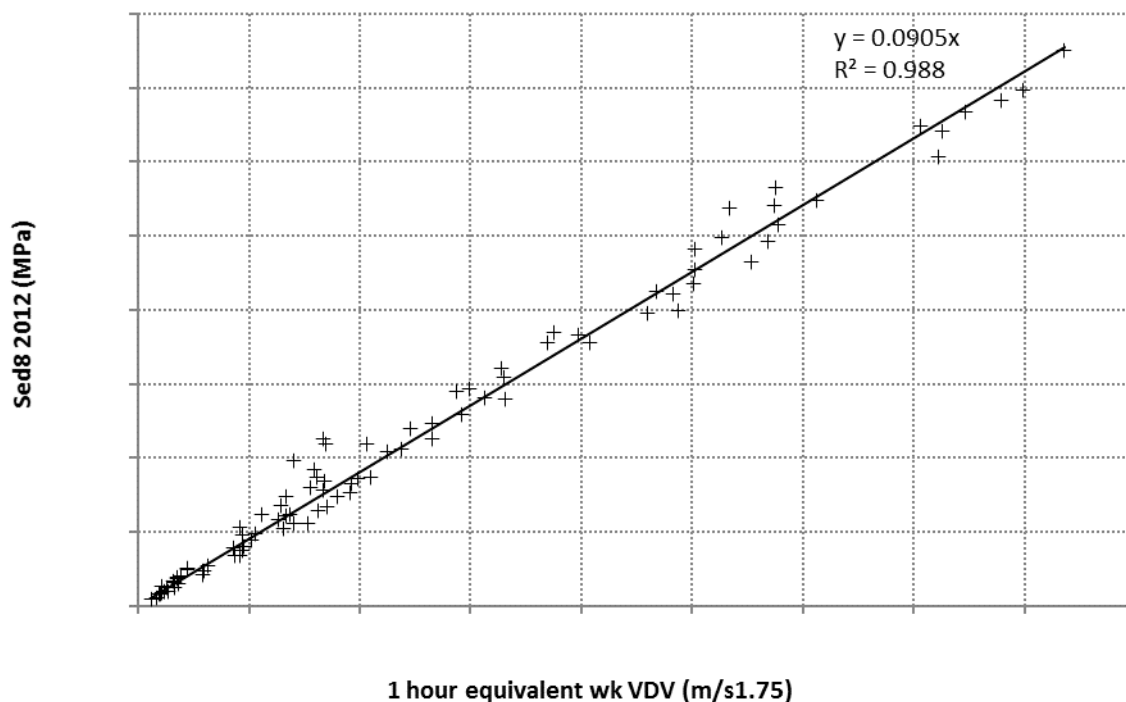
Figure 5 Least-squares linear correlation between 1-hour equivalent VDV and Sed8 values for 96 measurements taken on the deck or seat of various planing or semi-planing boats

These results suggest that a reduction in exposure severity assessed in terms of the Sed8 is likely to be proportionally similar to that assessed in terms of the VDV. It is, in the author's opinion, unlikely that any epidemiological study comparing methods for predicting injury would be sufficiently sensitive to be able to differentiate between these two methods, even assuming enough injuries were ever sufficiently well documented to make any such a study possible. We hope that this will never be the case.

For the present analysis, the decision was taken to use Wk as defined in ISO 2631-1, rather than a zero-phase alternative or another analysis method, because:
a) using the VDV maintains consistency with previous research; and
b) using the VDV is consistent with current risk assessment methods and associated Regulations as used in the UK; and we have seen no evidence that any other technique is a more appropriate predictor of injury risk.

2.3   Identification of impacts and calculation of Vibration Dose Values

Two alternative methods (A and B) were considered for splitting a time history into 'wave by wave' samples.

Method A was based on the 'overlapping windows' approach used in some frequency domain analysis techniques such as Welch's Power Spectral Density method (Welch, 1967).

Consecutive, 50% overlapped, 10 second samples of each Wk weighted acceleration time history which were extracted and a 1-second cosine taper was applied to each end of the 10-second sample, giving 8 seconds of non-attenuated measurement. The VDV of each 10-second sample was calculated and values below a threshold of 0.5g were disregarded as too low to be relevant to the performance of the seats in response to wave impacts.

The 50% overlap ensures that all significant impacts are included in the analysis. It was possible that an impact could occur over the transition between two non-overlapping 10-second samples, in which case only part of an impact would be analysed, giving a potentially misleading result. Use of an overlap and taper overcomes this to some extent.

This method was relatively simple to implement, but was not strictly 'wave by wave' as there could be two or more waves within each sample. It was also possible that some waves would be analysed twice, in consecutive overlapping samples, and some once, potentially affecting the distribution of the results.

Method B was developed to reduce the occurrence of such duplications.

Impact detection method B involved detecting peak accelerations as defined as the maximum (upward) acceleration between two consecutive zero crossings of the normalised, Wk weighted acceleration time history as recorded on the deck, at the base of the seat.

Peak weighted accelerations below an arbitrary threshold of 0.5g were disregarded as they probably did not indicate a wave impact. A 10-second duration sample of the Wk weighted acceleration time history on the deck and on the seat was extracted, centered on each remaining peak as detected on the deck. By centering the sample on the peak of interest, a longer, 2.5 second, cosine taper could be applied to more greatly attenuate any adjacent impacts without affecting the impact of interest. An example is shown in Figure 6. Again, the VDV of each tapered 10-second sample was calculated.
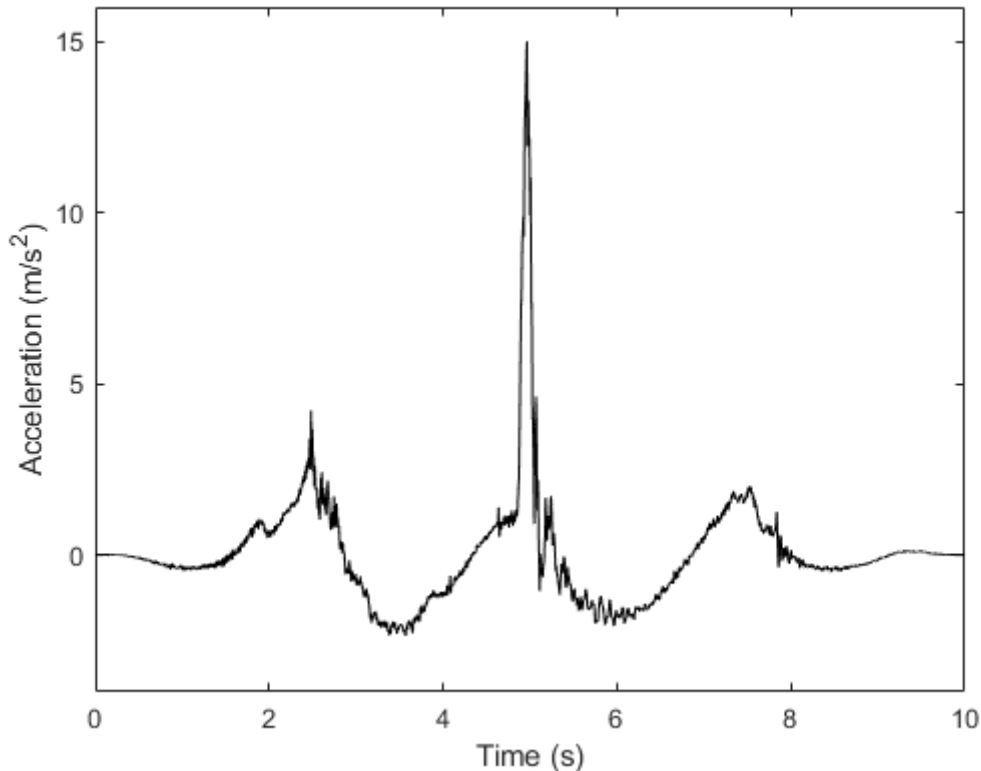
Figure 6 Example of a Wk-weighted, tapered, 10-second acceleration time history centered on an impact

This method will not eliminate duplications as it is possible that two or three impacts could occur very close together, and differences in wave period and craft speed would benefit from different choices in sample length and taper time, but it was considered an improvement over Method A.

In practice, for this trial, the overall results obtained with both methods were found to be similar. The remainder of this paper uses results from Method B.

2.4 Calculation of SEAT values, binning and averaging

The ratio of the VDV recorded on the seat to that on the deck was calculated to obtain the seat performance ratio, or SEAT (pronounced see-at) value, for each 10-second sample centered on each identified wave impact. A total of 2,689 SEAT values were obtained, each nominally associated with the effect of one wave on:
a) a seat type and configuration;
b) a seat occupant weight; and
c) a wave severity, as defined by the VDV measured on the deck.

These SEAT values were binned into groups as follows.

The range of seat occupant weights was divided into three bins, less than 80 kg overall standing mass, 80 to 100 kg, and greater than 100kg. These were not based on any anthropometric standard but were considered reasonably representative of the range of weights of fully dressed and equipped lifeboat crews.

The range of wave severities was divided into 14 bins, a number arrived at empirically. Too few bins would provide too little resolution for assessing seat performance, but too many bins would result in many bins with few or no samples.

The 2,689 SEAT values were therefore collated into 336 bins (14 amplitudes x 3 occupant weights x 8 seats) and the mean SEAT value for each bin was calculated.

For the present analysis, no minimum number of samples in each bin was specified for each average. Introduction of such a minimum would increase the confidence in each average at the expense of discarding some results or reducing the resolution of the results. For the present analysis, a decision was taken to view all results at the reasonably high (14 bin) amplitude resolution chosen, but with sight of the underlying values from which the average SEAT values were calculated.

The results are shown in Figure 7, with the deck motion for scaled in terms of 1-hour equivalent VDVs.
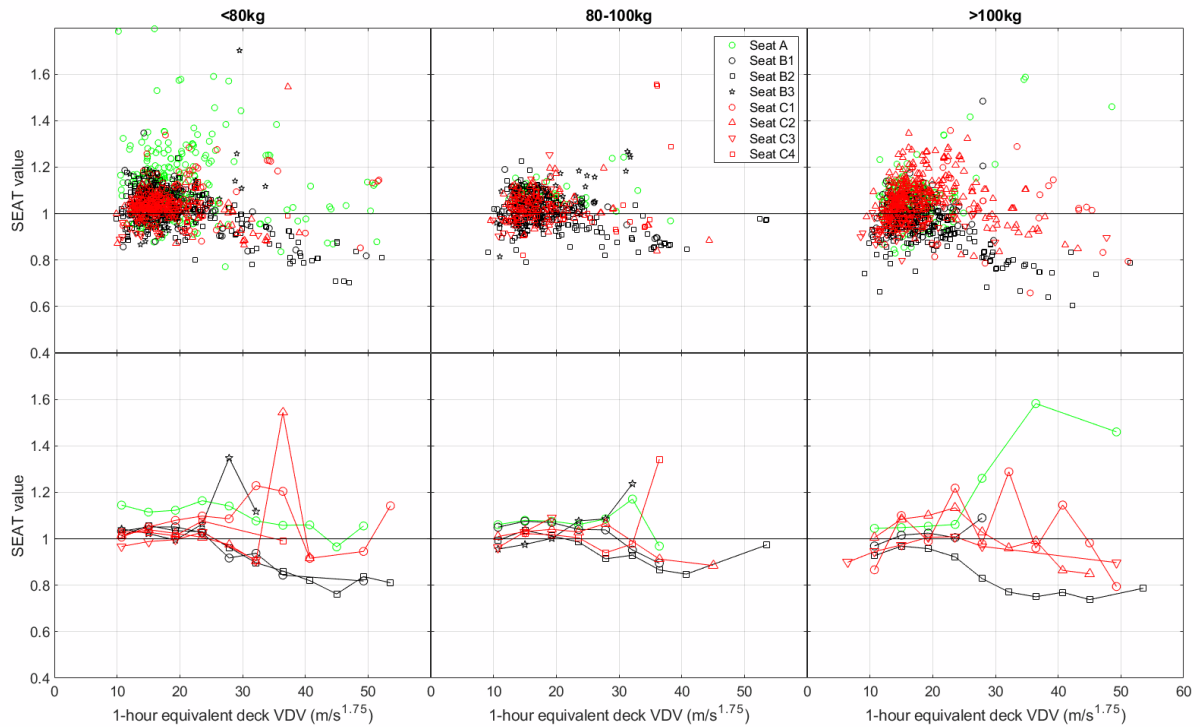
Figure 7 Individual (upper graphs) and average (lower graphs) SEAT values obtained with eights seat variants, various weights of test subject, in response to 10-second tapered samples of various magnitude of deck motion

Trends similar to those in Figure 2 are apparent. In general, for motions with 1-hour equivalent VDVs of less than perhaps 20 m/s$^{1/75}$, all seats, on average, do not show substantial attenuation or amplification, although there is a lot of variation in individual results. As the amplitude increases some seats, on average, improve in performance while some get worse. Feedback from trials crews suggested that the large amplification of Seat A with heavy subjects was associated with suspension overtravel, whereas seats that showed overall improvements with increasing amplitude were apparently freeing up from friction but remaining within their operational stroke.

2.5   Seat Comparison

Overall seat performance was assessed using a series of two-sided non-parametric rank sum (Mann-Whitney U) tests on all SEAT values for all test conditions where the 1-hour-equivalent deck VDV exceeded 20 m/s$^{1.75}$. This threshold was used as a simple method of limiting the analysis to the more severe motions where good seat performance is more important.

This statistical test is essentially looking to determine which of each pair of seats shows the greatest median attenuation over all conditions in which it was measured, irrespective of the number of results obtained with different occupant weights or at different magnitudes.

Due to the variable quantity of data available for each seat for difference amplitudes and payloads, the use of parametric methods, or of more complex non-parametric methods, was not considered appropriate or useful.

Each seat variant was compared with each other seat with the significances obtained divided by the number of paired comparisons made. Corrected significances for each paired comparison are shown in Table 1.

Table 1 Significant differences at the 1% (**), 5% (*), and non-signifcant [>5%](-) level from Mann-Whitney U-tests between SEAT values obtained between each pair of seats

Seat	C4	C3	C2	C1	B3	B2	B1
A	**	**	**	-	**	**	-
B1	**	**	**	-	**	**	
B2	**	*	**	**	**		
B3	-	-	-	*			
C1	-	-	-				
C2	-	-					
C3	-						

This analysis, and inspection of the SEAT values obtained, suggested that the seats might be grouped into three performance classes.

Group 1: Seat B2 only. This seat was significantly better than all the others. The overall median SEAT value for the conditions assessed in the statistical analysis was around 0.9, indicating useful attenuation overall. As can be seen in Figure 7, however, the seat performance was substantially better than this average value for some conditions, especially at higher magnitudes. Individual SEAT values for similar occupant weights and magnitudes were also less scattered compared to results obtained for some of the other seats, suggesting more consistent performance.

Group 2: Seats B3, C2, C3 and C4. These seats were not significantly different from each other, although this was partly due to the large scatter in the SEAT values with some seats, and the limited dataset for some seats. Median SEAT values were around 1.0. This is probably better than could be achieved with a cushion seat, and greater attenuation was provided in some conditions.

Group 3: Seats A, B1, and C1. These seats and generally did not perform well, and/or behaved inconsistently.

3   CONCLUSIONS

This paper describes the use of a 'wave by wave' analysis method to assess the performance of suspension seats under consideration for use on an offshore lifeboat, leading to identification of a preferred option.

By assessing the seat performance in response to each individual wave, this approach does not require testing in consistent sea conditions for sustained periods of time. Each test run produces a large number of individual SEAT values over a range of conditions, rather than one average value for a single, nominal condition.

This method might be applicable to other environments where seat performance in response to repeated shock is of interest, although some refinement may be necessary depending on the nature of the trial. For instance, a variable length window and taper, derived from some characteristic of the motion such as zero crossing or relative amplitude, might allow better focus on individual peaks if a seat was exposed to many shocks close together.

This analysis method was not used, on its own, to determine the seat to be selected. Many factors must be taken into account in selecting a marine craft suspension seat including weight, cost, footprint, vertical space requirements, integration with controls, ease of adjustment and repair, robustness, and consideration of the severity of motions that are likely to be experienced regularly

and in extreme circumstances. The ability of a seat to offer useful attenuation of shock and vibration in the environment in which it will be used is, however, a critical requirement.

4 REFERENCES

British Standards , 2019. *Minutes of the 21 February 2018 meeting of GME/021/06/03: Mechanical vibration, shock and condition monitoring - Human exposure to mechanical vibration and shock - Whole body vibration and shock.,* s.l.: s.n.

Fairley, T. & Griffin, M., 1989. The apparent mass of the seated human body: vertical vibration. *Journal of Biomechanics,* Volume 22, p. 81 – 94.

Gunston, T., 2002. *The sensitivity analysis of a suspension seat dynamic model..* PhD Thesis ed. s.l.:University of Southampton.

Health and Safety Executive, 2005. *HSE Publication L141: Whole body Vibration..* s.l.:Health and Safety Executive.

HMSO, 2005. *The Control of Noise at Work Regulaions.* [Online] Available at: http://www.legislation.gov.uk/uksi/2005/1643/contents/made

ISO/TC 108/SC 4, 1997. *ISO 2631-1 Mechanical vibration and shock -- Evaluation of human exposure to whole-body vibration -- Part 1: General requirements.* [Online].

ISO/TC 108/SC 4, 2016. *ISO 10326-1 Mechanical vibration – Laboratory method for evaluating vehicle seat vibration – Part 1: Basic requirements.* [Online].

ISO/TC 108/SC 4, 2018. *ISO 2631-5 Mechanical vibration and shock -- Evaluation of human exposure to whole-body vibration -- Part 5: Method for evaluation of vibration containing multiple shocks..* [Online].

ISO/TC 23/SC 2, 2002. *ISO 5008 Agricultural wheeled tractors and field machinery -- Measurement of whole-body vibration of the operator..* [Online].

Lewis, C. & Griffin , M., 1998. *The implementation of an improved anthropodynamic dummy for testing the vibration isolation of vehicle seats.* Buxton, Derbyshire, s.n.

Maritime and Coastguard Agency, 2007. *The Merchant Shipping and Fishing Vessels (Control of Vibration at Work) Regulations.* [Online] Available at: http://www.legislation.gov.uk/uksi/2007/3077/pdfs/uksi_20073077_en.pdf

Welch, P., 1967. The use of Fast Fourier Transform for the estimation of power spectra: A method based on time averaging over short, modified periodograms. *IEEE Transactions on Audio and Electroacoustics,* Volume AU-15, p. 70–73.

Wu, X. & Griffin, M., 1996. Towards the standardisation of a testing method for the end-stop impacts of suspension seats.. *Journal of Sound and Vibration ,* Volume 192(1), pp. 307-319.

13 Session 6: Keynote Presentation

Session chair: Mark Taylor

Professor Peter W. Johnson, University of Washington
Peter Johnson is a Professor in the Occupational and Environmental Exposure Sciences program, specializing in ergonomics. He earned his Doctorate in Bioengineering from the University of California - Berkeley and has worked as a researcher at the National Institutes of Occupational Health in the United States, Sweden and Denmark. Dr. Johnson and his lab are nationally and internationally recognized for their work evaluating seating alternatives to reduce vehicle operator exposures to Whole Body Vibration (WBV). Currently, in cooperation with Northeastern University, the University of Connecticut, Oregon State University and Pontifical Xavierian University, his lab is conducting studies to evaluate ways to reduce WBV exposures in the semi-truck, bus and mining industries. Dr. Johnson is a member of the American National Standards Institute's (ANSI) Whole Body Vibration Committee and an American Delegate on the International Standards Organization (ISO) Whole Body Vibration Committee and participates in the annual standard meetings of these organizations. In addition, Dr. Johnson has worked with Microsoft, Hewlett-Packard and Logitech assisting with the design, and evaluation and introduction of new tablets, notebook computers, keyboards and mice, and with Steelcase on the design and introduction of new ergonomic office furniture.

14   Session 7: WBV 3

Session chair: Kazuhito Kato

Shaking Table Tests for Development of Seismic Response Analysis Model of Human Body for Estimation of Injury During Earthquake

Takenori Hida [1], Tatsuya Itoi [2], and Tsuyoshi Takada [3]
The University of Tokyo, Department of Architecture, Graduate School of Engineering
7-3-1 Hongo, Bunkyo-ku, Tokyo, Japan
hida@load.arch.t.u-tokyo.ac.jp, tatsuya.itoi@arch.t.u-tokyo.ac.jp, takada@load.arch.t.u-tokyo.ac.jp

ABSTRACT

So many people suffered damages during massive earthquakes occurred before now in Japan. The cause of injury were not only due to overturning of furniture, but also hitting their head to the wall or falling over themselves. To develop a prediction methodology of human injury caused by hitting to the wall or falling due to shaking is important to draw up a strategy for prevention of human damage. A seismic analysis model of human body would be useful to predict human injury during an earthquake.

In this study, shaking table tests with a human subject were conducted to develop a seismic response analysis model of a human body for evaluation of injury during an earthquake. Mechanisms of standing postural control of a human subject were investigated based on the subject's behaviour measured by 3D motion capture system. Next, a seismic response analysis model of a human body was developed based on a cart-type double inverted pendulum with feedback controller. The model allows us to predict foot displacement and head velocity of a human. Finally, we evaluated head injury probability of human by using head injury criterion (HIC) derived from the head velocity calculated by the human model.

1   INTRODUCTION

When the accident of the Fukushima Daiichi Nuclear Power Plant occurred in the 2011 Great East Japan Earthquake, the accidents were prevented from expanding by desperate efforts of the manager and operators at the site. Although immediate operations during and just after huge earthquake should not rely on human efforts, various human control operations after the earthquake and damage mitigating operations in case of accidents would be needed, as experienced at the 2011 Fukushima Daiichi NPP accident.

In the event of a huge disaster such as the earthquake directly below Tokyo or the Nankai Trough earthquake, which could occur in the near future in Japan, damage reduction and societal restoration activities by human are essential. Therefore, evaluation of whether human can perform disaster reduction and recovery activities after the earthquake is required.

There are some previous studies dealing with human behaviour during an earthquake. Nachi et al. [1] investigated the human injury caused by strong shaking. Takahashi et al. [2] and Hida et al. [3] evaluated the psychological effects of seismic motion on human. Takahashi et al. [4] also investigated the influence on the human body due to overturning of furniture during earthquake. However, objectives of these studies are not to propose the methodology for evaluation of injury considering the human response to earthquake shaking.

The seismic response analysis model of a human is needed to evaluate injury due to shaking, because it is impossible to conduct an experiments dealing with falling over of human and injuries under a huge earthquake. Numerous models have been proposed to analyse the physical behaviour of human body against disturbances in various fields such as automobiles, railroads, robotics, CG, biomechanics etc. (Kudoh et al. [5], Uenishi et al. [6]). In the structural engineering field, Yamamoto [7] proposed the vibration response analysis model of the human body subjected to sinusoidal sweep excitation under a standing position with a simple single mass system. However, the model is not aimed to evaluate the dynamic behaviour of humans subjected to random alternate dynamic disturbance such as earthquake shaking.

In this study, the shake table tests with human subject were conducted to develop the seismic response analysis model of a human body for evaluation of injury during an earthquake. The model was developed based on the cart-type double inverted pendulum model with feedback controller. The model allows us to estimate the foot displacement and head velocity of the human. Finally, we evaluated the injury probability of human by using the head injury criterion derived from the head velocity calculated by the human model.

2   OUTLINE OF SHAKE TABLE TEST

Figure 1 illustrates the setup of shake table test. The size of the shake table is 5 m x 5 m. After each excitation, a questionnaire on condition and mental burden was conducted, and attention was paid to assure safety of the subjects. In addition, after obtaining the approval of the ethics committee of the University of Tokyo, the objective of this experiments and safety measures were explained to the subject in advance and gained consent from the subject. The human subject was made to stand on the force plate. Six video cameras (1920x1080, 60 fps) were set on the handrail constructed on the shake table.
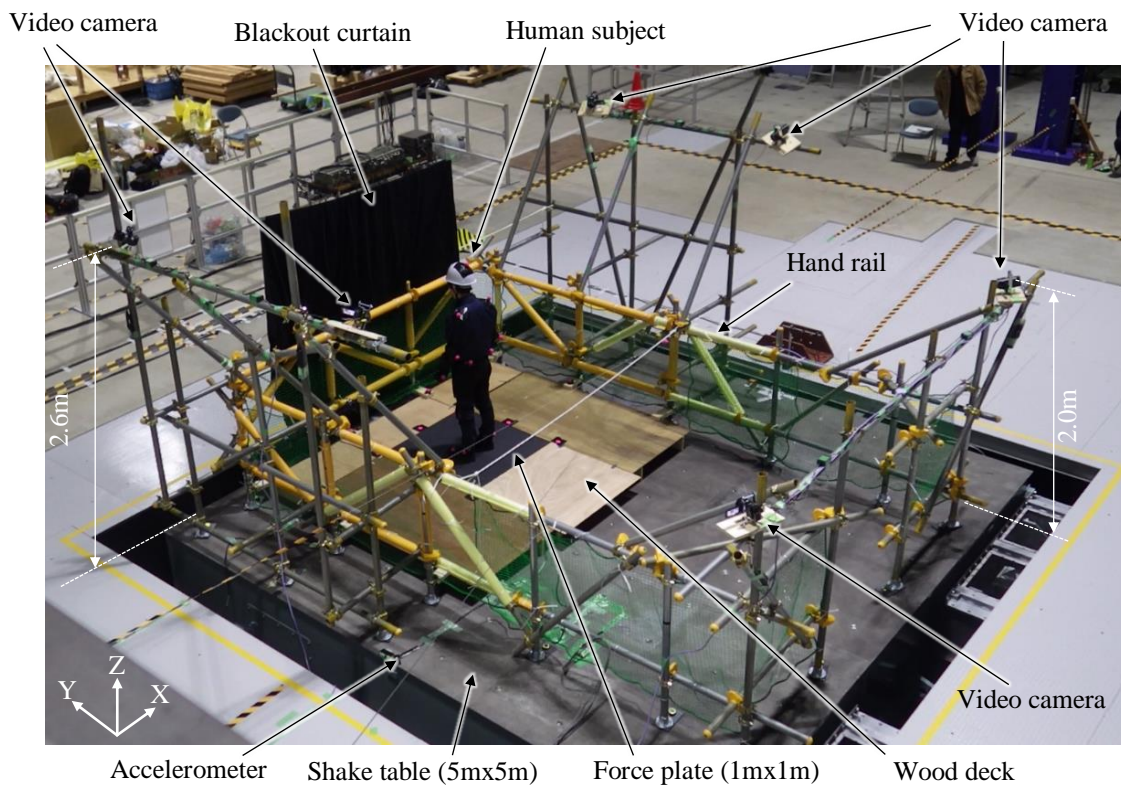
Figure 1: Bird View of Shake Table Test.

2.1 Human subject

The human subject (male, 24 years old, 169 cm, 57 kg) is shown in figure 2. The subject was put on a helmet and protectors for safety. In order to measure the behaviour of each body parts of the subject by using 3D motion capture system, markers coloured in pink were attached on each position of the subject. The displacement waveform of each markers attached to the human subject were obtained by using 3D motion capture system (DIPP-Motion V/3D). The subject was instructed to take the balance by swinging his own body or stepping, not to grab the handrail as much as possible, not to squat down, and to maintain the standing posture during the excitation.
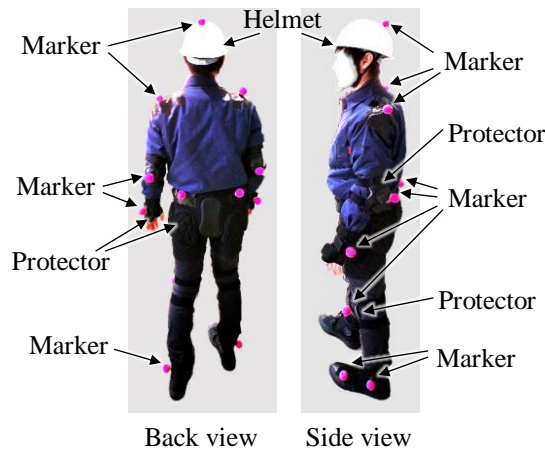
Figure 2: Human Subject

2.2 Force plate

The force plate was set on the shaking table to measure the displacement of center of pressure (CoP) of human acting on the floor. Figure 3 shows the force plate. The plate was made by honeycomb panel. Tile carpets were laid on the plate. The panel was supported vertically by four load cells, and was supported horizontally by rollers not to move in a horizontal direction. The load cells were supported by adjuster bolts to adjust height of each load cells

Center of mass (CoM) is a point that is at the center of the total body mass. The vertical projection of the CoM is defined as the center of gravity (CoG). The base support (BoS) is defined as the area of the body that is in contact with the support surface [8].
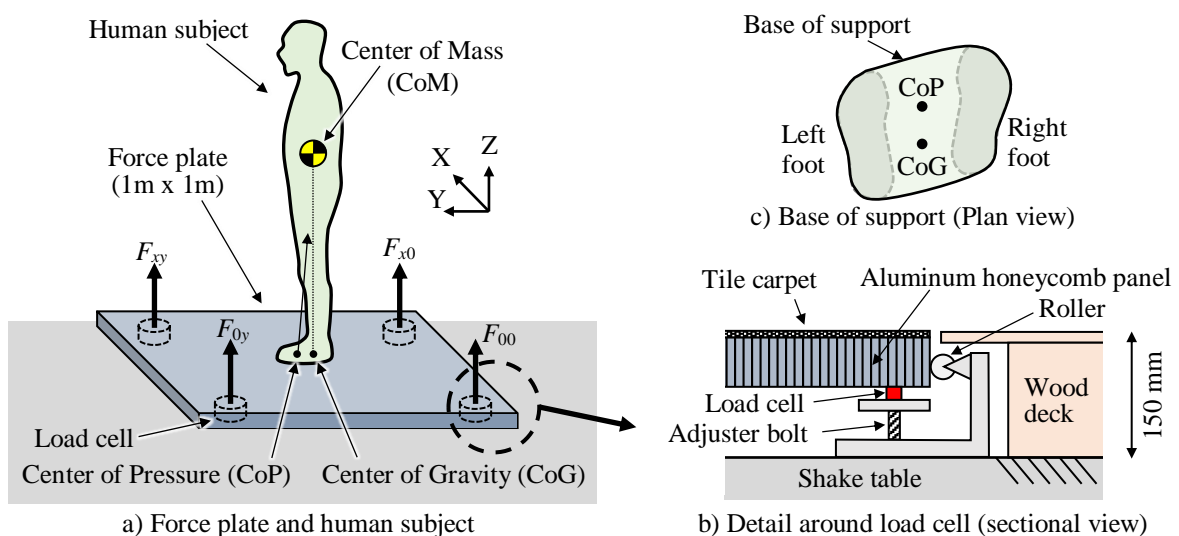
Figure 3: Force Plate

The displacement of CoP in x direction (x_{CoP}) and y direction (y_{CoP}) are calculated by the following equations, respectively.

$$x_{\text{CoP}} = \frac{L_x}{2}\left\{1 + \frac{F_{x0} + F_{xy} - \left(F_{00} + F_{0y}\right)}{F_{sum}}\right\} \tag{1}$$

$$y_{\text{CoP}} = \frac{L_y}{2}\left\{1 + \frac{F_{0y} + F_{xy} - \left(F_{00} + F_{x0}\right)}{F_{sum}}\right\} \tag{2}$$

Where, L_x and L_y are the distance of two load cells in x and y direction, respectively. F_{00}, F_{x0}, F_{0y} and F_{xy} are the vertical load measured by each load cells, shown in figure 3. F_{sum} is the summation of all loads.

2.3 Input motion

The strong motion records shown in Table 1 were used for the excitation. The records were observed on the operation floor of a reactor building of nuclear power plants during the 2011 off the Pacific Coast of Tohoku Earthquake and Niigata-ken Chuetsu-oki Earthquake in 2007 occurred in Japan [9], [10].

Table 1 Input Motion.

Name	Earthquake name	Observation site	Amp. factor
Case 1			0.50
Case 2	The Niigataken Chuetsu-oki Earthquake in 2007	Kashiwazaki-Kariwa Nuclear Power Plant, 3rd floor of Unit 7 reactor building	0.70
Case 3			1.00
Case 4			0.50
Case 5	The 2011 off the Pacific coast of Tohoku Earthquake	Fukushima Daiichi Nuclear Power Plant, 6th floor of Unit 6 reactor building	0.85
Case 6			1.00
Case 7		Fukushima Daiichi Nuclear Power Plant, seismically isolation building	1.00

Figure 4 and 5 respectively show the acceleration waveform and acceleration response spectrum of each input motion. In order to restage the situation at the actual earthquake occurrence as much as possible, the order of the input motion was made random, and excitation was carried out without telling the subject the names of the input motions.
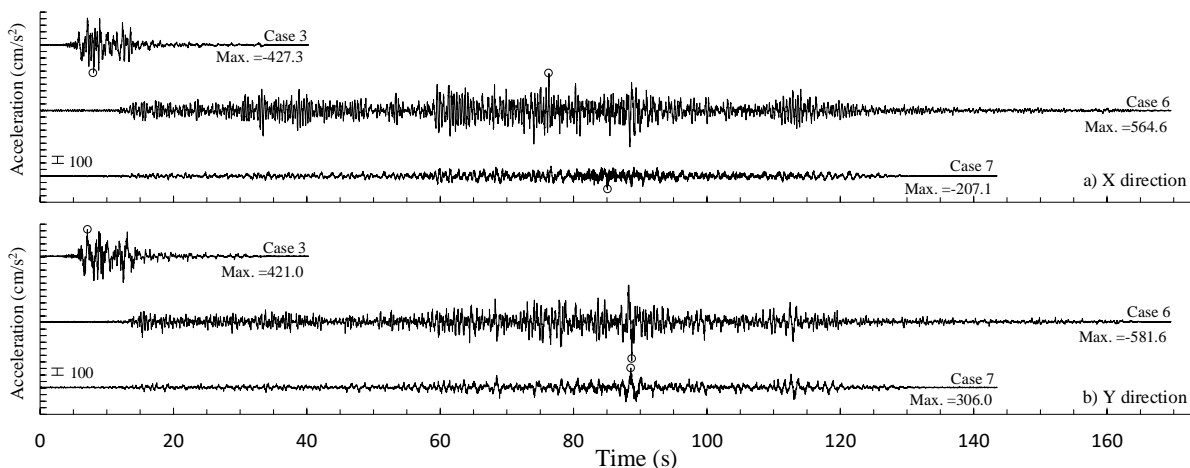
Figure 4: Acceleration Time History of Input Motion [9], [10]
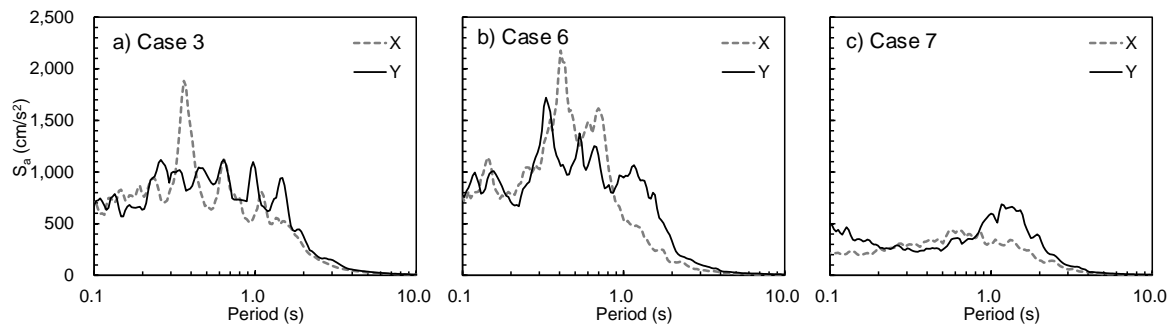
Figure 5: Acceleration Response Spectrum of Input Motion (h =5%) [9], [10]

3 MECHANISM OF STANDING POSTURAL CONTROL DURING EARTHQUAKE

Figure 6 shows time histories of relative displacement of the CoP, the CoG, shaking table, and acceleration of shaking table. Not only the acceleration of shaking table measured by the accelerometer installed on the shaking table, but also the acceleration evaluated by 3D motion capture are shown in the figure (c). For acceleration obtained by motion capture, a high-cut filter was used to remove frequency components above 8 Hz. The waveform observed by the accelerometer and the waveform obtained by motion capture are in good agreement, indicating that the measurement by motion capture is appropriate.

In figure 6, the shaking table was displaced forward from 6 to 6.8 seconds. After that, the shaking table was displaced backward around 7 seconds. At the time, the CoG was displaced forward by about 20 cm, and the CoP is also displaced forward by about 10 cm. When the subject stepped forward his left foot and the foot landed on the floor, the BoS expanded and the CoP rapidly moved forward. The CoP was displaced about 30 cm and overshot the CoG. Then, the CoG started moving backward.
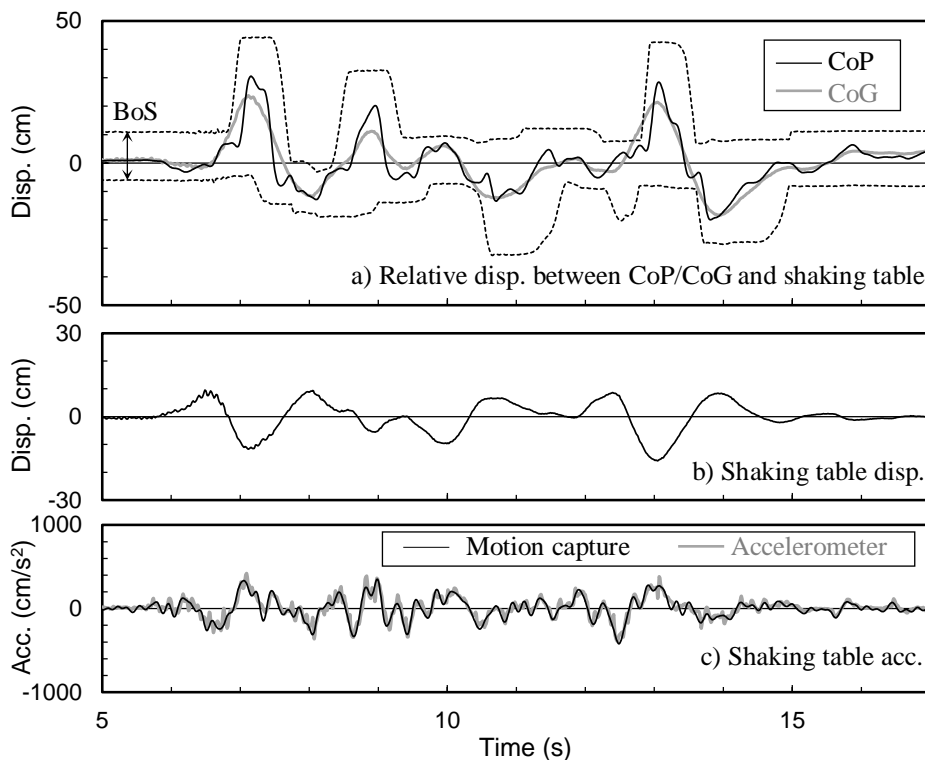
Figure 6: Time Histories of Displacement of CoP, CoG, BoS, Shaking Table, and Acceleration of Shaking Table (Case 3, y direction)

3-5

Based on the above-mentioned behavior of the human subject, a mechanisms of standing postural control of human during shaking is discussed. Figure 7 shows a conceptual diagram of the positional relationship of the CoG, the CoP, and the BoS during the stepping when the shaking table is displaced backward. In standing posture control, the purpose is to keep the CoG within the BoS. When the floor is displaced backwards by excitation, inertial force acts on the human body and the body tilts forward. Then, the CoG moves forward and deviates from the BoS (Figure 7 a). The subject then begins to step forward his foot to extend the BoS (Figure 7 b). At this time, the foot that has been stepped is in a state of floating in the air, and the BoS is only on the other foot sole that has not been stepped on, and the CoP stays within that the BoS. Subsequently, when his foot landed, the BoS expanded rapidly (Figure 7 c). As a result, the CoP is immediately displaced forward and overshoots the CoG. This corrects the posture by generating a reaction force that raises the body backward. In other words, when the CoG is moved due to shaking of the floor, a human holds his standing posture by controlling the position of the CoP.

Based on these considerations, in the next chapter, we will build a seismic response analysis model of human body based on a cart-type double inverted pendulum model that can reproduce the behavior of human body including displacement of the CoP.
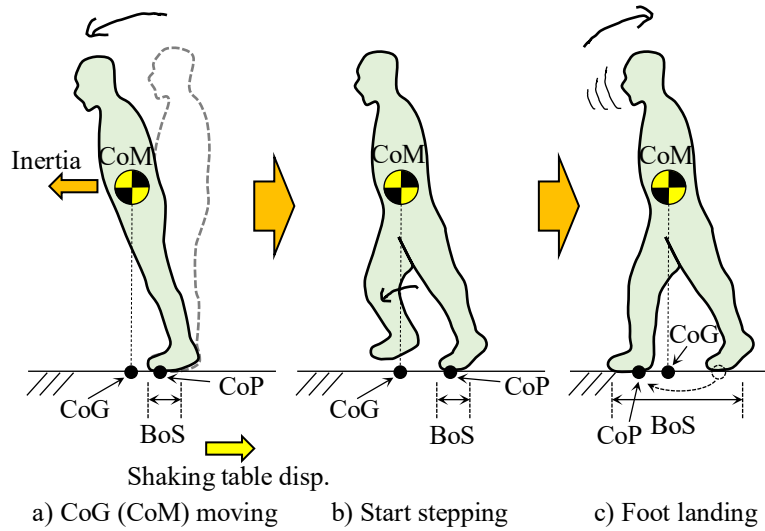
Figure 7: Behavior of CoP, CoG and BoS during Stepping

4 SEISMIC ANALYSIS MODEL OF HUMAN BODY

Figure 8 shows the seismic response analysis model of the human body based on a cart-type double inverted pendulum with feedback control system. Human body is modelled by two rigid rods. The upper rod corresponds to upper body, whereas the lower rod corresponds to lower body. Movement of the CoP due to foot stepping of human could be considered by cart moving. Hip torque of human could be considered by a torque applied on a hinge between upper and lower rods.

Assuming that the angle of the upper and lower pendulum is sufficiently small, the linearized equation of motion is given as follows.

$$d_1\left\{\ddot{\xi}(t) + \ddot{\xi}_0(t)\right\} + d_2\ddot{\theta}_1(t) + d_3\ddot{\theta}_2(t) + \mu_c\dot{\xi}(t) = f_c(t) \qquad (3)$$

$$d_2\left\{\ddot{\xi}(t) + \ddot{\xi}_0(t)\right\} + d_4\ddot{\theta}_1(t) + d_5\ddot{\theta}_2(t) - d_7\theta_1(t) = -\tau(t) \qquad (4)$$

$$d_3\left\{\ddot{\xi}(t) + \ddot{\xi}_0(t)\right\} + d_5\ddot{\theta}_1(t) + d_6\ddot{\theta}_2(t) - d_8\theta_2(t) = \tau(t) \qquad (5)$$

Where, $\theta_1(t)$ and $\theta_2(t)$ are angles with respect to the vertical line of the lower pendulum and the upper pendulum at time t, $\xi(t)$ is the relative displacement between the cart and the floor, $\xi_0(t)$ is the absolute displacement of the floor. $f_c(t)$ is horizontal force applied on the cart, and $\tau(t)$ denotes torque applied on the hinge between lower and upper pendulum. $f_c(t)$ and $\tau(t)$ are control forces as mentioned later. Note that d_1 to d_8 in the above equations are expressed by the following equations.

$$\begin{aligned}
&d_1 = m_1 + m_2 + m_c & &d_2 = m_1 l_1 + m_2 L_1 & &d_3 = m_2 l_2 \\
&d_4 = J_1 + m_1 l_1^2 + m_2 L_1^2 & &d_5 = m_2 l_2 L_1 & &d_6 = J_2 + m_2 l_2^2 \\
&d_7 = (m_1 l_1 + m_2 L_1) g & &d_8 = m_2 l_2 g
\end{aligned} \tag{6}$$

Where, m_1, m_2 and m_c are the masses of lower pendulum, upper pendulum and cart, l_1 and l_2 are the height from the lower end to the center of mass of the lower pendulum and the upper pendulum, L_1 is the total length of lower pendulum. μ_c is the damping coefficient of the cart.
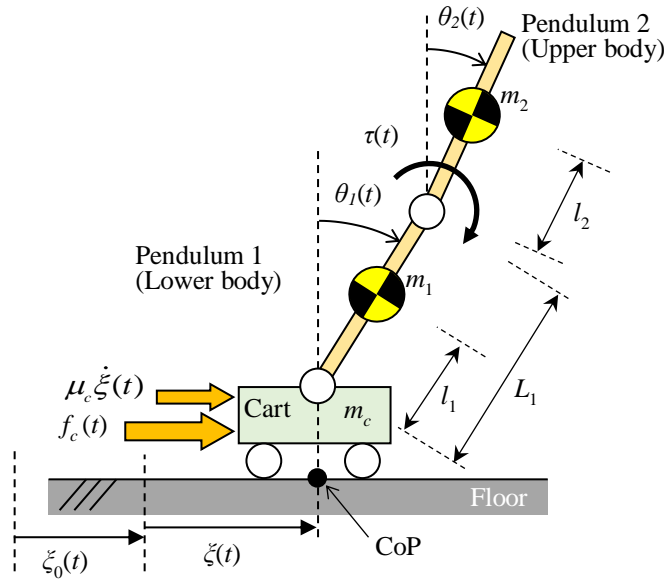
Figure 8: Seismic Analysis Model of Human Body Based on Cart-type Double Inverted Pendulum.

The equations (3)-(5) are summarized as the following equation.

$$\mathbf{D}\ddot{\boldsymbol{\theta}}(t) + \mathbf{C}\dot{\boldsymbol{\theta}}(t) + \mathbf{G}\boldsymbol{\theta}(t) = \mathbf{H}\mathbf{u}(t) \tag{7}$$

Where, the matrices $\mathbf{D}$, $\mathbf{C}$, $\mathbf{G}$, $\mathbf{H}$ are given by the following equations.

$$\mathbf{D} = \begin{bmatrix} d_1 & d_2 & d_3 \\ d_2 & d_4 & d_5 \\ d_3 & d_5 & d_6 \end{bmatrix}, \quad \mathbf{C} = \begin{bmatrix} \mu_c & 0 & 0 \\ 0 & 0 & 0 \\ 0 & 0 & 0 \end{bmatrix}, \quad \mathbf{G} = \begin{bmatrix} 0 & 0 & 0 \\ 0 & -d_7 & 0 \\ 0 & 0 & -d_8 \end{bmatrix}, \quad \mathbf{H} = \begin{bmatrix} -d_1 & 1 & 0 \\ -d_2 & 0 & -1 \\ -d_3 & 0 & 1 \end{bmatrix} \tag{8}$$

The displacement vector $\boldsymbol{\theta}(t)$ and the input vector $\mathbf{u}(t)$ in equation (7) are expressed by the following equations.

$$\boldsymbol{\theta}(t) = \begin{bmatrix} \xi(t) & \theta_1(t) & \theta_2(t) \end{bmatrix}^T \tag{9}$$

$$\mathbf{u}(t) = \begin{bmatrix} \ddot{\xi}_0(t) & f_c(t) & \tau(t) \end{bmatrix}^T \tag{10}$$

From equation (7), the following state equation is obtained.

$$\dot{\mathbf{x}}(t) = \mathbf{A}\mathbf{x}(t) + \mathbf{B}\mathbf{u}(t) \tag{11}$$

The state vector $\mathbf{x}(t)$, matrices $\mathbf{A}$ and $\mathbf{B}$ in the above equation are given by the following equations.

$$\mathbf{x}(t) = \begin{bmatrix} \boldsymbol{\theta}(t) & \dot{\boldsymbol{\theta}}(t) \end{bmatrix}^{\mathrm{T}} \tag{12}$$

$$\mathbf{A} = \begin{bmatrix} \mathbf{0} & \mathbf{I} \\ -\mathbf{D}^{-1}\mathbf{G} & -\mathbf{D}^{-1}\mathbf{C} \end{bmatrix}, \qquad \mathbf{B} = \begin{bmatrix} \mathbf{0} \\ \mathbf{D}^{-1}\mathbf{H}_2 \end{bmatrix} \tag{13}$$

The block diagram of the model is shown in figure 9.
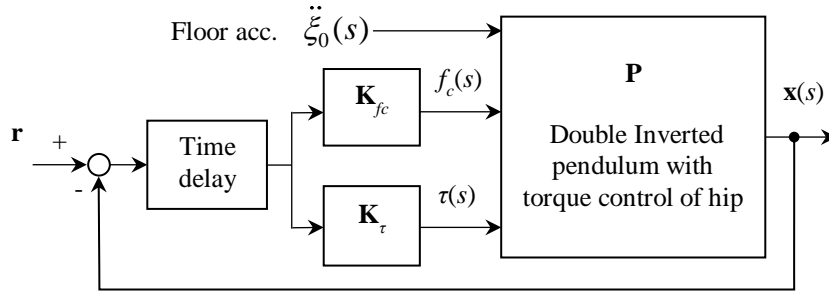
Figure 9: Block Diagram of Seismic Analysis Model of Human Body.

When a human controls his standing posture, there is a time delay of control force generation due to nerve transmission time lag, information processing time lag in the brain, control force generation time lag in the nerve-muscle-skeletal system, and so on. In this study, this time delay is considered as a dead time (L) in the feedback control system, and the difference between the state ($\mathbf{x}$) and the reference value ($\mathbf{r}$) is delayed for a certain time before being input to the controller. Considering the dead time (L), the Laplace transform of the control force applied to the cart $f_c(s)$ and of the control torque applied to the hip $\tau(s)$ is expressed by the following equations.

$$f_c(s) = -\mathbf{K}_{fc}\mathbf{x}(s)e^{-Ls} \tag{14}$$

$$\tau(s) = -\mathbf{K}_{\tau}\mathbf{x}(s)e^{-Ls} \tag{15}$$

Where, $\mathbf{K}_{fc}$ and $\mathbf{K}_{\tau}$ are the feedback gain expressed by the following equations.

$$\mathbf{K}_{fc} = \begin{bmatrix} k_{f\xi} & k_{f\theta_1} & k_{f\theta_2} & k_{f\dot{\xi}} & k_{f\dot{\theta}_1} & k_{f\dot{\theta}_2} \end{bmatrix} \tag{16}$$

$$\mathbf{K}_{\tau} = \begin{bmatrix} k_{\tau\xi} & k_{\tau\theta_1} & k_{\tau\theta_2} & k_{\tau\dot{\xi}} & k_{\tau\dot{\theta}_1} & k_{\tau\dot{\theta}_2} \end{bmatrix} \tag{17}$$

Where, $k_{f\xi}$, $k_{f\theta1}$, $k_{f\theta2}$, $k_{f\dot{\xi}}$, $k_{f\dot{\theta}_1}$ and $k_{f\dot{\theta}_2}$ are the feedback gains of f_c, multiplied to the state variables (the relative displacement between the cart and the floor, the angles of the lower and upper pendulum, the relative velocity of the cart, and the angular velocity of the lower and upper pendulum). Similarly, $k_{\tau\xi}$, $k_{\tau\theta1}$, $k_{\tau\theta2}$, $k_{\tau\dot{\xi}}$, $k_{\tau\dot{\theta}_1}$ and $k_{\tau\dot{\theta}_2}$ denote the feedback gains of τ, multiplied to the state variables, respectively.

5   ANALYTICAL RESULT OF SEISMIC RESPONSE ANALYSIS MODEL OF HUMAN BODY

Table 2 shows the parameters of the inverted pendulum. The length and weight of the pendulum were set based on the height and weight of the human subject of the shaking table test. The rotational

inertias J_1 and J_2 were calculated from the height of the human subject's center of mass of body segments and the mass distribution. The dead time L was set to 0.1 s.

Table 2 Parameter of Cart-type Double Inverted Pendulum Model.

m_1	m_2	l_1	l_2	L_1	J_1	J_2	μ_c	g
18.3 kg	38.7 kg	0.432 m	0.376 m	0.863 m	1.66 kgm^2	5.12 kgm^2	10000 Ns/m	9.8 m/s^2

In this study, the behaviour in the Y direction, the backward and forward direction of the subject, is dealt with. After finding the optimum feedback gain with a linear quadratic regulator (LQR), the feedback gains were adjusted so that the analytical result corresponds to the behaviour of the test subject in case 3 of the shaking table test. Table 3 shows the feedback gains.

Table 3 Feedback Gain.

$k_{f\xi}$	$k_{f\theta1}$	$k_{f\theta2}$	$k_{f\dot{\xi}}$	$k_{f\dot{\theta}1}$	$k_{f\dot{\theta}2}$
0	-39450	-15100	-15660	-13360	-6160

$k_{\tau\xi}$	$k_{\tau\theta1}$	$k_{\tau\theta2}$	$k_{\tau\dot{\xi}}$	$k_{\tau\dot{\theta}1}$	$k_{\tau\dot{\theta}2}$
0	-150	100	-50	-30	40

Figure 10 shows the time history waveforms of the relative velocity and the relative displacement of the head with respect to the shaking table, and the relative displacement of the CoP by experiments and analysis. The waveforms analysed by the inverted pendulum model corresponded well to the experimental results in both phase and amplitude.
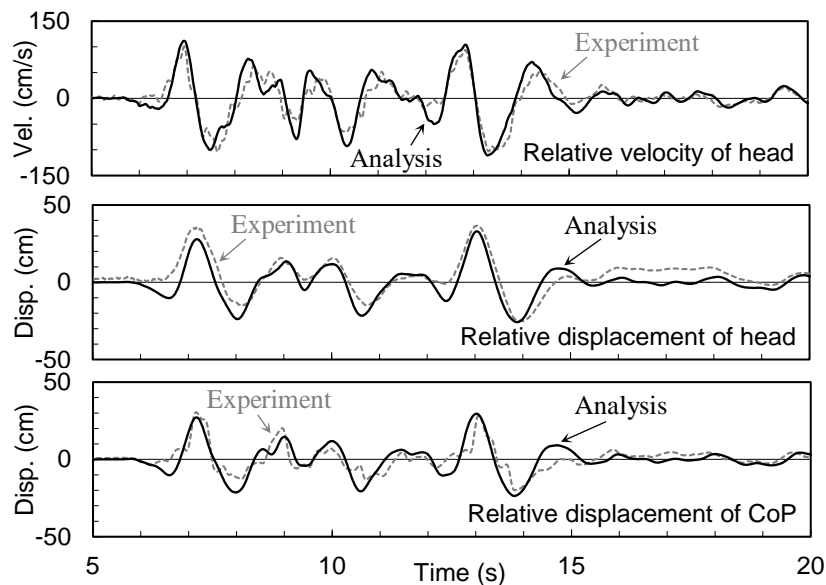
Figure 10: Time Histories of Motion of Head and CoP

In order to further examine the validity of the analysis model, the shaking table accelerations in all the excitation cases of Cases 1 to 7 were input to the analysis model, and the calculated behaviours of the head and the CoP were compared with the experimental results. Figure 11 shows the relationship between the experimental results and the analytical results of the maximum relative displacement of the CoP and that of head, and the maximum relative velocity of head. The numbers in the figure indicate the excitation case numbers. The maximum values calculated by the model showed good agreement with those of the experimental results. Therefore, the displacement of foot and head, and the velocity of head can be predicted accurately by using the cart-type double inverted pendulum model.

a) Relationship between maximum displacements
of experiments and those of analyses
(Number: Case No. of experiment)

b) Relationship between maximum head
velocities of experiments and those of analyses
(Number: Case No. of experiment)
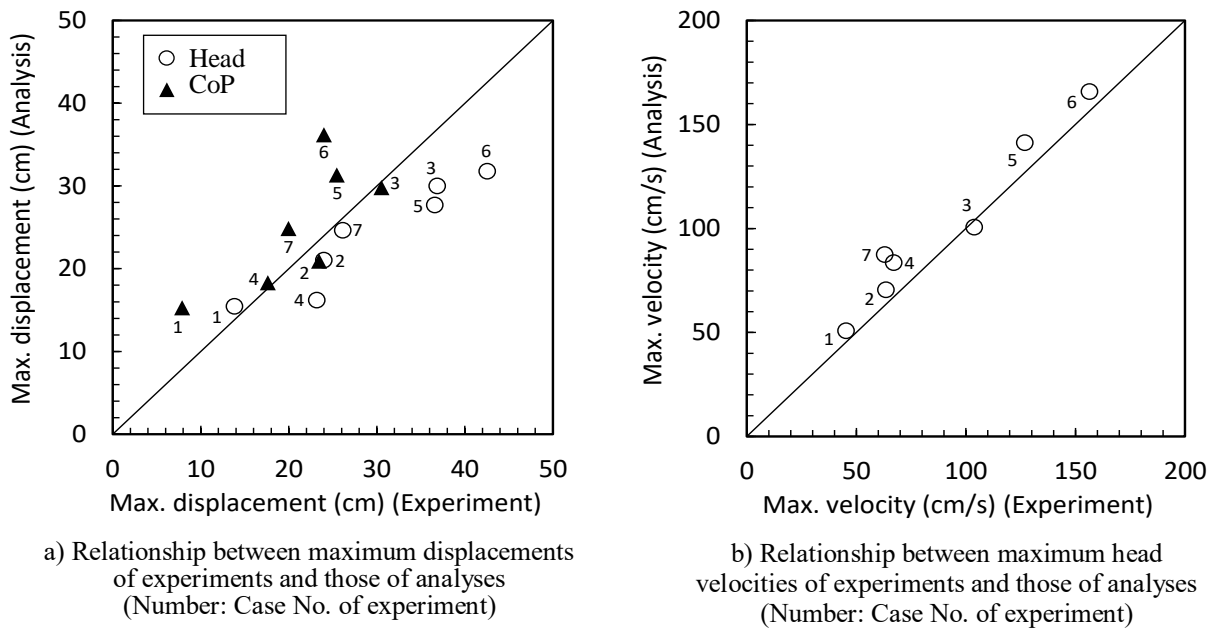
Figure 11: Comparison of Motion between Experiment and Analysis Model.

6   EVALUATION OF HUMAN INJURY BY USING HEAD INJURY CRITERION

The maximum value of relative displacement of head relates to the possibility of hitting to object, and the maximum displacement of CoP relates to an increased risk of falling over in narrow spaces or falling down from staircases and so on. Furthermore, human can suffer severe damage if they hit their head to object such as wall and furniture. Considering those facts, we evaluated the possibility of human injury based on maximum displacement of head and CoP, and Head Injury Criterion (HIC) score developed by National Highway Traffic Safety Administration [11]. The HIC score is defined by the following equation.

$$HIC = \left\{ \left[\frac{1}{t_2 - t_1} \int_{t_1}^{t} a(t)dt \right]^{2.5} (t_2 - t_1) \right\}_{max} \tag{18}$$

Where, $a(t)$ is the acceleration of the head at the time of hitting to an object, t_1 and t_2 denote integration interval, t_2-t_1 was set to 15 msec. "Max" denotes to select the integration interval to

maximize HIC. We assumed that the amplitude of acceleration acting on the head is constant during hitting time Δt. Furthermore, by using the relative velocity of the head with respect to the object right before the hitting, V_0, and the coefficient of restitution between the head and the object, e, we get the following equation.

$$HIC = 0.015 \left\{ \frac{V_0}{\Delta t}(1+e) \right\}^{2.5} \tag{19}$$

Note that the HIC calculated by equation (19) is derived by the maximum velocity of head and assuming that human hit his head to rigid plane. This assumption can lead overestimation of human injury.

The coefficient of restitution, e, and hitting time, T, were set based on previous researches [12]. HIC values reaches 50% probability of injury levels are showed in table 4 [13]. The table also shows the relationship between head velocities (V_0) and HIC score derived by equation (19).

Table 4 HIC score and Head Velocity Corresponds to Injury Level.

Injury (p=50%)	HIC score	Head velocity (cm/s)
Minor (head injury without disturbance of consciousness)	331	205
Moderate (skull fracture)	593	259
Critical (cerebral contusion)	1848	408
Fatal (death)	2175	435

In addition to the waveforms used in this experiment, the strong motion records observed in Japan during the 1995 Hyogoken Nanbu Earthquake (JMA Kobe NS and JR Takatori NS), the 2016 Kumamoto Earthquake (KiK-net Mashiki EW), and 1968 Tokachi-oki Earthquake (Hachinohe NS), were used to investigate probability of injury further. HIC and the maximum values of the relative displacement of the head and that of CoP are shown in figure 12.
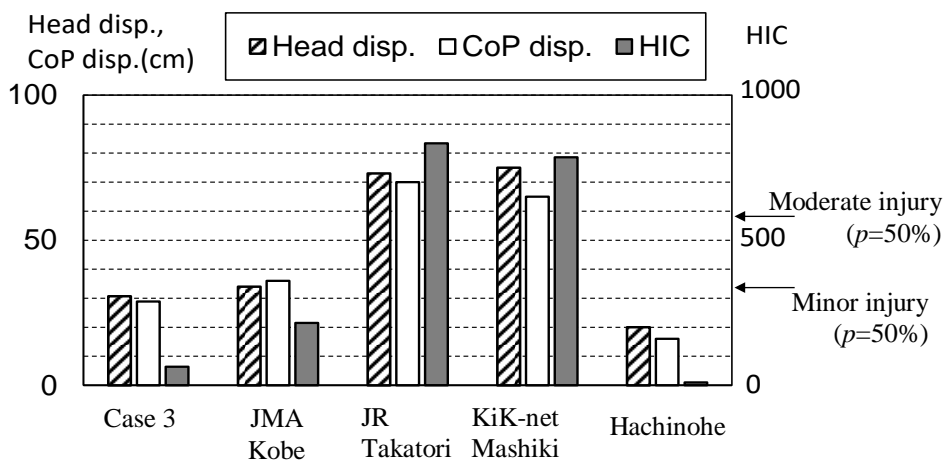
Figure 12: Maximum Displacement of Head and CoP, and HIC Score

The displacement of the head and the CoP are small in Hachinohe case. In addition, the HIC score is extremely small in the case. In the JMA Kobe case, the displacement of the head and the CoP are less than 40 cm, and HIC score is below the level at which the probability of minor injuries is 50%. On the other hand, in the JR Takatori case and the Kik-net Mashiki case, the displacements of the head and the CoP are beyond 60 cm. In the cases, the HIC scores are extremely high at around 800, and are beyond the 50% probability of moderate injury in those cases. Thus, the characteristics of strong motions significantly affect the probability of injury. By using the seismic response analysis model of the human body developed in this study, it is possible to quantitatively evaluate the possibility of human injury during an earthquake.

7 CONCLUSION

In this study, we developed a seismic response analysis model of human body based on the shaking table tests. The model was constructed by cart-type double inverted pendulum model with feedback control system. Then, the probability of human injury was evaluated by using HIC score derived from head velocity calculated by the seismic analysis model of human body. The obtained findings are shown below.

1) When CoG is moved due to shaking of the floor, a human holds his standing posture by controlling the position of CoP.

2) Relative displacement of CoP and head, and relative velocity of head with respect to the floor could be evaluated accurately by using the cart-type double inverted pendulum model.

3) The characteristics of strong motions significantly affect the probability of injury.

4) By using the seismic response analysis model of the human body constructed in this study, it is possible to quantitatively evaluate the possibility of injury.

REFERENCES

[1] Nachi, N., and Okada, S., "Probabilistic Seismic Casualty Models and Simplified Method to Evaluate Seismic Casualty Risk", Journal of Structural and Construction Engineering, AIJ, 72(616), 97-104, 2007 (in Japanese)

[2] Takahashi, T., Saito, T., Azuhata, T., and Ohtomo, K., "Shake table Test for Indoor Human Response and Evacuation Limit," Journal of 5th International Conference on Earthquake Engineering, 187-193, 2010

[3]   Hida, T., Nagano, M., Takehiko, T., and Kaneko, T., "Impossibility Ratio of Evacuation in Super High-Rise Residential Buildings Based on Questionnaire Survey After The 2011 Off The Pacific Coast of Tohoku Earthquake and Shake table Tests," AIJ Journal of Technology and Design, 20(45), 521-526, 2014 (in Japanese)

[4]   Takahashi, T., Watanabe, S., Nakamura, Y., and Saito, T., "Study on the Impact of Furniture Turnover onto Human during Strong Motion -Experimental study of furniture turnover using dummy doll-," Journal of JAEE, 16(3), 126-136, 2016 (in Japanese)

[5]   Kudoh, S., Komura, T., and Ikeuchi K., "Modeling and Generating Whole Body Motion of Balance Maintenance," IEICE Transactions on Information and Systems, D-II, Vol. J88-D-II, No.8, 1582-1591, 2005 (in Japanese)

[6]   Uenishi, K., Matsuhisa, H., Utsuno, H., and Park, J., "Dynamic Model for Car Occupants in Head-on Collisions," IEICE Transactions on Information and Systems, C, 71(704), 2005

[7]   Yamamoto, M., "human body dynamics under horizontal ground motions: shake table tests and simplified modeling under standing conditions," Journal of Structural and Construction Engineering, AIJ, 76(667), 1631-1637, 2011 (in Japanese)

[8]   A. S. Cook and M. H. Woollacott, "Motor Control ,Translating Research into Clinical Practice," Fifth Edition, Wolters Kluwer, 2017

[9]   Japan Association for Earthquake Engineering, Main Shock Record of The 2011 off the Pacific coast of Tohoku Earthquake Observed at Fukushima Daiichi and Daini Nuclear Power Plant, TEPCO Corp., Revised Edition (CD-ROM).

[10]   Japan Association for Earthquake Engineering, All Strong Motion Records at Kashiwazaki-Kariwa Nuclear Power Plant, TEPCO Corp., Revised edition (DVD).

[11]   NHTSA (1999), Development of improved injury criteria for the assessment of advanced restraint systems-II, 1999

[12]   Anata, K., Konosu, A., Isshiki, T., Mori, K., Morita, T. and Yoshinari, S., "Development of Safe and Comfortable Protective Headwear," LIFE2012, Japan Human Factors and Ergonomics Society, 2012 (in Japanese)

[13]   Nakano, M., Matsuura, H., Tamagawa, M., Yamanaka, M., and Yukimasa, T., "Theoretical Analysis of Head Injury Criterion (HIC)", Journal of Biomedical Fuzzy Systems Association, 12(2), 57-63, 2010 (in Japanese)

Shaking Table Test On Quantification Of Anxiety Using Head Mount Display During Strong Vibration

Jinglin Xu [1], Satoshi Ishikawa [1], Toru Takahashi [2]
Chiba University
1-33, Chiba, 263-8522, Japan
ayfa6114@chiba-u.jp, basketball_center_1020@yahoo.co.jp, takahashi.toru@faculty.chiba-u.jp

Takuzo Yamashita [3]
National Research Institute for Earth Science and Disaster Resilience (NIED)
3-1, Ibaraki, 305-0006, JAPAN
tyamashi@bosai.go.jp

ABSTRACT

Nowadays, more and more people pay attention to the safety and health of human body under strong vibration. Quantifying the level of anxiety under vibration is valuable for clarifying the structural performance needed for human safety and will facilitate the communication between structural designers and clients about comfort. Chiba University has been devoting itself to the study of the anxiety of human-body induced by earthquake vibration since 2000, and has preliminarily obtained a curve to describe the Anxiety quantitatively. It is defined as "Anxiety curve of Human Body under Vibration"(AHV). In this study, a shaking-table test for humans who are wearing a head-mounted display (HMD) was performed to quantify the levels of anxiety during strong vibration. A virtual scene consisting of a living room with several pieces of furniture was simulated using virtual reality (VR). The period, speed, and shape of input vibration were varied for each VR-based situation. The results of the test show that a longer shaking period produced lower levels of anxiety. The results of this study will further advance our understanding about how vibration in a building affects the anxiety of its occupants during strong vibration.

1   INTRODUCTION

When a strong vibration occurs, evaluating the ability to evacuate according to factors such as human anxiety is very important for ensuring human-body safety. In this study, a shaking-table test for humans using a head-mounted display (HMD) was performed to quantify anxiety during strong ground vibration. To evaluate the influence of strong vibration, virtual reality (VR) was used to simulate a living room with a table, sofa, chairs, television, bookshelf, and sideboard during strong vibration. The aim was to assess the difference in the level of anxiety experienced by subjects using a shaking table and an HMD that displayed views of a virtual scene in which the furniture either fell to the side or forward under the vibration.

2   SHAKING-TABLE TEST

The shaking-table test (Fig.1) were performed as early as from Oct, 2000. The recent experiment was operated in Jul 22th, 2019. We conducted experiments on 140 subjects (95% male and 5% female), using a simple vibration table installed in the Building Engineering Laboratory at

Chiba University, Japan. We asked subjects to answer a questionnaire after experiencing multiple vibration that were presented with a virtual scene of falling furniture, displayed under the same vibration conditions. In each experiment, the subject's bioinformatics were measured and the acceleration was measured by accelerometers attached to the shaking table and one subject's head.
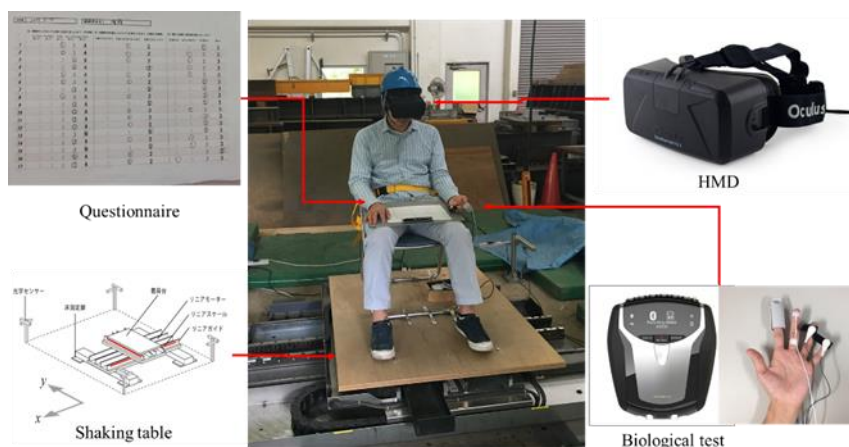
Fig. 1 experimental setup

2.1 HMD

In the experiment, we use HMD (Oculus rift) as the display device. It can block the visual contact between the experimenter and the outside environment during the experiment. It can output the specified sound, image and other information according to the needs of the experiment. while the shaking table operates with the input waves, the display device can simultaneously play the three-dimensional video image, such as the collapse and offset of indoor furniture. It can help us to obtain the most real anxiety data of the subjects.
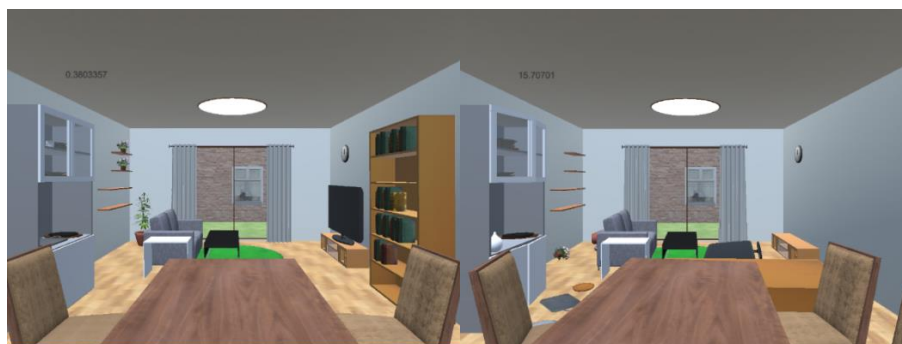
Fig. 2 Virtual scene in which furniture collapses:
(left) before vibration and (right) after vibration.

2.2 The experiment wave of the vibration

In the test, six vibration periods (0.4, 0.6, 1.0, 2.0, 3.0, and 4.0 s), four levels of input vibration (0.1, 0.15, 0.3, and 0.6 m/s), and five input directions (x-direction, y-direction, O-shape, 8-shape, and ∞-shape) were performed for each viewpoint of the virtual scene. However, some of these inputs were abandoned because of the limitations of the stroke and maximum acceleration of the vibration table. Therefore, each participant was subjected to a total of 142 inputs in this experiment. Vibration was continued for a duration of 12 to 32 s, and the excitation sequence was random to take into account the psychological impact on the subject. The magnitude of the internal change has a significant impact on three indoor conditions: whether the bookshelf falls, the television falls, or the table falls.
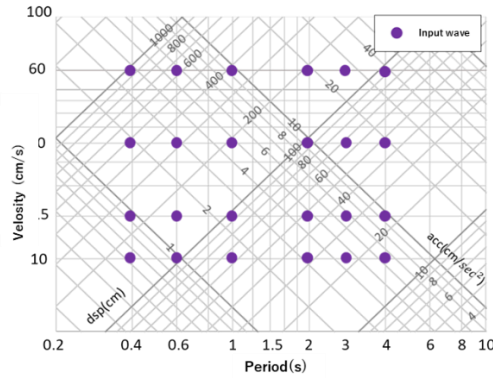
Fig. 3 the experiment wave of the vibration.

2.3 Questionnaire

The subjects were asked to answer a questionnaire after each shaking-table vibration was completed. The questionnaire evaluated three main aspects: the degree of anxiety (on a scale from 0 to 4), ability to take action (on a scale from 0 to 2), and difference between shaking and display. The questions (Partial content) are shown in Table 1.

2.4 Biological test

In order to identify the validity of the anxiety questionnaire, we installed NeXus-10 MarkIIon one hand of the subjects. It consists of blood volume pulse (BVP), electro dermal activity (EDA), temperature (TMP). By comparing the data, some probabilistic errors can be eliminated from the data of the questionnaire.

Table 1 Questionnaire (Partial content)

(A) How did you feel in the shaking table experiments? (Degree of anxiety)	
0. I had no anxiety.	1. I felt a little anxiety.
2. I felt anxiety.	3. I felt some anxiety.
4. I felt a lot of anxiety.	
(B) Do you think you could take action if it were the real earthquake? (Ability to take action)	
0. I can take action.	1. I am not sure whether I can take action or not.
2. I do not think I can take action.	
...	

3 TEST RESULTS

By comparing the effects of three generations of HMD used in the past, it is found that the standard deviation is smaller in the case where HMD is mounted, and the stability of the data is improved.

3.1 Analysis of questionnaire

The results of the questionnaire after each input vibration are presented with the bubble charts (Fig. 4). The X axis is the maximum speed of input wave and the Y axis is the level of anxiety. The size of the bubble is related to the number of subjects who gave the same answer. Finally, a straight line was fitted to the data using the weighted least squares method. In this study, we focus on the degree of anxiety in the questionnaire results.

According to figure 4, the degree of anxiety of type O is relatively high, and It's guessed that it is due to the large eccentricity of type O. On the other hand, the degree of anxiety of type Y is relatively low. It's guessed that the seat is supported in the front and rear directions, part of the body sloshing is eliminated. In the vibration video of HMD, the long edge of furniture is set in the Y direction. so it is not easy for the experimenter to catch the furniture's moving in this direction, which indirectly reduces the occurrence of anxiety.

According to figure 5, Under the same speed of vibration, the shorter the period, the higher the degree of anxiety. In other words, a longer shaking period produced lower levels of anxiety. The author thinks that it is caused by the rising of the acceleration with the shortening of the period. Under the same period of vibration, the faster the speed, the higher the degree of anxiety.

Based on the Figure 6 it is found that the value of anxiety increases with the increase of acceleration. This shows that in addition to speed, acceleration is also an important factor affecting human-body anxiety. When the acceleration exceeded 600 cm/s2, the value of anxiety was close to 4, which indicated that the subjects felt great anxiety.
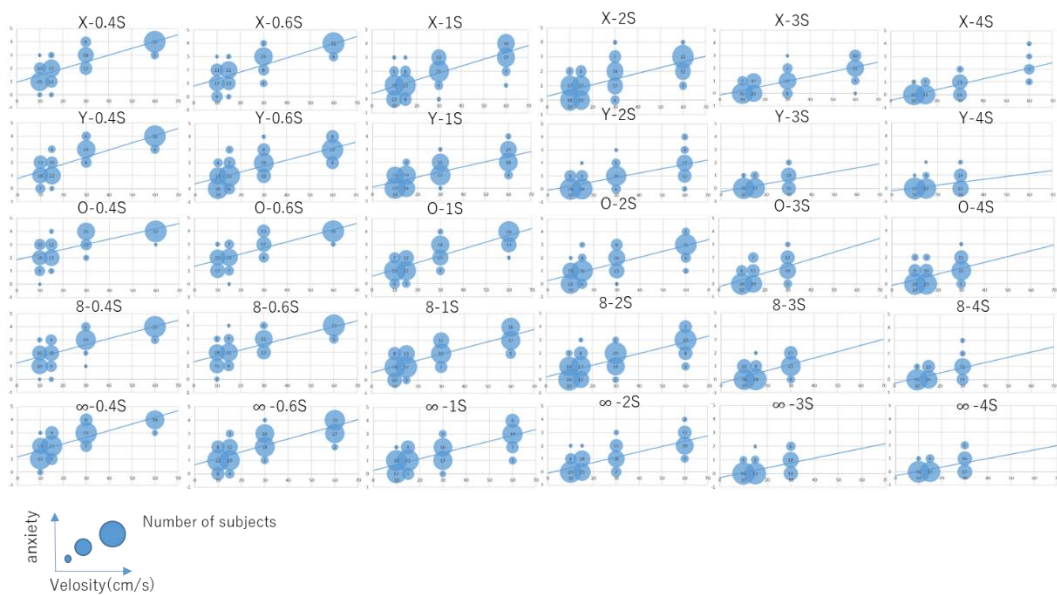
Fig. 4 Bubble charts of anxiety
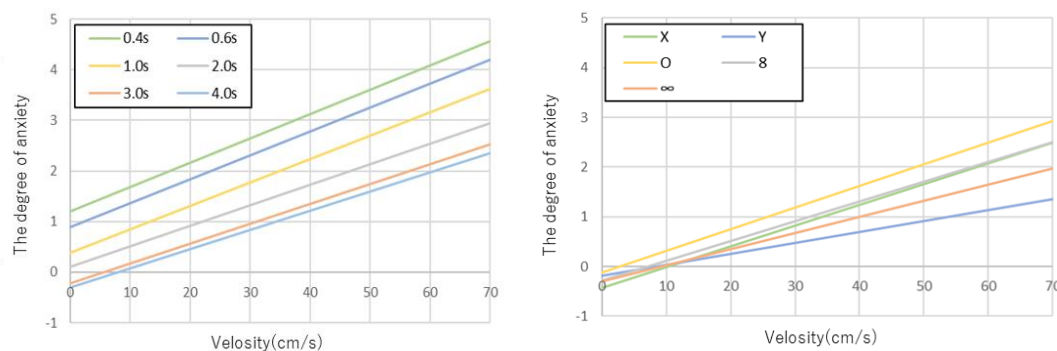
Fig.5 comparison of anxiety line
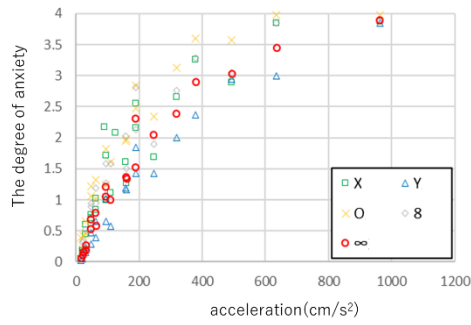
Fig.6 The correlation of anxiety and acceleration

3.2   Analysis of Biological test

In this study, three biological information such as BVP (blood volume pulse), EDA (electro dermal activity), and TMP (temperature: skin temperature) are measured. However, the noise was added to the result of BVP with the strong vibration. Some analytical values were overvalued.

According to Fig.7, It shows that the value of EDA is inversely proportional to the period of vibration. The smaller the period of vibration, the larger the value of EDA. On the other hand, the value of EDA is proportional to the speed of vibration. As the speed increases, the value of EDA increases. Especially when the acceleration of vibration exceeds 200 cm/s2, there is an obvious increase of the value of EDA. Among all the formation of vibration, the increasing trend of O-type is the most obvious.

The reaction value of TMP becomes larger as the speed increases. when the acceleration of vibration exceeds 100 cm/s2, there is an obvious correlation between the acceleration and TMP.

The above analysis of the data is basically consistent with the results of the questionnaire, which proves the validity of the questionnaire.
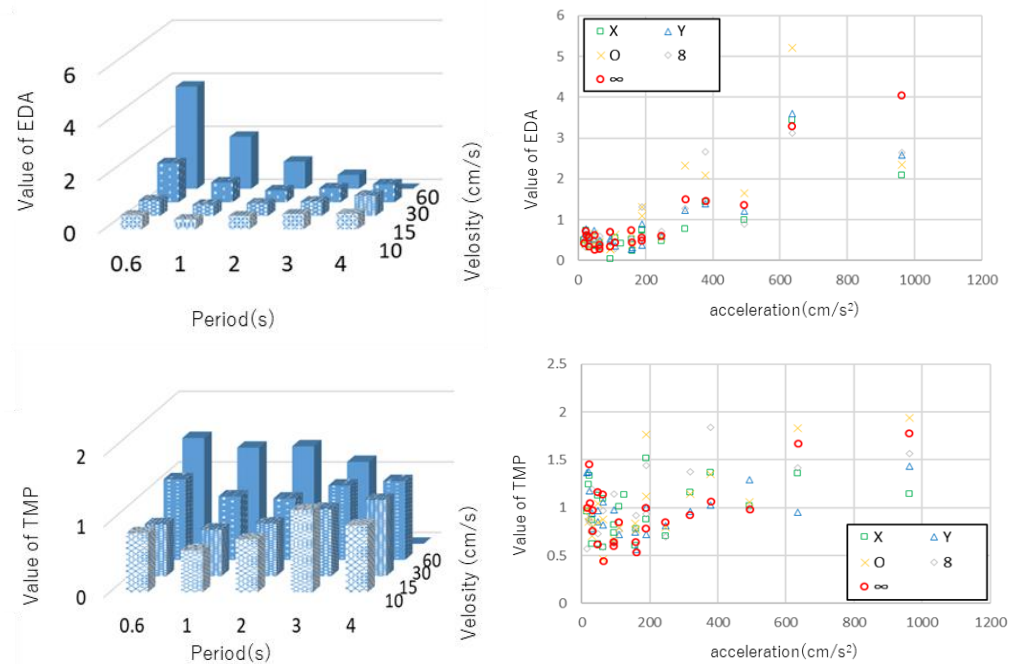
Fig. 7 anxiety analysis of Biological test

4-5

3.3   Anxiety curve of Human Body under Vibration (AHV)

Based on the results of the questionnaire and biological test, Fig.8 is produced to evaluate the anxiety of the strong vibration. Firstly, divide bubble graph from each periodic zone, and draw an approximate straight line. Then, an approximate straight line is used to obtain the velocity for each anxiety value. Period of building is plotted on the trapetite diagram on the X-axis and the velocity of vibration is plotted on the Y-axis. It is connected with the same anxiety values. Do it at each vibration type, and a performance evaluation curve was obtained (Fig.8). Connect the lowest point of the evaluation curve in all vibration types and produce the most dangerous AHV curve.

Comparing with each vibration type, it is understood that the degree of anxiety in the O-type is higher than in the Y type. In addition, the slope of AHV is especially larger in the short period side in the region where the speed is from 0 to 40 cm/s. From this fact, it is understood that the rise in the acceleration leads to the rise of the anxiety. On the other hand, the slope of the evaluation curve is smaller in the long period side, and the rise of the velocity affects the rise of the anxiety. Especially, when the speed exceeds 40 cm/s, the slope of the anxiety evaluation curve on the short period side is smaller than the long period side. It shows that the speed of vibration has a great influence on the value of the anxiety than the acceleration of the vibration.
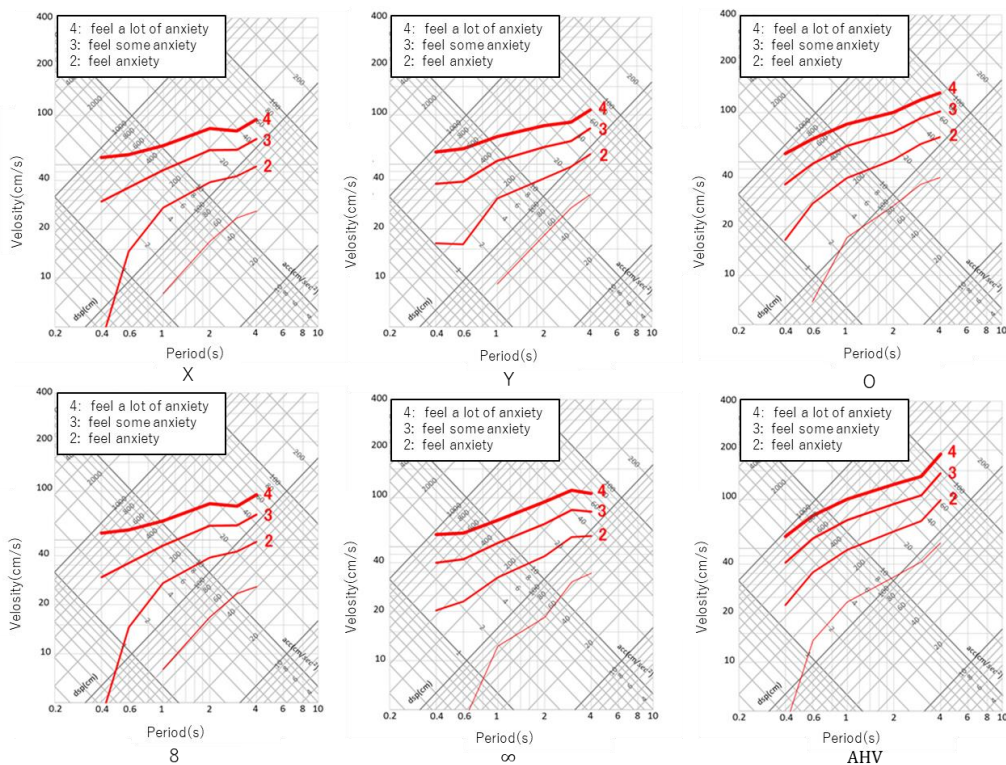
Fig. 8 Anxiety curve of Human Body under Vibration (AHV)

4   CONCLUSION

In this study, we investigated the effect of vibration parameters on human anxiety from questionnaires and biometric test using HMD. As the result, it was found that: the anxiety of human body under vibration is closely related to the formation, speed, acceleration and period of the vibration. It is easier to feel anxiety under the vibration of O type than the vibration of Y type. A longer shaking period produced lower levels of anxiety. It also can be concluded that in the short period of vibration, The greater the speed, the greater the anxiety. In the long period, the greater the acceleration, the greater the anxiety. However, there are still some defects in this experiment. For example, the age and sex ratio of the subjects are still not uniform. The stock of experimental data is still not large

enough. In the next experiments, we will constantly improve the shortcomings in this area to get more accurate expressions about anxiety of human-body under vibration.

REFERENCES

[1] T. Takahashi, T. Suzuki, T. Saito, T. Azuhata, and K. Morita: Shaking Table Test for Indoor Human Response and Evacuation Limit, Joint Proc. 7CUEE & 5ICEE, Tokyo Institute of Technology, Paper No. 17, pp. 187-193, 2010.

[2] T. Takahashi, M. Sadahiro, T. Saito, T. Azuhata, K. Morita, K. Noguchi, and C. Minowa: Shaking Table Test on Indoor Seismic Safety of High-rise Buildings, Part I. Performance Test on BRI Large Stroke Shaking Table. Part II. Movement of Furniture Under Long Period Earthquake Ground Motion, Proc. 14WCEE, Paper IDs: S10-024 and S10-014, 2008.

[3] T. Takahashi, M. Sadahiro, T. Suzuki, T. Saito, T. Azuhata, K. Noguchi, and C. Minowa: Shaking Table Test on Indoor Human Performance Limit in Strong Motion for High-Rise Buildings, Proc. 8th Pacific Conference on Earthquake Engineering, Paper No.131, 2007.

[4] T. Takahashi, A. Mazaki, T. Saito, T. Azuhata, and K. Noguchi: Shaking Table Test on Indoor Human Performance Limit in Strong Motion, Proc. 12JEES, Paper No. 0322, 2006.

[5] T. Takahashi, T. Azuhata, T. Saito, and K. Ohtomo: Structural Performance Considering Human Response Limit During Strong Earthquake, Proc. JCOSSAR2003, JSME, Vol. 5, pp. 825-828, 2003.

[6] T. Takahashi, T. Azuhata, K. Noguchi, D. Kounsana, and Y. Watanabe: Shaking table test on indoor human response and its feeling in strong ground motion, Summaries of Technical Papers of Annual Meeting of the AIJ, B2 pp. 861–864, 2001.

[7] M. Wada, A. Masuzawa, T. Yamashita and T. Takahashi: Experimental Study on Quantification of Anxiety under Strong Motion using Two Dimensional Small Shaking Table, Journal of Structural Engineering, Architectural Institute of Japan, Vol. 64B, pp. 345-350, March 2018.

[8] Yohji Watanabe, Ginga Kimura, Yukiko Nakamura, Toru Takahashi: Experimental study on the quantification of anxiety level during strong earthquake, Part 1 Consideration from the questionnaire results, Architectural Institute of Japan Academic Papers Summary pp. 919-920, 2014.9.

[9] Akira Masuzawa, Yuudai Ohno, Ginga Kimura, Yukiko Nakamura, Toru Takahashi: Experimental study on the quantification of anxiety level during strong earthquake, Part 3 Reproduction of the situation during strong earthquake using HMD, Architectural Institute of Japan Academic Papers Summary pp. 865-866, 2015.9.

A consideration of earthquake vibration sense of human in buildings by using real-time questionnaire system

Mutsuhiro Yoshizawa [1], Harumi Yoneda [2], Masashi Yamamoto [3]
Takenaka Corporation, Research and Development Institute
Otsuka 1-5-1, 270-1395 Inzai, Chiba, Japan
yoshizawa.mutsuhiro@takenaka.co.jp, nishimura.harumi@takenaka.co.jp,
yamamoto.masashia@takenaka.co.jp

ABSTRACT

In Japan, social needs for the building seismic performance are changing not only to the life safety but also to the maintenance of functionality after the earthquake. So the human condition during building shaking by earthquakes is also beginning to be considered as a part of the functionality of the building.

The Great East Japan Earthquake is mentioned as an example that the building shaking by earthquakes affected the maintenance of human physiological functions. Many questionnaire surveys were conducted targeting the Great East Japan Earthquake, and it was revealed that high-rise building users felt fear and anxiety during earthquake.

However, since such questionnaires are limited to large-scale earthquake disasters, there is a problem that answers to relatively small tremors cannot be obtained, and investigation cannot be conducted immediately after the earthquake. Regarding the influence that the earthquake motion has on the psychological anxiety and human physiology, there is a possibility that a correct answer cannot be obtained after a long time has passed since the earthquake occurred. Therefore, we have developed a system for questionnaires in real time after earthquakes for building users. This paper introduces the sense of human vibration obtained by the questionnaire system.

1   INTRODUCTION

On March 11, 2011, Japan was shaken by the 2011 Great East Japan Earthquake. During the 2011 Great East Japan earthquake, the Japan Meteorological Agency(JMA) Seismic Intensity 6 lower or more was observed in a large area throughout Tohoku and Kanto region, and the long-time strong shaking and the long-period ground motion were widely observed. And the high-rise buildings in urban area, which have long natural period, were easy to sway by the long-period ground motions. JMA conducted a questionnaire survey on the shaking of these high-rise buildings, and pointed out that the long-time strong shaking and the long-period ground motion caused anxiety and discomfort to users of high-rise buildings.

In order to clarify human response of such abnormalities, Yoshizawa et al. applied some human response evaluation methods, such as ISO 2631-1, to the earthquake observation records of the 2011 Great East Japan Earthquake. To explain the results of the questionnaire conducted after the earthquake using the MSDV (The motion sickness does value defined in ISO2631-1), it was pointed out that expansion of the MSDV evaluation was necessary. (M. Yoshizawa et al., 2014)

Takahashi et al conducted 1-direction shake table test in order to clarify the evacuation action limit in the strong ground motion, and proposed human performance limit curves for action difficulty and human performance limit curves for anxiety (Takahashi T. et al., 2010). Hida et al. also conducted the questionnaire survey to people in the high-rise buildings after the Great East

Japan earthquake, and compared the limit curves for anxiety derived from the questionnaire survey with the one derived from the shaking table test. Both derived curves for anxiety tended to be higher with an increase in velocity, but the anxiety felt during an actual earthquake might be higher than that felt during a shaking table test (T. Hida et al., 2012).

The human subject experiment by shaking table tests is an effective method for the evaluation of the motor function against building shaking, but may be inadequate for the psychological evaluation, such as fear or anxiety, because the object person is not in a real building.

The questionnaire survey after the earthquake is very useful, because it is possible to reflect the situation in the real building. But time lag between the time when the object person felt shaking and the time when the object person answered the questionnaire might be big. There is a possibility that a correct answer cannot be obtained if this time lag is big.

So, using the information of the seismometer installed in the building, a quasi-real-time questionnaire system for the shaking of the building was developed (M.Yoshizawa et al., 2015). In this paper, a part of the questionnaire results were introduced.

2   FINDINGS FROM RESEARCH ON THE GREAT EAST JAPAN EARTHQUAKE

2.1   Questionnaire survey by Japan Meteorological Agency

In the Great East Japan Earthquake, high-rise buildings resonated due to long-period ground motion, and it was widely recognized that it was difficult for people to walk and act in the high-rise buildings due to long-lasting tremors. Figure 1 is a part of the results of the questionnaire for high-rise building inhabitants. The question was intended for the health condition during roughly one hour after the main shock. In the Figure 1, a few percent of the inhabitants on the upper floors may have vomiting. And about 50% inhabitants felt some abnormalities.
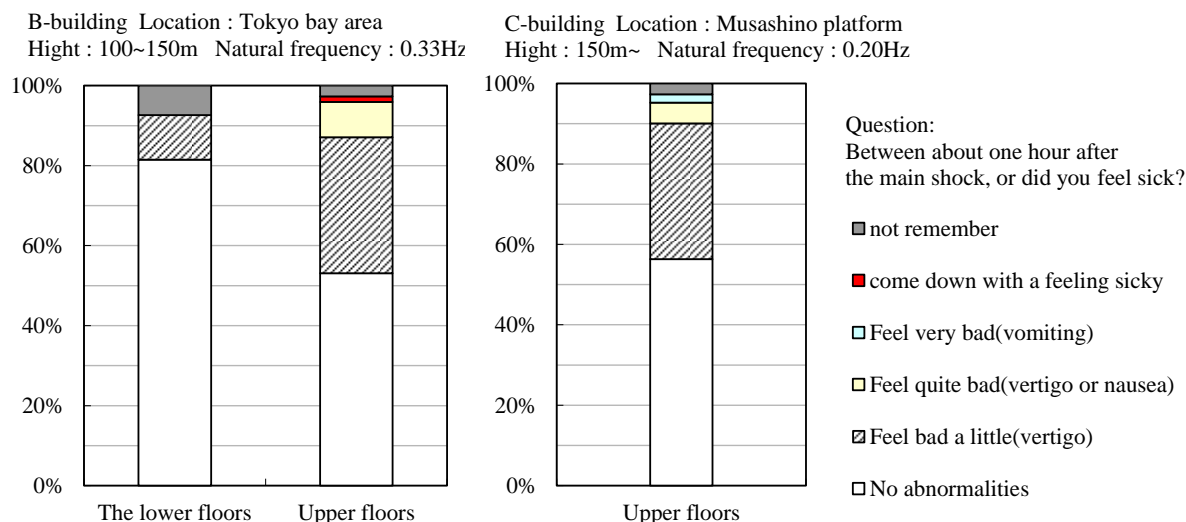
Figure 1: Part of the results of the questionnaire for high-rise buildings in areas around Tokyo (JMA, 2011)

2.2   Index of earthquake shaking in Japan

The JMA seismic intensity scale is a seismic scale used in Japan and is widely known. As a rule, seismic intensities announced by JMA are values observed using seismic intensity meters installed on the ground. Figure 2 shows the procedure of calculating the JMA instrumental seismic intensity. To calculate the JMA seismic intensity, three-component (North-South component, East-

West component, Up-Down component) acceleration time history is needed. The three-component acceleration is processed according to the procedure shown in Figure 2, and the JMA seismic intensity, I_{JMA} , is obtained as a real number. (Japan Meteorological Agency, 1996) Table. 3 shows the explanation of the JMA Seismic Intensity Scale.

(a) Flow chart

(b) Bandpass filter
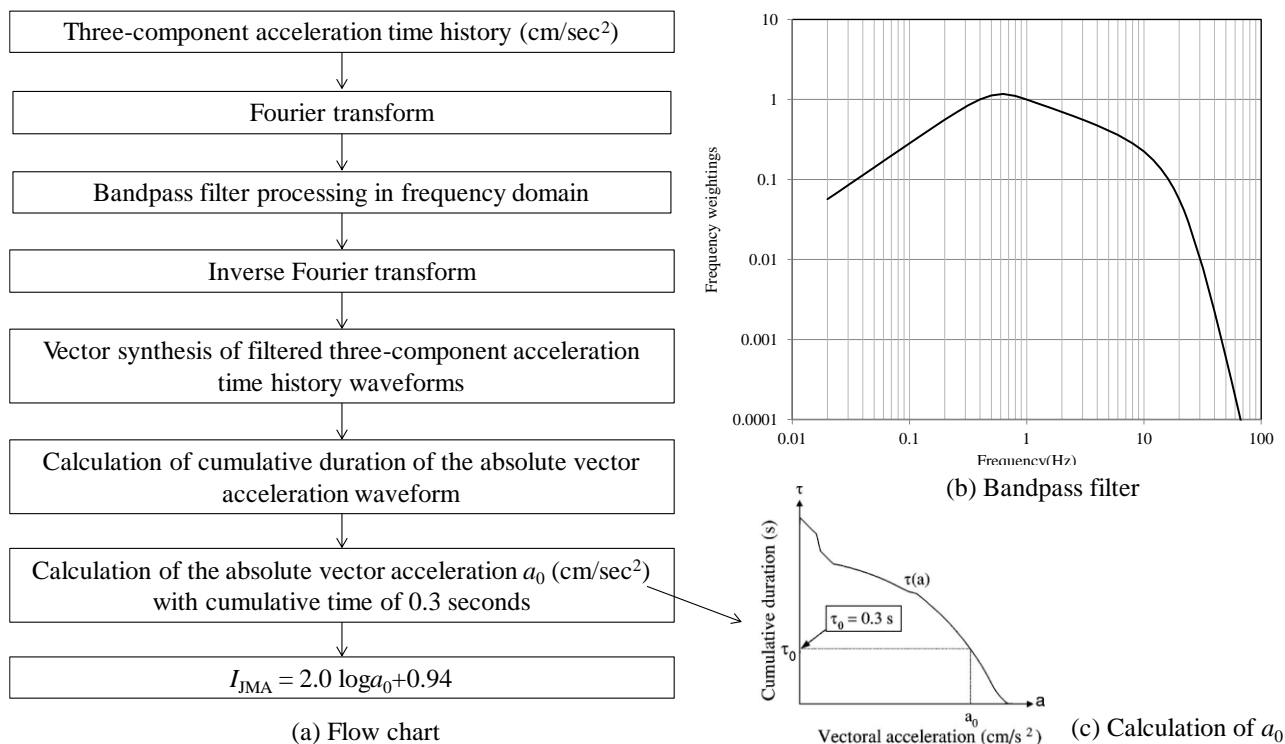
(c) Calculation of a_0

Figure 2: Procedure of calculating the JMA instrumental seismic intensity

Table 1 Explanation of the JMA Seismic Intensity Scale

Seismic intensity	Instrumental seismic intensity	Human perception and reaction	Seismic intensity	Instrumental seismic intensity	Human perception and reaction
0	0-0.4	Imperceptible to people, but recorded by seismometers.	5 Lower	4.5-4.9	Many people are frightened and feel the need to hold onto something stable.
1	0.5-1.4	Felt slightly by some people keeping quiet in buildings.	5 Upper	5.0-5.4	Many people find it hard to move; walking is difficult without holding onto something stable.
2	1.5-2.4	Felt by many people keeping quiet in buildings. Some people may be awoken.	6 Lower	5.5-5.9	It is difficult to remain standing.
3	2.5-3.4	Felt by most people in buildings. Felt by some people walking. Many people are awoken.	6 Upper	6.0-6.4	It is impossible to remain standing or move without crawling. People may be thrown through the air.
4	3.5-4.4	Most people are startled. Felt by most people walking. Most people are awoken.	7	6.5 and up	

As shown in Figure 2(b), the JMA instrumental seismic intensity uses the band pass filter, there is a possibility to cut the component of long-period ground motion (0.1~0.4Hz). So the JMA seismic intensity may underestimate the structural damage of high-rise buildings shaken by the long-period ground motion, and also may underestimate the human damage in high-rise buildings.

For this reason, in order to achieve the support of post-earthquake disaster prevention in high-rise buildings, JMA administers observed information about the long-period ground motion to inform about the probability of occurrence of the damage in the high-rise building. Figure 3 and Table 2 is a summary of the long-period ground motion class.

According to observations by JMA during the Great East Japan Earthquake, seismic intensity 5 lower to 5 upper were observed in the 23 wards of Tokyo, and the long-period seismic ground motion class was the largest class 4.

Class	Absolute velocity response
Long-period ground motion Class 4	100cm/s $\leqq$ Sva
Long-period ground motion Class 3	50cm/s $\leqq$ Sva < 100cm/s
Long-period ground motion Class 2	15cm/s $\leqq$ Sva < 50cm/s
Long-period ground motion Class 1	5cm/s $\leqq$ Sva < 15cm/s
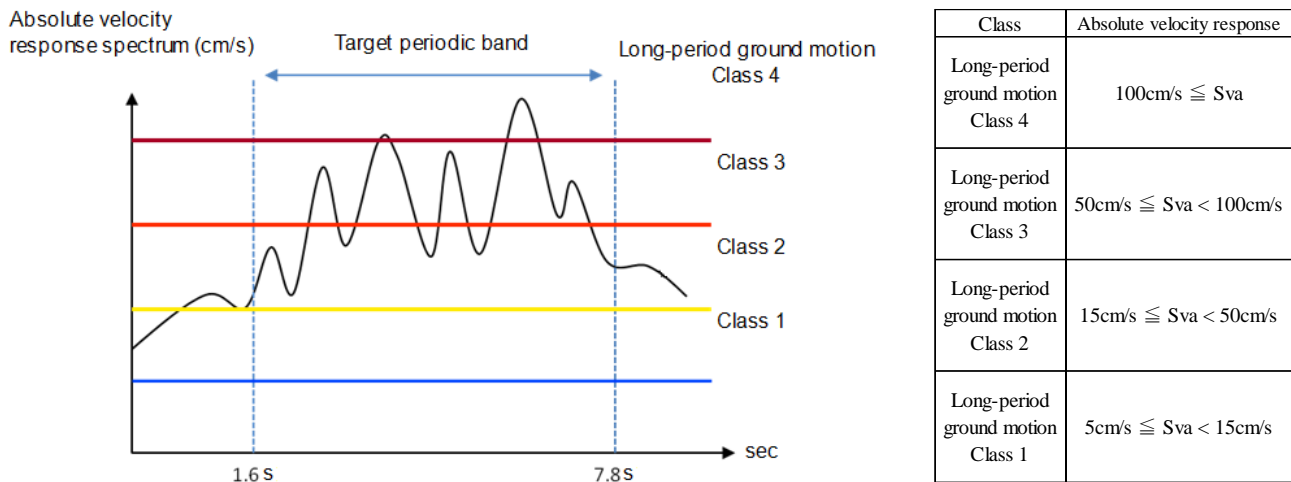
Figure 3: Concept of long-period ground motion class (JMA ,2013)

Table 2 Explanation of the JMA long-period ground motion class

Class	Human feeling and action	Interior space condition	Absolute velocity response spectrum (cm/s)
Long-period ground motion Class 1	Most people who were in the room feel the shaking. Some people surprised.	Suspended interior decorating ,such as blind, swing broadly.	5cm/s $\leqq$ Sva < 15cm/s
Long-period ground motion Class 2	Feel a great shaking in the room, and feel a strong need to hold on to something. Feel difficulty for usual action , such as holding on to something for walking.	Furniture and fixtures on casters move slightly. Storage goods, such as dishes on the shelf or books in bookshelf, may fall	15cm/s $\leqq$ Sva < 50cm/s
Long-period ground motion Class 3	Difficult to keep standing	Furniture and fixtures on casters move widely. Some unsteadfast furnitures may move and unbalanced ones may overturn.	50cm/s $\leqq$ Sva < 100cm/s
Long-period ground motion Class 4	Impossible to keep standing. Be tossed up and down by the shaking.	Furniture and fixtures on casters move widely and some furniture may overturn. Most of unsteadfast furnitures move and some of them overturn.	100cm/s $\leqq$ Sva

2.3 Study on application of ISO 2631-1 to building seismic response

ISO 2631-1 defines methods for the measurement of periodic, random and transient whole-body vibration. It indicates the principal factors that combine to determine the degree to which a vibration exposure will be acceptable. Informative annexes indicate current opinion and provide guidance on the possible effects of vibration on health, comfort and perception and motion sickness. The frequency range considered is

- 0.5 Hz to 80 Hz for health, comfort and perception, and
- 0.1 Hz to 0.5 Hz for motion sickness.

The vibration evaluation according to this part of ISO 2631-1 shall always include measurements of the weighted root-mean-square (r.m.s.) acceleration. The weighted r.m.s.

acceleration is expressed in meters per second squared (m/s^2) for translational vibration. The weighted r.m.s. acceleration shall be calculated in accordance with the following equation:

$$a_w = \left(\frac{1}{T} \int_0^T a_w(t)^2 \, dt \right)^{1/2} \tag{1}$$

$$a_w(t) = \left(a_{wx}(t)^2 + a_{wy}(t)^2 + a_{wz}(t)^2 \right)^{1/2} \tag{2}$$

$a_w(t)$ is the frequency weighted acceleration as a function of time history, in (m/s^2)
$a_{wx}(t)$, $a_{wy}(t)$, $a_{wz}(t)$ are the frequency weighted accelerations in the direction x, y, z
T is the exposure duration, in second.

The motion sickness does value (MSDV) in ISO 2631-1 consists of a low pass filter and total period T during which motion could occur, so it seems to be appropriate to evaluate the phenomenon of seasickness by long-period ground motion. MSDV$_z$ is given by the square root of the integral of the square of the z-axis acceleration after it has been frequency-weighted:

$$MSDV_z = \left(\int_0^T a_{wz}(t)^2 \, dt \right)^{1/2} \tag{3}$$

$a_{wz}(t)$ is the frequency weighted acceleration in the z direction, in (m/s^2)
T is the exposure duration, in second.

After calculating $MSDV_z$, the percentage of vomiting rate is calculated by the following equation:

$$Vomiting \quad percentage = K_m \cdot MSDV_z \tag{4}$$

The percentage of people who may vomit is approximately $K_m MSDV_z$, where K_m is a constant which may vary according to the exposed population, but, for a mixed population of unadapted male and female adults, $K_m = 1/3$. Figure 4 shows the outline of the acceleration evaluation procedure according to ISO2631-1.
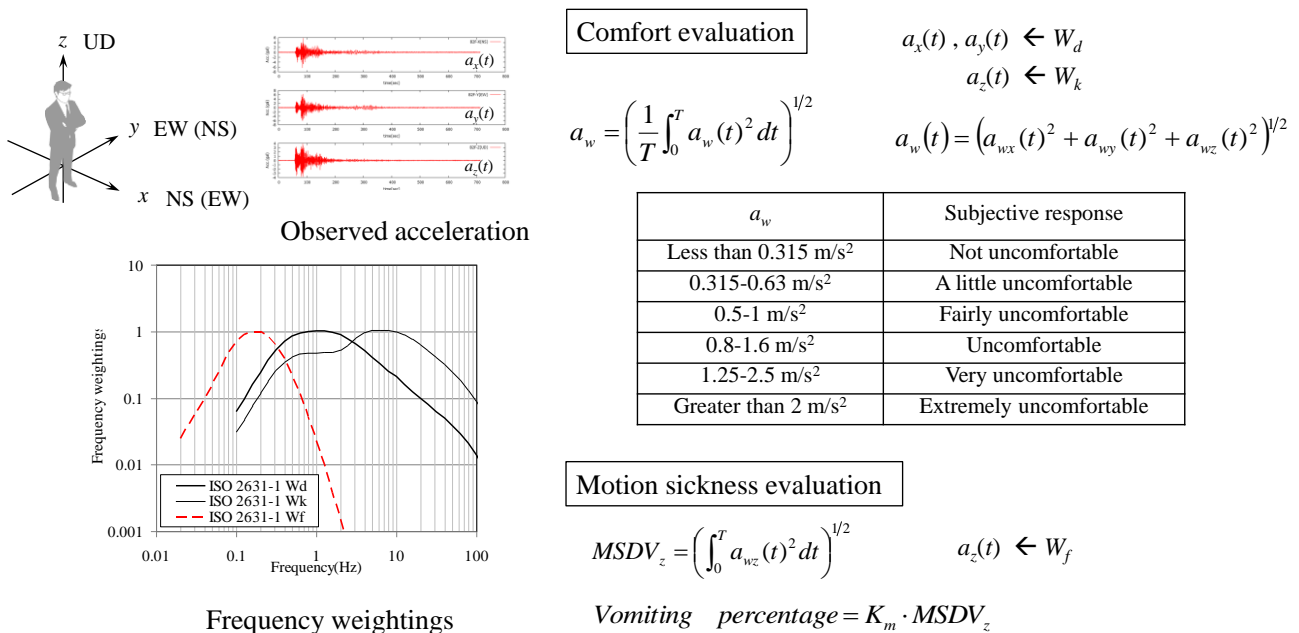
Figure 4: Outline of evaluation of vibration by ISO2631-1 (JMA, 2013)

In order to verify the applicability of ISO 2631-1 to the response of buildings due to an earthquake, reproduction of the questionnaire results in Figure 1 was examined. The building floor response were calculated from observed ground motion data. To evaluate the response of the building in a simplified manner, single degree of freedom model was used. The natural period of the building was supposed from the empirical prediction from the number of building stories, and the damping ratio was supposed 2%. To verify the results of the questionnaire C-building in Figure 1, the data of ground motion at the Nishi-Shinjyuku point was used for the input motion.

MSDV is given by the square root of the integral of the square of the z-axis acceleration as shown in equation (3). In general, the earthquake shaking in the horizontal direction(x and y) is larger than the vertical direction(z). So following the precedent study (Kouhei M. 2005), combining vibrations in three directions is adopted as equation (2). $a_{wx}(t)$ and $a_{wy}(t)$ are the same frequency-weighted acceleration as $a_{wz}(t)$.

$$MSDV_{xyz} = \left(\int_0^T a_w(t)^2 \, dt \right)^{1/2} \tag{5}$$

Figure 5 shows the comparison of MSDV time series using equation (3) and (5). When the vomiting ratio was calculated by $MSDV_{xyz}$, the vomiting ratio of the case of 56 stories building was 1.7%. The case of 56 stories building was close to the C-building in Figure 1, the calculated vomiting ratio was good agreement with the result of Figure 1.

Floor response acceleration obtained from response analysis of one mass system with equivalent period

number of stories	height (m)	natural period(sec)			
		horizontal		vertical	
56	170	4.50	(0.22Hz)	0.54	(1.87Hz)
30	90	2.40	(0.42Hz)	0.32	(3.15Hz)
20	60	1.60	(0.63Hz)	0.23	(4.29Hz)
10	30	0.80	(1.25Hz)	0.15	(6.71Hz)
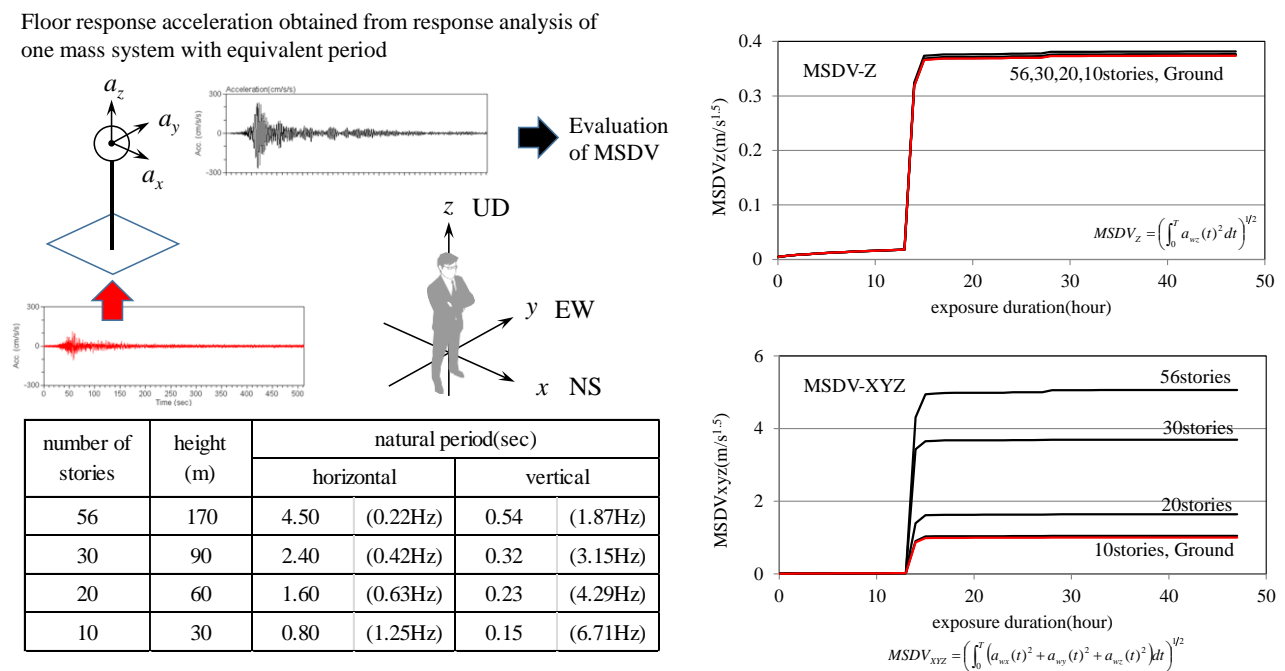
Figure 5: Comparison of MSDV time series

3 DEVELOPMENT OF REAL-TIME QUESTIONNAIRE SYSTEM

In order to reduce human damage during a large earthquake, research has been conducted to clarify human vibration characteristics during an earthquake. Although subject experiments using shaking tables and questionnaire surveys after a major earthquake have been conducted, these studies have been conducted under limited conditions. Therefore, in order to compensate the obtained knowledge, a real-time questionnaire system was developed in the building where the seismometer was installed. It has been operating since 2015.

3.1 Overview of the questionnaire system

The building as a target of the questionnaire system is seven, Miyagi, Chiba, Tokyo, Kanagawa, Aichi, Osaka, and Fukuoka (as shown in Figure 6). Figure 7 shows the flow of the questionnaire system processing. The seismographs in these seven buildings are connected for 24 hours on the intranet. So, if the intranet can be used after the earthquake, a questionnaire survey is possible in almost real time immediately after the earthquake.

The UC building is the only high-rise building in the questionnaire conducted this study. The UC building is not connected to the intranet, but long term observation of the seismograph is conducted in the UC building. Occasionally it is reported that only upper floors in the UC building resonate due to the long-period ground motion. Therefore, in this study, questionnaire surveys of the same contents were conducted for the UC building users, although not in real time.

Table 3 shows the contents of the questionnaire. The questionnaire items are set in reference to the items in the former study of the questionnaire survey carried out for the resident of the high-rise building in the case of the Great East Japan Earthquake (K. Tamura et al. 2012). The questionnaire item was selected as a selection formula of about 10 questions at the maximum so as not to bear the burden of respondents. Since this questionnaire system also covers small earthquakes, "I did not feel shaking" was set up as an option.
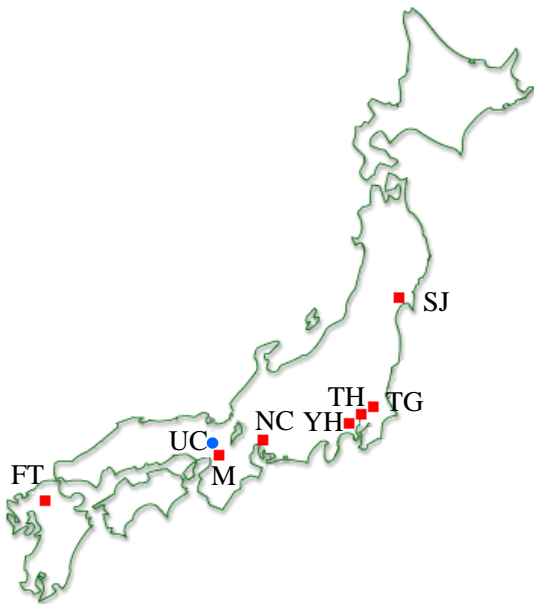
Building	Number of stories	Place
SJ	B2・F12・P1	Sendai, Miyagi
TG	B1・F4	Inzai, Chiba
TH	F7	Koto ward, Tokyo
YH	B1・F13	Yokohama, Kanagawa
NC	B4・F10	Nagoya, Aichi
M	B4・F9	Osaka, Osaka
FT	B2・F12	Fukuoka, Fukuoka
UC	B2・F32・P1	Osaka, Osaka

Figure 6: Buildings with the developed questionnaire system
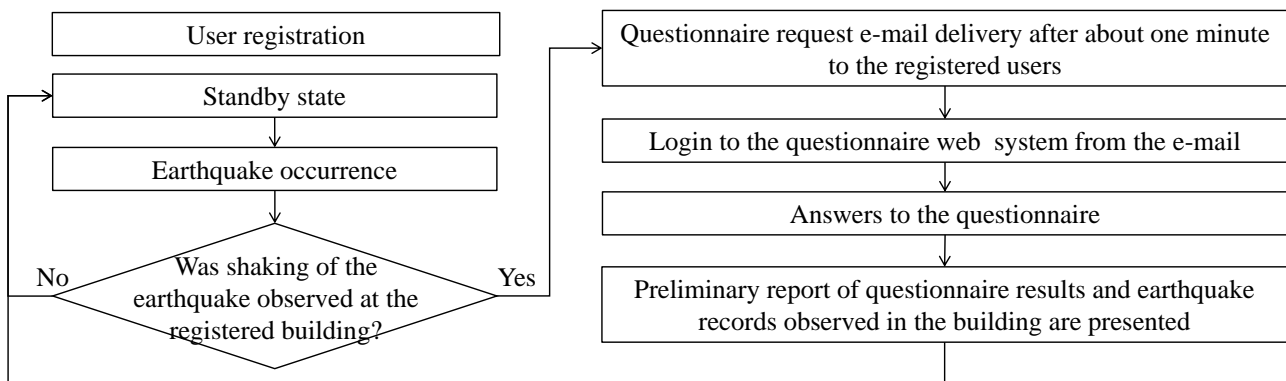
Figure 7: The flow of the questionnaire processing

Table 3 Explanation of the JMA long-period ground motion class

No.	Question	Answer Choices
Q1	Where did you feel the shaking of the earthquake?	☐Nth Floor ☐Not in the building ☐Not remembered
Q2	Please choose the situation when you feel the earthquake.	☐sitting position ☐standing position ☐walking ☐other, do not remember
Q3	Did you feel the shaking of the earthquake and take evacuation action?	☐I did not feel shaking ☐I did nothing ☐I sank under the desk ☐I protected a body from falling objects (helmet wearing etc.) ☐I opened the door for immediate evacuation ☐other, do not remember
Q4	How big was the earthquake you felt?	☐I did not feel shaking ☐I slightly felt shaking ☐I felt a clear shook, but there was no trouble in the action ☐There was a little trouble for walking or moving, ☐It was not possible to standing ☐I couldn't do anything at my will ☐other, do not remember
Q5	What kind of shake did you feel? (Multiple answers allowed)	☐I did not feel shaking ☐Long-period tremors with slow repetition ☐Shaking which goes around around in north, south, east and west ☐Shaking which moves in left and right small tremblingly ☐Shaking which pushes up and down ☐Shaking that its amplitude increases suddenly ☐other, do not remember
Q6	How long did you feel the shaking?	☐I did not feel shaking ☐Less than 10 seconds ☐About 30 seconds ☐About 1 minute ☐About 2 minutes ☐More than 2 minutes ☐other, do not remember
Q7	While the earthquake shook, did you feel anxious?	☐I did not feel shaking ☐Not anxious ☐Anxious a little ☐Anxious ☐Anxious very much ☐other, do not remember
Q8	After the earthquake, did you come to feel sick?	☐I did not feel shaking ☐No problem with physical condition ☐Such as feeling dizzy, I came to feel sick slightly ☐Quite feel bad in dizziness and nausea ☐Such as vomiting, I came to feel sick very much ☐I fell asleep ☐other, do not remember
Q9	How much shaking did you feel it with in the scale of the JMA seismic intensity scale?	☐I did not feel shaking ☐Less than seismic intensity 1 ☐1 ☐2 ☐3 ☐4 ☐5 Lower ☐5 upper ☐More than seismic intensity of 6 Lower ☐other, do not remember
Q10	In addition, please describe impressions about the shaking freely.	(Optional)

3.2 Example of the results with the questionnaire system

About 400 earthquake records have been observed throughout the questionnaire system. However, if the earthquake does not occur in office hours, the number of questionnaire responses will be small. Here, we introduce the questionnaire results of three earthquakes observed in Osaka. Figure 8 shows the outline of the target earthquakes. In No.1 and No.2, the JMA seismic intensity 2-3 was observed in Osaka Prefecture, and long-period ground motion class 1-2 was also observed. On the other hand, No.3 was a near-field earthquake around Osaka Prefecture, and a maximum seismic intensity of 6 lower was observed.
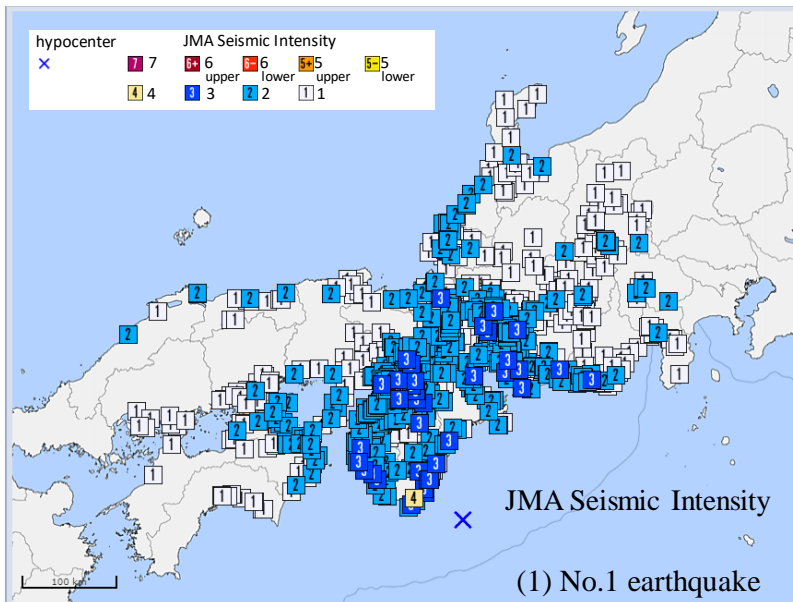
Southeastern part of Mie pref.
Apr. 1, 2016 11:39
Epicenter position
33° 19.4′N   136° 22.9′E
Depth 29km   JMA Magnitude 6.5

JMA Seismic Intensity

(1) No.1 earthquake

Class 1   Class 2   Class 3   Class4

JMA long-period
ground motion class
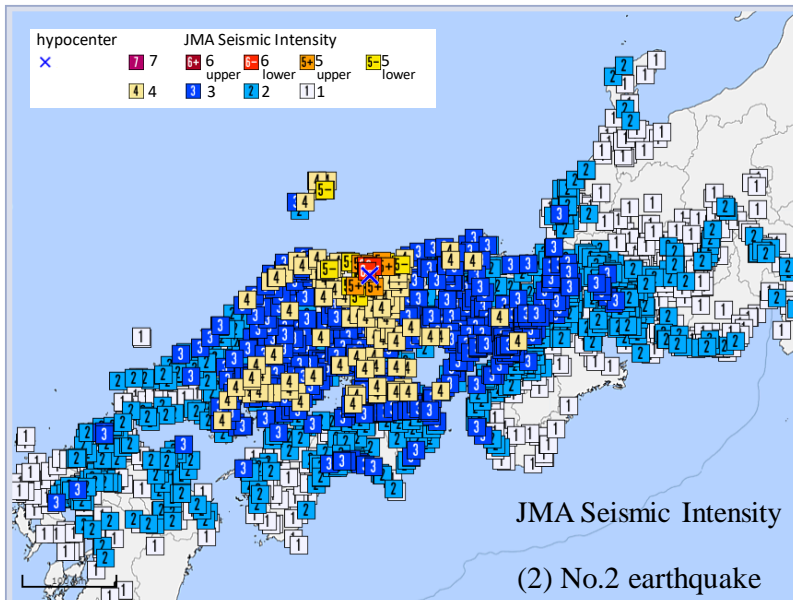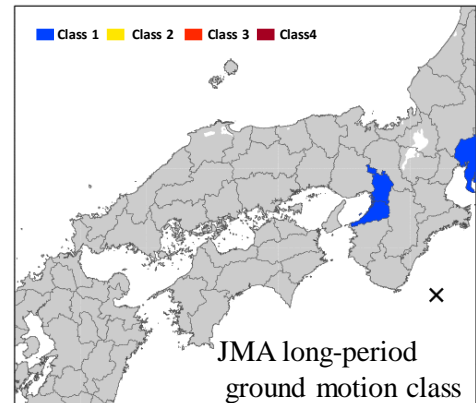
Central Tottori pref.
Oct. 21, 2016 14:07
Epicenter position
35° 22.8′N   133° 51.3′E
Depth 11km   JMA Magnitude 6.6

JMA Seismic Intensity

(2) No.2 earthquake

Class 1   Class 2   Class 3   Class4

JMA long-period
ground motion class
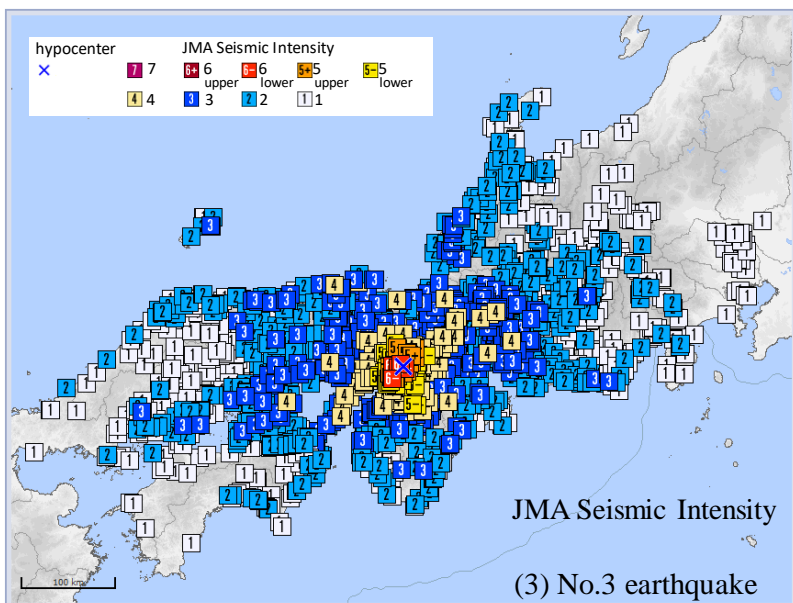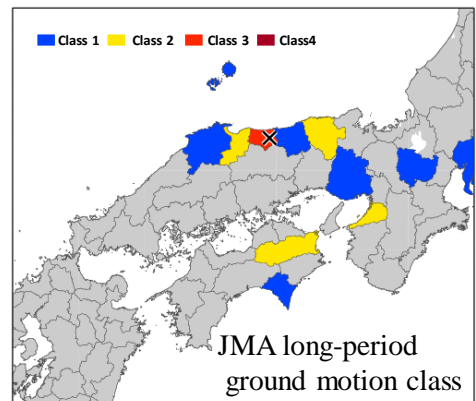
Northern Osaka pref.
June 18, 2018 07:58
Epicenter position
34° 50.6′N   133° 37.3′E
Depth 13km   JMA Magnitude 6.1

JMA Seismic Intensity

(3) No.3 earthquake

Class 1   Class 2   Class 3   Class4

JMA long-period
ground motion class
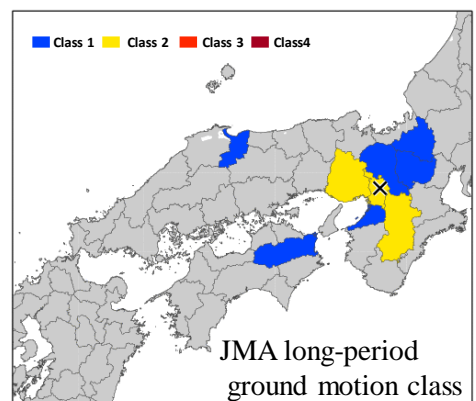
Figure 8: Outline of the target earthquakes of the questionnaire system
(Map images quoted from the Japan Meteorological Agency website)

Table 4 shows the records of observations of earthquakes in the M building and the UC building. Table 4 shows the maximum acceleration value, the ISO2631-1 comfort and motion sickness evaluation index, the JMA seismic intensity, and the long-period ground motion class using the observed acceleration.

Table 4 Records of observations of earthquakes in buildings

(1) The M building

Eathquake	Floor	Max. Acc.(m/s^2)			a_w (m/s^2)	$MSDV_Z$	Vomiting ratio(%)	JMA S. I.	JMA Long period ground motion class
		NS	EW	UD					
No.1	9	0.19	0.11	0.04	0.029	0.0156	0.0052	3.1	Class1
	B4	0.05	0.03	0.02	0.009	0.0158	0.0053	2.3	(5.3cm/s)
No.2	9	0.24	0.29	0.11	0.048	0.0202	0.0067	3.6	No Class
	B4	0.06	0.07	0.05	0.010	0.0202	0.0067	2.4	(3.7cm/s)
No.3	9	0.88	2.69	1.52	0.145	0.0352	0.0117	5.2	Class1
	B4	0.62	1.65	1.02	0.063	0.0349	0.0116	4.5	(14.7cm/s)

(2) The UC building

Eathquake	Floor	Max. Acc.(m/s^2)			a_w (m/s^2)	$MSDV_Z$	Vomiting ratio(%)	JMA S. I.	JMA Long period ground motion class
		NS	EW	UD					
No.1	31	0.12	0.14	0.05	0.030	0.0171	0.0057	3.1	No Class
	15	0.08	0.10	0.04	0.024	0.0152	0.0051	2.9	(4.5cm/s)
	B2	0.04	0.04	0.02	0.017	0.0153	0.0051	2.3	

Figure 9 shows the part of questionnaire results at the M Building. The answer to No.1 took one week, and the answer to No.2 ended during the day of the earthquake. All respondents were on the 5th floor at the time of the earthquakes.

No.3 is the first earthquake in Osaka Prefecture that has observed tremors with a maximum seismic intensity of 6 since 1995 Great Hanshin-Awaji Earthquake, and the majority of people were affected by the earthquake. Since No. 3 occurred about 30 minutes before the start of the business day, many building users were working at M building. As for No.3, in addition to a web real-time questionnaire, an offline questionnaire was conducted and a total of 66 questionnaire results were collected in one week. In Figure 9, No.3 respondents were the people who experienced earthquakes on the 5th floor.

In Figure 9(3), No.2 is the largest percentage of respondents who chose "Long-period tremors with slow repetition" due to the shaking of the M building. Comparing No.1 and No.2 with similar levels of shaking, the JMA long period ground motion class in Table 4(1) may not be able to evaluate the tendency of Figure 9(3). Although the $MSDV_Z$ in Table 4(1) is small, it shows the tendency of Figure 9(3). This is probably because the long-period ground motion class is defined by the maximum value of the absolute velocity response spectrum and does not include the effect of the duration of shaking as in MSDV.

In No.3, the largest MSDV and long-period ground motion class are calculated. However, since the intensity of shaking of the short period component was large, it is considered that the influence of shaking due to the long period component did not appear in the questionnaire results.
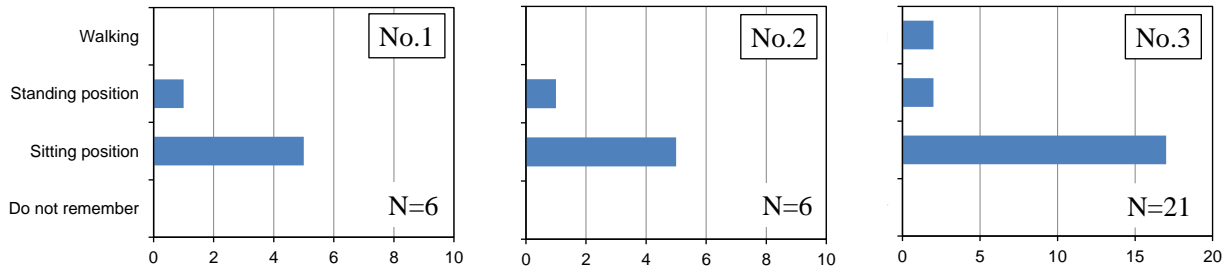
(1) Answers of Q2 : Please choose the situation when you feel the earthquake.
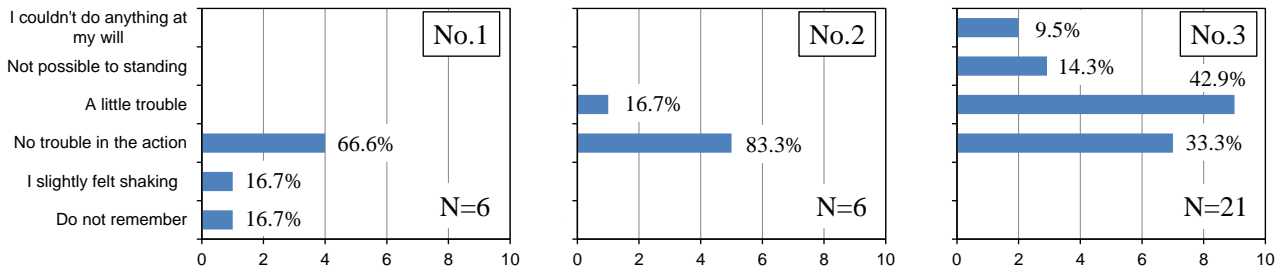
(2) Answers of Q4 : How big was the earthquake you felt?
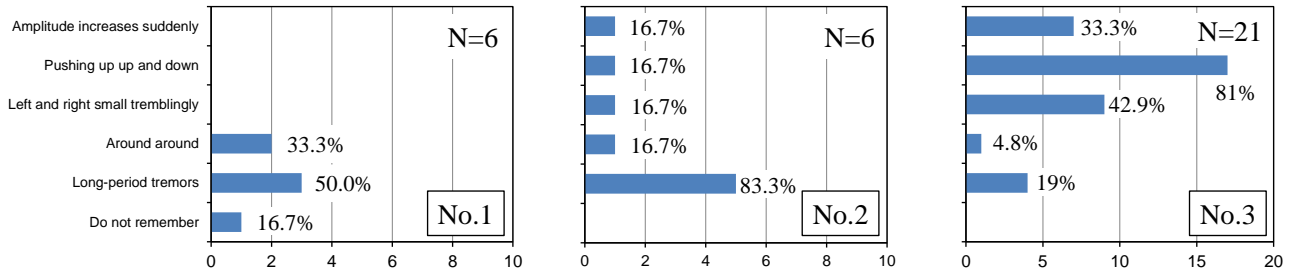
(3) Answers of Q5 : What kind of shake did you feel? (Multiple answers allowed)
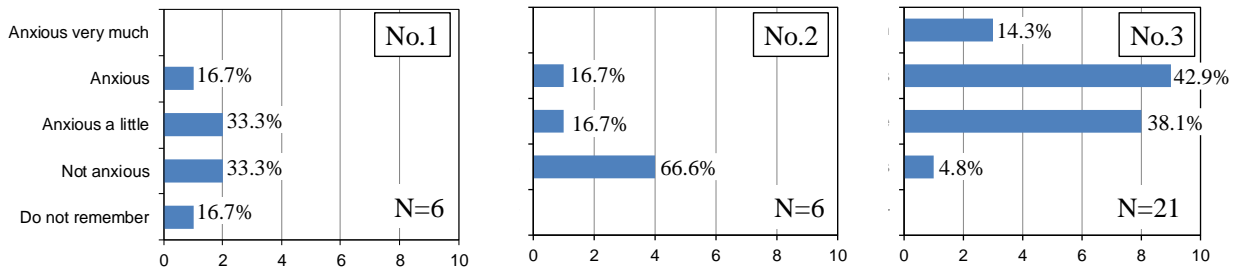
(4) Answers of Q7 : While the earthquake shook, did you feel anxious?
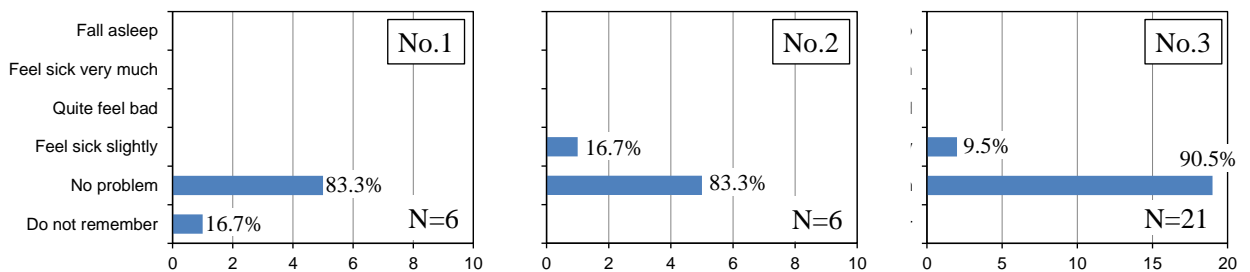
(5) Answers of Q8 : Did you feel sick because of the earthquake?

Figure 9: Part of questionnaire results at the M Building

Figure 10 shows the results of the questionnaire against No.1 earthquake at the UC building. In this questionnaire results, the respondents who were above the 16th floor were analyzed as upper floors. The distribution of floors where respondents were at the time of the earthquake is shown in the lower right of Figure 10.

About half of the respondents on the lower floors chose "I did not feel shaking". On the other hand, some respondents on the upper floors chose "Such as feeling dizzy, I came to feel sick slightly". Figure 10 shows the results that the shaking of high-rise buildings due to long-period ground motions is greatly different between the high and low floors.

Answers of Q6 : How long did you feel the shaking?
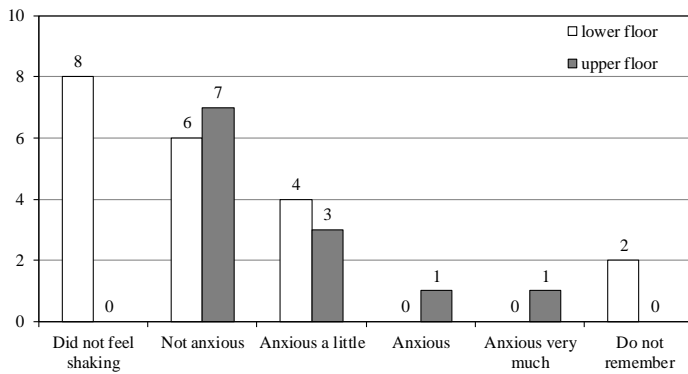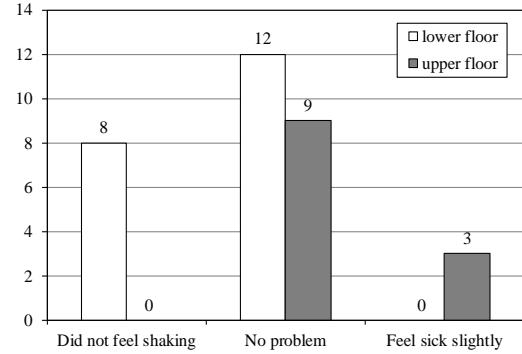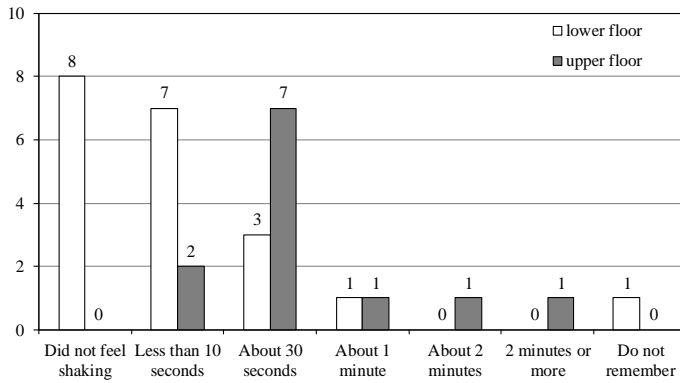
Answers of Q8 :
After the earthquake, did you come to feel sick?

Answers of Q7 : Did you feel scared while the earthquake was shaking?

Distribution of questionnaire respondents in the UC building

	floor	Male	Female	Each total
upper floor	30	0	1	1
	26	1	0	1
	19	1	0	1
	16	6	3	9
lower floor	3	4	0	4
	1	9	3	12
	B1	2	0	2
	B2	2	0	2
	Do not remember	1	0	1
	Absent in building	3	0	3
	total	29	7	36

Figure 10: Part of questionnaire results at the UC Building against earthquake No.1

3.3 Consideration of questionnaire results

As shown in Figure 5, the motion sickness index $MSDV_{xyz}$ shown in Equation (5) was in good agreement with the questionnaire results in the high-rise building. Therefore, $MSDV_{xyz}$ was calculated for this observation record and compared with the questionnaire results.

Table 5 shows the $MSDV_{xyz}$ calculation results for the M building during No.3 earthquake and the UC building during No.1 earthquake. There is an impression that the proportion of people with feeling physically sick condition in the questionnaire results (Q8) is considerably larger than the vomiting rate evaluated by $MSDV_{xyz}$. Although there were problems such as the small number of people in the questionnaire, cross tabulation was performed between the questionnaire questions.

Table 6 is cross tabulation between Q8 and Q1, it shows the tendency of the number of floors that people who felt physically sick during the earthquake. The number of floors of the M building and the UC building are very different, but those who felt physically sick are on the upper floors of both buildings.

Table 7 is cross tabulation between Q8 and Q6, it is a comparison based on the difference in how the duration of shaking was felt. It was assumed that people who were sensitive to shaking were more easily influenced in physical condition, but no clear correlation was found.

Table 5 Records of observations of earthquakes in buildings

Building	Eathquake	Floor	$MSDV_z$	Vomiting ratio(%)	$MSDV_{xyz}$	Vomiting ratio(%)
M	No.3	9F	0.035	0.012	0.102	0.034
		B4F	0.035	0.012	0.087	0.029
UC	No.1	31F	0.017	0.006	0.444	0.148
		15F	0.015	0.005	0.212	0.071
		B2	0.015	0.005	0.043	0.014

Table 6 Cross tabulation between Q8 and Q1

(1) Results at the M Building during the No.3 earthquake

Q8 \ Q1	B3F	B1F	1F	3F	4F	5F	6F	8F	Other
I did not feel shaking									
No problem	3	1	2	1	6	19	9	4	1
Feel sick slightly					2	2	1	3	1
Quite feel bad					1				

(2) Results at the UC Building during the No.1 earthquake

Q8 \ Q1	B2F	B1F	1F	3F	10F	16F	19F	26F
I did not feel shaking	1	2	2	2				
No problem	1		10	2		7	1	1
Feel sick slightly					1	2		
Quite feel bad								

Table 7 Cross tabulation between Q8 and Q6

(1) Results at the M Building during the No.3 earthquake

Q8 \ Q6	Less than 10 seconds	About 30 seconds	About 1 minute	About 2 minutes	Other
No problem	17 37.0%	24 52.2%	5 10.9%		
Feel sick slightly	2 22.2%	4 44.4%	3 33.3%		
Quite feel bad		1 100.0%			

(2) Results at the UC Building during the No.1 earthquake

Q8 \ Q6	Less than 10 seconds	About 30 seconds	About 1 minute	About 2 minutes	Other
No problem	8 27.6%	9 31.0%	1 3.4%	2 6.9%	9 31.0%
Feel sick slightly	1 33.3%	1 33.3%	1 33.3%		
Quite feel bad					

Table 8 is cross tabulation between Q8 and Q7, it is a comparison between psychological anxiety and physical condition. It was assumed that psychological anxiety about the shaking of the earthquake had an effect on the physical condition, and the tendency was seen in the M building, but it was not clearly confirmed in the UC building. Since the respondents who answered "Feel sick slightly" in Table 8(2) were significantly different in age, there may be differences in psychological responses.

Table 8 Cross tabulation between Q8 and Q7

(1) Results at the M Building during the No.3 earthquake

Q8 \ Q7	Not anxious	Anxious a little	Anxious	Anxious very much	Other
No problem	3 6.5%	22 47.8%	15 32.6%	6 13.0%	
Feel sick slightly			7 77.8%	2 22.2%	
Quite feel bad				1 100.0%	

(2) Results at the UC Building during the No.1 earthquake

Q8 \ Q7	Not anxious	Anxious a little	Anxious	Anxious very much	Other
No problem	20 69.0%	6 20.7%	1 3.4%		2 6.9%
Feel sick slightly	1 33.3%	1 33.3%		1 33.3%	
Quite feel bad					

4   CONCLUSION

Social needs for the building seismic performance are changing not only to the life safety but also to the maintenance of functionality after the earthquake. So the human condition during building shaking by earthquakes is also beginning to be considered as a part of the functionality of the building and some research on human vibration characteristics during an earthquake has begun.

In order to collect basic information of human anxieties and abnormalities during big earthquakes, we have developed quasi-real-time questionnaire system for shaking of buildings caused by earthquakes and have been operating since 2015. In this paper, we introduced examples of relatively large earthquake shaking from the collected questionnaire results.

Focusing on the results of questionnaires on the physical condition of people, it was pointed out that people on the upper floors of the building tend to be more affected, and psychological anxiety about shaking may affect the physical condition.

It is considered that the psychological anxiety or fear for the earthquake is promoted not only by the shaking itself but also by the imagination of how the environment in which the person is in becomes. Since shaking of a building due to an earthquake cannot be avoided, providing appropriate information can be considered as a measure to reduce psychological anxiety of building users.

Since the number of responses by the developed questionnaire system is still small, it is necessary to increase the number of survey respondents in the questionnaire and improve the reliability of the questionnaire result data. In addition, with the aim of reducing the psychological anxiety of building users, we are planning to consider an appropriate method of providing information to survey respondents immediately after the earthquake.

REFERENCES

[1] Japan Meteorological Agency, "Know the JMA seismic intensity - Basic knowledge and its utilization", Gyosei, 1996(in Japanese).

[2] International Organization for Standardization, "Mechanical vibration and shock - Evaluation of human exposure to whole-body vibration -", ISO 2631-1 Second edition, 1997

[3] Kouhei M. and Kousuke O., "Study on Method of Measurement and Analysis for Motion Sickness Evaluation", JSME annual meeting, 239-240, 2005(in Japanese).

[4] Takahashi T., Suzuki T., Saito T., Azuhata T., Morita K., Shaking table Test for Indoor Human Response and Evacuation Limit, Journal of 5Th International Conference on Earthquake Engineering, pp.187-193, 2010.3

[5] Seismology and Volcanology Department, Japan Meteorological Agency, Report of a way of information about long-period ground motion, 2012(in Japanese).

[6] K. Tamura, M. Kaneko, H. Kitamura and T. Saito, "A Questionnaire on Seismic Indoor Damage and Occupant's Behavior of Tall Residential Buildings in Tokyo", AIJ J. Technol. Des. Vol.18, No.39, pp.453-458, Jun., 2012(in Japanese).

[7] T. HIDA and M. NAGANO, "Study on Shaking and Damages of Super High-Rise Residential Buildings During The 2011 Off The Pacific of Tohoku Earthquake Based on Questionnaire Survey", 15th World Conference on Earthquake Engineering, 2012

[8] Japan Meteorological Agency, "Observation information about the long-period ground motion (Trial*)", 2013(in Japanese). *Transition from trial to official operation in 2019 http://www.data.jma.go.jp/svd/eew/data/ltpgm_explain/kaisetsu.html

[9] M. Yoshizawa, K. Kajiwara, S. Maeda, "A study on human body sensitivity for shaking from main shock of major earthquake to some aftershocks", Proceedings of the 22nd Japan Conference of Human response to vibration, 2014

[10]   M. Yoshizawa and M.Yamamoto, "Development of questionnaire system for shaking of buildings caused by earthquakes", Proceedings of the 23rd Japan Conference of Human response to vibration, 2015

15 Session 8: WBV 4

Session chair: Mohammed Fard

Validation of smart insoles for the measurement of vibration exposure of workers and athletes

Pietro Marzaroli [1], Arash Valiesfahani [1], Marco Tarabini[1]
Politecnico di Milano – Department of Mechanical Engineering
Via Previati, 1/C 23826 Lecco, Italy
pietro.marzaroli@polimi.it, arash.valiesfahani@polimi.it

Alex P. Moorhead [1,2]
Politecnico di Milano – Department of Electronics, Information and Bioengineering
Via Golgi, 39 20133 Milan, Italy
alexpatten.moorhead@polimi.it

Manuela Galli[2,3]
Politecnico di Milano – E[4]sport Lab
Via Golgi, 39 20133 Milan, Italy
manuela.galli@polimi.it

Filippo Goi[4]
Vibram s.p.a.
Via Colombo, 5 21041 Albizzate, Italy
filippo.goi@vibram.com

ABSTRACT

Wearable sensors are becoming increasingly common in daily life for medical care, athletic training, or even daily activity monitoring [1]-[3]. As these systems advance, so do their potential application, but their use for monitoring vibration exposure is limited or absent, despite the adverse effects of vibration on health being well known among the scientific community. To address this deficit, we propose a system of sensorized smart insoles capable of measuring triaxial vibration exposure according to ISO 2631-1. Each insole allows measurement of the vibration exposure and contact pressure at the forefoot and rearfoot, as well as the temperature inside the shoe. We used the insoles to measure the vibration exposure of five male subjects in three different testing conditions: 1) indoor condition (Politecnico di Milano laboratory, atop a triaxial shaker; 2) outdoor condition riding a mountain bike; and 3) skiing. The vibration exposure along the three mutually perpendicular axes was compared with that measured using instrumentation compliant with the current standards (ISO 8041). Results show that the proposed system allows direct monitoring of vibration exposure at the feet, also accounting for the vibration reduction provided by the shoe sole.

1   INTRODUCTION

The measurement of vibration exposure is very important to prevent risks deriving from whole-body vibration. Different measurement systems provide the ability to study vibration exposure at the workplace or during athletic activities [4], [5]. These systems can be classified into two categories: laboratory-based systems (compliant with ISO 2631-1 and ISO 8041 standards) and portable (wearable) systems. Laboratory instrumentation can be used on field for short time periods and provide highly accurate and reliable measurements. In comparison, developments in microelectromechanical systems (MEMS) have resulted in the miniaturization of sensors which can be placed directly on the body or integrated into clothing [6]-[9]. These sensors, referred to as

'wearable', allow long-term monitoring of workers in ecological conditions and provide a compromise between accuracy and costs.

Different wireless, MEMS-based systems have been proposed to measure hand-arm vibration (HAV) and whole-body vibration (WBV) [10], [11] and the possibility of measuring the human vibration using smartphones and tablets have been proposed by Cutini et al. [12].

In the last two decades, foot-worn sensors such as instrumented insoles became popular for the monitoring and classification of human activity. Research using this sub-set of wearable sensors, has shown that they are highly accurate, especially for basic activities such as sitting, standing and locomotion [13]. Foot worn inertial measurement units (IMUs) combine accelerometers and gyroscopes to evaluate various kinematic and spatiotemporal gait parameters by obtaining foot orientation and trajectory, heel strike, and toe off. In addition, by integrating plantar pressure or force sensors in the shoe insoles, it is possible to estimate kinetic variables such as load and center of pressure (CoP) trajectory during different activities [1], [13]. So far, these sensors have not yet been used for measuring vibration exposure.

In this paper, we describe the design and validation of novel instrumented insoles. Each insole contains two sensors capable of measuring three-axes of accelerations on each foot's toe and heel. The measured data are transmitted wirelessly through the corresponding smartphone application and stored in the cloud. The system has been validated in laboratory conditions and used to measure vibration exposure during outdoor biking and skiing. We hypothesize that these insoles will provide an accurate and convenient way to monitor the human response to vibration exposure both during occupational and sport activity.

2   METHODS

2.1   Design and Participants

The vibration level at the interface between the feet and the supporting surface was directly measured through two sensors system placed inside the insoles of the shoes, in dedicated slots, one below the heel and one beneath the forefoot. The sensors which compose each system are triaxial MEMS accelerometers, model ST LIS3DH, (STMicroelectronic Plan-les-Ouates (HQ), Switzerland) and the force sensitive resistor 402 FSR, manufactured by Interlink Electronics (Westlake Village (HQ), CA United States 31248 Oak Crest Dr #110). The acceleration data of the three axis of the four accelerometers inside the insoles are used to compute the exposure to vibration according to ISO 2631-1. The system was validated by comparing the exposure to vibration measured by the instrumented insoles with the exposure to vibration measured through a reference accelerometer (compliant with the ISO 8041 specifications) in laboratory conditions.

Figure 1: Photograph of the data acquisition and transmission system inside the insole

Our study consisted of two stages; lab-based validation with and without shoes, followed by outdoor testing on a mountain bike and skis.

The indoor, lab-based validation involved one subject (32 years old, 178cm, 75kg). The mountain bike testing involved three male subjects; mean ($\bar{x} \pm SD$) age, mass, and height was 26.7±1.5 years, 73.7±19.5 kg and 178.3±6.5 cm, respectively. The ski tests involved two male subjects; mean age, mass and height is, 28.5±4.9 years, 73.0±2.8 kg 177.5±3.5 cm, respectively

2.2 Laboratory Testing

Four different sets of instrumented insoles were placed directly over the vibrating platform (3D shaker based on linear delta kinematics) one at a time and were subjected to the four signals explained in Table 1. To assess whether shoes can affect the measured exposition of vibration, one set has been chosen randomly and it has been put inside three different pair of shoes, which were again placed on the vibrating platform and subjected to the same signals as before.

Table 1: Characteristics of the signals used for the laboratory testing of the sensorized insoles

Signal ID	Direction	Waveform	Passband [Hz]	Duration [s]	Nominal RMS [m/s^2]
1	X	White Noise	0.5 - 20	60	0.5
2	Y	White Noise	0.5 - 20	60	0.5
3	Z	White Noise	0.5 - 20	60	0.5
4	X, Y, Z simultaneous	Pseudo-Random	0.5 - 50	120	0.5

The test order was randomized and the rest between each test was modulated according to the needs of the subject. The reference accelerometer was a triaxial 356A22 unit manufactured by PCB Piezotronics (3425 Walden Avenue Depew, NY 14043-2495 USA); the pickup was placed in the middle of the vibrating platform. Data were sampled with a rate of 2048 Hz through the acquisition board National Instruments 9234 (11500 N Mopac Expwy Austin, TX 78759-3504).

Figure 2: Subject standing on the sensorized insoles, without shoes on the three-axis shaker, shown with the reference system used.

2.3   Outdoor Testing: Mountain Bike & Skiing

The mountain bike testing took place inside the PoliMi Campus of Lecco. Each subject was asked to repeat the same path inside the campus 5 times. During the tests, participants were asked not to use the saddle of the bike. The ski testing took place in the ski area of Piani di Bobbio (LC, Italy). Both subjects had to cover 9 different paths in randomized order.

2.4   Data Analysis

The vibration exposure at the location of the 4 accelerometers inside the insoles was summarized, in each test, by the weighted vibration level as per RMS ISO 2631-1. For the lab validation, the sensorized insole system was tested by imposing controlled vibrations in the X, Y, Z axes and finally by combining vibration along all three axes simultaneously. The RMS of the four vibrations measured by the insoles was then compared to the vibration exposure measured by a reference accelerometer; both per test, as well as the average of the five tests. In the lab tests, since vibration was imposed by a controlled shaker, all four sensors within the insoles should be exposed to the same amount of vibration.

Once the sensorized insoles were validated in the lab, the total RMS vibration exposure was measured during the outdoor tests. Since dynamic movements and the distribution of force within the shoes/boots affected the amount of vibration exposure measured by each sensor, the vibration exposure was calculated as the total mean vibration exposure of the four sensors rather than comparing the measurement of any single sensor.

3   RESULTS

3.1   Lab testing

Tables 2 and 3 show a summary of the weighted vibration level measured by each sensor during all the controlled, shaker-induced trials in 3 different axes as well as during a 3D test. Table 2 reports results of tests performed without shoes, while Table 3 reports data of tests performed with shoes. Without shoes, the largest difference between the insoles and the reference accelerometer was in the X axis test and the smallest difference was in the Z axis test. With shoes, the largest difference was during the 3D test while the smallest difference was in the Y axis test. It can be seen however, that the differences overall were smaller when wearing shoes than when testing without shoes.

Table 2: Vibration exposure measurements in lab without shoes. Units are in m/s^2.

	R Toe	R Heel	L Toe	L Heel	Total	Ref.	Diff.	
Test X	0.23	0.24	0.25	0.24	0.24	0.18	0.07	
Test Y	0.23	0.24	0.22	0.20	0.22	0.17	0.05	
Test Z	0.35	0.35	0.36	0.35	0.35	0.38	0.02	
Test 3D	0.53	0.54	0.53	0.58	0.55	0.49	0.06	

Table 3: Vibration exposure measurements in lab with shoes. Units are in m/s^2.

	R Toe	R Heel	L Toe	L Heel	Total	Ref.	Diff.	
Test X	0.20	0.20	0.21	0.21	0.20	0.18	0.02	
Test Y	0.19	0.19	0.20	0.21	0.20	0.18	0.02	
Test Z	0.35	0.34	0.35	0.35	0.35	0.38	0.03	
Test 3D	0.50	0.57	0.49	0.59	0.54	0.50	0.04	

3.2   Outdoor testing: Mountain bike & Skiing

Table 4 shows the vibration exposure measured by each sensor, during each trial, the global vibration exposure for each trial, as well as the RMS of each sensor across all trials. During the ski testing, there were four tests from one of the subjects in which the instrumented insoles did not record data.

Table 4: Vibration exposure measurements of sensorized insoles during mountain bike trials with subjects and trials labelled as Subject#.Trial#. Units are in m/s^2.

	Mountain Bike				
	R Toe	R Heel	L Toe	L Heel	Total
S1.1	0.22	0.43	0.29	0.21	0.30
S1.2	0.65	0.65	3.89	1.98	2.23
S1.3	3.84	2.91	2.86	2.38	3.05
S1.4	3.42	2.64	3.24	2.04	2.89
S1.5	3.92	2.75	3.99	1.93	3.26
RMS S1	2.91	2.17	3.16	1.87	2.58
S2.1	2.61	2.35	2.82	2.40	2.55
S2.2	1.13	3.16	1.07	0.32	1.77
S2.3	4.44	3.27	4.85	1.38	3.73
S2.4	4.71	3.49	5.09	3.11	4.18
S2.5	4.45	3.85	5.39	3.15	4.29
RMS S2	3.74	3.26	4.19	2.34	3.45
S3.1	4.73	3.29	0.23	1.40	2.97
S3.2	4.22	3.17	3.88	2.96	3.59
S3.3	4.59	2.88	4.14	2.79	3.68
S3.4	5.74	3.72	5.31	3.69	4.70
S3.5	4.76	3.60	5.05	3.16	4.22
RMS S3	4.84	3.35	4.14	2.90	3.88

Table 5 shows the vibration exposure measured by each sensor, during each trial and the global vibration exposure for each trial. During three of the trials for subject #1, one or more of the sensors failed to transmit data. During four of the trials for subject #2, the system was unable to gather data from any of the sensors.

Table 5: Vibration exposure measurements of sensorized insoles during skiing tests with subjects and trials labelled as Subject#.Trial#. Units are in m/s^2.

	Ski				
	R Toe	R Heel	L Toe	L Heel	Total
S1.1	2.66	3.47	2.74	0.95	2.62
S1.2	5.23	5.56	5.84	3.08	5.05
S1.3	5.63	5.17	4.17	5.95	5.28
S1.4	5.00	3.72	0.87	4.15	3.77
S1.5	2.01	2.60	0.10	2.35	2.02
S1.6	x	1.70	1.46	1.77	1.65
S1.7	4.16	x	x	4.34	4.25
S1.8	2.32	2.83	x	2.77	2.65
S1.9	2.36	3.04	2.28	2.79	2.64
S2.1	3.31	2.93	3.32	4.45	3.55
S2.6	1.97	1.48	2.09	1.47	1.78
S2.7	2.66	2.14	3.06	2.31	2.57
S2.8	3.37	3.10	3.67	3.16	3.33
S2.9	2.24	2.10	2.46	2.40	2.31

4   CONCLUSION

This paper presents a new kind of insoles for the measurement of vibration exposure, in accordance with ISO 2631-1. Each insole is equipped with two triaxial accelerometers, and the data acquired are used to automatically compute the vibration exposure. These instrumented insoles have been validated in controlled conditions, through the comparison of their measurement with the measurement of a reference accelerometer, and then have been used to measure the exposure to vibration during outdoor activities. The maximum error between the vibration exposure measured by

the insoles and the one measured by the reference accelerometer was 0.065 m/s^2. Given that the limit proposed by ISO 2631-1 for an exposure to WBV for a period between 4 and 8 hours is between 0.5 and 1, the validation process can be considered successful.

The experimental data acquired during outdoor activities show that skiers and cyclists are exposed to dangerous levels of vibration. Values of vibration exposure exceeding 4 m/s^2, in fact, are considered dangerous even for periods lower than 10 minutes. These results are compatible with the data already presented in literature [4]; however, it is important to remark a key difference. Although the instrumented insoles are affected by a larger error on the measurement in respect to the reference accelerometers already used, their main advantage is to make direct measurement on the interface between the feet and the supporting surface, as it was not possible with standard equipment. As a further advantage, each insole can measure the whole acceleration vector in two different points. The difference in terms of vibration exposure between the two legs, or between the heels and the toes may in fact be not negligible, as shown by the data acquired during cycling, where the vibration exposure measured on the toes is consistently larger than the one measured on the heels.

Therefore, the instrumented insoles, thanks to their unobtrusiveness and to their greater number of sensors, could allow the acquisition of a more complete and direct set of measurements of vibration exposure during hazardous activities, thus improving the overall safety of athletes and workers.

6   REFERENCES

[1] C. Liedtke *et al*, "Evaluation of instrumented shoes for ambulatory assessment of ground reaction forces," *Gait Posture,* vol. 26, *(1),* pp. 39-47, 2007.

[2] S. C. Mukhopadhyay, "Wearable sensors for human activity monitoring: A review," *IEEE Sensors Journal,* vol. 15, *(3),* pp. 1321-1330, 2015.

[3] S. Spinsante and L. Scalise, "Measurement of elderly daily physical activity by unobtrusive instrumented shoes," in *2018 IEEE International Symposium on Medical Measurements and Applications (MeMeA),* 2018, pp. 1-5.

[4] M. Tarabini, B. Saggin and D. Scaccabarozzi, "Whole-body vibration exposure in sport: four relevant cases," *Ergonomics,* vol. 58, *(7),* pp. 1143-1150, 2015.

[5] I. Pavón *et al*, "Wearable technology usefulness for occupational risk prevention: Smartwatches for hand-arm vibration exposure assessment," in *Proceedings of the Occupational Safety and Hygiene V: Selected Papers from the International Symposium on Occupational Safety and Hygiene (SHO 2017),* 2017, pp. 65.

[6] M. Tarabini *et al*, "The potential of micro-electro-mechanical accelerometers in human vibration measurements," *J. Sound Vibrat.,* vol. 331, *(2),* pp. 487-499, 2012.

[7] M. Tarabini *et al*, "Measurement of the force exchanged by orthodontic masks and patients," in *2018 IEEE International Symposium on Medical Measurements and Applications (MeMeA),* 2018, pp. 1-6.

[8] M. Tarabini *et al*, "Monitoring the human posture in industrial environment: A feasibility study," in *2018 IEEE Sensors Applications Symposium (SAS),* 2018, pp. 1-6.

[9] M. Tarabini *et al*, "Real-time monitoring of the posture at the workplace using low cost sensors," in *Congress of the International Ergonomics Association,* 2018, pp. 678-688.

[10] G. Aiello *et al*, "Real time assessment of hand–arm vibration system based on capacitive MEMS accelerometers," *Comput. Electron. Agric.,* vol. 85, pp. 45-52, 2012.

[11] R. Morello, C. De Capua and A. Meduri, "A wireless measurement system for estimation of human exposure to vibration during the use of handheld percussion machines," *IEEE Transactions on Instrumentation and Measurement,* vol. 59, *(10),* pp. 2513-2521, 2010.

[12] M. Cutini and C. Bisaglia, "Whole-body vibration monitoring using a smartphone," in *Proceedings of the International Conference of Agricultural Engineering (AgEng),* 2014, pp. 1-8.

[13] C. Moufawad El Achkar, *Instrumented Shoes for Daily Activity Monitoring in Healthy and at Risk Populations,* 2016.

Development of a simplified two-dimensional biodynamic model of the foot-ankle system exposed to vibration

Delphine Chadefaux[1]
Université Paris 13 Nord, Institut de Biomecanique Humaine Georges Charpak
Boulevard de l'Hôpital 151, 75013 Paris,France
delphine.chadefaux@univ-paris13.fr

Katie Goggins[2], Tammie Eger[2]
Laurentian University, Centre for Research in Occupational Safety and Health,
Ramsey Lake Road 935, Sudbury, ON P3E 2C6, Canada
kx_goggins@laurentian.ca, teger@laurentian.ca

Stefano Marelli [3], Cesare Cazzaniga[3], Marco Tarabini[3], Pietro Marzaroli[3]
Politecnico di Milano, Dipartimento di Meccanica
via la Masa 1, 20156 Milano, Italy
stefano1.marelli@polimi.it, cesare.cazzaniga@polimi.it, pietro.marzaroli@polimi.it,
marco.tarabini@polimi.it

Reuven Katz[4]
Technion - Israel Institute of Technology, Department of Mechanical Engineering,
Haifa, 3200003, Israel
reuvenk@technion.ac.il

ABSTRACT

A wide range of workers is exposed to Foot-Transmitted Vibration (FTV). Exposure to this kind of vibration is associated with an increased risk of developing vibration-induced white foot. This paper presents a two-dimensional biodynamic lumped element model describing the response of the foot-ankle system to vibration. The model is composed of four segments linked together and connected to the ground by three couples of springs and dampers elements. The stiffness and damping were estimated by minimizing the difference between the modelled transmissibility and the average transmissibility taken from literature data. Five different points of the feet were taken into account, in the frequency range of 10 Hz – 100 Hz. The results showed that the model correctly describes the experimental data (maximum transmissibility error lower than 0.11 and 0.70 rad for the modulus and the phase), especially with respect to the inter-participant variability experimentally observed (in average 0.52 and 1.65 rad for the modulus and the phase). This contribution can aid in the development of materials and equipment to attenuate FTV and, consequently, to lower the risk of developing vibration-induced white foot.

1   INTRODUCTION

Millions of workers all over the world are exposed to foot-transmitted vibration (FTV), that can lead low-back disorders, neck pain and other diseases [1], [2]. FTV is for example associated with drilling/bolting off platforms, and workers can develop vibration-induced white feet (VIWFt), which induces pain and numbness in the toes and feet, increases sensitivity to cold and joint pain.

In literature, a few studies recently focused on the response to the foot to FTV; Goggins et al. [3] reported that the vibration transmissibility is different in the various regions of the foot. Lumped parameters models were developed to describe the foot behavior under vibration at very low frequencies. Gefen [4] proposed a model that reproduces the foot's longitudinal arch, and used such a model to estimate the in-vivo elastic properties of the plantar fascia through unobtrusive tests. Simkin and Leichter [5] used a similar model to estimate the energy stored inside the foot while walking. Later, Kim and Voloshin [6] added to the previous model the damping properties of the plantar fascia. All these models represent the foot in a very simple way, as they are composed by two rigid beams, connected by a hinge at one end, and by an elastic or visco-elastic elements on the other end.

This paper proposes a lumped parameter model to reproduce foot transmissibility at specific locations. A degree of freedom is dedicated to reproduce also all the fingers' resonances evidenced by Goggins et al. (2018) [3]. This model has been implemented to reproduce the foot-ankle system (FAS) behavior when exposed to FTV between 10-100Hz.

2   METHOD

The model is composed of masses, springs and dampers, connected in such a way to represent the foot anatomy. Bones were represented as masses, while tendons and muscles were represented as Kelvin Voight elements. Inertia, masses and lengths values of each segment were derived from the literature, while stiffnesses and damping coefficients were obtained by fitting experimental transmissibility measured in five-foot locations with the numerical curves.

2.1   Experimental data used for model construction

Foot transmissibility experimental data were collected from 21 healthy participants exposed to vertical vibration while standing in natural position on a rigid plate, that was fixed on an electrodynamic shaker. The detailed test procedure is described by Goggins et al. [3]. Experimental data were considered between 10-100 Hz, where the applied stimulus was a sine sweep of 51 s, with maximum vibration amplitude of 30 mm/s. Figure 1(a) shows foot measured locations, indicated with different colors and letters: rearfoot (A), midfoot (C), ankle (B), forefoot (D) and toes (E). According to similarities in transmissibility responses [3], the tridimensional foot can be reduced to a 2D model, by averaging at the foot position just described. In this way, the measured 24 anatomical locations were averaged to obtain five average transmissibility functions (one for each letter).
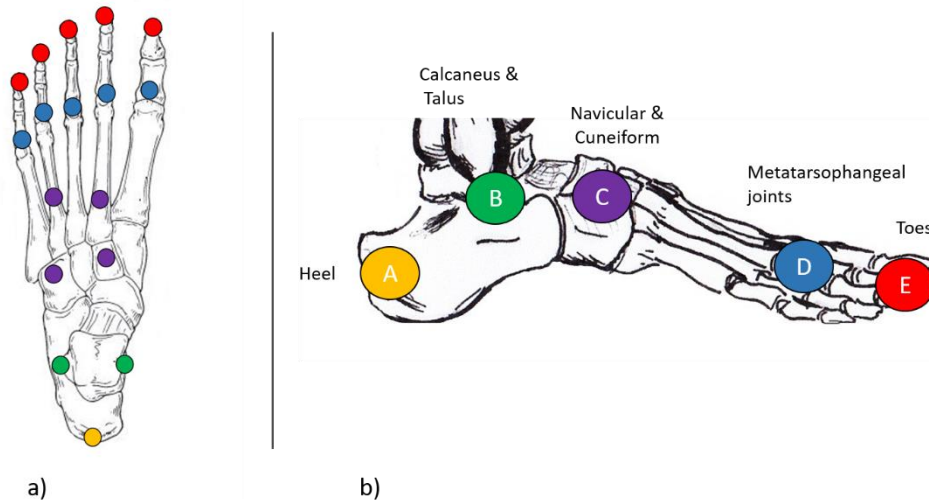
Figure 1: Transmissibility measurement locations averaged (a) used to design model segments corresponding to the anatomy of the foot (b).

2.2 Model of the foot-ankle system

The simplified 2D model of the FAS describes the dynamical behaviour of one foot supporting a mass m corresponding to the half of the total human body mass (Figure 2). Mass m is the average half body mass of the participants, i.e. 35 kg. The model was composed of four homogeneous segments:

- the talus and the calcaneus (i.e. rearfoot),
- the cuneiforms and the navicular (i.e. midfoot),
- the metatarsals (i.e. forefoot),
- the toes.

All segments were assumed to be rigid body of and moment of inertia $I_{I...IV}$, mass $m_{I...IV}$ and length $L_{I...IV}$. All inertial and geometrical properties of each segment were derived from (Isman and Inman, 1969; Lee et al., 2011; Zatsiorsky, 2002) and are summarized in Table 1.

Table 1: Geometrical and inertial characteristics of the four segments composing the foot (Isman and Inman, 1969; Lee et al., 2011; Zatsiorsky, 2002).

	Segment I	Segment II	Segment III	Segment IV
m (kg)	0.294	0.294	0.196	0.098
L (m)	0.046	0.085	0.07	0.06
I (kg·m^2)	$28 \cdot 10^{-5}$	$1 \cdot 10^{-6}$	$14 \cdot 10^{-6}$	$15 \cdot 10^{-7}$

Figure 2 shows the foot model, made of the four segments just mentioned, connected to each other by Kelvin-Voight models of stiffnesses and dampers. k_a and c_a reproduce viscoelastic properties of ligaments and tendons between ankle and mass m, while $k_{b, c}$ and $c_{b, c}$, are torsional spring and dampers that connects segments II, III and IV. The plantar aponeurosis behaviour was expressed by stiffness and damping coefficients k_d and c_d. Finally, $k_{e, f, g}$, and $c_{e, f, g}$ represent the absorbing capability of the fat pad and soft tissues composing the foot sole. This model has six degrees of freedom, four called $\theta_{1..4,}$ that are four rotations occurring between each segments. $y_A(t)$ and $y_B(t)$ are the vertical displacement of ankle and of the whole body except the foot respectively. The motion of the human body centre of mass $y_B(t)$ was assumed to be vertical. The static values of FAS posture for θ_1, θ_2, and θ_3 were derived from literature and corresponded to 49°, 69°, and 82° respectively. An imposed harmonic displacement $y_{in}(t)$ drove the sole of the foot. To evaluate numerical

transmissibility in the same location of the measured one, the foot response in the frame of reference (x, y) was estimated at:

- the middle of the rearfoot segment $(x_1(t), y_1(t))$,
- the distal end of the midfoot $(x_2(t), y_2(t))$,
- the distal end of the forefoot $(x_3(t), y_3(t))$,
- the distal end of the toes $(x_4(t), y_4(t))$.
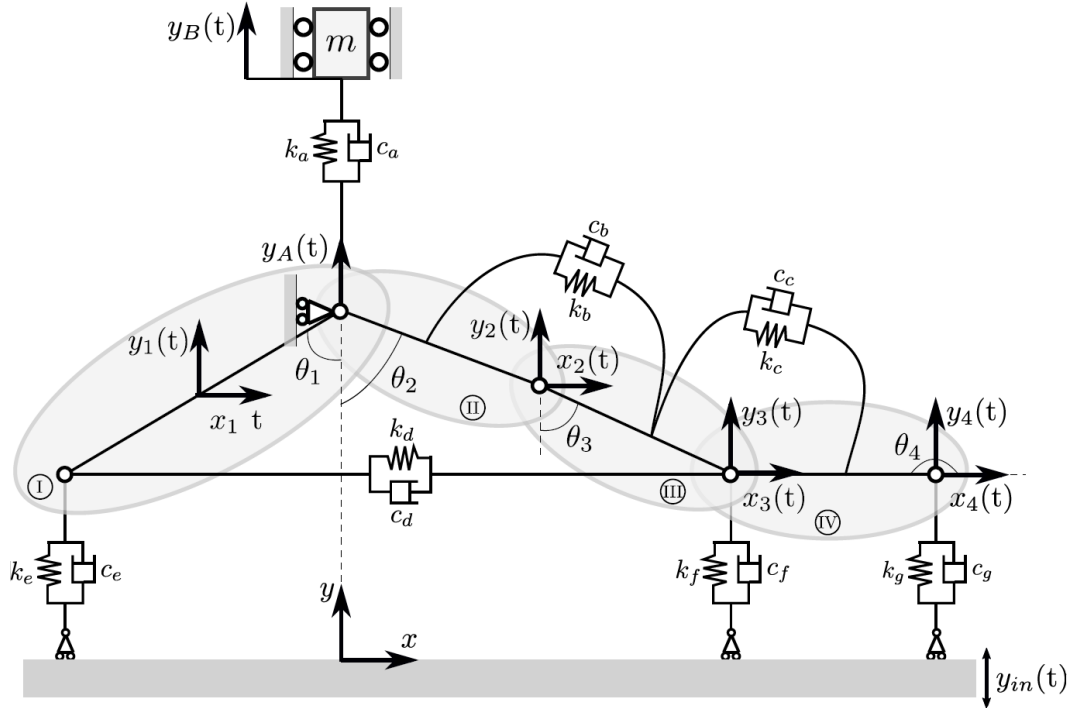
Figure 2: Biodynamic model of the FAS. The four segments are referring to the rearfoot (I), the midfoot (II), the forefoot (III), and the toes (IV). The equivalent dynamical properties $k_{a...g}$ and $c_{a...g}$ are describing each joint behavior. $\theta_{1...4}$, and $y_{A,B}$ correspond to the system's degrees of freedom.

2.3 Equations of motions

By applying the Lagrangian approach, it was possible to derive the non-linear equation of motion on the lumper parameter model. Under the hypothesis that the transmitted vibration induced only small perturbations around the equilibrium position, geometric nonlinearities were simplified to the first two terms of the Taylor series expansion. This linearization procedure led to a simplification of the problem and hence a reduction of the computation time for dynamic simulation, and it is justified by the limited nonlinear effects in the biodynamic response of standing participants, as reported by Tarabini et al. [7].

2.4 Identification of the model parameters

The stiffnesses and damping properties were computed by minimizing the mean-squared error between the moduli of numerical transmissibility functions and the measured ones. The computation was carried out through the '*lsqcurvefit*' function implemented in MATLAB R2017b. The initial guess values implemented in the procedure were of 10000 N·m^{-1} and 100 N·s·m^{-1} for the stiffness and damping elements based on (Wee, 2012), while the parameters' lower bounds were set at zero and no upper bounds were specified to the solver. Finally, the reconstruction quadratic error was estimated for each transmissibility function as:

$$\varepsilon = \sqrt{\frac{1}{N} \sum_{f=10}^{100} \left| \tilde{T}(f) - T(f) \right|^2}, \tag{1}$$

where f is the frequency vector, $\tilde{T}$ and T are the modelled and the measured transmissibility functions, and N is the length of the discrete transmissibility functions.

3 RESULTS

3.1 Model of the foot-ankle system

Table 2 lists the optimized parameters. Stiffness coefficients were estimated within a range from 8 N·rad^{-1} up to 147 kN·m^{-1}. The lowest values were obtained for k_a, k_b, and k_c, describing the ligaments and tendons between the ankle and the body (k_a = 228 N·m-1), between the segments II and III (k_b = 53 N·rad^{-1}), and between the segments III and IV (k_c = 8 N.rad^{-1}), respectively. Further, the plantar aponeurosis stiffness k_d was ten times higher than the stiffness of the ligaments and tendons between the ankle and the body (k_d = 3498 N·m^{-1}). The foot sole stiffnesses greatly varied in the different foot locations. The forefoot sole stiffness (k_f = 147 kN·m^{-1}) was about 10 times higher than the rearfoot (k_e = 13650 N·m-1) and about 300 times higher than the toes (k_g = 536 N·m^{-1}). Damping coefficients were estimated within a range from 0 to 124 N·s·m^{-1}. As for the lowest stiffness coefficients, the lowest damping coefficients were estimated for the ligaments and tendons (c_a = 0.2 N.s.m-1, c_b = 0.2 N·s·rad^{-1}, and c_c = 0.4 N·s·rad^{-1}). The plantar aponeurosis damping coefficient was increased compared to the ligaments and tendons (c_d = 48 N·s·m^{-1}). The forefoot sole damping coefficient c_f was 0 N·s·m^{-1}, the rearfoot damping coefficient c_e was 71 N·s ·m^{-1}, and the toes damping coefficient was even greater (c_g = 124 N·s·m-1).

Table 2: Estimated stiffness and damping coefficients of each model segment.

Parameter	Unit	Value	Description
k_a	N·m^{-1}	228	stiffness of the ankle/body joint
k_b	N·rad^{-1}	53	stiffness of the segments II/III joint
k_c	N·rad^{-1}	8	stiffness of the segments III/IV joint
k_d	N·m^{-1}	3 500	stiffness of the plantar aponeurosis
k_e	N·m^{-1}	13 650	stiffness of the rearfoot sole
k_f	N·m^{-1}	147 000	stiffness of the midfoot sole
k_g	N·m^{-1}	536	stiffness of the forefoot sole
c_a	N·s·m^{-1}	0.2	damping of the ankle/body joint
c_b	N·s·rad^{-1}	0.2	damping of the segments II/III joint
c_c	N·s·rad^{-1}	0.4	damping of the segments III/IV joint
c_d	N·s·m^{-1}	48	damping of the plantar aponeurosis
c_e	N·s·m^{-1}	71	damping of the rearfoot sole
c_f	N·s·m^{-1}	0	damping of the midfoot sole
c_g	N·s·m^{-1}	124	damping of the forefoot sole

Figure 3 shows the resulting magnitude and phase of the transmissibility functions for the five locations on the foot. The reconstruction quadratic error of the modulus was ε=0.08 ±0.03. The reconstruction error of the phase was ε=0.31 ±0.21 rad. For all investigated transmissibility functions, results showed that modelled transmissibility were included in the standard deviation estimated experimentally based on both, the inter-participant repeatability and the two-dimensional reduction of the model. Differences between modelled transmissibility and experimental transmissibility increased with frequency, where the effect of soft tissues is more relevant.
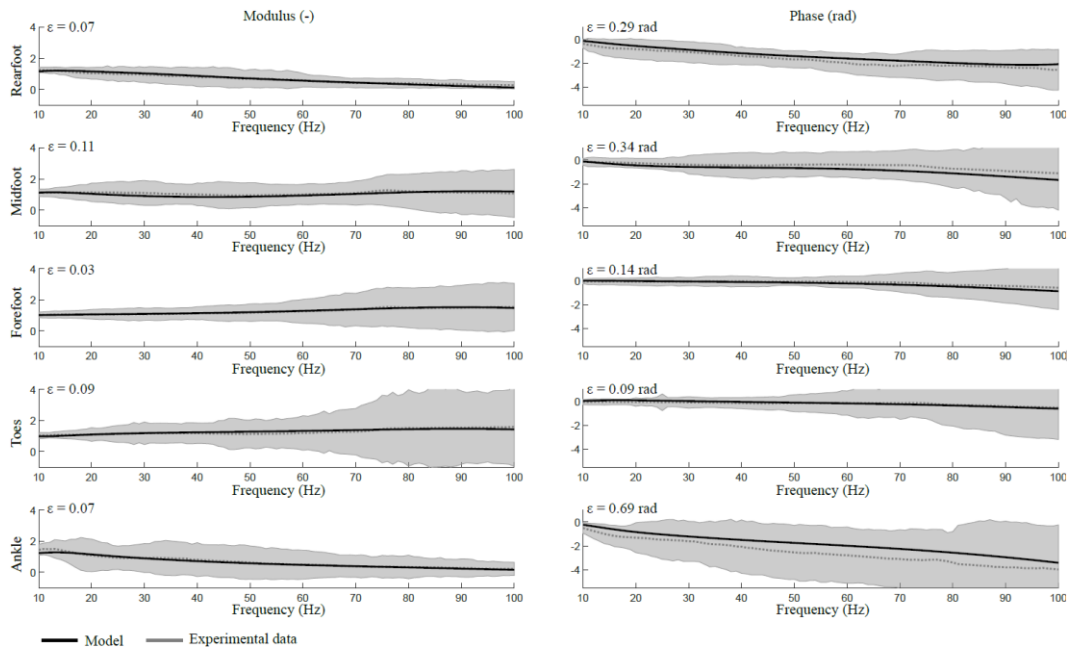
Figure 3: Modelled (black curves) and measured (grey curves) amplitude and phase of the vibration transmissibility functions computed at five locations of the FAS. The reported uncertainty represents a 95% confidence interval. The reconstruction quadratic error ε is reported for each modelled curve.

4   DISCUSSION AND CONCLUSION

The 2D lumped-parameter model of the Foot-Ankle system proposed in this paper was validated with experimental data in the frequency range from 10 to 100 Hz. The foot response was estimated at five locations using experimental data measured on 21 healthy participants standing in a natural position. The values of stiffness and damping were estimated through an optimization procedure of the computed transmissibility functions with respect to experimentally measured transmissibility functions [3]. The results obtained show that FAS model, with the optimized parameters, can represent the transmissibility at five locations on the foot, with reconstruction errors lower than 0.11 (moduli) and 0.34 rad (phase).

The FAS model correctly reproduces the foot response to vertical WBV as the errors are small in comparison with experimental data variability, with errors that usually increase with the frequency. This observation is explained by the preponderance of the bones and tendons in the FAS dynamical behaviour at low frequency, while the human skin and tissues govern the FAS dynamical behaviour at higher frequencies (Lundström, 1985).

The parameters resulting from the optimization process are consistent with the existing literature works. For instance, the majority of the energy dissipation occurs at the forefoot/toes, and the apparent mass is mainly concentrated on the talon, consistently with what was evidenced by Tarabini et al. [7] at lower frequencies. Furthermore, Gefen [4], and Jorgensen and Bojsen-Moller [8] reported that the rearfoot and forefoot of the sole had the highest damping ratios while the lowest absorbing capability in the entire FAS was estimated at the sole's midfoot. Material and structural differences between the foot segments have also been reported, suggesting that heel pad stiffness was higher than the second metatarsal head stiffness [9]. Results of the FAS model in this paper are also comparable to HTV models where the stiffness values are higher and the damping values are lower at the skin directly in contact with the vibrating sources [10], [11].

As a future step, also the information about the apparent mass will be included in the objective function of the optimization, to obtain a model that can describe completely the interaction between the human foot and a vibration on the supporting surface. To date, the results obtained from the validation of a more complex FAS model, able to reproduce both transmissibility and DPMI, is under

evaluation for publication on Journal of Biomechanics [12]. This model will help to investigate which FAS segments are responsible of the transmissibility variations. Further investigation on the shoe effect will identify the transmissibility change due to presence of the shoe, modelled as a spring between the supporting surface and the FAS.

To conclude, this contribution opens new perspectives in modelling human-body response to vibrations and could aid in the development of future models to evaluate materials to attenuate FTV associated with VIWFt.

REFERENCES

[1] T. Hashiguchi *et al*, "Pathological changes of finger and toe in patients with vibration syndrome," *Nagoya J. Med. Sci.,* vol. 57, *(Suppl),* pp. 129-136, 1994.

[2] U. Hedlund, "Raynaud's phenomenon of fingers and toes of miners exposed to local and whole-body vibration and cold," *Int. Arch. Occup. Environ. Health,* vol. 61, *(7),* pp. 457-461, 1989.

[3] K. A. Goggins *et al*, "Anatomical locations for capturing magnitude diffferences in foot-transmitted vibration exposure," *Ace-Crosh 2018,* pp. 92, 2018.

[4] A. Gefen, "The in vivo elastic properties of the plantar fascia during the contact phase of walking," *Foot & Ankle International,* vol. 24, *(3),* pp. 238-244, 2003.

[5] A. Simkin and I. Leichter, "Role of the calcaneal inclination in the energy storage capacity of the human foot—a biomechanical model," *Medical and Biological Engineering and Computing,* vol. 28, *(2),* pp. 149-152, 1990.

[6] W. Kim and A. S. Voloshin, "Role of plantar fascia in the load bearing capacity of the human foot," *J. Biomech.,* vol. 28, *(9),* pp. 1025-1033, 1995.

[7] M. Tarabini *et al*, "Analysis of non-linear response of the human body to vertical whole-body vibration," *Ergonomics,* vol. 57, *(11),* pp. 1711-1723, 2014.

[8] U. Jørgensen and F. Bojsen-Møller, "Shock absorbency of factors in the shoe/heel interaction—with special focus on role of the heel pad," *Foot Ankle,* vol. 9, *(6),* pp. 294-299, 1989.

[9] J. C. Teoh, Y. B. Lim and T. Lee, "Minimum indentation depth for characterization of 2nd sub-metatarsal head and heel pad tissue properties," *J. Biomech.,* vol. 48, *(10),* pp. 2096-2101, 2015.

[10] R. Dong *et al*, "Vibration energy absorption (VEA) in human fingers-hand-arm system," *Med. Eng. Phys.,* vol. 26, *(6),* pp. 483-492, 2004.

[11] D. Reynolds and R. Falkenberg, "Three-and four-degrees-of-freedom models of the vibration response of the human hand," in *Vibration Effects on the Hand and Arm in Industry*Anonymous Wiley New York, 1982, pp. 117-132.

[12] D. Chadefaux *et al*, "A Development of a two-dimensional dynamic model of the foot-ankle system exposed to vibration" *J. Biomech.*, (under evaluation)

Influence of leg posture on vibration characteristics of a passenger car

Massimo Cavacece[1]
University of Cassino and Southern Lazio, Department of Civil and Mechanical Engineering,
Via G. Di Biasio n.43, 03043 Cassino (FR), Italy
cavacece@unicas.it

Graziella Aghilone[2]
University La Sapienza of Rome, Pharmacy and Medicine Faculty,
Piazzale Aldo Moro n.5, 00185, Rome (RM), Italy
graziella.aghilone@uniroma1.it

ABSTRACT

The present study was conducted with the car driven at speed of 60 and 80 [km/h]. The purpose of the study was to investigate the effect of different seating conditions and different speed on the vibration transmitted through the seat pan, in all directions, to the seated human body. The vibration dose value was measured on the seat along x-, y- and z- directions. It is proposed an integrating finite element method and multi-body simulation for seated human body. The analysis of power spectrum density shows how the vehicle seats should have the capability of attenuating the vibration at frequencies coinciding with the resonance frequencies of the human body to avoid discomfort or health problems due to vibration.

1   INTRODUCTION

Vibration transmitted from the road to the passengers (or driver) of a vehicle through the seat pan and seat backrest can affect ride comfort [1]. The person posture (e.g. sitting with an erect or normal posture) [8] or the seating conditions (e.g. with or without a backrest, seat surface angle and backrest angle) can be considered the independent variables [6]. The behaviour of the seat affects the response of the occupant.

Toward and Griffin concluded that the biodynamic response affects the transmission of vibration through seats [7]. If the dynamics of seats is evaluated, the foot position should be considered.

If the subjects place their feet away from the seat compared to placing their feet close to the seat, it can be observed an increase in apparent mass at resonance frequency and at low frequencies [2].

Rakheja et al. illustrated that the effect of foot position on the apparent mass at resonance frequency is more pronounced in the driver posture (hands on steering wheel posture) than in the passenger posture (hands in lap posture) [3]. Nawayseh and Griffin reported an increase in the fore-and-aft cross-axis apparent mass (complex ratio between the fore-and-aft force and the vertical acceleration on the seat) at low frequencies when subjects extended their legs compared to a vertical lower legs position [4].

The correlation between the peak frequency of the vertical apparent mass and the peak frequency of the fore-and-aft cross-axis apparent mass has been found to be affected by the position of the legs [5].

The objective of this study is to investigate the effect of different seating conditions on the vibration received by the seat occupant from the seat pan. The factors considered in this paper are the postures of lower leg position. Different seating conditions indicate different sitting postures. Different body postures give different biodynamic responses. The seated human system is a coupled system. Therefore, the body postures generate an effect on the vibration received by the occupant of the seat.

The effects of different seating conditions and speed of the car on the vibration dose value (VDV) and on power spectrum density (PSD) have been investigated on the seat pan along all directions. It is proposed a comparison between ISO 2631 standard and BS 6841 standard to calculate the vibration transmitted to the human body from the seat. The results of this study show no effect of leg posture on the VDVs measured on the seat pan in any direction.

The analysis of PSD shows how the vehicle seats should have the capability of attenuating the vibration at frequencies coinciding with the resonance frequencies of the human body to avoid discomfort or health problems due to vibration.

2   FINITE ELEMENT MODEL

The finite element method considers the dynamical system as an assemblage of elements. The joint displacements $u_i(t)$ and $u_{i+1}(t)$ are chosen along the axial direction of the element. Each bar element can have an orientation qi respect to horizontal axis as shown in Fig.1.
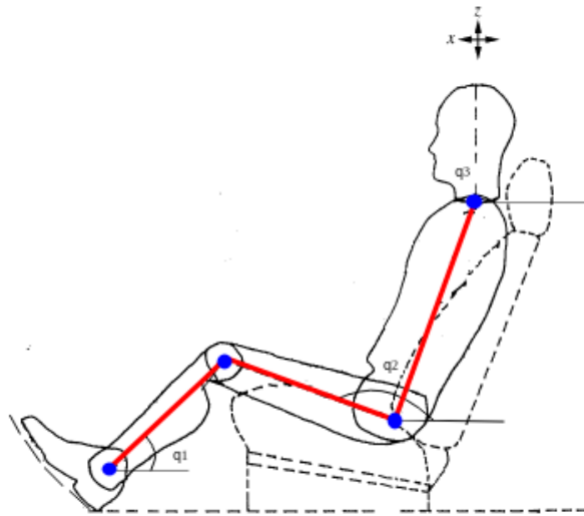
Figure 1: Arrangement of the seat and finite element model of seated human body

The vectors of the joint displacements in the local and the global coordinate system can be written as the following relation:

$$\vec{u}(t) = [\lambda]\vec{U}(t) ,\tag{1}$$

where [λ] is the coordinate transformation matrix given by

$$[\lambda] = \left[\begin{array}{cccc} \cos q_i & \sin q_i & 0 & 0 \\ 0 & 0 & \cos q_i & \sin q_i \end{array} \right] ,\tag{2}$$

Equations (1) and (2) can be used to obtain the equations of motion of a single finite element in the global coordinate system

$$[m]\,\ddot{\vec{U}}(t) + [c]\,\dot{\vec{U}}(t) + [k]\,\vec{U}(t) = [\lambda]^T \vec{f}(t)\,, \tag{3}$$

with
- [m], mass matrix;
- [c], damping matrix;
- [k], stiffness matrix;
- f(t), external load.

3   EXPERIMENTAL DESIGN

In the experimental investigation, the car was driven several times on the same road segment at the required speed of 60 and 80 [km/h] and keeping the same speed for T = 1 min. The same driver was used in all experiments reported in this study. The weighted r.m.s. values obtained at the seat pan in the x, y and z-directions were measured by a more advanced measuring device (Human Vibration Meter and Analyzer, SVANTEK SV 106). In each experiment, the accelerations in the x, y and z–directions were measured at the seat pan of the front passenger seat using MEMS type SVANTEK SV 38V tri-axial accelerometer housed in SAE pads. The data were acquired and analyzed using SVANTEK SV 106 Human Vibration Meter and Analyzer.

Ten male subjects, with average mass 79.9 kg (range 62-109 kg), stature 1.72 m (range 1.63-1.78 m), and body mass index (BMI) 26.8 [(kg · m^{-2})], were driven 6 times on the same road segment while sitting in the front passenger seat. Each time, the subject sat with one of two different seating conditions (Fig.2). The characteristics of seating conditions are the following aspects:
- Posture 1: Contact with backrest at 110°, contact with the headrest, vertical lower legs;
- Posture 2: Contact with backrest at 110°, contact with the headrest, extended lower legs.

(a) Posture 1   (b) Posture 2
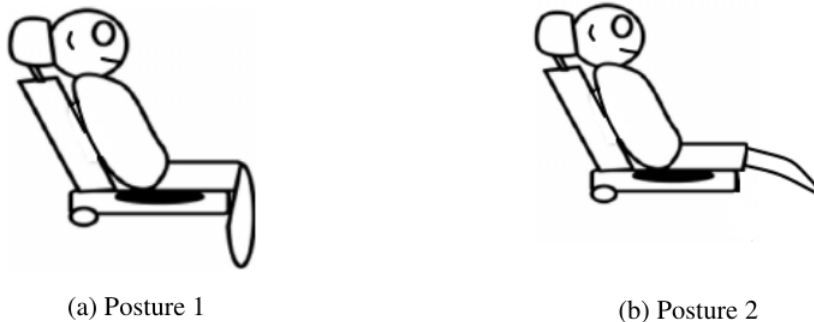
Figure 2: Schematic diagrams of the studied seating conditions

4   ANALYSIS OF VIBRATION DOSE VALUE

The Vibration Dose Value (VDV) was used to represent the data obtained from the experimental investigation of this study. The VDV takes into consideration the magnitude, frequency and duration of the exposure. The VDVs were obtained directly from the measuring device after programming the device with the axis multiplication factors and frequency weighting filters as described in the ISO 2631. The formula used to calculate VDVs is the following relation:

$$\text{VDV} = \left[\int_{t=0}^{t=T} a_w^4(t) \right]^{1/4}. \tag{4}$$

where $a_w(t)$ is the frequency weighted acceleration and T is the signal duration (60 s in this study).

After obtaining the VDVs for each axis (x, y, and z on the seat), the total VDV on the seat was evaluated by the following relation

$$\text{VDV}_{\text{seat}} = \left(\text{VDV}^4_{\text{seat,x}} + \text{VDV}^4_{\text{seat,y}} + \text{VDV}^4_{\text{seat,z}}\right)^{1/4} , \qquad (5)$$

Statistical analysis was performed on the measured data using Python Language and Software package.

Wilcoxon Signed Rank Test was used to look for statistically significant differences between the seating conditions in order to identify the effect of the studied independent variables (Posture 1 and Posture 2) on the transmission of vibration through the seat pan. The significance level was taken as 0.05.
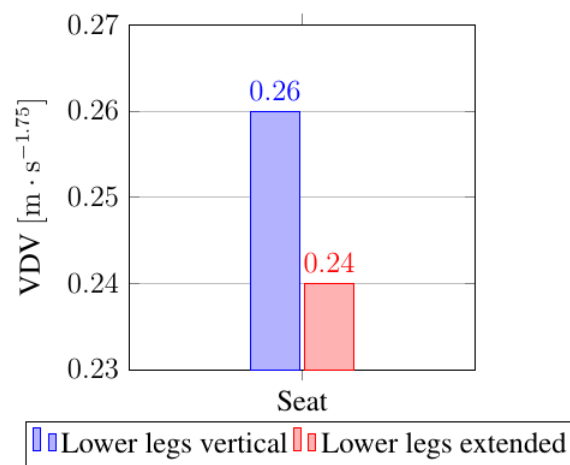
Figure 3: Effect of Posture 1 and Posture 2 on the VDVs measured on the seat
along the x-direction with v=60 km/h
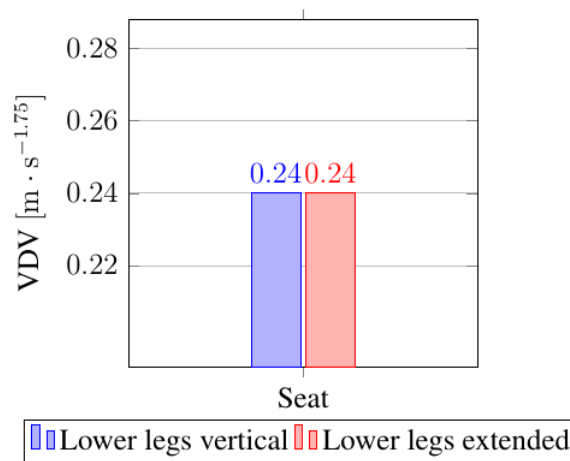
Figure 4: Effect of Posture 1 and Posture 2 on the VDVs measured on the seat
along the y-direction with v=60 km/h

No statistically significant differences were found in the VDVs measured on the seat along x (Fig.3), y (Fig.4) and z–directions (Fig.5) between Posture 1 and Posture 2 (Wilcoxon, p > 0.05). Similar conclusion were obtained by effect of Posture 1 and Posture 2 on the total VDVs measured on the seat (Fig.6).
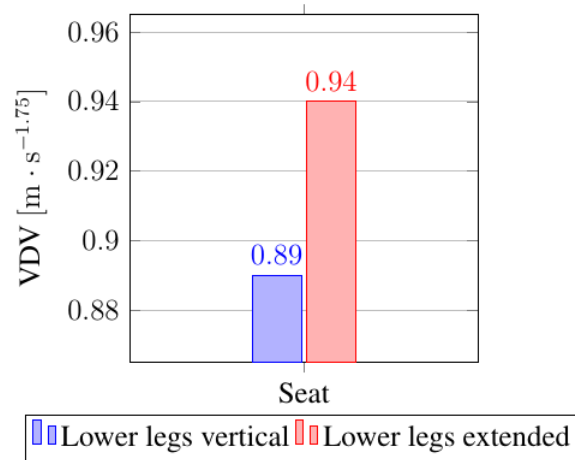
Figure 5: Effect of Posture 1 and Posture 2 on the VDVs measured on the seat
along the z-direction with v=60 km/h
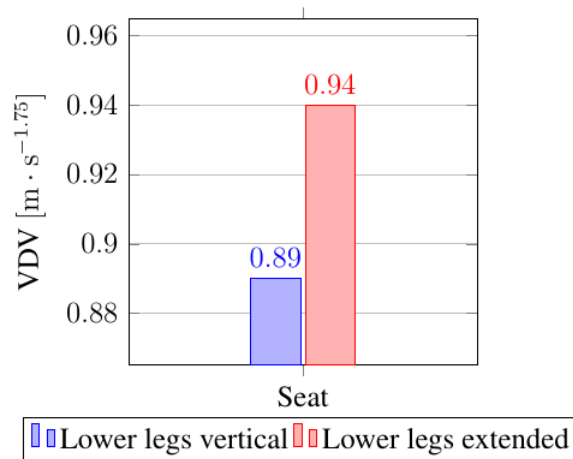
Figure 6: Effect of Posture 1 and Posture 2 on the total VDVs
measured on the seat with v=60 km/h

5   ANALYSIS OF POWER SPECTRUM DENSITY

The results of Power Spectrum Density (PSD), evaluated along z direction on the seat by effect of different seating conditions and speed of the car, are shown in Figures 7, 8, 9 and 10.
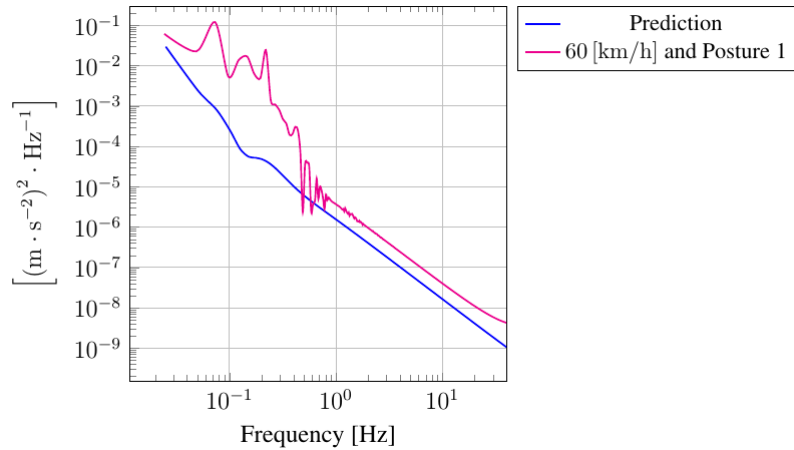
Figure 7: Comparison between predicted PSD by finite element method and measured PSD on the seat by effect of Posture 1 and speed of 60 [km/h]
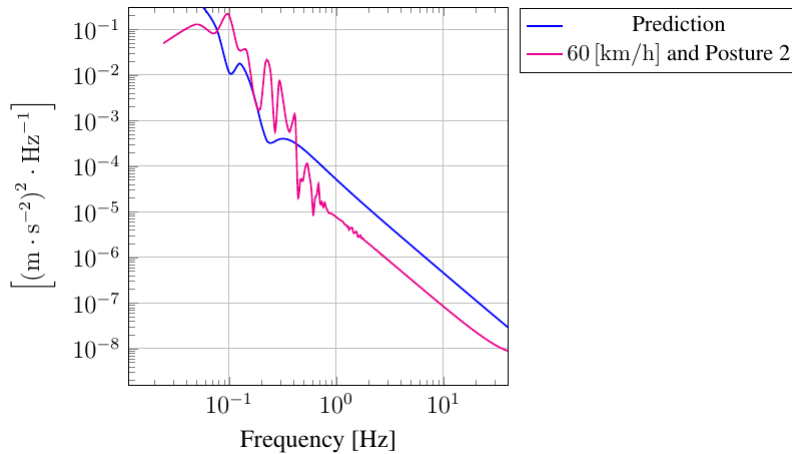
Figure 8: Comparison between predicted PSD by finite element method and measured PSD on the seat by effect of Posture 2 and speed of 60 [km/h]

The comparison between predicted PSD, by finite element method, and measured PSD, by experimental investigation, on the seat by effect of posture 1, posture 2 and speed of the car shows a good agreement.

The PSDs, obtained by experimental investigation, show that the vibration in the z-direction occurs in the frequency range 0-20 Hz. The resonance frequency of the human body, in the vertical direction, is about 5 Hz. The resonance frequency of the human body in z-direction is in the frequency range 0-20 Hz and coincides with some of the peak frequencies shown in the PSDs. Vehicle seats should have the capability of attenuating the vibration at frequencies coinciding with the resonance frequencies of the human body to avoid discomfort or health problems due to vibration.

If the speed of the car increases from 60 to 80 [km/h], it can seen that the power spectrum density, evaluated along z direction on the seat, is amplified in the frequency range 0-20 Hz.
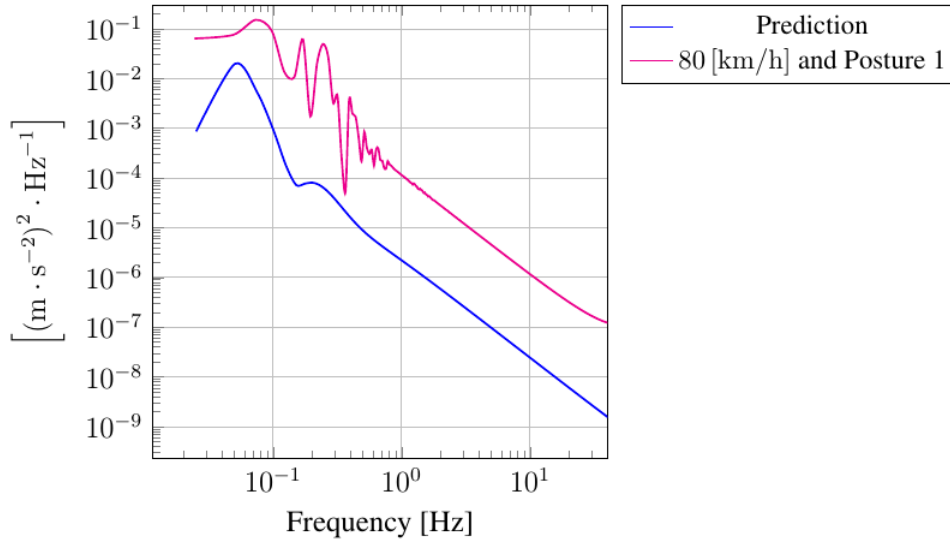
Figure 9: Comparison between predicted PSD by finite element method and measured PSD on the seat by effect of Posture 1 and speed of 80 [km/h]
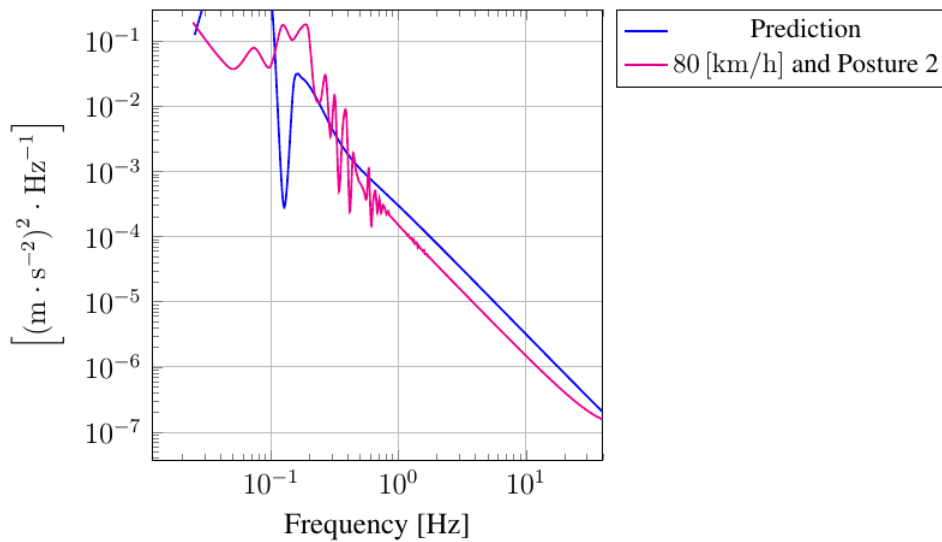
Figure 10: Comparison between predicted PSD by finite element method and measured PSD on the seat by effect of Posture 2 and speed of 80 [km/h]

6   DISCUSSION

The present study was conducted with the car driven at speed of 60 and 80 [km/h]. The purpose of the study was to investigate the effect of different seating conditions and different speed on the vibration transmitted through the seat pan, in all directions, to the seated human body.

Generally speaking, ISO 2631 uses the worst axis for assessment of vibration at the interface between the body and the vibrating surface based on the axis with the highest weighted acceleration r.m.s. value. The assessment of vibration in BS 6841 is based on calculating the

combined Vibration Dose Value (VDV) from different axes. This paper compares ISO 2631 standard and BS 6841 standard to calculate the vibration transmitted to the human body from the seat. The difference between total VDV on the seat, evaluated by BS 6841 standard, and VDV of worst axis, according to ISO 2631 standard, is very negligible.

The seating conditions, examined in this work, are passengers seating conditions and hence cannot be generalized to the driver. One main difference is that unlike the passenger, the driver will be in contact with a steering wheel which could act as a support for the body and as another source of vibration. The contact with the steering wheel might change the sitting posture and this might lead to difference between the VDVs measured for a passenger and those measured for the driver.

No statistically significant differences were found in the VDVs measured on the seat along x, y and z–directions between Posture 1 and Posture 2. Similar conclusion was obtained by effect of Posture 1 and Posture 2 on the total VDVs measured on the seat.

The PSDs of the vibration, transmitted to the seat along z-direction, were amplified in the frequency range 0-20 Hz. The resonance frequency of the human body, along z-direction, can coincide with some of the peak frequencies shown in the PSDs.

7   CONCLUSION

The effects of different seating conditions on the VDVs and PSDs on the seat pan have been investigated. Foot position showed no effect on the VDVs. Foot position and speed of the car influences the PSDs evaluated along z-direction on the seat in the frequency range 0-20 Hz. This research evaluates the effect of the seating condition on the transmission of vibration through the seat pan of a car seat. This research may help seat manufacturers recommend seating conditions that reduce discomfort caused by whole-body vibration.

REFERENCES

[1] M.J. Griffin, "Handbook of Human Vibration", Academic Press, London, 1990.

[2] N. Nawayseh, M.J. Griffin, "Non-linear dual-axis biodynamic response to vertical whole-body vibration", Journal of Sound and Vibration, 268, 503-523, 2003.

[3] S. Rakheja, I. Stiharu, P.E. Boileau, "Seated occupant apparent mass characteristics under automotive postures and vertical vibration", Journal of Sound and Vibration, 253 (1), 57-75, 2002.

[4] N. Nawayseh, M.J. Griffin, "Tri-axial forces at the seat and backrest during whole body fore-and-aft vibration", Journal of Sound and Vibration, 281, 921-942, 2005.

[5] N. Nawayseh, M.J. Griffin, "Effect of seat surface angle on forces at the seat surface during whole-body vertical vibration", Journal of Sound and Vibration, 284, 613-634, 2005.

[6] W. Wang, S. Rakheja, P.E. Boileau, "Effects of sitting postures on biodynamic response of seated occupants under vertical vibration", International Journal of Industrial Ergonomics, 34, 289-306, 2004.

[7] M.G.R. Toward, M.J. Griffin, "Apparent mass of the human body in the vertical direction: effect of a footrest and a steering wheel", Journal of Sound and Vibration, 329, 1586-1596, 2010.

[8] M. Cavacece, G. Aghilone, "Optimisation of the contact damping and stiffness coefficients to attenuate vertical whole-body vibration", 6th International Conference on Whole-Body Vibration Injuries, ISBN 978-91-85971-64-0, Gothenburg, 2017

16 Session 9: Conference Close

Session chair: Setsuo Maeda

The 55th UK Conference on Human Responses to Vibration will be held at the University of Exeter in September 2020. For further information contact J.A.B.Lewis-Thompson@exeter.ac.uk
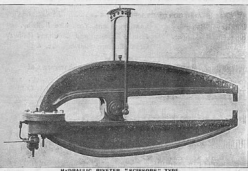
17 Conference Special Tour: the Forth Bridge

The tour will depart from the Craiglockhart campus by coach. We will be travelling to South Queensferry and North Queensferry where we will spend some time admiring the work of designer's Benjamin Baker and Sir John Fowler. However, the work of the great Scottish civil engineer Sir William Arrol will be the focus of our attention as we discuss his innovative machines that inevitably reduced the vibration exposure of the men engaged in this work. The coach will return to the city centre.

A regular ferry operated between North and South Queensferry as far back as the 12th century. By the 18th century it was reckoned to be the busiest ferry in Scotland, linking the North East of the country with Edinburgh and the south. The coming of the 19th century brought a major improvement in the form of ramped piers on either side of the Forth, which could be used by sailing ships at any stage of the tide. These piers, built between 1808 and 1817, were used by ferries right up until 1964, when the Forth Road Bridge opened.

There were plans for an alternative crossing which was not weather dependent, with a 1806 proposal for a tunnel under the Forth and a design for a suspension bridge submitted in 1818. It was the spreading of the railway network in the middle years of the century, however, that underlined the need for a bridge.

A young engineer called Thomas Bouch arrived in 1849, determined to solve the problem of the Forth and Tay estuaries. He first devised a system

261
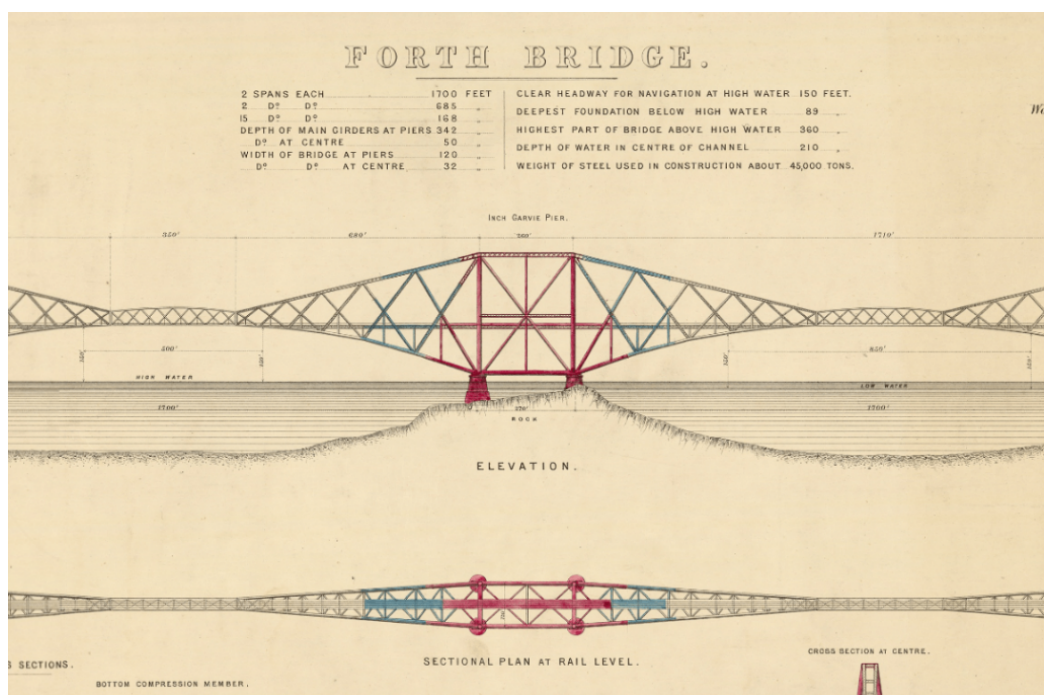
where trains were floated over the water on platforms, which impressed the directors of the North British Railway enough to listen to his ideas for bridges across the two estuaries. The Tay Bridge was begun in 1871 and the foundation stone laid for a suspension bridge across the Forth in 1873. However, this project came to an abrupt end when, three days after Christmas 1879, the Tay Bridge collapsed in a storm, with the loss of an estimated 75 train passengers.

The tragedy meant an end to Bouch's bridge plans – in fact he died the following year – but the momentum for a crossing had grown and a new design, by John Fowler and Benjamin Baker, was submitted to the Forth Bridge Company in May 1881, with construction authorised by Parliament in July 1882.

The following year, in 1883, work began on the Forth Bridge we know today, an iconic marvel of design and engineering skills known the world over.

18 List of Conference Papers

The following papers have been submitted for presentation at the conference. The conference papers are identified by a unique number. The paper identification number is used to identify papers being presented at each of the conference sessions.